

1 Kv1.2 contributes to pattern separation by regulating the hippocampal CA3  
2 neuronal ensemble size

3

4 Kisang Eom<sup>\*1,2</sup>, Hyoung Ro Lee<sup>\*1</sup>, Jung Ho Hyun<sup>\*1,†</sup>, Hyun-Hee Ryu<sup>1</sup>, Yong-Seok Lee<sup>1</sup>, Inah Lee<sup>2</sup>, Won-  
5 Kyung Ho<sup>1,2</sup>, Suk-Ho Lee<sup>1,2</sup>.

6 <sup>1</sup>Cell Physiology Lab. Department of Physiology, Seoul National University College of Medicine;

7 <sup>2</sup>Department of Brain and Cognitive Science, Seoul National University College of Natural Science, 103  
8 Daehak-ro, Jongno-gu, 03080, Seoul, Republic of Korea.

9

10 <sup>#</sup>The present address is Department of Neuroscience, Johns Hopkins University School of Medicine.  
11 Baltimore, MD 21205

12

13 \*K Eom, HR Lee and JH Hyun equally contributed to this study

14

15 Corresponding author:

16 Lee, Suk-Ho M.D., Ph.D.

17 Department of Physiology,

18 Seoul National University College of Medicine.

19 103 Daehak-ro, Jongno-gu, Seoul, 03080, Republic of Korea

20 Tel: +82-2-740-8222; Fax: +82-2-763-9667

21 e-mail address: [leesukho@snu.ac.kr](mailto:leesukho@snu.ac.kr)

22

23

24     Abstract

25     Kv1.2 expression in rodent CA3 pyramidal cells (CA3-PC) is polarized to distal apical dendrites, and  
26     regulate the synaptic responses to perforant pathway (PP) inputs. Accordingly, Kv1.2 haploinsufficiency  
27     (*Kcna2*<sup>+/−</sup>) in CA3-PCs, but not Kv1.1 (*Kcna1*<sup>+/−</sup>), lowered the threshold for long-term potentiation at  
28     PP-CA3 synapses. The *Kcna2*<sup>+/−</sup> mice, but not *Kcna1*<sup>+/−</sup>, displayed impairments in contextual fear  
29     discrimination task. The size and overlap of CA3 ensembles activated by the first visits to slightly  
30     different contexts were not different between wildtype and *Kcna2*<sup>+/−</sup> mice, but these ensemble parameters  
31     diverged over training days between genotypes, suggesting abnormal plastic changes in the CA3 network  
32     of *Kcna2*<sup>+/−</sup> mice. Eventually, the *Kcna2*<sup>+/−</sup> mice exhibited larger ensemble size and overlap upon  
33     retrieval of two contexts, compared to wildtype or *Kcna1*<sup>+/−</sup> mice. These results suggest that Kv1.2  
34     subunits prevent promiscuous plastic changes at PP-CA3 synapses, and contribute to sparse  
35     representation of memories and pattern separation in the CA3 network.

36

## 37 Introduction

38 Hippocampal CA3 region is implicated in rapid formation of episodic memories (Kesner, 2013). Synaptic  
39 inputs from entorhinal cortex (EC) converge on hippocampal CA3 pyramidal cells (CA3-PCs) directly via  
40 perforant pathway (PP) and indirectly through dentate gyrus (DG) via mossy fibers (MFs). DG is thought  
41 to segregate overlapping input patterns (pattern separation) by expansion re-coding of input patterns on  
42 the large number of dentate granule cells (GCs) that exhibit sparse firings (Senzai and Buzsaki, 2016;  
43 GoodSmith et al., 2017). Because MFs sparsely innervate CA3-PCs (Amaral et al, 1990) and convey  
44 ensemble patterns pre-processed by DG to CA3, computational models propose that MF inputs contribute  
45 to discrete and decorrelated representation of memories in the CA3 network, indicative of pattern  
46 separation (Leutgeb et al., 2004; Rolls and Kesner, 2006; Leutgeb et al., 2007). In contrast to MFs, PP  
47 densely innervates CA3-PCs and makes weak and Hebbian synapses (Amaral et al., 1990; McMahon and  
48 Barrionuevo, 2002). A formal model implies that cued memory retrieval of a pattern stored in recurrent  
49 network requires afferent inputs mediated by large number of associatively modifiable synapses, which  
50 correspond to PP-CA3 synapses (Treves and Rolls, 1992). Moreover, PP inputs are expected to be more  
51 informative for retrieval than MF inputs, because noisy part of a cue from EC can be amplified by an  
52 intervening layer, DG (O'Reilly and McClelland, 1994). To avoid interference between patterns stored in  
53 recurrent network, each pattern should be represented by a small number of principal neurons (sparse  
54 coding; Treves & Rolls, 1992). Given that associational/commissural (A/C) synaptic inputs are weakened  
55 under a high cholinergic level (Vogt and Regehr, 2001), the model assumes that MF inputs dominate the  
56 firing pattern of CA3-PCs during a learning phase. Because unit synaptic inputs incoming via PP are not  
57 strong sufficient to elicit somatic action potentials (APs) in the postsynaptic CA3-PCs, there would be  
58 low probability for PP synaptic inputs alone to trigger long-term potentiation (LTP) at PP-CA3 synapses.  
59 During learning phase, memory representation in a CA3 network is considered to be formed by Hebbian  
60 LTP at PP and A/C synapses in a subset of CA3-PCs chosen by decorrelated DG inputs (McMahon and

61 Barrionuevo, 2002; Mishra et al., 2016). A previous lesion study, however, showed that MF inputs are  
62 dispensable for retrieval of acquired memories, whereas MF inputs are required for the memory  
63 acquisition (Lee and Kesner, 2004; but see Bernier et al., 2017), implying that PP inputs initiate retrieval  
64 of memory representations stored in CA3 network. In order for PP inputs to activate a decorrelated CA3  
65 ensemble on retrieval, LTP at PP synapses should be induced in a small number of CA3-PCs (sparse  
66 encoding) during hippocampal learning. For sparse encoding at PP synapses, induction of LTP at PP  
67 synapses should be tightly regulated, and thus it would be of crucial importance to keep the LTP threshold  
68 (the minimal strength of synaptic inputs required for LTP induction) high at PP-CA3 synapses.

69 The CA3 region displays the highest expression of Kv1.2 transcripts in the rodent hippocampus  
70 (<http://mouse.brain-map.org/gene/show/16263>). Somatodendritic expression of Kv1.2 is polarized to  
71 distal apical dendrites, at which PP synaptic inputs arrive (Hyun et al. 2015). Consistent with the notion  
72 that D-type K<sup>+</sup> current (I<sub>K(D)</sub>) is activated by low voltage depolarization near the AP threshold (Storm,  
73 1988), distal dendritic Kv1.2 subunits regulate the threshold for dendritic Na<sup>+</sup> channel-dependent  
74 amplification of PP-evoked EPSPs (PP-EPSPs) (Hyun et al., 2015). Because PP synapses exhibit Hebbian  
75 plasticity, we hypothesized that downregulation of Kv1.2 and consequent enhancement of EPSP-to-spike  
76 (E-S) coupling would have a profound effect on the propensity of LTP induction at PP synapses. Here, we  
77 show that insufficiency of Kv1.2 in CA3-PCs, whether it is caused by activity-dependent downregulation  
78 or heterozygous knock-out of *Kcna2* (*Kcna2*+/‐), lowers the LTP threshold at PP-CA3 synapses. The  
79 non-specific lowering of LTP threshold at PP-CA3 synapses caused by genetic haploinsufficiency of  
80 *Kcna2* was well correlated with abnormal enlargement of CA3 ensembles during contextual fear  
81 discrimination task and impaired pattern separation of CA3 ensembles representing slightly different  
82 contexts.

83

84 **Results**

85 *The threshold for PP-LTP is lowered by haploinsufficiency of Kcna2*

86 Homosynaptic LTP of PP-EPSCs (referred to as PP-LTP) in the CA3-PCs of wildtype (WT) mice was  
87 induced under the current clamp mode by high frequency stimulation (HFS) of PP, which consists of 10  
88 bursts repeated every 10 s with each burst being comprised of 20 pulses at 100 Hz (PP-HFS, Figure 1Aa  
89 and Ab) (McMahon et al, 2002). We monitored PP-EPSCs of non-failure events before and after PP-HFS.

90 When PP-EPSC amplitudes were increased by more than 50% at 30 min after PP-HFS, it was regarded as  
91 induction of PP-LTP. To confirm stimulation of PP, effects of DCG-IV, a group II mGluR agonist, on

92 synaptic responses were tested at the end of experiments (Figure 1Ac) (Tsukamoto et al., 2003). The PP  
93 stimulation strength was quantified as the baseline amplitudes of PP-EPSC. The PP-LTP threshold was

94 determined by the minimal amplitude of baseline PP-EPSCs that induces PP-LTP. At weak stimulation

95 strength, which evoked the baseline EPSCs less than 12 pA, PP-HFS induced neither somatic firing nor  
96 PP-LTP (Figure 1Aa and open circles in Figure 1Ac;  $8.48 \pm 1.02$  to  $8.52 \pm 0.95$  pA,  $n = 5$ ,  $t = -0.137$ ,  $p =$

97 0.898, paired t-test). We repeated the same experiments with stronger stimulation intensities, which  
98 elicited baseline EPSCs amplitudes larger than 12 pA. The strong PP-HFS always drove the postsynaptic

99 CA3-PCs to fire APs (Figure 1Ab), and induced PP-LTP (black dots in Figure 1Ac;  $14.61 \pm 0.78$  to  $27.55$   
100  $\pm 2.72$  pA,  $n = 5$ ,  $t = -6.415$ ,  $p = 0.003$ , paired t-test), indicative of the Hebbian property of PP synapses.

101 The mean values for potentiation of EPSCs by the weak and strong PP-HFS are summarized in Figure

102 1Ad. After the CA3-PCs underwent PP-LTP, CA3-PCs responded to the same burst stimulation of PP (20  
103 pulse at 100 Hz) with the significantly higher number of somatic spikes (Figure 1 – figure supplement 1),

104 implying that PP-LTP may contribute to spike transfer from EC to CA3.

105 Because somatodendritic distribution of Kv1.2 is polarized to distal apical dendrites of CA3-PCs and  
106 downregulation of Kv1.2 in a CA3-PC enhances E-S coupling of PP synaptic inputs (Hyun et al., 2015),

107 we tested whether haploinsufficiency of Kv1.2 has any effects on the threshold for induction of PP-LTP.

108 Previously, it was confirmed that the D-type K<sup>+</sup> current ( $I_{K(D)}$ ) in CA3-PCs of *Kcna2*<sup>+/−</sup> mice is reduced to

109 c.a. 58% of that of their WT littermates (Hyun et al., 2015).  $I_{K(D)}$  is primarily mediated Kv1.1 and Kv1.2  
110 subunits in central neurons (Guan et al, 2006), and both subunits are equipped with molecular domains  
111 required for axonal targeting (Gu et al., 2003; Gu et al., 2006). Previous studies indicate that Kv1.1 and  
112 Kv1.2 subunits are expressed in axonal and dendritic compartments of CA3-PCs, respectively (Sheng et  
113 al. 1994; Grosse et al. 2000; Hyun et al. 2015; Rama et al. 2017), while the soma of CA3-PCs express  
114 both subunits (Rama et al. 2017). Axonal expression of Kv1.2, however, is still obscure in CA3-PCs.  
115 Moreover, PP expresses both Kv1.1 and Kv1.2 (Monaghan et al., 2001). Therefore, we cannot rule out  
116 possible contributions of axonal Kv1.2 expressed in PP and/or in CA3-PCs to the PP-LTP threshold. To  
117 test this possibility, we compared the *Kcnal*<sup>+/−</sup> CA3-PCs with *Kcna2*<sup>+/−</sup> CA3-PCs for the PP-LTP  
118 threshold. The excitability of *Kcnal*<sup>+/−</sup> CA3-PCs was enhanced similar to *Kcna2*<sup>+/−</sup>. The intrinsic  
119 excitability was evaluated by two parameters: the input conductance ( $G_{in}$ ) and first spike latency (AP  
120 latency) (See Materials and Methods) (Hyun et al. 2013). Both of  $G_{in}$  and AP latency were lower in  
121 *Kcnal*<sup>+/−</sup> and *Kcna2*<sup>+/−</sup> CA3-PCs than their WT littermates, but not different between *Kcnal*<sup>+/−</sup> and  
122 *Kcna2*<sup>+/−</sup> (Figure 1B).

123 The LTP threshold and degree of potentiation were measured for *Kcnal*<sup>+/−</sup> and *Kcna2*<sup>+/−</sup> CA3-PCs using  
124 the same methods as in the WT mice (Figure 1C). Potentiation of PP-EPSCs estimated at 30 min after  
125 strong PP-HFS was not different between WT, *Kcnal*<sup>+/−</sup> and *Kcna2*<sup>+/−</sup> (Figure 1Ad and Cb;  $F_{(2,16)} =$   
126 0.881,  $p = 0.436$ , one-way ANOVA; WT,  $187.0 \pm 10.6\%$ ,  $n = 5$ ; *Kcnal*<sup>+/−</sup>,  $177.4 \pm 16.8\%$ ,  $n = 5$ ;  
127 *Kcna2*<sup>+/−</sup>,  $203.1 \pm 14.0\%$ ). The PP-LTP level was measured as a normalized amplitude of EPSCs 30 min  
128 after HFS relative to the baseline. The plot for the PP-LTP levels as a function of PP stimulation  
129 intensities, quantified as the baseline amplitude of PP-EPSCs, shows that the threshold for the induction  
130 of PP-LTP is left-shifted in *Kcna2*<sup>+/−</sup> (10.2 pA), compared to those of *Kcnal*<sup>+/−</sup> (12.8 pA) and WT (12.4  
131 pA) (Figure 1Da), indicating that the expression level of Kv1.2 regulates the PP-LTP threshold. Whereas  
132 the LTP threshold was lower in *Kcna2*<sup>+/−</sup>, *Kcna2*<sup>+/−</sup> was not different from other genotypes in that PP-  
133 HFS always elicited somatic APs whenever it induced PP-LTP (Fig. 1Db).

134

135 *Activity-dependent downregulation of Kv1.2 lowers the threshold for PP-LTP*

136 Insufficiency of Kv1.2 can be induced not only by genetic mutation but also by repetitive stimulation of  
137 afferent MFs or the soma of a CA3-PC. The latter results in a decrease in input conductance and enhanced  
138 E-S coupling of PP synaptic inputs, collectively referred to as long-term potentiation of intrinsic  
139 excitability (LTP-IE) (Hyun et al., 2013; Hyun et al., 2015; Eom et al., 2019). Notably, LTP-IE enhances  
140 PP-EPSPs but not PP-EPSCs, supporting the notion that it is attributed to intrinsic excitability changes of  
141 dendrites (Hyun et al., 2015). Given that *Kcna2* insufficiency lowers the threshold for PP-LTP, we tested  
142 whether LTP-IE induced by 10 Hz somatic stimulation also lowers the PP-LTP threshold (referred to as  
143 metaplasticity). Because *Kcna2*<sup>+-</sup> as well as *Kcna2*<sup>-/-</sup> CA3-PCs lack LTP-IE (Hyun et al., 2015), and  
144 *Kcna2*<sup>-/-</sup> mice die within the 3<sup>rd</sup> postnatal week (Brew et al., 2007), we examined the effects of LTP-IE on  
145 the PP-LTP threshold in WT, *Kcnal*<sup>+-</sup> and *Kcna2*<sup>+-</sup> CA3-PCs to confirm involvement of Kv1.2 in the  
146 metaplasticity. To this end, we adjusted the PP stimulation intensity which evokes EPSCs lower than 10  
147 pA. At this intensity PP-HFS by itself does not induce PP-LTP in naïve CA3-PCs of the all three  
148 genotypes. Since PP-EPSPs are influenced by intrinsic excitability, EPSCs were monitored, and EPSPs  
149 were measured at the start and the end of EPSC monitoring. Somatic stimulation at 10 Hz did not alter  
150 PP-EPSCs (blue arrow in Figure 2Ac) in all three genotypes (Figure 2Ba), but it enhanced PP-EPSPs  
151 measured 6 min after priming in WT and *Kcnal*<sup>+-</sup>, but not in *Kcna2*<sup>+-</sup> (Figure 2Bb). To prevent  
152 washout of intracellular milieu necessary to induce LTP, the PP-HFS was delivered within 20 min after  
153 the patch break-in (Malinow and Tsien, 1990). Distinct from the naïve CA3-PCs (Figure 1Aa), subsequent  
154 weak PP-HFS (PP-EPSC < 10 pA) readily elicited AP firing in the WT and *Kcnal*<sup>+-</sup> CA3-PCs which  
155 underwent 10 Hz somatic stimulation (Figure 2Aa), but such E-S potentiation did not occur in *Kcna2*<sup>+-</sup>  
156 CA3-PCs (Figure 2Ab). Accordingly, weak PP-HFS induced PP-LTP in WT and *Kcnal*<sup>+-</sup>, but not in  
157 *Kcna2*<sup>+-</sup> CA3-PCs (Figure 2Ac) ( $F_{(2,16)} = 22.510$ ,  $p < 0.001$ ; WT vs. *Kcnal*<sup>+-</sup>,  $p = 1.00$ ; For WT or  
158 *Kcnal*<sup>+-</sup> vs. *Kcna2*<sup>+-</sup>,  $p < 0.001$ ; one-way ANOVA, Bonferroni post-hoc test). Figure 2C summarizes

159 the dependence of PP-LTP level on the baseline EPSC amplitudes. This plot demonstrates that 10 Hz  
160 somatic stimulation lowers the threshold for PP-LTP induction in WT and *Kcnal*<sup>+/−</sup> mice. In contrast, the  
161 threshold for PP-LTP in naïve *Kcna2*<sup>+/−</sup> CA3-PCs was already lower than other genotypes, and not  
162 affected by 10 Hz somatic stimulation. These results suggest that downregulation of Kv1.2 mediates both  
163 of LTP-IE and metaplasticity induced by 10 Hz somatic stimulation, **but we cannot rule out a possibility**  
164 **that the 10 Hz somatic stimulation may lower the PP-LTP threshold by cellular mechanisms other than**  
165 **downregulation of Kv1.2**. The effect of 10 Hz somatic APs on the LTP threshold was even larger than  
166 *Kcna2* haploinsufficiency, reflecting our previous observations that  $I_D$  in CA3-PCs was more reduced by  
167 10 Hz somatic APs (to c.a. 30% of control; Hyun et al., 2013) than by *Kcna2*<sup>+/−</sup> (to c.a. 58%; Hyun et al.,  
168 2015).

169 It should be noted that 10 Hz somatic stimulation in Figure 2 was used as a surrogate of high frequency  
170 MF stimulation, and that MF inputs are privileged for the induction of LTP-IE (Eom et al., 2019). Indeed,  
171 we confirmed that repetitive stimulation of afferent MFs (20 Hz, 2 s) induces metaplasticity at PP  
172 synapses similar to 10 Hz somatic APs (Figure 2-figure supplement 1). Taken together, above results  
173 indicate that insufficiency of Kv1.2, whether it is induced by genetic mutation or by 10 Hz somatic APs,  
174 facilitates induction of PP-LTP. **Assuming that the probability that PP inputs alone induce Hebbian**  
175 **plasticity is fairly low**, our results together with McMahon et al (2002) imply that induction of PP-LTP  
176 may be allowed in the PCs receiving concurrent MF inputs and in PCs primed by previous strong MF  
177 inputs, both of which anyway depend on MF inputs.

178

179 *Kv1.2*<sup>+/−</sup> mice, but not *Kv1.1*<sup>+/−</sup> mice, are impaired in rapid contextual discrimination  
180 Given that PP-LTP enhances spike transfer from EC to CA3, lowered threshold for PP-LTP would  
181 potentially increase the size and overlap of CA3 ensembles. Both MF-induced LTP-IE and genetic *Kcna2*  
182 insufficiency have potential to exert adverse influence on pattern separation. In WT mice the PP-LTP

183 threshold is lowered selectively in a CA3-PC primed by MF inputs, and thus only limited number of PCs  
184 would be primed owing to the sparseness of MF innervation and firings of dentate GCs. In contrast, PP-  
185 LTP threshold in *Kcna2+/-* mice is lowered not in a subset of CA3-PCs but over the whole CA3-PC  
186 population. Therefore, Kv1.2 insufficiency may increase the chance for MF input-independent induction  
187 of PP-LTP, and promiscuous encoding at PP synapses would ensue. We hypothesized that non-specific  
188 lowering of PP-LTP threshold caused by haploinsufficiency of Kv1.2 may result in impairment in a  
189 pattern-separation task, in which mice must learn association of different behaviors with two slightly  
190 different contexts.

191 Although *Kcna2-/-* mice had a reduced life span (3 weeks; Brew et al., 2007), we found that their  
192 heterozygous littermates (*Kcna2+/-*) had a normal life span. There were no changes in activity, feeding,  
193 reproductive, or parental behaviors in *Kcna1+/-* (n = 10) and *Kcna2+/-* (n = 9) mice, compared to WT (n  
194 = 11) mice. To examine behavioral pattern separation, the three genotype mice (WT littermates, *Kcna1+/-*  
195 and *Kcna2+/-*) were subject to the contextual fear discrimination task (McHugh et al., 2007; Kim et al.,  
196 2020). This task is comprised of three phases: contextual acquisition phase (day 1-3), generalization test  
197 phase (day 4-5), and the discrimination training phase (day 6-14) (Figure 3A). In the first phase, all  
198 genotype mice were given by a foot shock 180 s after being placed in context A (conditioned context) for  
199 consecutive 3 days. In the 2nd phase (day 4 and 5), the freezing behavior of such conditioned mice was  
200 assessed without a foot shock in context A and context B (safe context). The context B had the same  
201 sound noise level, metal grid floor, sidewalls and roof as in context A, but differed from context A in  
202 having a unique odor (1% acetic acid), dimmer light (50%) and a slanted grid floor by 15° angle (Figure  
203 3-figure supplement 1). On the subsequent 9 days (day 6 -14, phase 3), mice daily visited both contexts  
204 with a foot shock only in context A (Figure 3A). The kinetics of freezing in context A was not different  
205 among the three genotypes (Figure 3Ba, Table 1 for statistics). All genotypes showed similar levels of  
206 freezing behavior in context B as in contexts A suggesting that all genotypes displayed equivalent  
207 generalization on day 4 and 5 (Figure 3Bb, Table 1). WT and *Kcna1+/-* mice began to distinguish the two

208 contexts on the 2nd day of phase 3 (day 7), as shown by the increase in the discrimination ratio [freezing  
209 in A/(A+B)] (Figure 3Bc). *Kcna2<sup>+/−</sup>* mice, however, exhibited significant delay in the acquisition of the  
210 discrimination (Figure 3Bc, Table 1; WT vs. *Kcna1<sup>+/−</sup>*,  $p = 1.00$ ; For WT or *Kcna1<sup>+/−</sup>* vs. *Kcna2<sup>+/−</sup>*,  $p <$   
211 0.001). On day 9, the *Kcna2<sup>+/−</sup>* mice exhibited elevated freezing level not only in A but also in B,  
212 whereas WT and *Kcna1<sup>+/−</sup>* mice showed significantly lower freezing in context B (Figure 3Bd, Table 1;  
213 WT vs. *Kcna1<sup>+/−</sup>*,  $p = 0.135$ ; For WT or *Kcna1<sup>+/−</sup>* vs. *Kcna2<sup>+/−</sup>*,  $p < 0.001$ ; 2-way ANOVA, Bonferroni  
214 post-hoc test). On the last day of the discrimination training phase (day 14), all mice discriminated the  
215 two contexts to a similar degree (Figure 3Be), suggesting that normal expression of Kv1.2 channel  
216 subunit is required for rapid pattern separation between slightly different contexts.

217 To rule out possible impairment in basic hippocampal contextual learning in *Kcna2<sup>+/−</sup>* mice, WT and  
218 *Kcna2<sup>+/−</sup>* mice were assessed for fear acquisition and retrieval of contextual freezing behavior based on  
219 Cravens et al. (2006). We examined the context specificity for fear conditioning by assessment of freezing  
220 behavior in two distinct contexts (A and C) 24 hours after pairing context A with a shock (Figure 3Ca).  
221 For context A, both genotype mice acquired and retained the fear conditioning to a similar degree after a  
222 single context-footshock pairing. The distinct context (context C), however, caused significantly lower  
223 freezing levels than the conditioned context in both genotype mice (Figure 3Cb, Table 1).

224 Next, we examined the capability of WT and *Kcna2<sup>+/−</sup>* mice for pattern completion-based memory  
225 retrieval using the pre-exposure-mediated contextual fear conditioning (PECFC) paradigm (Fanselow,  
226 1990; Nakashiba et al., 2008) (Figure 3Da). The PECFC task requires retrieval of contextual memories  
227 from a very brief exposure to previously experienced context, which is impaired by disruption of synaptic  
228 output from CA3-PCs (Nakashiba et al. 2008). We found no difference between WT and *Kcna2<sup>+/−</sup>* mice  
229 in freezing response under the PECFC paradigm (Figure 3Db) (genotype,  $F_{(1,46)} = 0.286$ ,  $p = 0.596$ ;  
230 context,  $F_{(1,46)} = 77.173$ ,  $p < 0.001$ ; shock,  $F_{(1,46)} = 77.173$ ,  $p < 0.001$ , 3-way ANOVA), implying that the  
231 *Kcna2<sup>+/−</sup>* mice are normal in CA3-dependent pattern completion-based retrieval. Finally, we assessed  
232 basal anxiety level using an elevated plus maze (EPM). Exemplar trials of WT, *Kcna2<sup>+/−</sup>* mice on the

233 EPM (tracking for 5 min; Figure 3Ea). The total distances that mice explored in EPM was not  
234 significantly different between WT and *Kcna2*+/− mice (Figure 3Ea and 3Eb). The mean values for time  
235 spent in the closed and open arms were not significantly different between two genotype mice (Figure  
236 3Ec).

237

238 *Table 1, Statistical test for experiments shown in Figure 3*

Experiment	Statistical test	1 <sup>st</sup> Variable (Genotype)	2 <sup>nd</sup> Variable (Context / Time / Day)	Interaction (Genotype x Time/Context/Day)
Figure 3Ba	RM- ANOVA	$F_{(2,27)} = 0.89$ $p = 0.422$	Time, $F_{(9,243)} = 4.248$ , $p < 0.001$ .	Geno x Time, $F_{(18,243)} = 1.117$ $p = 0.336$
Figure 3Bb (Day 4-5)	Two-way ANOVA	$F_{(2,54)} = 0.610$ $p = 0.547$	Context, $F_{(1,54)} = 0.110$ $p = 0.741$	Geno x Context, $F_{(2,27)} = 0.504$ $p = 0.607$
Figure 3Bc (Discrimination ratio)	RM- ANOVA Bonferroni post-hoc test	$F_{(2,27)} = 14.243$ $p < 0.001$	Day, $F_{(8,216)} = 17.487$ $p < 0.001$	Geno x Day, $F_{(16,216)} = 4.216$ $p < 0.001$
Figure 3Bd (Day 9)	Two-way ANOVA,	$F_{(2,54)} = 14.240$ $p < 0.001$	Context, $F_{(1,54)} = 60.777$ $p < 0.001$	Geno x Context, $F_{(2,54)} = 15.775$ $p < 0.001$
Figure 3Be (Day 14)	two-way ANOVA	$F_{(2,54)} = 0.292$ $p = 0.748$	Context, $F_{(2,54)} = 288.49$ $p < 0.001$	Geno x Context, $F_{(2,54)} = 0.740$ $p = 0.482$
Figure 3Cb	two-way ANOVA	$F_{(1,19)} = 0.137$ $p = 0.716$	Context, $F_{(1,19)} = 133.125$ $p < 0.001$	Geno x Context. $F_{(1,19)} = 0.007$ $p = 0.933$

239

240 *Kv1.2, but not Kv1.1, is crucial for pattern separation in the CA3*  
241 Above results indicate that *Kcna2+/-* mice are impaired in rapid discrimination of the contexts A and B  
242 tested in Figure 3A. We hypothesized that the impaired contextual discrimination in *Kcna2+/-* mice may  
243 be caused by larger overlap between neuronal ensembles representing the two slightly different contexts  
244 in the hippocampal CA3 region. To test this hypothesis, we examined CA3 cell ensembles activated upon  
245 memory retrieval of contexts A and B for the three genotype mice. An ensemble of active cells in each  
246 context was detected using catFISH (cellular analysis of temporal activity by fluorescence *in situ*  
247 hybridization) of immediate early genes (IEG) transcripts, Arc and Homer1a (H1a), which are expressed  
248 after patterned neuronal activities associated with synaptic plasticity (Guzowski et al., 2005). Designing  
249 Arc/H1a RNA probes targeting different locations from transcriptional initiation sites [22 bases for Arc  
250 and 51.6 kilobases (exon 5) for H1a] allows us to detect intra-nuclear foci (INF) of Arc/H1a transcripts at  
251 different timing from cellular activities (Vazdarjanova et al., 2002; Vazdarjanova and Guzowski, 2004).  
252 Typically, INF of Arc and H1a transcripts are expressed 5 and 30 min after cellular activity, respectively  
253 (Vazdarjanova et al., 2002). **We confirmed the previous notion that most CA3-PCs are devoid of INF of**  
254 **H1a and Arc transcripts detected by catFISH 5 min or 30 min after an animal was exposed to a novel**  
255 **context, respectively (Figure 4 - Supplement 1).**

256 As a control, we estimated an overlap between CA3 ensembles activated upon acquisition and retrieval of  
257 context A. To this end, WT and *Kcna2+/-* mice were handled daily for a week before the experiment to  
258 habituate to the general handling procedure. Little expression of c-fos was confirmed in the CA3 region  
259 of the handled mice compared to the mice that visited context A (Figure 4 - Supplement 2). The handled  
260 WT and *Kcna2+/-* mice visited the context A twice for 4 min with a 20 min interval, during which mice  
261 were kept in their home cage (Figure 4Aa). In the first visit, the mice received a footshock 3 min after  
262 being placed. After the second visit, mice were sacrificed, and their hippocampi underwent the Arc/H1a  
263 catFISH procedure. In the exemplar catFISH images of WT and *Kcna2+/-* CA3 cells (Figure 4Ab-Ac),  
264 H1a (green) and Arc (red) INF represent transcripts expressed upon 1<sup>st</sup> and 2<sup>nd</sup> visits, respectively. **The**

265 fractions of H1a (+) and Arc (+) CA3 cells were not significantly different between WT and *Kcna2*<sup>+/−</sup> mice, suggesting that the increased distal dendritic excitability in *Kcna2*<sup>+/−</sup> CA3-PCs has little effect on 266 the ensemble size activated by a novel context (For WT, H1a:  $7.34 \pm 0.49\%$ , Arc:  $7.21 \pm 0.37\%$ , n = 12 267 slices from 4 mice; For *Kcna2*<sup>+/−</sup>, H1a:  $6.66 \pm 0.83\%$ , Arc:  $6.61 \pm 0.35\%$ , n = 6 slices from 3 mice; 589  $\pm$  268 92 cells per a slice; genotype,  $F_{(1,36)} = 0.419$ , p = 0.522; context,  $F_{(1,36)} = 2.797$ , p = 0.104; genotype  $\times$  269 context,  $F_{(1,36)} = 0.154$ , p = 0.697, two-way ANOVA; Figure 4Aa). The overlap between H1a (+) and Arc 270 (+) ensembles was  $3.70 \pm 0.32\%$  for WT and  $3.00 \pm 0.34\%$  for *Kcna2*<sup>+/−</sup> (cells indicated by yellow 271 arrowhead in Figure 4Aa;  $t = 1.363$ , p = 0.192, independent t-test). The conditional probability for re- 272 activation of ensemble cells of the 1<sup>st</sup> visit (A<sub>1</sub>) among ensemble cells of the 2<sup>nd</sup> visit (A<sub>2</sub>) [ $P(A_1|A_2)$ ] was 273 not different between the two genotypes either (WT,  $51.21 \pm 3.47\%$ ; *Kcna2*<sup>+/−</sup>,  $45.9 \pm 3.11\%$ ). 274

275 Next, we estimated the proportion of ensemble cells re-activated upon retrieval of contexts A and B in the 276 same mice. After handling for a week, mice were subject to a contextual fear discrimination (CFD) 277 protocol as shown in Figure 4Ba. Mice daily visited twice each of contexts A and B with receiving a 278 footshock always in context A and never in B. The configurations of context A and B were the same as in 279 Figure 3A (see Materials and Methods). On day 3, WT (n = 4) and *Kcna1*<sup>+/−</sup> (n = 4) mice began to 280 distinguish the two contexts, whereas *Kcna2*<sup>+/−</sup> (n = 4) mice did not as shown by the difference in the 281 freezing ratio (Figure 4Bb-Bc; Table 2 for statistics). On day 4, each genotype mice were divided into two 282 subgroups. One subgroup was exposed to context A for 4 min with no footshock, returned to its home 283 cage for 20 min, and then exposed to context B for 4 min (A/B). The other subgroup was subject to the 284 same protocol except switching the order of A and B (B/A). On day 4, *Kcna2*<sup>+/−</sup> mice still did not 285 distinguish the two contexts, in contrast to WT and *Kcna1*<sup>+/−</sup> (Figure 4Bb-Bc, Table 2). After visiting the 286 second context, the mice were killed, and their hippocampi were examined for expression of Arc/H1a 287 transcripts. Figure 4C shows exemplar Arc/H1a catFISH images of CA3 regions of the three genotype 288 mice. For parameters of ensemble size and overlap, no difference was found between the two subgroups 289 (A/B and B/A), and thus results are presented with respect to the context in Figure 4D. The fraction of

290 CA3 cells activated in context A and that in context B were about 1.5 times larger in *Kcna2*<sup>+-</sup> compared  
291 to WT ( $p < 0.001$ ), and those in *Kcna1*<sup>+-</sup> mice were marginally larger than WT ( $p = 0.053$ ) (Table 2 and  
292 3, Figure 4Da). The fraction of CA3 cells active in both of contexts A and B [denoted as  $P(A \cap B)$ ] was not  
293 different between WT and *Kcna1*<sup>+-</sup> mice, but it was about three times higher in *Kcna2*<sup>+-</sup> than other  
294 genotypes (Table 2 and 3). To test whether larger ensemble size in *Kcna2*<sup>+-</sup> is responsible for larger  
295 overlap, we calculated the conditional probability for reactivation of the A ensemble cells among the B  
296 ensemble cells [ $P(A|B)$ ] as an overlap index. The overlap index for *Kcna2*<sup>+-</sup> was significantly higher  
297 than those of *Kcna1*<sup>+-</sup> and WT (Table 2, Figure 4Db), and rather similar to the value for WT and  
298 *Kcna2*<sup>+-</sup> mice which visited context A twice [denoted as WT(AA) and *Kcna2*<sup>+-</sup>(AA), respectively]  
299 [WT(AA) vs. *Kcna2*<sup>+-</sup>(AB),  $p = 0.188$ ; *Kcna2*<sup>+-</sup>(AA) vs. *Kcna2*<sup>+-</sup>(AB),  $p = 1.00$ ; one-way ANOVA,  
300 Bonferroni post-hoc test; Figure 4Db and Table 2]. The cumulative distribution of the overlap index  
301 shows a significant shift of the curve to the right in *Kcna2*<sup>+-</sup>(AA), *Kcna2*<sup>+-</sup>(AB) and WT(AA),  
302 compared to WT(AB) and *Kcna1*<sup>+-</sup> [WT(AA) vs. WT(AB),  $Z = 2.4$ ,  $p < 0.001$ ; WT(AA) vs. *Kcna1*<sup>+-</sup>,  
303  $Z = 2.4$ ,  $p < 0.001$ ; WT(AA) vs. *Kcna2*<sup>+-</sup>(AB),  $Z = 1.255$ ,  $p = 0.083$ ; WT(AA) vs. *Kcna2*<sup>+-</sup>(AA),  $Z =$   
304  $0.667$ ,  $p = 0.766$ , Kolmogorov-Smirnov test, Figure 4Dc), indicating larger overlap between A and B  
305 ensembles in *Kcna2*<sup>+-</sup>. If the overlap index of *Kv1.2*<sup>+-</sup> were the same as that of WT [WT(AB),  $23.6 \pm$   
306  $1.4\%$ ], the expected overlap between A and B ensembles should be 2.6% considering that  $P(B)$  in  
307 *Kcna2*<sup>+-</sup> was  $11.2 \pm 0.7\%$ . The measured value for overlap in *Kcna2*<sup>+-</sup> was, however,  $4.7 \pm 0.4\%$ ,  
308 which is 1.8 times larger than the value expected under the same overlap index as WT. Therefore, larger  
309 overlap in *Kcna2*<sup>+-</sup> cannot be explained by larger ensemble size alone, suggesting involvement of  
310 additional factors, [probably less dependence of PP-LTP induction on concurrent MF inputs](#) (see  
311 Discussion). Taken together with the results of Figure 3, pattern separation of CA3 ensembles are well  
312 correlated with the performance of CFD task across the three genotypes, implying that impaired pattern  
313 separation of CA3 ensembles may underlie the impairment of the rapid acquisition of contextual  
314 discrimination in *Kcna2*<sup>+-</sup> mice.

315

316 *Table 2, Statistical test for experiments shown in Figure 4*

Experiment	Statistical test	Genotype	Context	Genotype x Context	WT vs. <i>Kcnal</i> +/-	WT vs. <i>Kcna2</i> +/-	<i>Kcna2</i> +/- vs. <i>Kcnal</i> +/-
Figure 4Bb-Bc Day 3	two-way ANOVA, Bonferroni post-hoc test	$F_{(2,18)} = 20.817$ $p < 0.001$	$F_{(1,18)} = 69.689$ $p < 0.001$	$F_{(2,18)} = 13.91$ $p < 0.001$	$p = 0.652$	$p < 0.001$	$p < 0.001$
Figure 4Bb-Bc Day 4		$F_{(2,18)} = 31.00$ $p < 0.001$	$F_{(1,18)} = 86.22$ $p < 0.001$	$F_{(2,18)} = 24.14$ $p < 0.001$	$p = 0.292$	$p < 0.001$	$p < 0.001$
Figure 4Da (Ensemble size)		$F_{(2,96)} = 28.87$ $p < 0.001$	$F_{(1,96)} = 0.27$ $p = 0.603$	$F_{(2,96)} = 0.443$ $p = 0.643$	$p = 0.053$	$p < 0.001$	$p < 0.001$
Figure 4Da (Ensemble overlap)	one-way ANOVA	$F_{(2,48)} = 48.99$ $p < 0.001$	irrelevant	irrelevant	$p = 1.00$	$p < 0.001$	$p < 0.001$
Figure 4Db P(A B)		$F_{(4,65)} = 33.50$ $p < 0.001$	irrelevant	irrelevant	$p = 1.00$	$p < 0.001$	$p = 0.119$

317

318 *Table 3, Mean values for size and overlap of neuronal ensembles activated by context A and B (mean  $\pm$  SEM)*

Genotype (n=4 mice each)	P(A) (%)	P(B) (%)	P(A $\cap$ B) (%)	P(A)P(B) (%)	P(A B) (%)
WT	$7.00 \pm 0.34$	$6.83 \pm 0.27$	$1.56 \pm 0.10$	$0.48 \pm 0.04$	$23.2 \pm 1.53$
<i>Kcnal</i> +/-	$7.15 \pm 0.44$	$9.24 \pm 0.61$	$1.69 \pm 0.13$	$0.67 \pm 0.06$	$19.3 \pm 1.95$
<i>Kcna2</i> +/-	$10.6 \pm 0.66$	$11.2 \pm 0.65$	$4.69 \pm 0.41$	$1.21 \pm 0.12$	$42.6 \pm 3.15$

320

321 *CA3 ensembles of WT and *Kcna2*+- mice differently evolve over training days*

322 To further confirm the correlation between contextual discrimination and the overlap of CA3 ensembles,  
323 we examined the CA3 ensemble size and their overlap before WT and *Kcna2*+- mice discriminate the  
324 contexts A and B. To this end, mice were subject to the same protocol of Figure 4Ba, but were killed for  
325 catFISH after one paired visits (session 1) on day 1 (D1) or after the session 1 on day 2 (D2) (Figure 5A).  
326 Figure 5B shows exemplar Arc/H1a catFISH images of CA3 regions of WT (upper row) and *Kcna2*+-  
327 (lower row) mice for D1 (Ba and Bb), D2 (Bc and Bd). For comparison, catFISH data on retrieval of  
328 contexts on day 4 (D4) were adopted from Figure 4.

329 Because the ensemble sizes measured from H1a and Arc in the same slice were not statistically different  
330 (probe,  $F_{(1,136)} = 0.893$ ,  $p = 0.436$ ; probe  $\times$  genotype,  $F_{(1, 136)} = 0.201$ ,  $p = 0.655$ , probe  $\times$  day,  $F_{(2,136)} =$   
331  $0.105$ ,  $p = 0.900$ , probe  $\times$  genotype  $\times$  day,  $F_{(2,136)} = 0.380$ ,  $p = 0.685$ ; three-way ANOVA, Table 4), the  
332 ensemble size on each day was measured as the averaged number of H1a(+) plus Arc(+) cells on each  
333 slice. The CA3 ensemble size increased over training days in both genotypes, but the expansion of CA3  
334 ensemble size in *Kcna2*+- (red) was more pronounced compared to WT (gray) (Fig. 5Ca; genotype,  $F_{(1,68)}$   
335  $= 36.528$ ,  $p < 0.001$ ; day,  $F_{(2,68)} = 51.758$ ,  $p < 0.001$ ; genotype  $\times$  day,  $F_{(2, 68)} = 12.303$ ,  $p < 0.001$ ; WT vs  
336 *Kcna2*+- for day 1:  $p = 0.635$ , day 2:  $p = 0.008$ , day 4:  $p < 0.001$ ; two-way ANOVA and simple effect  
337 analysis). Whereas in WT mice the fraction of CA3 cells active in both of contexts A and B [denoted as  
338  $P(A \cap B)$ ] decreased over training days, it rather increased in *Kcna2*+- mice (genotype,  $F_{(1,68)} = 38.687$ ,  $p$   
339  $< 0.001$ ; day,  $F_{(2, 68)} = 3.159$ ;  $p = 0.024$ , genotype  $\times$  day,  $F_{(2,68)} = 20.287$ ,  $p < 0.001$ ; two-way ANOVA;  
340 Figure 5Cb). The increase of  $P(A \cap B)$  in *Kcna2*+- mice can be attributed to the increase in the ensemble  
341 size, because the overlap index [ $P(A|B)$ ] remained static over days (Figure 5Cc). In contrast,  $P(A|B)$  in  
342 WT mice decreased over days (gene,  $F_{(1,68)} = 10.40$ ,  $p = 0.002$ ; day,  $F_{(2, 68)} = 14.719$ ;  $p < 0.001$ , genotype  $\times$   
343 day,  $F_{(2,68)} = 12.383$ ,  $p < 0.001$ ; two-way ANOVA). Figure 5Cd shows the changes in the cumulative  
344 distribution of the overlap index over training days for two genotypes. On day 1, the distribution in  
345 *Kcna2*+- mice was not different from that in WT ( $Z = 1.118$ ,  $p = 0.164$ ; Kolmogorov–Smirnov test). The

346 distributions in WT mice shifted to the left over training days ( $\chi^2 = 25.983$ ,  $p < 0.001$ ; Kruskal-Wallis  
347 test) (D1 vs. D2:  $Z = -2.756$ ,  $p = 0.006$ ; D2 vs. D4:  $Z = -3.708$ ,  $p < 0.001$ ; Kolmogorov-Smirnov test),  
348 whereas the distribution of *Kcna2*<sup>+/−</sup> mice remained unaltered ( $\chi^2 = 0.223$ ,  $p = 0.895$ ; Kruskal-Wallis  
349 test). In summary, the size and overlap of A and B ensembles activated by the first visit were not different  
350 between WT and *Kcna2*<sup>+/−</sup> mice. In WT mice, the A and B ensembles evolved into more distinct ones  
351 over training days. In contrast, the same training induced little pattern separation in CA3 ensembles of  
352 *Kcna2*<sup>+/−</sup> mice with the ensemble size more enlarged compared to WT.

353

354 **Table 4**, Fractions of *H1a*(+) and *Arc*(+) cells in CA3 (mean ± SEM)

Day	Genotype	H1a (%)	Arc (%)	P(A∩B) (%)	P(A B) (%)
Day 1 (n=10 from 3 mice)	Wildtype	5.11 ± 0.28	5.07 ± 0.34	2.45 ± 0.14	49.3 ± 2.98
	<i>Kcna2</i> <sup>+/−</sup>	5.20 ± 0.31	5.55 ± 0.31	2.37 ± 0.12	43.5 ± 2.33
Day 2 (n=7 from 3 mice)	Wildtype	5.13 ± 0.35	5.80 ± 0.26	2.13 ± 0.11	36.9 ± 1.42
	<i>Kcna2</i> <sup>+/−</sup>	7.17 ± 0.34	7.43 ± 0.44	3.35 ± 0.30	45.2 ± 3.27
Day 4 (n=16 from 4 mice)	Wildtype	7.04 ± 0.30	6.57 ± 0.32	1.56 ± 0.10	23.2 ± 1.53
	<i>Kcna2</i> <sup>+/−</sup>	10.61 ± 0.66	11.19 ± 0.64	4.69 ± 0.41	42.6 ± 3.15

355

356 *Generation of CA3 region-specific hetero-knockout of Kcna2*

357 Above results indicate that haploinsufficiency of *Kcna2* lowers the threshold for PP-LTP and impairs  
358 behavioral pattern separation (Figure 1 and 3). However, Kv1.2 subunits are expressed not only in CA3-  
359 PCs but also in other brain regions (Sheng et al., 1994; Grosse et al., 2000). To confirm that insufficiency  
360 of Kv1.2 expressed in CA3-PCs is responsible for the impairment in behavioral pattern separation, we  
361 created CA3 region-specific *Kcna2*<sup>+/−</sup> (CA3-*Kcna2*<sup>+/−</sup>) mice using Cre-lox recombination techniques  
362 (see Materials and Methods). We labelled *Kcna2* transcripts in the hippocampus of each genotype mice  
363 (postnatal week 16) using an RNAscope probe (Wang et al., 2012), and counted the number of mRNA  
364 dots in the layer 2/3 of medial entorhinal cortex (MEC) and three hippocampal regions [indicated as a  
365 (MEC), b (DG), c (CA3) and d (CA1) in Figure 6A-B]. The *Kcna2* mRNA expression level was  
366 quantified as the ratio of the number of *Kcna2* mRNA particles to the number of nuclei in the region of  
367 interest (ROI) drawn on each region. The *Kcna2* mRNA in the CA3 of CA3-*Kcna2*<sup>+/−</sup> mice (n = 5, Figure  
368 6Bc) was lowered to c.a. 60% of that in the CA3 of *floxed-Kcna2* mice (*f-Kcna2*) (n = 5, Figure 6Ac),  
369 whereas the *Kcna2* mRNA in the MEC, DG and CA1 were not different between genotypes (Figure 6A-  
370 C; MEC, U = 7.00, p = 0.251; DG, U = 12.00, p = 0.917; CA3, U = 0.00, p = 0.009; CA1, U = 8.00, p =  
371 0.347; Mann-Whitney U test). As a parameter for the expression level of Kv1.2, the peak amplitudes of  
372 D-type K<sup>+</sup> current (I<sub>K(D)</sub>) were measured from CA3-PCs in *f-Kcna2* (Figure 6Da, left) and CA3-*Kcna2*<sup>+/−</sup>  
373 (right) mice. We regarded the slowly inactivating K<sup>+</sup> outward current sensitive to 30 μM 4-aminopyridine  
374 (4-AP) as I<sub>K(D)</sub> (Storm, 1988; Hyun et al. 2013, 2015). The peak amplitudes of I<sub>K(D)</sub> elicited by  
375 depolarizing steps from -70 mV were significantly lower in CA3-PCs of CA3-*Kcna2*<sup>+/−</sup> mice than those  
376 of *f-Kcna2* mice (Figure 6D; -40 mV, black, t = 2.282, p = 0.046; -30 mV, blue, t = 2.698, p = 0.022; -20  
377 mV, red, t = 3.885, p = 0.003; independent t-test).

378 To test if there is any alteration in the afferent inputs to CA3-PCs of CA3-*Kcna2*<sup>+/−</sup> mice, we assessed  
379 short-term synaptic plasticity of MF and PP-EPSCs, because reduction of axonal Kv1 channels is  
380 expected to broaden the axonal APs and increase in synaptic release probability to lower paired pulse ratio

381 of EPSCs (Kole et al., 2007). Previously, it was noted that PP expresses both of Kv1.1 and Kv1.2, while  
382 MFs express primarily Kv1.1 (Monaghan et al. 2001). Consistently, short-term facilitation (STF) of PP-  
383 EPSCs evoked by 5 pulses at 20 or 50 Hz was reduced in *Kcnal*<sup>+/−</sup> and *Kcna2*<sup>+/−</sup> mice, but not *CA3*-  
384 *Kcna2*<sup>+/−</sup> mice. For MF-EPSCs evoked by 3 pulses at 50 Hz, STF was reduced only in *Kcnal*<sup>+/−</sup> mice  
385 (Table 5, Figure 6-figure supplement 1).

386

387 *Table 5, Short term plasticity at PP and MF synapses of CA3-PCs*

Stimulation	Statistical test	Genotype	Genotype x Stim.	<i>f</i> - <i>Kcna2</i> <sup>+/−</sup> vs. <i>Kcna2</i> <sup>+/−</sup>	<i>f</i> - <i>Kcna2</i> <sup>+/−</sup> vs. <i>Kcnal</i> <sup>+/−</sup>	<i>f</i> - <i>Kcna2</i> <sup>+/−</sup> vs. CA3- <i>Kcna2</i> <sup>+/−</sup>	<i>Kcna2</i> <sup>+/−</sup> vs. <i>Kcnal</i> <sup>+/−</sup>
PP, 5 pulses at 20 Hz	RM- ANOVA, Bonferroni post-hoc test.	$F_{(3,16)} = 10.808$ $p < 0.001$	$F_{(3,16)} = 7.423$ $p < 0.001$	$p = 0.014$	$p = 0.006$	$p = 1.00$	$p = 1.00$
PP, 5 pulses at 50 Hz		$F_{(3,16)} = 3.471,$ $p < 0.001$	$F_{(3,16)} = 8.373$ $p < 0.001$	$p = 0.015$	$p = 0.009$	$p = 1.00$	$p = 1.00$
MF, 3 pulses at 50 Hz		$F_{(3,16)} = 6.532$ $p = 0.004$	$F_{(3,16)} = 6.663$ $p = 0.004$	$p = 1.00$	$p = 0.012$	$p = 1.00$	$p = 0.01$

388

389 Next, we examined MF-induced LTP-IE of CA3-PCs in CA3-*Kcna2*<sup>+/−</sup> mice and their WT littermates (*f*-  
390 *Kcna2*) in the third postnatal week because Cre/loxP recombination is detectable on postnatal day 14 in  
391 the CA3 region (Nakazawa et al., 2002). In addition, we previously reported that the degree of LTP-IE is  
392 not different between the third and 12th postnatal week mice (Eom et al., 2019). LTP-IE was assessed by  
393 input conductance ( $G_{in}$ ) and first spike latency, which were measured as in Figure 1B. In *f*-*Kcna2* CA3-  
394 PCs, 20 Hz MF stimulation reduced  $G_{in}$  ( $75.3 \pm 2.7\%$ ,  $n=6$ ,  $t = 7.714$ ,  $p = 0.001$ , paired t-test, Figure 7Aa-  
395 Ab) and first spike latency ( $t = 3.855$ ,  $p = 0.012$ ,  $n = 6$ , paired t-test, Figure 7Ac). In contrast, MF-induced  
396 LTP-IE was completely abolished at CA3-PCs of CA3-*Kcna2*<sup>+/−</sup> (Figure 7A;  $G_{in}$ ,  $99.07 \pm 2.8\%$ ,  $t =$

397 0.541,  $p = 0.612$ ; AP latency,  $n = 6$ ,  $t = -0.947$ ,  $p = 0.397$ , paired t-test). The baseline  $G_{in}$  and AP latency  
398 in CA3-*Kcna2*<sup>+/−</sup> CA3-PCs were lower than those of *f-Kcna2*, and was not significantly different from  
399 those of *Kcna2*<sup>+/−</sup> mice (Figure 7Ab-Ac). Next, we examined MF-induced heterosynaptic potentiation of  
400 PP-EPSPs for the CA3-*Kcna2*<sup>+/−</sup> and *f-Kcna2* mice. LTP of PP-EPSP was readily induced in the *f-Kcna2*  
401 CA3-PCs ( $185.46 \pm 2.59\%$ ,  $n = 5$ ,  $t = -5.874$ ,  $p = 0.004$ ; paired t-test), but it was abolished in the CA3-  
402 *Kcna2*<sup>+/−</sup> ( $91.30 \pm 11.91\%$ ,  $n = 6$ ,  $t = 0.348$ ,  $p = 0.742$ ; paired t-test; Figure 7Ba and 7Bb). Supporting the  
403 notion that LTP-IE underlies the heterosynaptic LTP of PP-EPSPs (Hyun et al., 2015), 20 Hz MF  
404 stimulation did not alter PP-EPSCs (Figure 7Bc).

405 Previously we demonstrated that downregulation of Kv1.2 after induction of LTP-IE enhances  
406 specifically PP-EPSPs with little effect on MF-EPSPs (Hyun et al., 2015). To test if a reduction of Kv1.2  
407 channels has any effect on E-S coupling of synaptic inputs to proximal dendrites, the number of APs  
408 elicited during 20 Hz MF stimulation for 2 s (Figure 7Ca) and the number of MF stimulation required to  
409 elicit the 1<sup>st</sup> AP in the postsynaptic CA3-PC (Figure 7Cb) was plotted as a function of baseline MF-EPSC  
410 in the three genotype mice (*f-Kcna2*, *Kcna2*<sup>+/−</sup>, CA3-*Kcna2*<sup>+/−</sup>). Both parameters were not different  
411 between the three genotypes, confirming that reduction of Kv1.2 has little effect on the proximal dendritic  
412 excitability.

413

414 *Insufficiency of Kv1.2 in CA3-PCs is responsible for the impaired pattern separation*  
415 To test whether haploinsufficiency of *Kcna2* confined to CA3-PCs is sufficient to impair the CFD task,  
416 we repeated the behavioural test of Figure 3A for *f-Kcna2* and CA3-*Kcna2*<sup>+/−</sup> mice. In CA3-*Kcna2*<sup>+/−</sup>  
417 mice the expression of Cre recombinase is driven by the promoter of a kainate receptor subunit, KA-1,  
418 which is strongly expressed in CA3. KA1, however, is expressed in 10% of dentate and cerebellar granule  
419 cells too (Nakazawa et al., 2002). To rule out the possibility that reduction of Kv1.2 in brain regions other  
420 than CA3 contributes to behavioural phenotype, we delivered AAV encoding Cre-mCherry or GFP under

421 the CaMKII $\alpha$  promoter (AAVcre and AAVgfp, respectively) to dorsal and ventral CA3 regions of *f*-  
422 *Kcna2* mice through stereotaxic techniques (see materials and methods). The AAV-injected mice were  
423 subject to behavioral test and post-hoc *ex vivo* experiments 4 weeks after the viral injection.

424 On day 4-5, all genotype and AAV-injected mice showed similar kinetics of freezing in context A (Figure  
425 8Aa, Table 6), and no difference was observed in freezing behavior among genotypes and AAV-injected  
426 mice [WT (n=11), *f*-*Kcna2* (n=4), *CA3-Kcna2* $^{+/-}$  (n=4), *Kcna2* $^{+/-}$  (n=9) mice, and AAVcre (n=4) or  
427 AAVgfp (n=4)-injected mice] and between contexts A and B (Figure 8Ab, Table 6), indicating that  
428 generalization between the two contexts is similar in the three genotype mice. On the subsequent 9 days  
429 (day 6 -14, phase 3), mice daily visited both contexts with receiving a foot shock only in context A. The  
430 discrimination ratio of *f*-*Kcna2* and AAVgfp-injected mice, but not *CA3-Kcna2* $^{+/-}$  and AAVcre-injected  
431 mice, began to rise already on day 7 (Figure 8Ba). During acquisition of the discrimination over the 9  
432 training days, *f*-*Kcna2* and AAVgfp-injected mice quickly discriminated context B from context A similar  
433 to WT mice, whereas *CA3-Kcna2* $^{+/-}$ , *Kcna2* $^{+/-}$  and AAVcre-injected mice showed significant delay for  
434 discrimination (Figure 8Ba, Table 6). Notably, the learning curves of *CA3-Kcna2* $^{+/-}$  were not different  
435 from that of *Kcna2* $^{+/-}$  mice ( $p = 1.00$ ) and AAVcre-injected mice ( $p = 1.00$ ), whereas it was different  
436 from those of WT ( $p < 0.001$ ), *f*-*Kcna2* ( $p = 0.02$ ), and AAVgfp-injected mice ( $p = 0.005$ ; RM-ANOVA  
437 Bonferroni post-hoc test, Figure 8Ba). The discrimination was impaired in the *CA3-Kcna2* $^{+/-}$  and  
438 AAVcre-injected mice on day 9 (Figure 8Bb; comparing with WT, *CA3-Kcna2* $^{+/-}$ :  $p < 0.001$ , *Kcna2* $^{+/-}$ :  
439  $p < 0.001$ , *f*-*Kcna2*:  $p = 0.680$ , AAVgfp:  $p = 0.466$ , AAVcre:  $p < 0.001$ , two-way ANOVA), but it was  
440 eventually acquired on day 14, similar to WT and *f*-*Kcna2* (Figure 6Bc, Table 6). After the behavioral  
441 test, AAV-injected mice were sacrificed and subject to *ex vivo* experiments to examine the AAV infection  
442 area and reduction of  $I_{K(D)}$  in CA3-PCs (Figure 8C-E). Confirming that mCherry or GFP signal is  
443 confined to the CA3 region (Figure 8C-D),  $I_{K(D)}$  was measured from GFP(+) and mCherry(+) CA3-PCs  
444 using the same methods as in Figure 6D (Figure 8E). The peak amplitude of  $I_{K(D)}$  activated by a  
445 depolarizing step to -20 mV from -70 mV in CA3-PCs of AAVcre-injected mice (Figure 8Eb) was

446 significantly lower than that of AAVgfp-injected mice (Figure 8Ea; AAVgfp,  $325.7 \pm 30.65$  pA; AAVcre,  
447  $168.74 \pm 25.73$  pA,  $t = 3.921$ ,  $p = 0.004$ , independent t-test, Figure 8Ec).

448 Altogether, despite that release probability at PP-CA3 synapses is enhanced both in *Kcnal*<sup>+/−</sup> and  
449 *Kcnal*<sup>+/−</sup> mice, *Kcnal*<sup>+/−</sup> mice was normal in CFD (Figure 3) and in pattern separation of CA3  
450 ensembles (Figure 4), suggesting that impaired pattern separation in *Kcnal*<sup>+/−</sup> mice cannot be attributed  
451 to presynaptic Kv1.2 haploinsufficiency. Because both *CA3-Kcnal*<sup>+/−</sup> mice and AAVcre-injected mice  
452 displayed impairments in the CFD task, it is unlikely that insufficiency of Kv1.2 in brain regions other  
453 than hippocampal CA3 is responsible for the impairment in CFD. Given that performance in CFD task is  
454 closely correlated with pattern separation in CA3 ensembles, insufficiency of Kv1.2 in CA3-PCs rather  
455 than other brain regions might be responsible for the impaired pattern separation of CA3 ensembles in the  
456 *Kcnal*<sup>+/−</sup> mice.

457

458 *Table 6, Statistical test for experiments shown in Figure 8*

Experiments	Statistical test	1 <sup>st</sup> variable (Genotype)	2 <sup>nd</sup> variable (Context / Time / Day)	Interaction
Figure 8Aa	RM- ANOVA	$F_{(5,30)} = 0.616$ $p = 0.689$	Time, $F_{(9,270)} = 9.799$ $p < 0.001$	Geno x Time, $F_{(9,270)} = 0.523$ $p = 0.996$
Figure 8Ab (Day 4-5)	two-way ANOVA	$F_{(5,67)} = 2.336$ $p = 0.054$	Context $F_{(1,67)} = 0.334$ $p = 0.566$	Geno x Context. $F_{(5,67)} = 0.226$ $p = 0.950$
Figure 8Ba (Discrimination ratio)	RM- ANOVA Bonferroni post- hoc test	$F_{(6,39)} =$ 11.614 $p < 0.001$	Day $F_{(8,312)} = 27.433$ $p < 0.001$	Geno x Day, $F_{(48,312)} = 2.930$ $p < 0.001$
Figure 8Bb (Day 9)	two-way ANOVA, simple effect analysis	$F_{(5,72)} = 13.408$ $p < 0.001$	Context $F_{(1,72)} = 47.450$ $p < 0.001$	Geno x Context, $F_{(5,72)} = 6.269$ $p < 0.001$
Figure 8Bc (Day 14)	two-way ANOVA,	$F_{(5,72)} = 3.529$ $p = 0.007$	Context $F_{(5,72)} = 438.86$ $p < 0.001$	Geno x Context. $F_{(5,72)} = 1.520$ $p = 0.197$

459

460 Discussion

461 Despite extensive studies on the synaptic plasticity in the CA3 region (reviewed in Rebola et al., 2017),  
462 the cognitive and behavioral consequences of altered synaptic plasticity in the CA3 network largely  
463 remains to be elucidated. For pattern separation, studies on its cellular mechanisms have mainly focused  
464 on DG (McHugh et al., 2007; Nakashiba et al., 2012; KimKR et al., 2020), but little understood in the  
465 CA3 region. In the present study, we found that insufficiency of Kv1.2 subunits in CA3-PCs enhances E-  
466 S coupling of PP synaptic inputs to lower the PP-LTP threshold (Figure 1 and 2), and closely correlates  
467 with deficit in rapid contextual discrimination (Figure 3 and 8) and with impaired pattern separation of  
468 CA3 ensembles activated by retrieval of two slightly different contexts (Figure 4).

469 The size and overlap of CA3 ensembles activated by the first visit to contexts A and B on day 1 were not  
470 different between WT and *Kcna2+/-* mice, but the two ensemble parameters diverged over training days  
471 (Figure 5). The *Kcna2+/-* mice displayed rapid enlargement of the CA3 ensemble size with the overlap  
472 index static over training days, while WT mice displayed relatively stable ensemble size with decreasing  
473 overlap index. Because the ensemble properties of *Kcna2+/-* mice were initially similar to WT, the  
474 abnormal evolvement of CA3 ensembles in *Kcna2+/-* mice cannot be explained by increased dendritic  
475 excitability alone, but implies that the CA3 networks of *Kcna2+/-* mice undergo plastic changes different  
476 from that of WT mice over subsequent training days. Given that the PP-LTP threshold is lowered by  
477 Kv1.2 haploinsufficiency, PP-LTP seems to be one of major players in the evolvement of CA3 ensembles  
478 during the training phase. Therefore, these results support the view that Kv1.2-dependent regulation of  
479 PP-LTP threshold may be crucial for stabilizing the ensemble size and pattern separation. It was  
480 previously shown that hippocampal learning induces growth of filopodia from MF terminals, which  
481 increases feedforward inhibition (FFI) triggered by MF inputs, and that the CA3 ensemble size is  
482 abnormally enlarged by contextual fear conditioning in the mutant mice in which the filopodial growth is  
483 abolished (Ruediger et al., 2011). This study together with our results suggest that balanced plastic

484 changes at excitatory and inhibitory synapses are essential for the CA3 ensemble size to be maintained  
485 stable during hippocampal learning, and this may be the case for the wildtype mice. On the other hand, as  
486 *Kcna2<sup>+-</sup>* mice are repeatedly exposed to the dangerous context, CA3 network may undergo too  
487 promiscuous plastic changes at PP synapses to be counterbalanced by plastic changes at inhibitory  
488 synapses such as new filopodial growth from MF terminals.

489 Previous studies indicate that Kv1.1 subunits are preferentially expressed in the soma and axonal  
490 compartments of CA3-PCs (Monaghan et al., 2001; Rama et al., 2017), whereas Kv1.2 subunits are in  
491 both of somatodendritic and axonal compartments (Sheng et al., 1994; Wang et al., 1994; Hyun et al.,  
492 2015). Moreover, PP expresses both Kv1.1 and Kv1.2, while MFs express Kv1.1 but not Kv1.2  
493 (Monaghan et al., 2001). Consistently, both of *Kcnal<sup>+-</sup>* and *Kcna2<sup>+-</sup>* CA3-PCs displayed similar  
494 increases in the intrinsic excitability of CA3-PCs (Figure 1B) and similar changes in short-term plasticity  
495 at PP synapses (Figure 6-figure supplement 1). Nevertheless, the PP-LTP threshold (Figure 1D),  
496 behavioral phenotype (Figure 3), and the CA3 ensemble overlap (Figure 4D) were not altered in *Kcnal<sup>+-</sup>*  
497 mice (Figure 1D, 3 and 4D). These results suggest that larger ensemble size in *Kcna2<sup>+-</sup>* cannot be  
498 attributed to insufficiency of *Kcna2* in the axonal compartment of afferent fibers but caused by subunits  
499 located in somatodendritic compartment. Supporting this view, performance in CFD task of *CA3-*  
500 *Kcna2<sup>+-</sup>* or AAVcre-injected mice were impaired similar to *Kcna2<sup>+-</sup>* mice (Figure 8B).

501

502 *PP-LTP threshold and CA3 ensemble size*

503 Our results imply that lowered PP-LTP threshold correlates with abnormal enlargement of the ensemble  
504 size during repeated exposure of the contexts. Given that PP synaptic inputs that were already  
505 strengthened during a previous episode contribute to the ensemble size on retrieval, sparse encoding at PP  
506 synapses would be essential for keeping the ensemble size stable. MF inputs are expected to activate a  
507 small number of CA3-PCs because of low convergence of MFs to CA3-PC together with sparse firing of

508 [dentate GCs. When PP-LTP depends on concurrent MF inputs or MF-dependent priming, the sparse MF](#)  
509 [inputs to CA3 may ensure sparse encoding of memories at PP-CA3 synapses.](#) In contrast to MFs, PP  
510 makes densely distributed synapses on CA3-PCs (Amaral et al, 1990), and thus nonspecific lowering of  
511 PP-LTP threshold caused by *Kcna2* haploinsufficiency is expected to have more profound effects on the  
512 CA3 ensemble size than lowering the threshold by MF-dependent priming. Therefore, Kv1.2 in CA3-PCs  
513 seems to [reduce the probability for PP inputs alone to induce LTP without a help of MF inputs](#) by keeping  
514 the LTP threshold high, and plays a crucial in limiting the expansion of CA3 neuronal ensemble size  
515 during hippocampal learning.

516

517 *MF-dependent encoding at PP synapses and pattern separation of CA3 ensembles*

518 Because MF inputs convey a decorrelated version of EC ensemble pattern to CA3 and dominate firing of  
519 CA3-PCs during a learning phase, limiting the LTP induction at PP synapses in CA3-PCs receiving strong  
520 MF inputs is thought to be essential for formation of sparse and discrete ensembles in CA3, and thus  
521 pattern separation. In *Kcna2<sup>+-</sup>* mice, however, non-specific lowering of PP-LTP threshold renders the  
522 PP-LTP induction less dependent of MF inputs, and thus the overlap between ensembles in the input layer  
523 (EC) may be transferred to the CA3 network without decorrelation. This view may explain why the  
524 overlap of CA3 ensembles in *Kcna2<sup>+-</sup>* mice is larger than that expected from their large ensemble size  
525 (Figure 4Da-Db). On the other hand, the pattern completion behavior probed by PECFC was not altered  
526 in *Kcna2<sup>+-</sup>* mice (Figure 3D). Given that pattern completion is mediated by A/C fibers, this result is  
527 consistent with our previous report that downregulation of Kv1.2 does not alter EPSPs evoked by A/C  
528 fibers (Hyun et al., 2015). Taken together, an increased probability for MF-independent PP-LTP may  
529 render the *Kcna2<sup>+-</sup>* mice impaired in formation of discrete representation of memories for two slightly  
530 different contexts during learning phase. Such impaired decorrelation of memories may result in  
531 generalization of the two contexts by a pattern completion process.

532

533 *Possible role of MF-induced metaplasticity at PP-CA3 synapses in the CA3 network computation*

534 We have previously shown that repetitive MF inputs to a CA3-PC downregulate Kv1.2 subunits in  $\text{Ca}^{2+}$ -  
535 and  $\text{Zn}^{2+}$ -dependent manner, resulting in LTP-IE and specific potentiation of PP-EPSPs (Hyun et al, 2013,  
536 2015; Eom et al., 2019). LTP-IE, which involves global excitability changes over the distal apical  
537 dendritic arbor, is unlikely to directly mediate memory encoding. Therefore, the role of LTP-IE in  
538 memory encoding should be studied with respect to the plastic changes of PP-EPSCs, which reflects  
539 synapse-specific events. The present study showed that LTP-IE greatly lowers the threshold of PP  
540 synaptic inputs required for subsequent plastic changes of PP-EPSCs (Figure 2), indicating that not only  
541 concurrent MF inputs but also previous history of MF inputs may facilitate encoding at PP-CA3 synapses.

542 **Lowering PP-LTP threshold by MF-induced metaplasticity may potentially increase the size and overlap**  
543 **of CA3 ensembles, and thus may have negative effects on pattern separation.** The CA3 ensemble size in  
544 *Kcan2<sup>+-</sup>* mice was 1.5 times larger on day 4 (Figure 4D), even though *Kcna2<sup>+-</sup>* CA3-PCs lack MF-  
545 induced metaplasticity, suggesting that non-specific lowering of PP-LTP threshold caused by *Kcna2*  
546 haploinsufficiency seems to exert more adverse effects on pattern separation compared to MF-induced  
547 metaplasticity. Although the CA3 neuronal ensemble size should be larger in the presence of MF-induced  
548 metaplasticity than without it, the increment may be very limited, because induction of LTP-IE requires  
549 high frequency MF inputs (Eom et al., 2019). **To figure out the role of MF-induced metaplasticity in**  
550 **pattern separation and CA3 network computation, it needs to be elucidated the cellular mechanisms**  
551 **underlying depotentiation of LTP-IE, because the role of MF-induced metaplasticity in CA3 network**  
552 **computation would heavily depend on how long the primed state of CA3-PCs is maintained *in vivo*.**  
553 **Although MF-induced LTP-IE, which corresponds to the metaplastic or primed state, lasts longer than 30**  
554 **min *in vitro* (Hyun et al., 2015; Eom, 2019; Figure 7A), it may not be the case *in vivo*. If the primed state**  
555 **of CA3-PCs is maintained until an animal experiences the next episode, which activates the second**

556 ensembles, such CA3-PCs would be re-activated by diffusely incoming PP inputs during the 2nd episode  
557 independent of MF inputs. This scenario raises a possibility that a subset of CA3-PCs primed during the  
558 1st episode may play a key role in bridging the two ensembles encoding the 1<sup>st</sup> and 2<sup>nd</sup> episodes even if  
559 the two episodes are temporally discontiguous. In this case, MF-induced metaplasticity should have more  
560 or less adverse effects on pattern separation because the primed subset will be activated by both contexts  
561 associated with the two episodes. If metaplastic states of CA3-PCs are relatively short lasting, however, it  
562 may simply subserve MF-dependent encoding at PP synapses of a single episodic memory, and thus may  
563 have little effect on pattern separation.

564

565 **Materials and Methods**

566 **Animals and ethical approval.** All of studies and experimental protocols described in this article were  
567 approved by the Institutional Animal Care and Use Committee (IACUC) of Seoul National University.  
568 The animals were maintained in standard environmental conditions (Temperature:  $25 \pm 2$  °C, Humidity:  
569  $60 \pm 5$  %, Dark/Light cycle: 12/12h) and monitored under veterinary supervision by Institute for  
570 Experimental Animals, Seoul National University College of Medicine.

571 **Kv1.1 or Kv1.2 mutant mice.** Heterozygous *Kcna1* and *Kcna2* knock-out mice (C3HeB/FeJ-*Kcna1*<sup>tm1tem</sup>  
572 and C3HeB/FeJ-*Kcna2*<sup>tm1tem</sup>, denoted as *Kcna1*<sup>+/−</sup> and *Kcna2*<sup>+/−</sup>, respectively) were kindly donated by  
573 Dr. Bruce Tempel (University Washington, Seattle) and purchased from The Jackson Laboratory  
574 (BarHarbor, ME, USA; Donating Investigator: Dr. Bruce Tempel, University of Washington School of  
575 Medicine), respectively. These mice were maintained under the veterinary supervision by Institute for  
576 Experimental Animals, Seoul National University College of Medicine. By inter-crossing heterozygote  
577 mice, we bred homozygous knock-out mice, heterozygote mice and wild-type littermate (WT) for two  
578 genotypes. For genotyping, DNA was isolated from the tail of each mouse in a litter aged 6–8 days as  
579 described by (Brew et al., 2007). Detailed protocols are available online (Kcna2:  
580 <https://www.jax.org/Protocol?stockNumber=010744&protocolID=24908>; Kcna1:  
581 <https://www.jax.org/Protocol?stockNumber=003532&protocolID=27668>). Although *Kcna2*<sup>−/−</sup> and  
582 *Kcna1*<sup>−/−</sup> mice had a severely reduced life span (range P18–P23; P4–6 wks, respectively) (Brew et al.,  
583 2007), they appeared normal during the first 2 weeks of their life.

584 **Generation of CA3 region-specific Kv1.2 mutant mice.** Generation of mice bearing the ‘Knockout-  
585 first’ allele of *Kcna2* <*Kcna2tm1a(EUCOMM)Wtsi*> was performed by Macrogen Inc. (Seoul, Republic  
586 of Korea). JM8A3.N1 ES cells (Clone ID: EPD0544\_3\_G05; Allele name: *Kcna2tm1a(EUCOMM)Wtsi*;  
587 Coat color: agouti) from C57BL/6N mice were imported from the EUCOMM (European Conditional  
588 Mouse Mutagenesis; Helmholtz Zentrum, München, Neuherberg, Germany) Project. The JM8A3.NA ES

589 cell was cultured to acquire enough number of ES cells to injection to C57BL/6N blastocysts to form new  
590 chimeric embryos. The embryos were transferred into the uteri of pseudopregnant recipient ICR female  
591 mice (5 blastocysts per conus uteri). Acquired male chimeric mice ( $F_0$ ) were bred with C57BL/6N  
592 wildtype females to transfer *Kcna2tm1a(EUCOMM)Wtsi* allele to germ cells. Germ-line transmission of  
593 the allele was analyzed by PCR in a F1 litter aged 6–8 days. After the screening of  
594 *Kcna2tm1a(EUCOMM)Wtsi* from F1 offspring mice (hereafter ‘tm1a’ mice), they were mated with  
595 general ‘FRT deleter’ mice (Protamine-FLPe) to cut of both the LacZ and neomycin site, leading to the  
596 generation of ‘*floxed-Kcna2*’ mice. A CA3-specific cre-expressing mice (C57BL/6-Tg(Grik4-cre)G32-  
597 4Stl/J) was mated with tm1c mice to cut exon 3 via Cre-lox recombination, leading to deletion of *Kcna2*  
598 in CA3 subregion (hereafter called ‘CA3-*Kcna2*+/-’).

599 **Stereotaxic surgery and intrahippocampal injection of adeno-associated virus.** A pair of adeno-  
600 associated virus (AAV) was kindly provided by Dr. Joung-Hun Kim (Dept. of Life sciences, POSTECH)  
601 (AAV-CaMKII $\alpha$ -GFP for control; AAV-CaMKII $\alpha$ -cre-mCherry for test group; titer,  $4.8 \times 10^{12}$  GC/ml for  
602 both). Surgery was performed on adult floxed-*Kcna2* mice (8 weeks). After anesthesia with isofluorane,  
603 mice were secured in a stereotaxic frame (Neurostar, Tubingen, Germany). Holes were drilled bilaterally  
604 in the skull at the injection sites (4 sites). Stereotaxic coordinates used for intrahippocampal injections  
605 were as follows (from bregma); for a dorsal hippocampus, anterior–posterior: -2.1 mm, mediolateral:  $\pm 2.2$   
606 mm, dorsoventral: 2.25 mm; for a ventral hippocampus, anterior–posterior -2.85 mm, mediolateral  $\pm 2.8$   
607 mm, dorsoventral 3.3 mm. A 33 gauge needle attached to a 50  $\mu$ l Hamilton syringe (#80908), mounted to  
608 the stereotaxic frame, and under control of a microinjection syringe pump UMP3T-1 controller (WPI,  
609 Sarasota, FL, USA) was used to inject 0.4  $\mu$ l of AAV at each site. Injections occurred at a rate of 0.04  
610  $\mu$ l/min, after which the needle was left in place for an additional 2 min. After injections were completed,  
611 the skin was sutured and the animals were allowed to recover for 1 h on a heating pad before returning to  
612 the home cage. Mice remained in the home cage for an additional 4 weeks before the start of behavioral

613 testing and post-hoc *ex vivo* experiments.

614 **Preparation of slices for electrophysiological recording.** Acute transverse hippocampal slices were  
615 obtained from Sprague-Dawley rats (P15-P22; P, postnatal days) or aforementioned mice (P15-P24) of  
616 either sex. Animals were anesthetized by inhalation of 5 % isoflurane. After decapitation, brain was  
617 quickly removed and chilled in ice-cold cutting solution contained 75 mM sucrose, 87 mM NaCl, 25 mM  
618 NaHCO<sub>3</sub>, KCl 2.5 mM, NaH<sub>2</sub>PO<sub>4</sub> 1.25 mM, D-glucose 25 mM, MgCl<sub>2</sub> 7 mM, and CaCl<sub>2</sub> 0.5 mM  
619 (equilibrated with carbogen mixture of 95% O<sub>2</sub> and 5% CO<sub>2</sub>). After mounting, 300  $\mu$ m-thick transverse  
620 slices were prepared in the cutting solution using a vibratome (Leica VT1200, Nussloch, Germany), and  
621 incubated at 34 °C for 30 min in the same solution, and thereafter stored at room temperature (22 °C). For  
622 experiments, slices were transferred to a submersion recording chamber superfused with standard  
623 recording solution contained 124 mM NaCl, 26 mM NaHCO<sub>3</sub>, 3.2 mM KCl, 1.25 mM NaH<sub>2</sub>PO<sub>4</sub>, 10 mM  
624 D-glucose, 2.5 mM CaCl<sub>2</sub>, and 1.3 mM MgCl<sub>2</sub>.

625 **Electrophysiological recordings.** Whole-cell voltage- or current-clamp recordings from CA3-PCs were  
626 performed at near-physiological temperature (34  $\pm$  1 °C) in standard recording solution while the  
627 recording chamber was perfused with the recording solution at 1 ~ 1.5 ml/min. Patch pipettes were pulled  
628 from borosilicate glass tubing (Outer diameter: 1.5 mm, Wall thickness: 0.225 mm) with a horizontal  
629 pipette puller (P-97, Sutter Instruments, Novato, CA, USA) and filled with the intracellular solution  
630 contained 130 mM K-gluconate, 7 mM KCl, 1 mM MgCl<sub>2</sub>, 2 mM Mg-ATP, 0.3 mM Na-GTP, 10 mM  
631 HEPES, 0.1 mM EGTA (pH = 7.20 with KOH, 295 mOsm with sucrose), and pipette resistance was 3 ~ 4  
632 M $\Omega$ . Recordings were preferentially obtained from the hippocampal CA3b. After formation of whole-cell  
633 configuration on the somata of CA3-PCs, recordings were performed from only cells that had stable  
634 resting membrane potential within -76 and -58 mV (cells that had more positive resting membrane  
635 potential or unstable resting membrane potential was discarded). Under this condition, input conductance  
636 ( $G_{in}$ ) was measured from subthreshold voltage responses to -30 pA and +10 pA current steps with 0.5 sec

637 (Hyun et al., 2015).  $G_{in}$  was monitored every 10 s before and after the activities delivered to CA3-PCs  
638 described below. The first spike latency (AP latency) was measured from voltage responses of CA3-PCs  
639 to a ramp current injection (250 pA/s for 1 s) (Hyun et al., 2013). All recordings were made using a  
640 MultiClamp 700B amplifier controlled by Clampex 10.2 through Digidata 1400A data acquisition system  
641 (Molecular Devices, Sunnydale, CA, USA)

642 **Synaptic stimulation for MF-, and PP-CA3 synapses.** Various stimulations were delivered to the  
643 synapses of CA3-PCs were delivered to evaluate the influence to the intrinsic excitability of CA3-PCs.  
644 Afferent MFs were stimulated with a recording solution-filled glass monopolar electrode with resistance  
645 of  $1 \sim 2 \text{ M}\Omega$  placed in striatum (st.) lucidum (SL; stimulus intensity with  $2 \sim 20 \text{ V}$ ) using minimal  
646 stimulation techniques (Hyun et al., 2015). Afferent PP and fibres were stimulated with a concentric  
647 bipolar electrode (CBAPB125; FHC Inc., Bowdoin, ME, USA). Brief stimulation pulses (100  $\mu\text{s}$ ) was  
648 generated by a digital stimulator (DS8000, WPI; Sarasota, FL, USA) and delivered to stimulation  
649 electrode through an isolation unit (DLS100 stimulus isolator, WPI). A stimulation electrode was  
650 positioned at st. lacunosum-moluculare (SLM) on the border of the subiculum and CA1 (for PP  
651 stimulation), and identified the type of synaptic inputs by the rise time of EPSCs and sensitivity to group  
652 II mGluR agonist, (2S,2'R,3'R)-2-(2',3'-Dicarboxycyclopropyl)glycine (DCG-IV, 2  $\mu\text{M}$ ). The attenuation  
653 of PP-EPSCs and MF EPSCs were 72.8%, 72.6 % (data not shown), consistent with previous reports  
654 (Tsukamoto et al., 2003).

655 **In situ hybridizaion.** Fluorescence in situ hybridization (FISH) for RNA transcripts was performed using  
656 RNAscope probes [Advanced Cell Diagnostics (ACD), Hayward, CA, USA] for target genes following  
657 the manufacturer's instructions. A harvested brain was quickly frozen on liquid nitrogen. Frozen sections  
658 of  $15 \sim 20 \mu\text{m}$  thick were serially and coronally cut through the habenula formation. Sections were thaw-  
659 mounted onto Superfrost Plus Microscope Slides (Fisher Scientific #12-550-15). The sections were fixed  
660 in 4% PFA for 10 min, dehydrated in increasing concentrations of ethanol for 5 min, and finally air-dried.

661 Tissues were then pretreated for protease digestion for 10 min at room temperature. For hybridization,  
662 prepared slides were incubated in HybEZ hybridization oven (ACD) for 30 min at 40°C. Unbound  
663 hybridization probes were removed by washing the sections three times with 1x wash buffer at room  
664 temperature for 2 min. For signal amplification, slides were incubated with amplification solutions  
665 (Amplifier #FL): #1 for 30 minutes at 40°C, #2 for 15 min at 40°C, #3 for 30 minutes at 40°C, #4 for 15  
666 min at 40°C. After the completion of each session, slides were washed twice with 1x wash buffer for 2  
667 min at room temperature. Nuclei were counterstained with 4',6-diamidino-2-phenylindole (DAPI, ACD).  
668 For detection of *Homer1a* (*H1a*), *Arc*, and *Kcna2* mRNA in Figure 4 and Figure 5, RNAscope Probes  
669 Mm-Homer1-tvS (Cat#, 433941), Mm-Arc-C3 (Cat#, 316911-C3), Mm-Kcna2-C2 (Cat#, 462811-C2)  
670 were used, respectively. The slides were viewed, analyzed, and photographed using TCS SP8 Dichroic/CS  
671 (Leica, Germany) or Olympus Fluoview FV1200 (Japan) confocal microscope equipped with 488 nm and  
672 633 nm diode lasers. For *H1a* and *Arc*, the settings for photomultiplier and laser power were optimized  
673 for detection of intra-nuclear foci and for minimizing weaker cytoplasmic signals (Almira et al., 2002).  
674 The number of *Kcna2* mRNA dots and intra-nuclear foci of *H1a* and *Arc* were counted on 60 x magnified  
675 photographs (N.A. = 1.2).

676 **Image acquisition and analysis for catFISH.** Hippocampal slices obtained from *WT*, *Kcna1+/-*, and  
677 *Kcna2+/-* mice were analysed with RNAscope assay (Advanced Cell Diagnostics, Hayward, CA, USA)  
678 using target probes for *Arc* (Cat No.: 540901) and *Homer1a* (Cat No.: 433261) for catFISH described in  
679 Figure 4. Confocal z-stacks composed of 1-μm-thick optical sections were collected in regions CA3 from  
680 3 slides/animal and stored for offline analysis. Stacks for CA3 (one stack per slide) were collected with a  
681 20× objective to collect comparable numbers of cells from each subjects. Non-neuronal cells, identified as  
682 small cells (c.a. 5 μm in diameter) with intensely bright and uniformly stained nuclei, were excluded from  
683 the analysis. Only large, diffusely stained nuclei present in the sections were regarded as neuronal cells,  
684 and included in our analysis. Neuronal nuclei from the CA3 region were classified as negative (containing  
685 no transcription foci), *H1a* (+) (containing only *H1a* transcription foci), *Arc* (+) (containing only *Arc*

686 transcription foci), or Arc/H1a (+) (containing transcription foci for both Arc and H1a) by an  
687 experimenter blind to the relationship between the image stacks and the behavioural conditions they  
688 represented. The number of nuclei corresponded to each classification and total number of neuronal  
689 nuclei were counted.

690 **Evaluation of CA3 region-specific Kv1.2 hetero-knockout mice.** Hippocampal slices obtained from  
691 CA3-Kcna2<sup>+-</sup> and floxed-Kcna2 mice were analysed with RNAscope assay (Advanced Cell Diagnostics,  
692 Hayward, CA, USA) using RNAscope<sup>®</sup> Probe- Mm-Kcna2-C2 (Cat No.: 462811-C2). Confocal z-stacks  
693 composed of 1- $\mu$ m-thick optical sections were collected in regions CA3 from 3 slides/animal and stored  
694 for offline analysis. The number of mRNA dot in CA3, CA1, and dentate gyrus (DG) region was counted  
695 by an experimenter blind to the relationship between the image stacks and the behavioural conditions they  
696 represented, based on an assumption that each RNA dot deriving from a single mRNA molecule (Wang et  
697 al., 2012).

698 **Contextual fear discrimination test.** We tested 39 male mice between 14 and 20 weeks of age (20 WT  
699 mice, 10 kcna1<sup>+-</sup> and 9 kcna2<sup>+-</sup> mice) for fear conditioning in a pair of similar contexts using a  
700 protocol adapted from (McHugh et al., 2007). This test assesses an animal's ability to discriminate  
701 between two similar contexts, A and B, through repeated experience of a foot shock that is associated with  
702 Context A but not with B. Context A (conditioning context) is a chamber (18 cm wide x 18 cm long x 30  
703 cm high; H10-11M-TC; Coulbourn Instruments 5583, PA 18052, USA) consisting of a metal grid floor,  
704 aluminium side walls, and a clear Plexiglass front door and back wall. The context A chamber was lit  
705 indirectly with a 12 W light bulb. The features of Context B (safe context) were the same as Context A,  
706 except for a unique odor (1% acetic acid), dimmer light (50% of A), and a slanted floor by 15° angle.  
707 Each chamber was cleaned with 70% ethanol before the animals were placed. On the first 3 days of the  
708 experiment, the mice were placed in Context A, where they were allowed a 3-min exploration, received a  
709 single foot shock (1 mA, for 2 s) and were returned to their home cage 60 s after the shock. Freezing

710 levels were measured during the 3 min before the shock delivery. On day 4, mice of each genotype were  
711 divided into two groups; one group of genotype visited Context A and the other Context B. On day 5, we  
712 had each mouse visit the context opposite to the one visited on day 4, and freezing levels were measured  
713 again. On day 4-5, neither group received a shock in Context A and B. The mice were subsequently  
714 trained to discriminate these two contexts by visiting the two contexts daily for 9 days (discrimination  
715 task day 6 to 14), always receiving a footshock 3 min after being placed in Context A but not B (Figure  
716 3A). The freezing ratio (measured during the first 3 min) in each context was used to calculate  
717 discrimination ratios for each animal in both groups over the 9 days of training. We defined freezing  
718 behavior as behavioral immobility except for movement necessary for respiration and assessed the  
719 freezing behavior of each mouse for the duration of 5 min (day 4-5) or 3 min (day 6-14) by observing its  
720 video image for 2 s bouts every 10 s and counting the number of 2 s bouts during which the mouse  
721 displayed freezing behavior (referred to as a freezing score). Freezing ratio was calculated as the freezing  
722 score divided by the total number of observation bouts (18 or 30). Discrimination ratios were calculated  
723 according to  $F_A / (F_A + F_B)$ , where  $F_A$  and  $F_B$  are freezing scores in Contexts A and B, respectively. All  
724 experiments and analyses were performed blind to the mice genotype.

725 **One-trial contextual fear conditioning.** We tested five WT mice and five *Kcna2<sup>+-</sup>* mice between 14  
726 and 16 weeks of age for fear conditioning in a pair of very distinct contexts using the experimental  
727 schedule of 3 days (acclimation, conditioning, assessment) according to (Cravens et al., 2006). The  
728 aforementioned Context A was used as the conditioning context. For the distinct context (Context C), we  
729 put a white acrylic blind end cylinder (15 cm in diameter, 18 cm in height, and 0.5 cm in thickness)  
730 vertically on the metal grid floor of the conditioning chamber, and covered the bottom inside the cylinder  
731 with cage bedding, on which mice were placed. The chamber and cylinder were cleaned using 70%  
732 ethanol between runs. On day 1, we first placed mice in Context A and then placed them in Context C an  
733 hour later. Mice were allowed to freely explore in both contexts for 5 min. On day 2, we had mice revisit  
734 Context A and receive a single foot shock (1 mA, for 2 s) 3 min later, and returned them to their home

735 cage 60 s after the shock. On day 3, mice were separated into two groups; mice of each group were placed  
736 in Context A or C for 3 min without a foot shock, during which the freezing score was measured. All  
737 experiments were conducted and analysed by scientists blind to the genotypes of the mice.

738 **Pre-exposure-mediated contextual fear conditioning (PECFC).** This task requires mice to retrieve  
739 contextual memory from a very brief exposure to a previously experienced context (Fanselow, 1990;  
740 Nakashiba et al. 2008). Male WT mice (n = 18) and male Kcna2<sup>+-</sup> (n = 18) mice between 15 to 25 weeks  
741 of age were tested for PECFC. The pre-exposure context was the same as the aforementioned ‘Context A’,  
742 whereas non-exposure context was the same as the aforementioned ‘Context C’. The chamber was  
743 cleaned with 70% ethanol between runs. On day 1, each group of genotypes was divided, and one  
744 subgroup were allowed to freely explore Context A for 10 min, and the other group were allowed to  
745 Context C for same time (pre-exposure). On the second day, each group were separated into conditioned  
746 and unconditioned groups. The conditioned subgroup mice were placed into Context A for 10 s, received  
747 a single foot shock (1 mA, for 2 s) and were immediately (30 s after the shock) returned to their home  
748 cages. Mice of the unconditioned subgroup were just brought back to the home cages 42 s after being  
749 placed in the Context A without a foot shock. On day 3, 24 h after experiencing Context A, mice of each  
750 group were placed in Context A and a freezing score was assessed for 3 min.

751 **Elevated plus maze (EPM).** We assessed basal anxiety level in WT mice (n = 5) and Kcna2 HT mice (n =  
752 10) between 13 and 16 weeks of age using the elevated plus maze. The apparatus consisted of two open  
753 (30x5 cm) and two closed (30 x 5 x 15 cm) arms facing each other with an open roof. The entire maze  
754 was elevated at a height of 40 cm and each animal was placed individually on the central platform (5 x 5  
755 cm), facing an open arm, and was allowed to explore the apparatus for 5 min. Anxiety was measured by  
756 the time spent in open arms. Data were collected using a video camera fixed to the ceiling of the room  
757 and connected to a video tracking equipment and a recorder using EthoVision software (Noldus  
758 Information Technology, Wageningen, Netherlands).

759 **Statistical Analysis.** Statistical data are expressed as mean  $\pm$  standard error of the mean (SEM), and the  
760 number of cells/animals measured (denoted as n; details were described in results). Statistical data were  
761 evaluated for normality and variance equality with Kolmogorov-Smirnov test and Levene's test,  
762 respectively. For data that satisfy normality and equality of variances, statistical evaluations were  
763 performed with student's t-test or ANOVA. For data that inappropriate for parametric tests, non-  
764 parametric tests were performed for evaluation. The number of cells and statistical tests for determining  
765 statistical significance are stated in the text using following abbreviations: n.s., no statistical significance;  
766 \*, P < 0.05; \*\*, P < 0.01; \*\*\*, P < 0.005. Statistical analyses were performed using PASW Statistics 18  
767 (SPSS Inc, 2009, Chicago, IL, USA).

768

769 **Acknowledgements:**

770 This study was supported by grants from National Research Foundation of Korea (Grant No.  
771 2020R1A2C2006438) and Seoul National University Hospital.

772

773 **Competing interests:**

774 The authors declare that they have no competing interests.

775    **References**

776    Amaral DG, Ishizuka NI, Claiborne B (1990) Neurons, numbers and the hippocampal network. *Progress*  
777    *in Brain Research*, **83**:1-11. doi: 10.1016/s0079-6123(08)61237-6.

778    Abraham WC (2008) Metaplasticity: tuning synapses and networks for plasticity. *Nat Rev Neurosci*  
779    **9**:387-400. doi: 10.1038/nrn2356.

780    Bernier BE, Lacagnina AF, Ayoub A, Shue F, Zemelman BV, Krasne FB, Drew MR (2017) Dentate Gyrus  
781    Contributes to Retrieval as well as Encoding: Evidence from Context Fear Conditioning, Recall,  
782    and Extinction. *J Neurosci* **37**:6359-6371. doi: 10.1523/JNEUROSCI.3029-16.2017.

783    Brew HM, Gittelman JX, Silverstein RS, Hanks TD, Demas VP, Robinson LC, Robbins CA, McKee-  
784    Johnson J, Chiu SY, Messing A, Tempel BL (2007) Seizures and reduced life span in mice lacking  
785    the potassium channel subunit Kv1.2, but hypoexcitability and enlarged Kv1 currents in auditory  
786    neurons. *J Neurophysiol* **98**:1501-1525. doi: 10.1152/jn.00640.2006.

787    Cravens CJ, Vargas-Pinto N, Christian KM, Nakazawa K (2006) CA3 NMDA receptors are crucial for  
788    rapid and automatic representation of context memory. *Eur J Neurosci* **24**:1771-1780. doi:  
789    10.1111/j.1460-9568.2006.05044.x

790    Eom K, Hyun J, Lee D, Kim S, Jeong H, Kang J, Ho W, Lee S (2019) Intracellular Zn<sup>2+</sup> Signaling  
791    Facilitates Mossy Fiber Input-Induced Heterosynaptic Potentiation of Direct Cortical Inputs in  
792    Hippocampal CA3 Pyramidal Cells. *J Neurosci* **39**:3812-3831. doi: 10.1523/JNEUROSCI.2130-  
793    18.2019.

794    Fanselow M (1990) Factors governing one-trial contextual conditioning. *Animal Learning & Behavior*  
795    **18**:264-270.

796    GoodSmith D, Chen X, Wang C, Kim SH, Song H, Burgalossi A, Christian KM, Knierim JJ (2017)  
797    Spatial Representations of Granule Cells and Mossy Cells of the Dentate Gyrus. *Neuron* **93**:677-  
798    690 e5. doi: 10.1016/j.neuron.2016.12.026.

799 Grosse G, Draguhn A, Höhne L, Tapp R, Veh R, Ahnert-Hilger G (2000) Expression of Kv1 potassium  
800 channels in mouse hippocampal primary cultures: development and activity-dependent regulation.  
801 *J Neurosci* **20**:1869-1892. 10.1523/JNEUROSCI.20-05-01869.2000.

802 Gu C, Jan YN, Jan LY (2003). A conserved domain in axonaltargeting of Kv1 (Shaker) voltage-gated  
803 potassium channels. *Science* **301**:646–649. doi: 10.1126/science.1086998.

804 Gu C, Zhou W, Puthenveedu MA, Xu M, Jan YN, Jan LY (2006) Required for Kv1 Voltage-Gated K<sup>+</sup>  
805 Channel Axonal Targeting. *Neuron*. **52**:803-816. doi: 10.1016/j.neuron.2006.10.022.

806 Guan D, Lee JCF, Tkatch T, Surmeier DJ , Armstrong WE, Foehring RC (2006) Expression and  
807 biophysical properties of Kv1 channels in supragranular neocortical pyramidal neurones. *J  
808 Physiol.* **571**:371-389. doi: 10.1113/jphysiol.2005.097006

809 Guzowski JF, Timlin JA, Roysam B, McNaughton BL, Worley PF, Barnes CA (2005) Mapping  
810 behaviorally relevant neural circuits with immediate-early gene expression. *Curr Opin Neurobiol*  
811 **15**:599-606. 10.1016/j.conb.2005.08.018.

812 Hyun J, Eom K, Lee K, Ho W, Lee S (2013) Activity-dependent downregulation of D-type K<sup>+</sup> channel  
813 subunit Kv1.2 in rat hippocampal CA3 pyramidal neurons. *J Physiol* **591**:5525-5540. doi:  
814 10.1113/jphysiol.2013.259002.

815 Hyun J, Eom K, Lee K, Bae J, Bae Y, Kim M, Kim S, Ho W, Lee S (2015) Kv1.2 mediates heterosynaptic  
816 modulation of direct cortical synaptic inputs in CA3 pyramidal cells. *J Physiol* **593**:3617-3643.  
817 doi: 10.1113/JP270372.

818 Kesner RP (2013) A process analysis of the CA3 subregion of the hippocampus. *Front Cell Neurosci*  
819 **7**:78. doi: 10.3389/fncel.2013.00078.

820 Kim KR, Yeon Lee S, Ho Yoon S, Kim Y, Jeong HJ, Lee S, Ho Suh Y, Kang JS, Cho H, Lee SH, Kim  
821 MH, Ho WK (2020) Kv4.1, a key ion channel for low frequency firing of dentate granule cells, is  
822 crucial for pattern separation. *J Neurosci* **11**:1541-1519. doi: 10.1523/JNEUROSCI.1541-  
823 19.2020.

824 Kole MH, Letzkus JJ, Stuart GJ (2007) Axon initial segment Kv1 channels control axonal action  
825 potential waveform and synaptic efficacy. *Neuron*. 55(4):633-647.  
826 doi:10.1016/j.neuron.2007.07.031

827 Lee I, Kesner R (2004) Encoding versus retrieval of spatial memory: double dissociation between the  
828 dentate gyrus and the perforant path inputs into CA3 in the dorsal hippocampus. *Hippocampus*  
829 14:66-76. doi: 10.1002/hipo.10167.

830 Leutgeb JK, Leutgeb S, Moser MB, Moser EI (2007) Pattern separation in the dentate gyrus and CA3 of  
831 the hippocampus. *Science* 315:961-966. doi: 10.1126/science.1135801.

832 Leutgeb S, Leutgeb JK, Treves A, Moser MB, Moser EI (2004) Distinct ensemble codes in hippocampal  
833 areas CA3 and CA1. *Science* 305:1295-1298. doi: 10.1126/science.1100265

834 Malinow R, Tsien R (1990) Presynaptic enhancement shown by whole-cell recordings of long-term  
835 potentiation in hippocampal slices. *Nature* 346:177-180. doi: 10.1038/346177a0.

836 McHugh TJ, Jones MW, Quinn JJ, Balthasar N, Coppari R, Elmquist JK, Lowell BB, Fanselow MS,  
837 Wilson MA, Tonegawa S (2007) Dentate gyrus NMDA receptors mediate rapid pattern separation  
838 in the hippocampal network. *Science* 317:94-99. doi: 10.1126/science.1140263.

839 McMahon D, Barrionuevo G (2002) Short- and long-term plasticity of the perforant path synapse in  
840 hippocampal area CA3. *J Neurophysiol* 88:528-533. doi: 10.1152/jn.2002.88.1.528.

841 Mishra RK, Kim S, Guzman SJ, Jonas P (2016) Symmetric spike timing-dependent plasticity at CA3-  
842 CA3 synapses optimizes storage and recall in autoassociative networks. *Nat Commun*. 7:11552.  
843 doi:10.1038/ncomms11552

844 Monaghan M, Trimmer J, Rhodes K (2001) Experimental localization of Kv1 family voltage-gated K<sup>+</sup>  
845 channel alpha and beta subunits in rat hippocampal formation. *J Neurosci* 21: 5973-83. doi:  
846 10.1523/JNEUROSCI.21-16-05973.2001.

847 Nakashiba T, Young JZ, McHugh TJ, Buhl DL, Tonegawa S (2008) Transgenic inhibition of synaptic  
848 transmission reveals role of CA3 output in hippocampal learning. *Science* 319:1260-1264. doi:

849 10.1126/science.1151120.

850 Nakazawa K, Quirk MC, Chitwood RA, Watanabe M, Yeckel MF, Sun LD, Kato A, Carr CA, Johnston D,  
851 Wilson MA, Tonegawa S (2002) Requirement for hippocampal CA3 NMDA receptors in  
852 associative memory recall. *Science* **297**:211–218. doi.org:10.1126/science.1071795.

853 O'Reilly R, McClelland J (1994) Hippocampal conjunctive encoding, storage, and recall: avoiding a  
854 trade-off. *Hippocampus* **4**:661-682. doi: 10.1002/hipo.450040605

855 Rama S, Zbili M, Fekete A, Tapia M, Benitez MJ, Boumedine N, Garrido JJ, Debanne D (2017) The role  
856 of axonal Kv1 channels in CA3 pyramidal cell excitability. *Sci Rep* **7**:315. doi: 10.1038/s41598-  
857 017-00388-1.

858 Rebola N, Carta M, Mulle C (2017) Operation and plasticity of hippocampal CA3 circuits: implications  
859 for memory encoding. *Nat Rev Neurosci.* **18**:208-220. doi: 10.1038/nrn.2017.10.

860 Rolls ET, Kesner RP (2006) A computational theory of hippocampal function, and empirical tests of the  
861 theory. *Prog Neurobiol* **79**:1-48. doi: 10.1016/j.pneurobio.2006.04.005

862 Ruediger S, Vittori C, Bednarek E, et al. (2011) Learning-related feedforward inhibitory connectivity  
863 growth required for memory precision. *Nature*. 473(7348):514-518. doi:10.1038/nature09946

864 Senzai Y, Buzsáki G (2006) Physiological Properties and Behavioral Correlates of Hippocampal Granule  
865 Cells and Mossy Cells. *Neuron*. **93**:691-704. doi:10.1016/j.neuron.2016.12.011

866 Sheng M, Tsaur M, Jan Y, Jan L (1994) Contrasting subcellular localization of the Kv1.2 K<sup>+</sup> channel  
867 subunit in different neurons of rat brain. *J Neurosci* **14**:2408-2417. 10.1523/JNEUROSCI.14-04-  
868 02408.1994.

869 Storm JF (1988) Temporal integration by a slowly inactivating K<sup>+</sup> current in hippocampal neurons. *Nature*  
870 **336**:379-381. doi: 10.1038/336379a0.

871 Treves A, Rolls E (1992) Computational constraints suggest the need for two distinct input systems to the  
872 hippocampal CA3 network. *Hippocampus* **2**:189-199. doi: 10.1002/hipo.450020209

873 Tsukamoto M, Yasui T, Yamada MK, Nishiyama N, Matsuki N, Ikegaya Y (2003) Mossy fibre synaptic

874 NMDA receptors trigger non-hebbian long-term potentiation at entorhino-CA3 synapses in the  
875 rat. *J Physiol* **546**:665-675. doi: 10.1113/jphysiol.2002.033803.

876 Vazdarjanova A, McNaughton B, Barnes C, Worley P, Guzowski J (2002) Experience-dependent  
877 coincident expression of the effector immediate-early genes arc and Homer 1a in hippocampal  
878 and neocortical neuronal networks. *J Neurosci* **22**:10067-10071. doi: 10.1523/JNEUROSCI.22-  
879 23-10067.2002.

880 Vazdarjanova A, Guzowski JF (2004) Differences in hippocampal neuronal population responses to  
881 modifications of an environmental context: evidence for distinct, yet complementary, functions of  
882 CA3 and CA1 ensembles. *J Neurosci* **24**:6489-6496. doi: 10.1523/JNEUROSCI.0350-04.2004.

883 Vogt K, Regehr W (2001) Cholinergic modulation of excitatory synaptic transmission in the CA3 area of  
884 the hippocampus. *J Neurosci* **21**:75-83. 10.1523/JNEUROSCI.21-01-00075.2001.

885 Wang F, Flanagan J, Su N, Wang LC, Bui S, Nielson A, Wu X, Vo HT, Ma XJ, Luo Y (2012) RNAscope:  
886 a novel in situ RNA analysis platform for formalin-fixed, paraffin-embedded tissues. *J Mol Diagn*  
887 **14**:22-29. doi: 0.1016/j.jmoldx.2011.08.002.

888 Wang H, Kunkel D, Schwartzkroin P, Tempel B (1994) Localization of Kv1.1 and Kv1.2, two K channel  
889 proteins, to synaptic terminals, somata, and dendrites in the mouse brain. *J Neurosci* **14**:4588-  
890 4599. doi: 10.1523/JNEUROSCI.14-08-04588.1994

891

892

893 **Figure Legends**

894 *Figure 1*

895 **Figure 1.** The threshold for homosynaptic LTP at PP-CA3 synapse (PP-LTP) is lower in *Kcna2+/-* than in  
896 WT and *Kcna1+/-* mice. **Aa.** Voltage responses of a CA3-PC (*red*) to weak HFS of PP (PP-HFS) protocol  
897 (*black*). PP-HFS is comprised of 10 bursts delivered every 10 s (*left*), and each bursts consists of 20  
898 stimuli at 100 Hz (*right*, corresponds to the gray dashed box on the left). This HFS protocol was applied  
899 while the postsynaptic membrane potential was adjusted at -60 mV in current-clamp mode. **Ab.** Strong  
900 PP-HFS protocol. The pulse protocol was the same as the weak PP-HFS (*Aa*) but higher stimulation  
901 intensity. Note that a burst of APs was elicited by strong PP-HFS in the CA3-PC. **Ac.** Monitoring of PP-  
902 EPSCs before and after the PP-HFS in CA3-PCs of WT mice. Weak HFS and strong HFS were  
903 categorized based on the induction of PP-LTP. *Insets:* Representative PP-EPSC traces before (*black*) and  
904 30 min after (*red*) weak (*upper*) or strong (*lower*) PP-HFS. **Ad.** Mean amplitude of EPSCs before and  
905 after weak or strong PP-HFS. All strong stimulation intensity elicited the baseline PP-EPSCs larger than  
906 12 pA. **B,** Mean values for input conductance ( $G_{in}$ , *Ba*) and first AP latency (*Bb*) measured in CA3-PCs of  
907 the three genotype mice. *Bc* and *Bd* show representative traces for voltage responses to subthreshold  
908 (+10/-30 pA) current injection (*Bc*), and those to ramp (250 pA/s for 1s) current injection (*Bd*), from  
909 which  $G_{in}$  and first AP latency were measured, respectively. Both parameters were lower in *Kcna1+/-* and  
910 *Kcna2+/-* than wildtype littermates (WT), but not different *Kcna1+/-* and *Kcna2+/-* CA3-PCs ( $G_{in}$ ,  $F_{(2,35)} =$   
911 7.539,  $p = 0.002$ ; WT vs. *Kcna1+/-*,  $p = 0.003$ ; WT vs. *Kcna2+/-*,  $p = 0.006$ ; *Kcna1+/-* vs. *Kcna2+/-*,  $p =$   
912 1.00; For AP latency,  $F_{(2,46)} = 11.539$ ,  $p = 0.002$ ; WT vs. *Kcna1+/-*,  $p = 0.003$ ; WT vs. *Kcna2+/-*, 0.006;,  
913 *Kcna1+/-* vs. *Kcna2+/-*,  $p = 1.00$ ; one-way ANOVA and Bonferroni post-hoc test).. **Ca.** Monitoring of PP-  
914 EPSCs before and after weak (*open symbols*) or strong (*closed symbols*) PP-HFS in CA3-PCs of  
915 *Kcna1+/-* (*blue*) and *Kcna2+/-* (*red*) mice. The same color code was used in insets. *Insets:* Representative  
916 traces of PP-EPSCs before (*black*) and 30 min after weak (*upper*) and strong (*lower*) PP-HFS. **Cb.** Mean  
917 amplitude of EPSCs before and after PP-HFS. **Da,** PP-LTP levels as a function of stimulation intensity

918 which was quantified as the baseline PP-EPSC amplitude. Note that the LTP threshold in *Kcna2+/-* (c.a.  
919 10.4 pA) was lowered than that of *WT* or *Kcna1+/-* (c.a. 12.1 pA). **Db**, PP-LTP levels as a function of the  
920 number of somatic APs evoked by PP-HFS. Note that PP-LTP was always associated with somatic APs  
921 evoked by PP-HFS.

922

923 *Figure 1-S1*

924 **Figure 1-figure supplement 1.** PP-LTP enhances the number of spikes in CA3-PCs elicited by a burst  
925 stimulation of PP facilitates the generation of AP spikes of CA3-PCs. **Aa**. potentiation of PP-EPSCs  
926 before and after PP-HFS (the same protocol as shown in Figure 1Ab (n = 5, Z = -2.06, p = 0.039,  
927 Wilcoxon signed rank test). **Ab**. Exemplar traces for PP-EPSCs before (black; t = -5 min) and after (red; t  
928 = 30 min) PP-HFS. **Ba**. In the same PP-CA3 synapses (denoted by the same symbols as in A), the number  
929 of APs by a single burst stimulation (20 pulses at 100 Hz) of PP-CA3 synapses was significantly  
930 increased after induction of PP-LTP (n = 5, Z = -2.06, p = 0.039). **Bb**. Exemplar traces for temporally  
931 summated PP-EPSPs and APs evoked by a single burst stimulation before (upper, black) and after (lower,  
932 red) the induction of PP-LTP.

933

934 *Figure 2*

935 **Figure 2.** Kv1.2 mediates the 10 Hz somatic stimulation-induced metaplasticity at PP-CA3 synapses. **Aa-**  
936 **Ab**, Postsynaptic voltage responses to weak PP-HFS in *Kcna1+/-* (*Aa*) and *Kcna2+/-* (*Ab*) CA3-PCs that  
937 underwent 10 Hz somatic stimulation. Gray dashed box regions are shown in expanded time scale on the  
938 right insets. **Ac**. Metaplasticity induced by somatic conditioning at *WT* (black), *Kcna1+/-* (blue), and  
939 *Kcna2+/-* (red) PP-CA3 synapses. PP-EPSCs are monitored before and after somatic conditioning at -5  
940 min (blue arrow) and subsequent weak PP-HFS at 0 min (red arrow). After the somatic stimulation, LTP  
941 was induced by weak HFS in *WT* and *Kcna1+/-*, but not in *Kcna2+/-* CA3-PCs. **Ad**. Representative traces

942 for PP-EPSPs (*left*) and PP-EPSCs (*right*) recorded in wildtype (*upper*), *Kcnal*<sup>+/−</sup> (*middle*), and  
943 *Kcna2*<sup>+/−</sup> (*lower*) CA3-PCs at three time points indicated in *Ac* by numbers (1, baseline, *black*; 4, after  
944 conditioning, *blue*; 5, after PP-HFS, *red*). **Ba-Bb.** Mean amplitudes for PP-EPSCs (*Ba*) and PP-EPSPs  
945 (*Bb*) recorded before (*Baseline*) and after (*Primed*) 10 Hz somatic stimulation, and 30 min after weak PP-  
946 HFS (*After HFS*) in the three genotype CA3-PCs. Note that somatic conditioning increased PP-EPSPs  
947 (WT, n = 6, t = -6.086, p = 0.002; *Kcnal*<sup>+/−</sup>, n = 7, t = -3.642, p = 0.022; *Kcna2*<sup>+/−</sup>, n = 5, t = 1.851, p =  
948 0.114; paired t-test) but not EPSCs (WT, t = -0.132, p = 0.900; *Kcnal*<sup>+/−</sup>, t = 0.518, p = 0.632; *Kcna2*<sup>+/−</sup>, t  
949 = 0.302, p = 0.773; paired t-test) in WT and *Kcnal*<sup>+/−</sup>. Neither EPSPs nor EPSCs was altered by  
950 conditioning in *Kcna2*<sup>+/−</sup>. Furthermore, PP-HFS failed the induction of PP-LTP. **C.** Dependence of the  
951 PP-LTP levels on the PP stimulation intensity quantified as the baseline PP-EPSC amplitudes in naïve  
952 (*light-colored*, adopted from Figure 1D) and primed CA3-PCs. Priming was induced by 10 Hz somatic  
953 stimulation. Note that no metaplasticity was induced in *Kcna2*<sup>+/−</sup> CA3-PCs by the priming.  
954

955 *Figure 2-S1*

956 **Figure 2-figure supplement 1.** Both 10 Hz somatic stimulation and 20 Hz MF stimulation lower the  
957 threshold for PP-LTP induction in the rat CA3-PCs. **Aa.** Weak PP-HFS protocol (*black*) and postsynaptic  
958 voltage responses (*red*). The pulse protocol for PP-HFS is the same as in Figure 1. *Right inset* corresponds  
959 to the gray-dashed box on the left. **Ab.** Weak PP-HFS (baseline PP-EPSC < 12 pA) induced no  
960 potentiation of PP-EPSPs. *Insets*, Representative traces for PP-EPSCs (*left*) and PP-EPSPs (*right*) before  
961 (black) and 30 min after HFS (*red*) at PP-CA3 synapses. EPSCs were measured at the start and the end of  
962 EPSP monitoring. **Ac.** Mean amplitude of EPSCs (*left*) and EPSPs (*right*) before and 30 min after PP-  
963 HFS. Under this weak stimulation intensity conditions, the baseline amplitudes for EPSPs and EPSCs of  
964 non-failure events were  $0.92 \pm 0.08$  mV and  $10.24 \pm 1.64$  pA, respectively. No significant change of  
965 EPSCs and EPSPs was induced by weak PP-HFS in the naïve CA3-PCs (EPSP, t = 0.264, p = 0.799, n =  
966 9; EPSCs, t = -0.620, p = 0.555, n = 8; independent t-test, measured at 30 min). **Ba.** Strong PP-HFS

967 protocol. The pulse protocol is the same as the weak version (*Aa*) but higher stimulation intensity. Note  
968 that a burst of APs was elicited by strong HFS in CA3-PCs. **Bb.** Normalized EPSPs monitored at PP-CA3  
969 synapses. *Insets*, Representative PP-EPSC and PP-EPSP traces before (*black*) and 30 min after HFS (*red*).  
970 Both EPSCs and EPSPs became larger after strong PP-HFS. **Bc.** Mean amplitudes of EPSCs (*left*) and  
971 EPSPs (*right*) before (Pre) and 30 min after HFS. Both EPSCs and EPSPs were potentiated by strong PP-  
972 HFS (EPSC,  $n = 5$ ,  $t = -7.312$ ,  $p = 0.002$ ; EPSP,  $n = 5$ ,  $t = -4.133$ ,  $p = 0.014$ ; independent t-test). **Ca.**  
973 Monitoring of PP-EPSCs before and after 20 Hz MF stimulation (*red*) or 10 Hz somatic APs (*blue*) for 2  
974 s, and subsequent weak PP-HFS. Note that EPSCs are not altered by conditioning, but potentiated by  
975 weak PP-HFS. **Cb.** CA3-PCs were primed by induced by consists of MF stimulation at 20 Hz for 2 s  
976 (*upper*) or repetitive somatic firing at 10 Hz for 2 s (*lower*). Each current injection is amplitude of 1200  
977 pA, duration of 2.2 ms. **Cc.** Diagram (*black*) and response (*red*) of weak HFS after the MF stimulation  
978 (*upper*; number of elicited APs for 2 s,  $27.5 \pm 3.44$ ) or somatic firing (*lower*). HFS consisted of 10 bursts  
979 delivered per 10 s, and each bursts consisted of 20 stimuli at 100 Hz (gray-dashed line box of *right*,  
980 corresponded to gray-dashed line box of *left*). This HFS protocol was applied at -60 mV, adjusted in  
981 current-clamp mode. The stimulation intensity of this HFS is sub-threshold, which is insufficient to  
982 induce LTP without conditioning (Refer to the Figure 1). **Cd.** Representative EPSCs (*left*) and EPSPs  
983 (*right*) traces before and after MF (*upper*) or somatic (*lower*) conditioning. *black*, baseline; *blue*, after  
984 conditioning; *red*, after PP-HFS. **Da-Db.** Summary for mean amplitudes of EPSCs (*left*) and EPSPs  
985 (*right*). Note that no change in EPSCs after MF conditioning (*Da*,  $t = -0.725$ ,  $p = 0.492$ ,  $n = 8$ ) and  
986 somatic conditioning (*Db*,  $n = 13$ ,  $t = -0.012$ ,  $p = 0.991$ ; independent t-test), while EPSPs were  
987 potentiated by MF conditioning (*Da*,  $n = 8$ ,  $t = -5.262$ ,  $p = 0.001$ ) and somatic conditioning (*Db*,  $n = 13$ ,  $t$   
988 =  $-9.409$ ,  $p < 0.001$ , independent t-test). Weak PP-HFS subsequent to MF conditioning increased EPSCs  
989 (*Da*,  $n = 8$ ,  $t = -9.027$ ,  $p < 0.001$ ), and EPSPs (*Da*,  $n = 8$ ,  $t = -6.380$ ,  $p < 0.001$ , independent t-test).  
990 Similarly, HFS after somatic conditioning also increased EPSCs (*Db*,  $n = 13$ ,  $t = -9.027$ ,  $p < 0.001$ ) and  
991 EPSPs (*Db*,  $n = 13$ ,  $t = -9.613$ ,  $p < 0.001$ , independent t-test). **Dc.** LTP of PP-EPSCs as a function of PP

992 stimulation intensity quantified as the baseline EPSC amplitude. PP-LTP in CA3-PCs conditioned by MF  
993 (red) or somatic firing (blue) is compared to that in naïve CA3-PCs (gray). Note that the induction  
994 threshold for PP-LTP is lowered by conditioning.

995 *Figure 3*

996 **Figure 3.** Kv1.2 is essential for rapid contextual discrimination. **A.** Protocol for contextual fear  
997 discrimination task. Each of the first 3 days, mice visited context A with receiving a single footshock (2 s,  
998 0.75 mA). Over the subsequent 2 days (Day 4-5), freezing was measured in chamber A and B. During  
999 days 6 to 14, mice daily visited the two context with an hour interval with receiving a shock in A.  
1000 Freezing behavior was assessed during the first 3 min in each context. **Ba.** Kinetics of freezing behavior  
1001 over 5 min test in context A on day 4 and 5. **Bb.** Freezing ratio on day 4 and 5 of WT, *Kcna1*<sup>+/−</sup> and  
1002 *Kcna2*<sup>+/−</sup> mice in context A (gray) and B (red bars). All genotype mice could not discriminate two  
1003 contexts. **Bc.** Daily improvements in discrimination ratio over the phase 3 (day 6 -14) estimated in the  
1004 three genotype mice. **Bd-Be.** Freezing ratio on day 9 (*Bd*) and 14 (*Be*) of three genotype mice in context A  
1005 (gray) and B (red bars). On day 9, comparing the freezing ratio for A vs. B context in each genotype, WT:  
1006  $p < 0.001$ , *Kcna1*<sup>+/−</sup>:  $p < 0.001$ , *Kcna2*<sup>+/−</sup>:  $p = 0.914$  (two-way ANOVA and simple effect analysis). **Ca.**  
1007 Protocol for one-trial contextual fear conditioning, in which the test context C is very distinct from the  
1008 conditioning context A. **Cb.** Freezing ratio of *Kcna2*<sup>+/−</sup> and their littermate *Kcna2*<sup>+/+</sup> mice in context A  
1009 and C measured 24 hours after conditioning in context A with a single 0.75 mA foot shock for 2 s  
1010 (genotype,  $F_{(1,19)} = 0.137$ ,  $p = 0.716$ ; Context,  $F_{(1,19)} = 133.125$ ,  $p < 0.001$ ; genotype  $\times$  context,  $F_{(1,19)} =$   
1011  $0.007$ ,  $p = 0.933$ , two-way ANOVA). **Da.** Protocol for pre-exposure mediated contextual fear conditioning  
1012 (PECFC). **Db.** Freezing levels for context A and C measured 1 day after re-exposure for the context A  
1013 (genotype,  $F_{(1,46)} = 0.286$ ,  $p = 0.596$ ; context,  $F_{(1,46)} = 77.173$ ,  $p < 0.001$ ; shock,  $F_{(1,46)} = 77.173$ ,  $p < 0.001$ ,  
1014 3-way ANOVA). **Ea.** Exemplar traces of WT and *Kcna2*<sup>+/−</sup> mice in the elevated plus maze (EPM) for a 5  
1015 min session. **Eb.** Total distance moved in the EPM for WT (n=5) and *Kcna2*<sup>+/−</sup> (n=10) mice was not  
1016 different significantly ( $t = 0.691$ ,  $p = 0.502$ , independent t-test). **Ec.** The time spent in closed arms ( $t = -$

1017 0.539,  $p = 0.599$ ) and opened arms ( $t = -0.421$ ,  $p = 0.680$ , independent t-test) for each animal were not  
1018 different significantly.

1019

1020 *Figure 3-SI*

1021 **Figure 3-figure supplement 1.** Photographs of contexts A and B. The context A (left) is a chamber  
1022 consisting of a metal grid floor, aluminium side walls, and a clear Plexiglass front door and back wall.  
1023 The context A chamber was lit indirectly with a 12 W light bulb. The context B (right) had the same  
1024 sound noise level, metal grid floor, sidewalls and roof as in context A, but differed from context A in  
1025 having a unique odor (1% acetic acid), dimmer light (50%) and a slanted grid floor by 15° angle.

1026

1027 *Figure 4*

1028 **Figure 4.** Insufficiency of Kv1.2 leads to impaired pattern separation of CA3 neuronal ensembles  
1029 representing two similar contexts. **Aa.** Proportion of H1a(+), Arc(+) and H1a/Arc(+) (*overlap*) cells in the  
1030 CA3 from *WT* (gray) and *Kcna2+/-* (red) mice, which explored the same context A twice with an interval  
1031 of 20 min. On the 1<sup>st</sup> visit, mice received a footshock. **Ab-c.** An exemplar fluorescence image of H1a and  
1032 Arc transcripts in CA3 cells in *WT* (*Ab*) and *Kcna2+/-* (*Ac*) mice. Scale bars, 10  $\mu$ m. **Ba.** Protocol for  
1033 modified contextual fear discrimination (CFD) test. For first 3 days, mice daily visited two similar  
1034 contexts with 20 min interval with receiving a footshock always in context A. Mice were assessed for  
1035 freezing for first 3 min after being placed in each context. On day 4, mice were allowed to freely explore  
1036 the context A or B for 4 min (epoch 1). After a 20 min rest period in the home cage, mice were exposed to  
1037 other context for 4 min (epoch 2). In 5 min after epoch 2, mice were killed for catFISH. **Bb-Bc.** Freezing  
1038 ratio of mice in context A (Bb) and B (Bc) over 4 days, during which mice underwent the modified CFD  
1039 test. WT and *Kcna1+/-* mice began to discriminate two contexts in day 3, but *Kcna2+/-* mice could not  
1040 even on day 4. **C.** Representative confocal images of *H1a* and *Arc* transcripts in nuclei (*blue*,

1041 counterstained with DAPI) of the CA3 pyramidal layer from WT (*Ca*), *Kcna1+/-* (*Cb*), and *Kcna2+/-* (*Cc*) mice. Nuclei expressing H1a alone, Arc alone, and both are indicated by green, red, and yellow arrowheads, respectively. *H1a* (green dots) and *Arc* (red) intra-nuclear foci are activated during epoch 1 and 2, respectively. Scale bars, 10  $\mu$ m. **Da.** Size of neuronal ensembles in CA3 activated in context A and B quantified as percentage of H1a(+) or Arc(+) cells among total cells in the CA3 pyramidal layer of each slice. The fraction of CA3 cells active in both of contexts A and B (denoted as A $\cap$ B) was not different between WT and *Kcna1+/-* mice, but higher in *Kcna2+/-* than other genotypes. The size of neuronal ensembles in *Kcna2+/-* was larger than that in WT and *Kcna1+/-*. **Db.** The conditional probability for ensemble cells active in context A among those active in context B [denoted as P(A|B)]. For comparison, conditional probability for re-activation of WT ensemble cells of the 1<sup>st</sup> visit of context A (A<sub>1</sub>) among ensemble cells of the 2<sup>nd</sup> visit (A<sub>2</sub>) [P(A<sub>1</sub>|A<sub>2</sub>)] is shown as WT(AA) and *Kcna2+/-*(AA). **Dc.** Cumulative probability histogram of the P(A|B) values for different genotypes. The overlap index between two ensembles in *Kcna2+/-* mice was significantly greater than that in *Kcna1+/-* or WT mice.

1054

1055 *Figure 4-S1*

1056 **Figure 4-figure supplement 1.** Test for non-specific expression of H1a and Arc INF. **A-B.** To evaluate  
1057 non-specific expression of H1a and Arc transcripts, catFISH for H1a (*A*) and Arc (*B*) mRNA was  
1058 performed at 5 min and at 30 min, respectively, after the mice being placed in a novel context (context A)  
1059 with a footshock. Scale bars, 30  $\mu$ m. **C.** catFISH image reproduced from Figure 4Aa for comparison.  
1060 Green and red arrowheads indicate H1a and Arc INF. **D.** Mean fractions of H1a and Arc-positive nuclei,  
1061 when each was detected at 5 or 30 min after the mice were exposed to a novel context. Note that most  
1062 nuclei were negative for H1a and Arc INF, when H1a and Arc mRNA were stained at 5 and 30 min after  
1063 the mice visited a novel context (H1a INF:  $7.34 \pm 0.49\%$  at 30 min,  $0.54 \pm 0.01\%$  for 5 min, Mann-  
1064 Whitney U = 0.00, p = 0.004, n = 4; Arc INF:  $7.21 \pm 0.37\%$  at 5 min,  $0.60 \pm 0.02\%$  for 30 min, Mann-

1065 Whitney U = 0.00, p = 0.004, n = 4).

1066

1067 *Figure 4-S2*

1068 **Figure 4-figure supplement 2. A-B,** Representative fluorescence images of c-fos in the dorsal  
1069 hippocampi from WT mice, which have been handled for a week. On day 8, the mice were killed  
1070 immediately from their home cage (A) or 30 min after being placed in a novel context (context A) with a  
1071 footshock (B), and then their hippocampi underwent immunostaining for c-fos (green) with DAPI  
1072 counterstaining of nuclei (blue). Antibody targeting c-fos and DAPI were purchased from Cell Signaling  
1073 (Cat# 2250, USA) and Sigma-Aldrich (St Louis, MO, USA), respectively. **C,** Proportions of c-fos(+)  
1074 nuclei in the CA3 area of mice from homecage (n = 4) and those from context A (n = 5 slices, two mice  
1075 for each).

1076

1077 *Figure 5*

1078 **Figure 5.** Changes in CA3 ensembles over training days of CFD task in WT and *Kcna2+/-* mice. **A.**  
1079 Experimental procedures for catFISH of CA3 ensembles during training phase (Day 1 and 2), when mice  
1080 do not discriminate the two contexts A and B. **B.** Representative confocal images of *H1a* and *Arc*  
1081 transcripts in nuclei (blue, counterstained with DAPI) of the CA3 pyramidal layer from WT and *Kcna2+/-*  
1082 mice in day 1 (Ba, WT; Bb, *Kcna2+/-*), day 2 (Bc, WT; Bd, *Kcna2+/-*). Nuclei expressing *H1a* alone, *Arc*  
1083 alone, and both are indicated by green, red, and yellow arrowheads, respectively. **Ca.** Neuronal ensemble  
1084 size activated by exposure of mice to context A and B on each day. Because there was no statistical  
1085 difference in the fraction of *H1a*(+) and *Arc*(+) cells in the same slice, the ensemble size was quantified as  
1086 the averaged percentage of *H1a*(+) or *Arc*(+) cells among total cells in the CA3 pyramidal layer. Note that  
1087 the CA3 ensemble size in *Kcna2+/-* mice (red) grew larger over training days compared to that in WT  
1088 (gray). **Cb.** The fraction of CA3 cells activated in both contexts (denoted as A $\cap$ B) over training days. The

1089 fraction of A $\cap$ B cells in *Kcna2*<sup>+/−</sup> mice (red) increased over days, whereas that in WT (gray) decreased.  
1090 Compared to day 1, for WT, day 2: p = 0.457, day 4: p = 0.017. For *Kcna2*<sup>+/−</sup>, day 2: p = 0.025, day 4: p  
1091 < 0.001 (two-way ANOVA, simple effect analysis). **Cc.** The conditional probability for ensemble cells  
1092 active in context A among those active in context B [denoted as P(A|B)]. The P(A|B) for WT mice  
1093 decreased over days, but that for *Kcna2*<sup>+/−</sup> mice did not. Compared to day1, for WT, day 2: p = 0.005,  
1094 day 4: p < 0.001. For *Kcna2*<sup>+/−</sup>, day 2: p = 0.678, day 4, p = 0.816 (two-way ANOVA, simple effect  
1095 analysis). **Cd.** Cumulative curves for P(A|B) on each day. The overlap index [P(A|B)] in *Kcna2*<sup>+/−</sup> mice  
1096 were not different from that in WT on D1. The overlap index curves of WT shifted to the left over training  
1097 days, but those of *Kcna2*<sup>+/−</sup> mice did not.

1098

1099 *Figure 6*

1100 **Figure 6.** Generation of CA3 region-specific *Kcna2* hetero-knockout mice. **A-B.** Confocal *Kcna2* FISH  
1101 images of dorsal hippocampi from *CA3-Kcna2*<sup>+/−</sup> (A) and *f-Kcna2* mice (*f-Kcna2*, B). *Kcna2*  
1102 transcripts were hybridized using the RNAscope probe, and visualized as green fluorescent dots. Nuclei  
1103 were counterstained with DAPI (blue). Scale bars, 200  $\mu$ m. The boxed regions [*a*, medial entorhinal  
1104 cortex (MEC); *b*, DG; *c*, CA3; *d*, CA1] in each of hippocampal figures were imaged at high magnification  
1105 (60 x), in which the number of red dots were counted. A part of each magnified image is shown on the  
1106 below (scale bars, 10  $\mu$ m). **C.** In MEC, DG and CA1, ratio of the number of *Kcna2* mRNA particles to  
1107 the number of nuclei were not significantly different between *f-Kcna2* mice and *CA3-Kcna2*<sup>+/−</sup> mice  
1108 (MEC, Mann-Whittney U = 7.00, p = 0.251; DG, U = 12.00, p = 0.917; CA1, U = 8.00, p = 0.347, n = 5).  
1109 In CA3, however, the mRNA ratio was decreased by c.a. 60% in *CA3-Kcna2*  $\pm$  mice compared to the *f-*  
1110 *Kcna2* mice (n = 4, U = 0.00, p = 0.009). **Da.** Representative traces for D-type K<sup>+</sup> currents ( $I_{K(D)}$ ) was  
1111 obtained by the arithmetical subtraction of outward potassium currents ( $I_K$ ) under the bath application of  
1112 30  $\mu$ M 4-AP from the total  $I_K$  elicited by a depolarizing step to -20 (red), -30 (blue), and -40 (black) mV  
1113 from -70 mV in the *f-Kcna2* (left) and *CA3-Kcna2*<sup>+/−</sup> (right) CA3-PCs. **Db.** Mean values for peak

1114 amplitudes of  $I_{K(D)}$  induced by a step depolarization to  $-20$ ,  $-30$  and  $-40$  mV for *f-Kcna2* (gray) and *CA3-Kcna2+/-* (red) CA3-PCs.

1116

1117 Figure 6-S1

1118 **Figure 6-Figure Supplement 1.** Short-term plasticity of PP and MF-CA3 synapses. **Aa, Ba and Ca**,  
1119 Representative traces for EPSCs evoked by 20 (*Aa*) or 50 Hz (*Ba*) PP stimulation and 50 Hz MF  
1120 stimulation (*Ca*) in CA3-PCs of *f-Kcna2* (black), *CA3-Kcna2+/-* (blue), *Kcna1+/-* (green), and *Kcna2+/-*  
1121 (red) mice. **Ab, Bb and Cb**, Relative amplitudes of EPSC trains normalized to the 1<sup>st</sup> EPSC evoked by 20  
1122 Hz (*Ab*) or 50 Hz (*Bb*) PP stimulation or 50 Hz MF stimulation (*Cb*). **Ac, Bc and Cc**, Mean amplitude of  
1123 the 1<sup>st</sup> EPSCs in different genotypes. No significant difference in the 1<sup>st</sup> EPSC amplitudes between  
1124 genotypes, because the afferent fiber stimulation intensity was adjusted such that the 1<sup>st</sup> EPSC amplitude  
1125 falls within a narrow range. wt, *f-Kcna2*; n.s., statistically not significant.

1126

1127 Figure 7

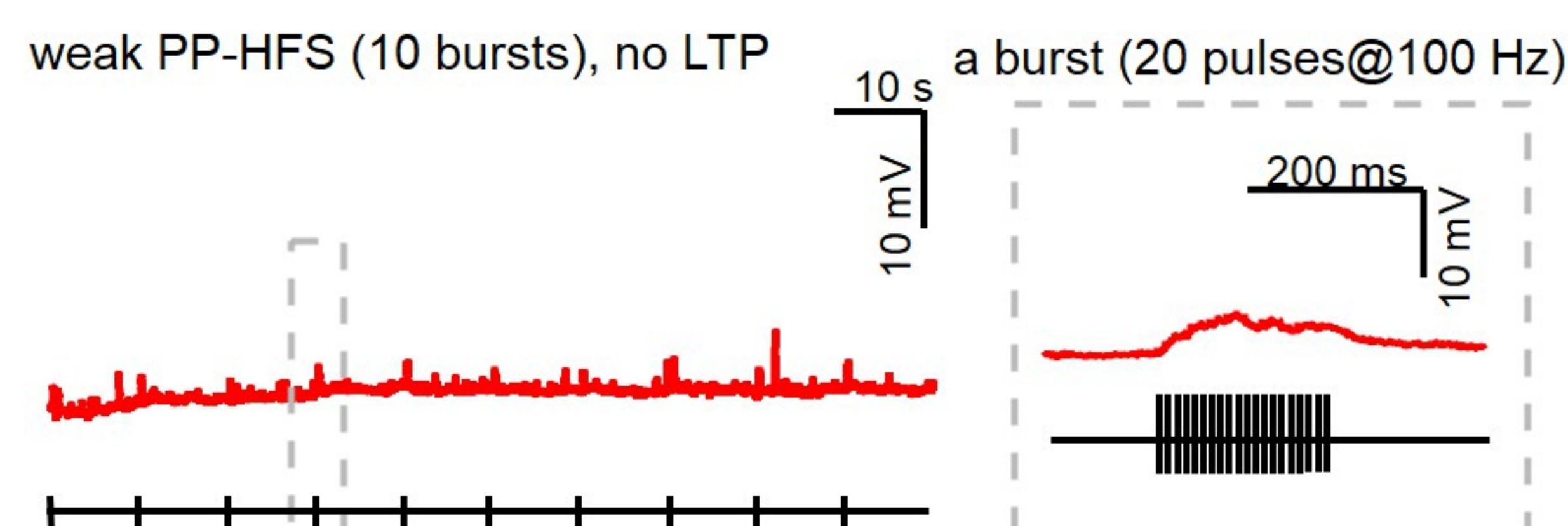
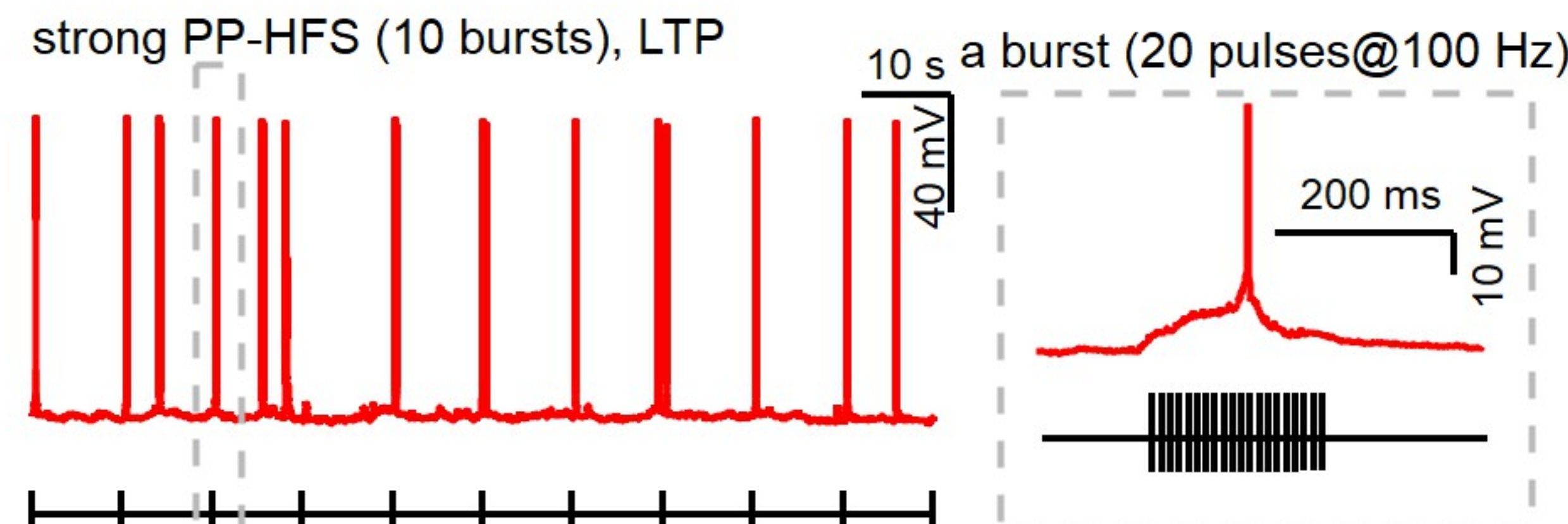
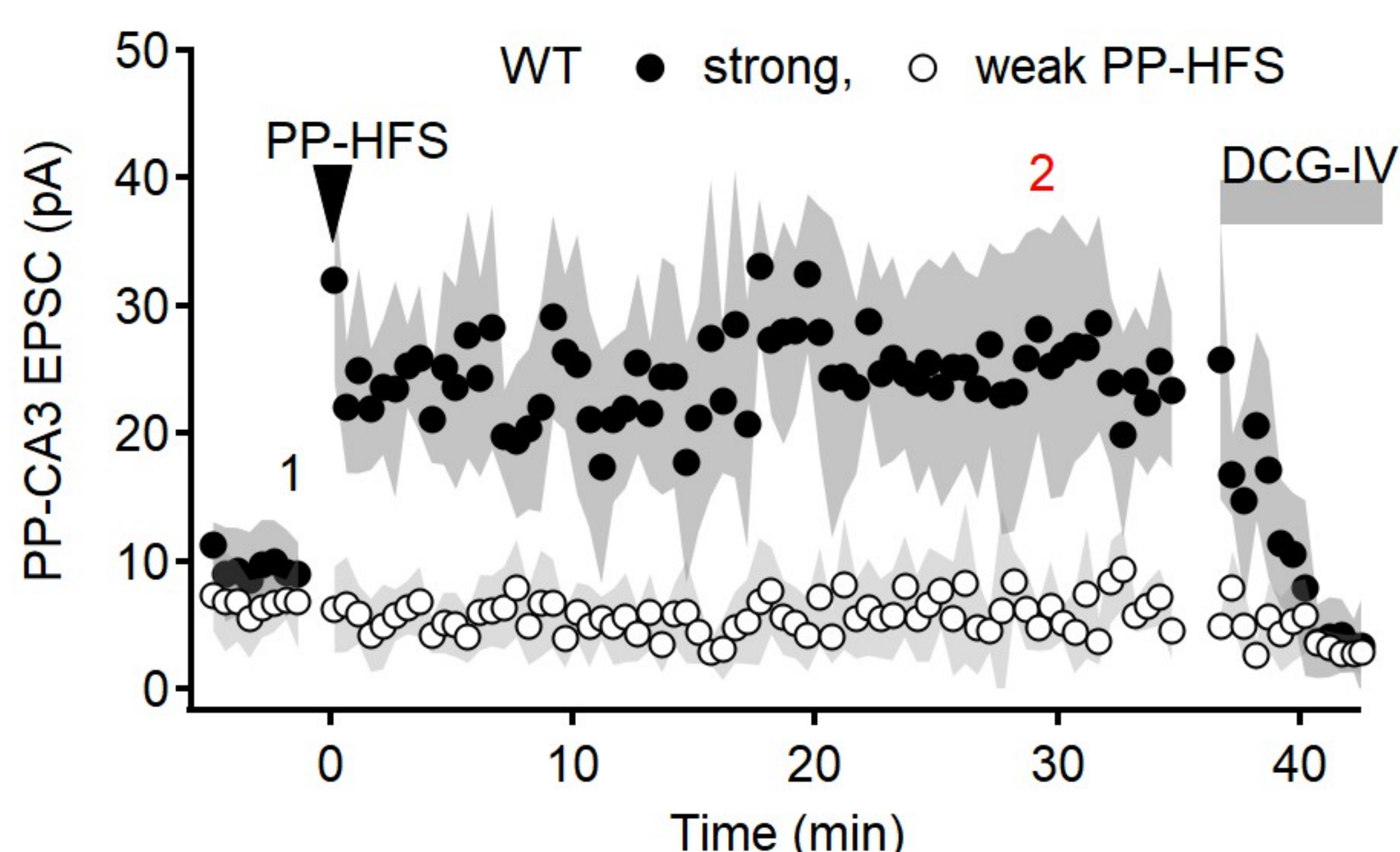
1128 **Figure 7.** CA3 region-specific *Kcna2* *+/-* mice lacks MF-induced LTP-IE. **Aa.** MF conditioning (20 Hz  
1129 MF stimulation, *blue arrowhead*) induced a decrease in input conductance ( $G_{in}$ ) in *f-Kcna2* (gray), but not  
1130 in *CA3-Kcna2+/-* (blue) and *Kcna2+/-* (red) CA3-PCs. *Insets:* Representative traces for postsynaptic  
1131 response to 20 Hz MF stimulation (*blue trace in the main figure*) and voltage responses to subthreshold  
1132 current injections (+10/-30 pA, *upper*). **Ab-Ac.** Mean values for baseline (gray) and post-conditioning  
1133 (red) input conductance (*Ab*) and first AP latency (*Ac*).  $G_{in}$  and first AP latency were measured in the  
1134 same way as in Figure 1B. The baseline  $G_{in}$  and first AP latency of *CA3-Kcna2+/-* CA3-PCs (n=6) were  
1135 lower than that of *f-Kcna2* (n=6), and the same as that of *Kcna2+/-* (n=14). (For  $G_{in}$ ,  $F_{(2,24)} = 6.036$ ,  $p =$   
1136 0.008; *f-Kcna2* vs. *CA3-Kcna2+/-*,  $p = 0.045$ ; *f-Kcna2* vs. *Kcna2+/-*,  $p = 0.008$ ; *CA3-Kcna2+/-* vs.  
1137 *Kcna2+/-*,  $p = 1.00$ ; For AP latency,  $F_{(2,28)} = 5.714$ ,  $p = 0.017$ ; *f-Kcna2* vs. *Kcna2+/-*,  $p = 0.112$ ; *CA3-*

1138 *Kcna2*<sup>+/−</sup> vs. *f-Kcna2*,  $p = 0.019$ ; CA3-*kcn2*<sup>+/−</sup> vs. *Kcna2*<sup>+/−</sup>,  $p = 1.00$ ; one-way ANOVA and  
1139 Bonferroni post-hoc test). **Ba.** MF conditioning-induced heterosynaptic potentiation of PP-EPSPs in *f-*  
1140 *Kcna2* (gray), CA3-*Kcna2*<sup>+/−</sup> (blue), and *Kcna2*<sup>+/−</sup> (red) CA3-PCs. *Insets:* Representative traces for PP-  
1141 EPSPs (*left*) and PP-EPSCs (*right*) before (*black*) and after MF conditioning. The color codes for post-  
1142 conditioning traces are same as the main figure. **Bb.** Amplitude of PP-EPSPs before (gray) and after (red)  
1143 MF conditioning induced heterosynaptic potentiation of PP-EPSP in *f-Kcna2* ( $n=5$ ), but  
1144 not in CA3-*Kcna2*<sup>+/−</sup> ( $n=6$ ) and *Kcna2*<sup>+/−</sup> ( $n=8$ ) CA3-PCs. **Bc.** Mean amplitude of PP-EPSCs was not  
1145 altered before and after MF conditioning (*f-Kcna2*,  $t = -0.451$ ,  $p = 0.675$ ; CA3-*Kcna2*<sup>+/−</sup>,  $t = 0.500$ ,  $p =$   
1146 0.638; *Kcna2*<sup>+/−</sup>,  $t = 0.518$ ,  $p = 0.632$ , paired t-test). **Ca** and **Cb.** The number of APs elicited by 20 Hz / 2  
1147 s MF stimulation (*Ca*) and MF stimulation required to elicit the 1st AP (*Cb*) as a function of baseline MF-  
1148 EPSC amplitude for *f-Kcna2* (black), CA3-*Kcna2*<sup>+/−</sup> (blue) and *Kcna2*<sup>+/−</sup> (red). No statistical difference  
1149 was found between genotypes in AP numbers (*Ca*,  $F_{(2,19)} = 0.294$ ,  $p = 0.749$ , one-way ANOVA) and MF  
1150 stimulation numbers (*Cb*,  $F_{(2,19)} = 0.864$ ,  $p = 0.439$ , one-way ANOVA). **Cc.** Representative EPSP traces  
1151 evoked by 20 Hz MF stimulation during which the first AP was evoked in the three genotype CA3-PCs.  
1152

1153 *Figure 8*

1154 **Figure 8.** Kv1.2 expressed in CA3-PCs is essential for rapid contextual discrimination. **Aa.** Kinetics of  
1155 freezing behaviour over 5 min in context A on day 4-5. **Ab.** On day 4 and 5, all genotype mice could not  
1156 discriminate the two contexts A and B. **Ba.** WT, *f-Kcna2* and AAVgfp-injected mice showed significantly  
1157 earlier rise in the discrimination ratio than CA3-*Kcna2*<sup>+/−</sup>, *Kcna2*<sup>+/−</sup> and , AAVcre-injected mice over the  
1158 day 6 to 14 (WT vs. *f-Kcna2*,  $p = 1.00$ ; WT vs. AAV-GFP injected,  $p = 1.00$ ; WT vs. CA3-*Kcna2*<sup>+/−</sup>,  $p <$   
1159 0.001; WT vs. *Kcna2*<sup>+/−</sup>,  $p < 0.001$ ; WT vs. AAVcre-injected:  $p < 0.001$ ; *f-Kcna2* vs. CA3-*Kcna2*<sup>+/−</sup>  $p <$   
1160 0.012; CA3-*Kcna2*<sup>+/−</sup> vs *Kcna2*<sup>+/−</sup>,  $p = 1.00$ ; AAVgfp vs. AAVcre:  $p = 0.036$ ; RM-ANOVA and  
1161 Bonferroni post hoc test). **Bb.** On day 9, WT, *f-Kcna2* and AAVgfp-injected mice discriminated the two  
1162 similar contexts, whereas CA3-*Kcna2*<sup>+/−</sup> and AAVcre-injected mice still could not. Comparing the

1163 freezing ratio for A vs B in each genotype, WT:  $p < 0.001$ ,  $fKcna2$ :  $p < 0.001$ , CA3- $Kcna2^{+/-}$ :  $p = 0.185$ ,  
1164  $Kcna2^{+/-}$ :  $p = 0.899$ , AAVcre:  $p = 0.446$ , AAVgfp:  $p < 0.001$  (two-way ANOVA, simple effect analysis).  
1165 **Bc.** On day 14, initial discrimination deficit for CA3- $Kcna2^{+/-}$  was rescued by repetitive training. **C-D**,  
1166 IR-DIC (*Ca* and *Da*, left) and epifluorescence images (right, excited by 488 or 588 nm for GFP or  
1167 mCherry, respectively) of the hippocampi from the AAVcre-injected (*Ca*) or AAVgrp-injected (*Da*) mice.  
1168 Corresponding magnified IR-DIC (*Cb* and *Db*, upper) and epifluorescence images (lower). **Ea-b**,  $I_{K(D)}$  in  
1169 GFP(+) and mCherry(+) CA3-PCs from acute slices prepared from AAVgfp-injected and AAVcre-  
1170 injected mice, respectively.  $I_{K(D)}$  (lower, red) was obtained from difference in the  $K^+$  outward current  
1171 activated by a depolarizing step to -20 mV from -70 mV before (upper left, black) and after the bath  
1172 application of 30  $\mu$ M 4-AP (upper right, gray) in CA3-PCs of AAVgfp-injected (*Ea*) and AAVcre-injected  
1173 (*Eb*) mice. **Ec**, Mean values for peak amplitudes of  $I_{K(D)}$ .

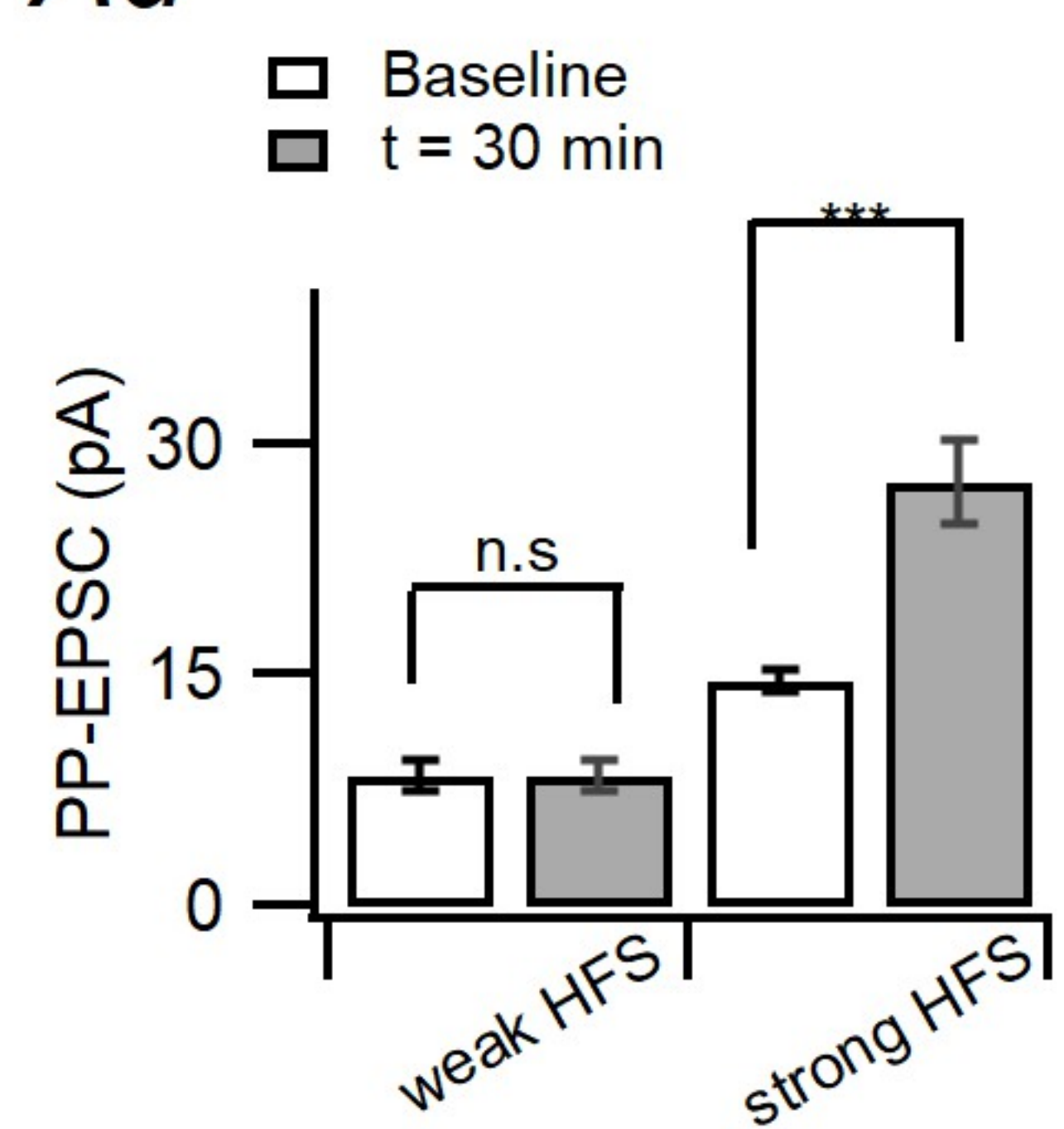
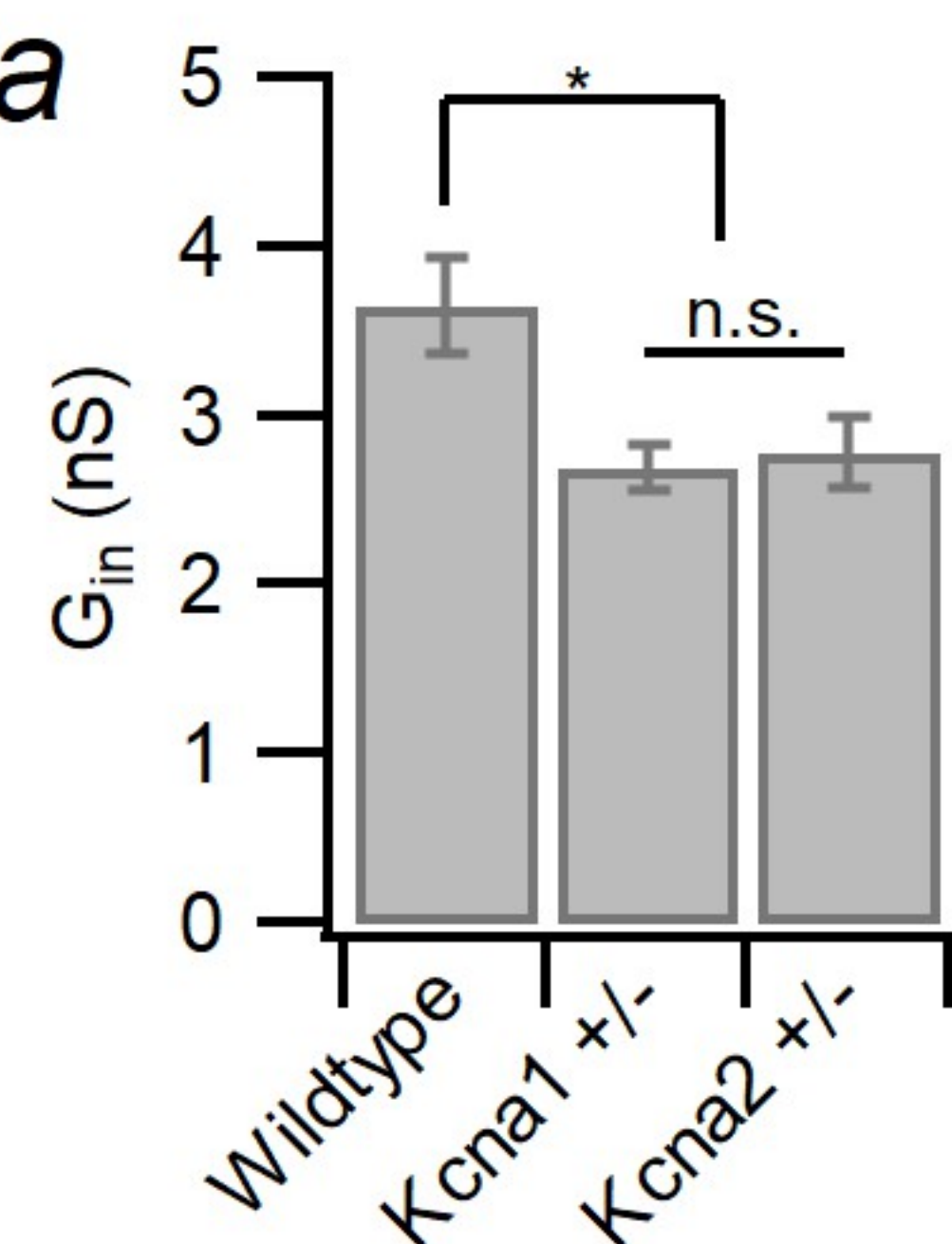
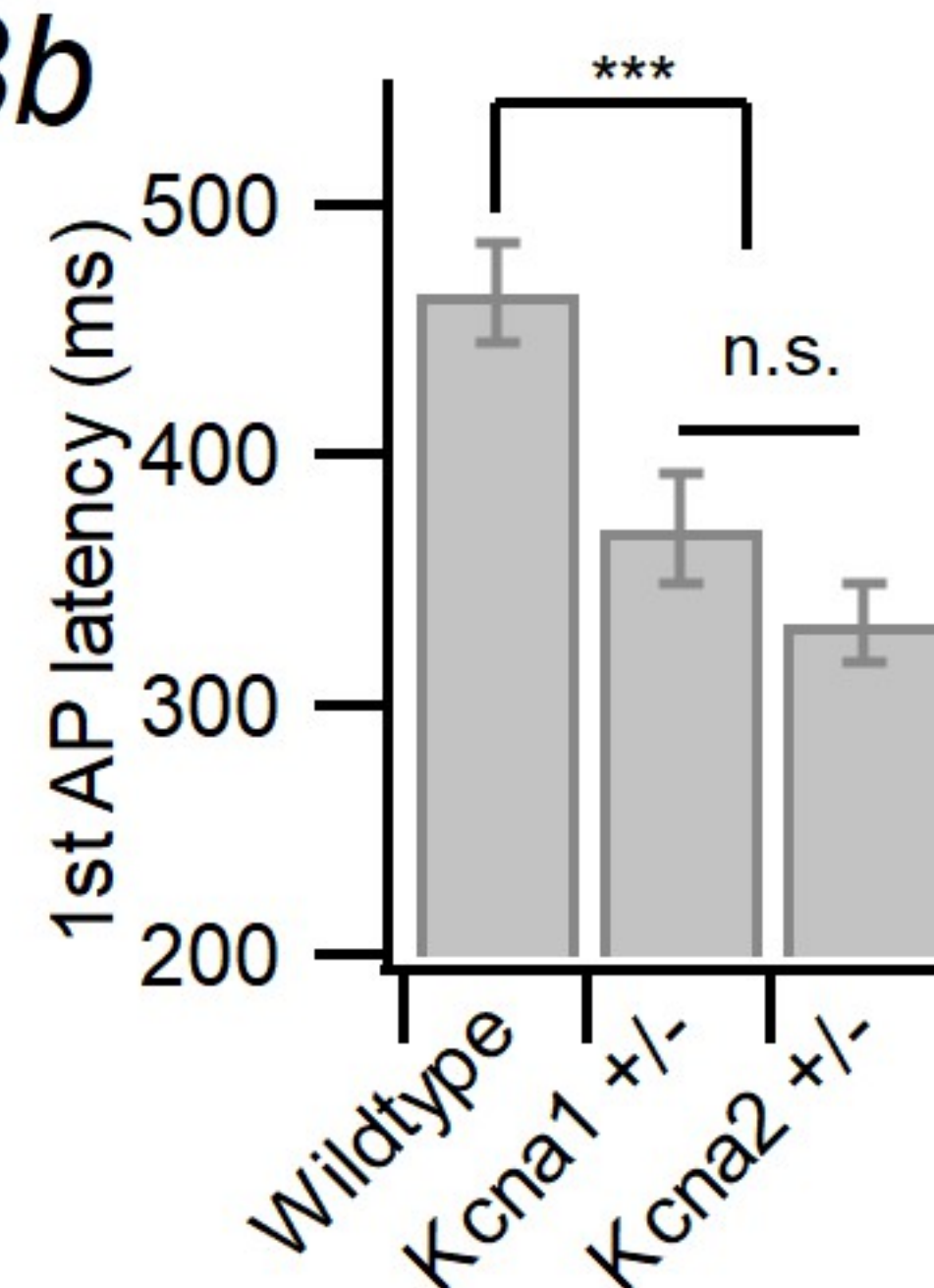
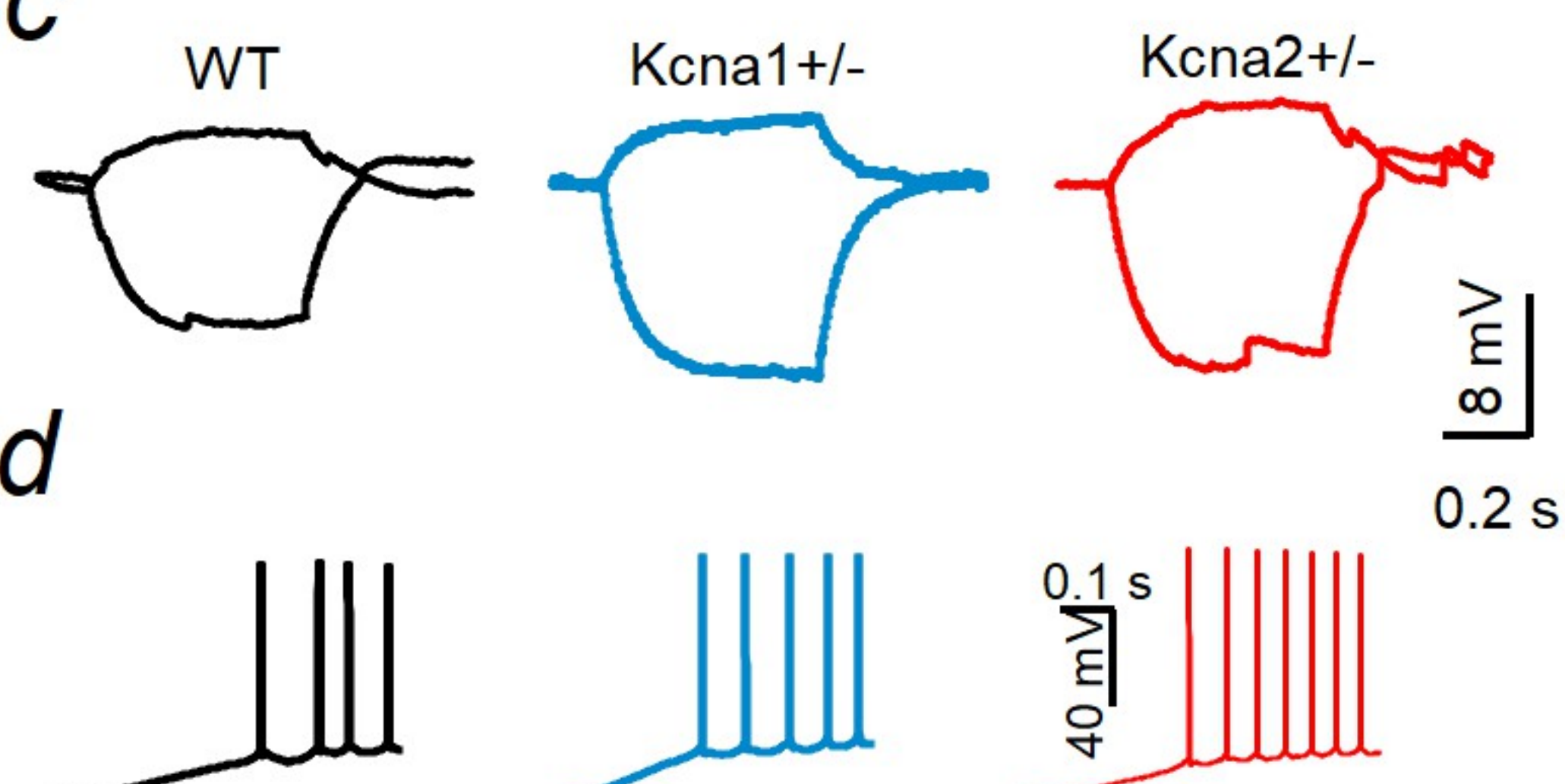
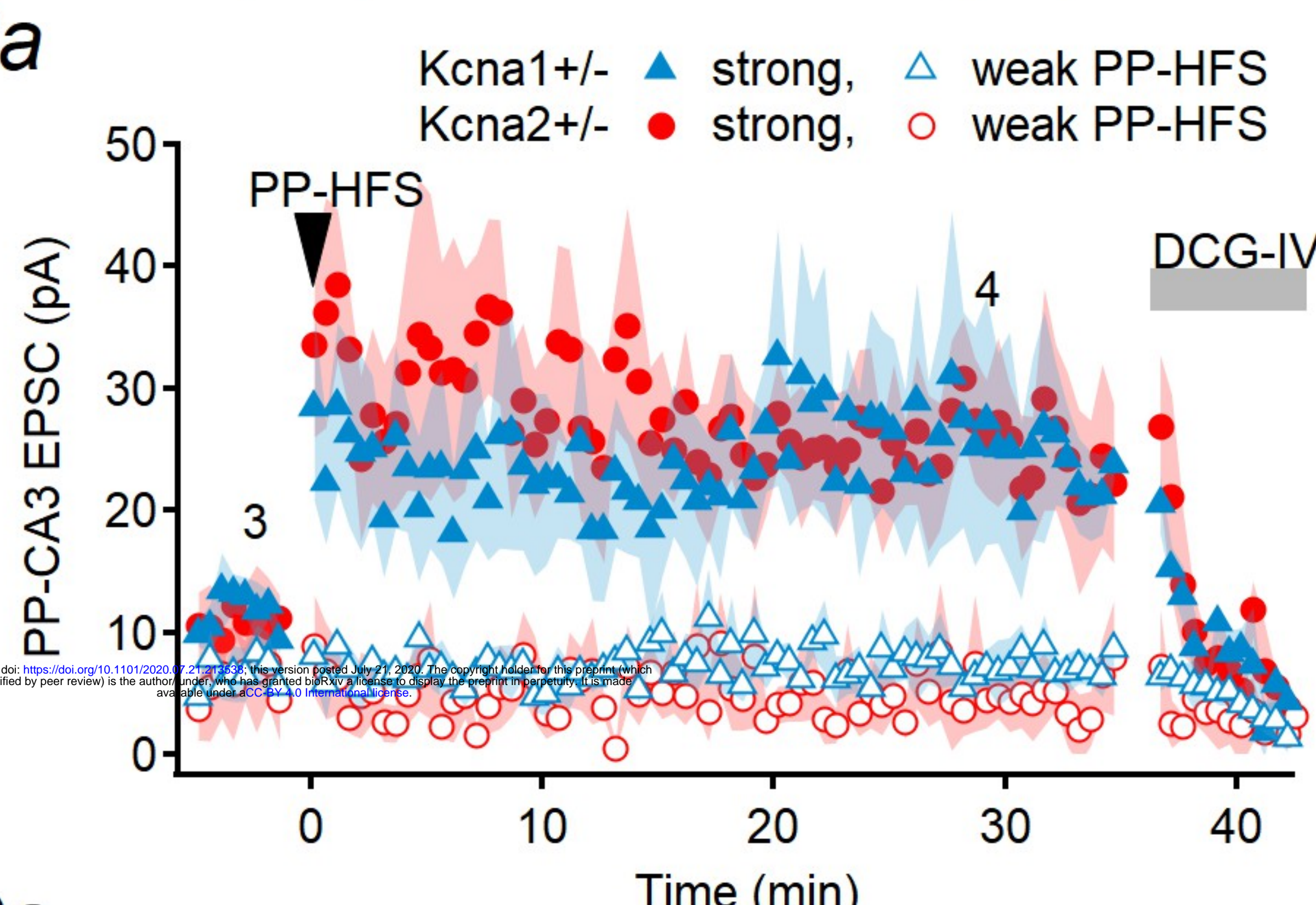
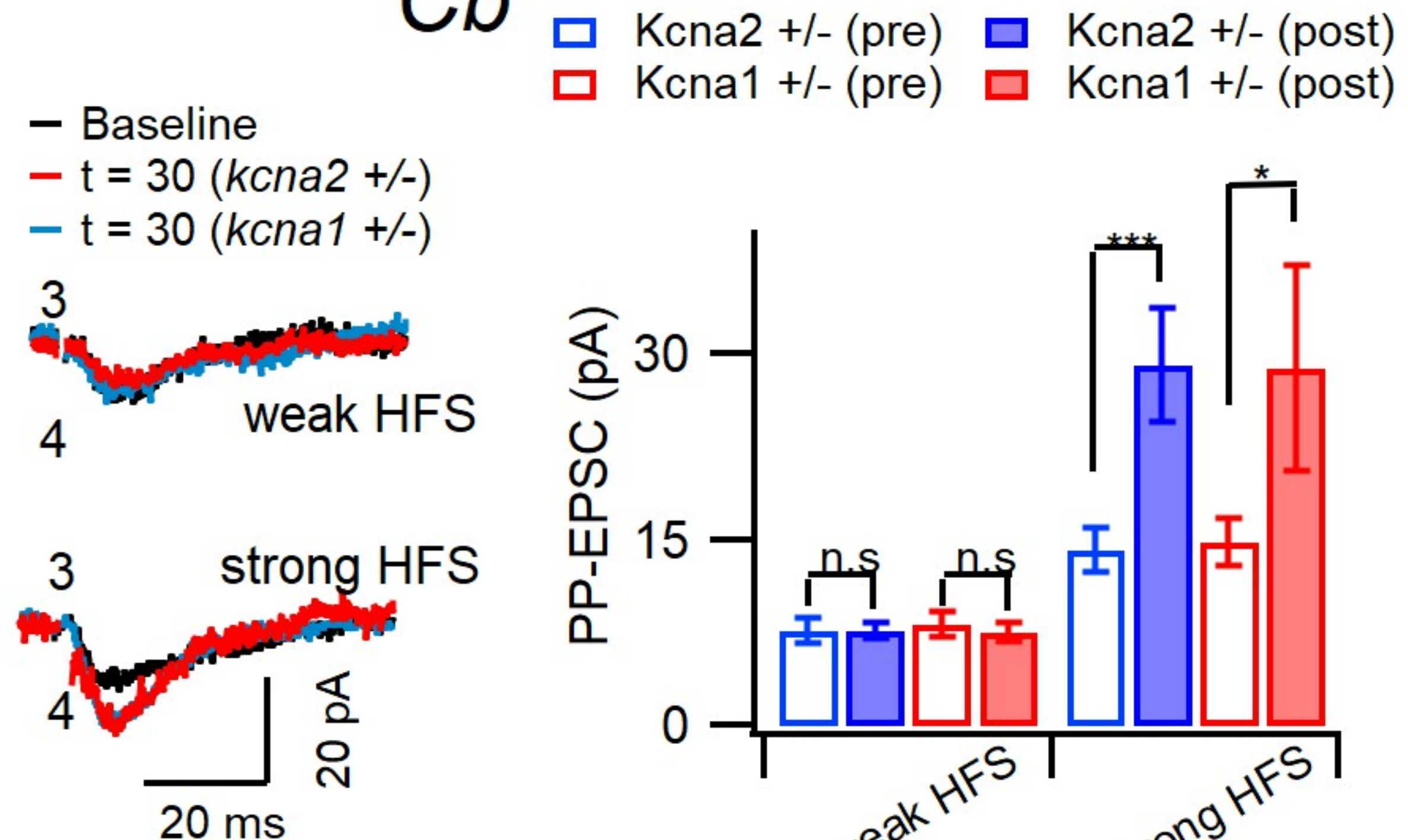
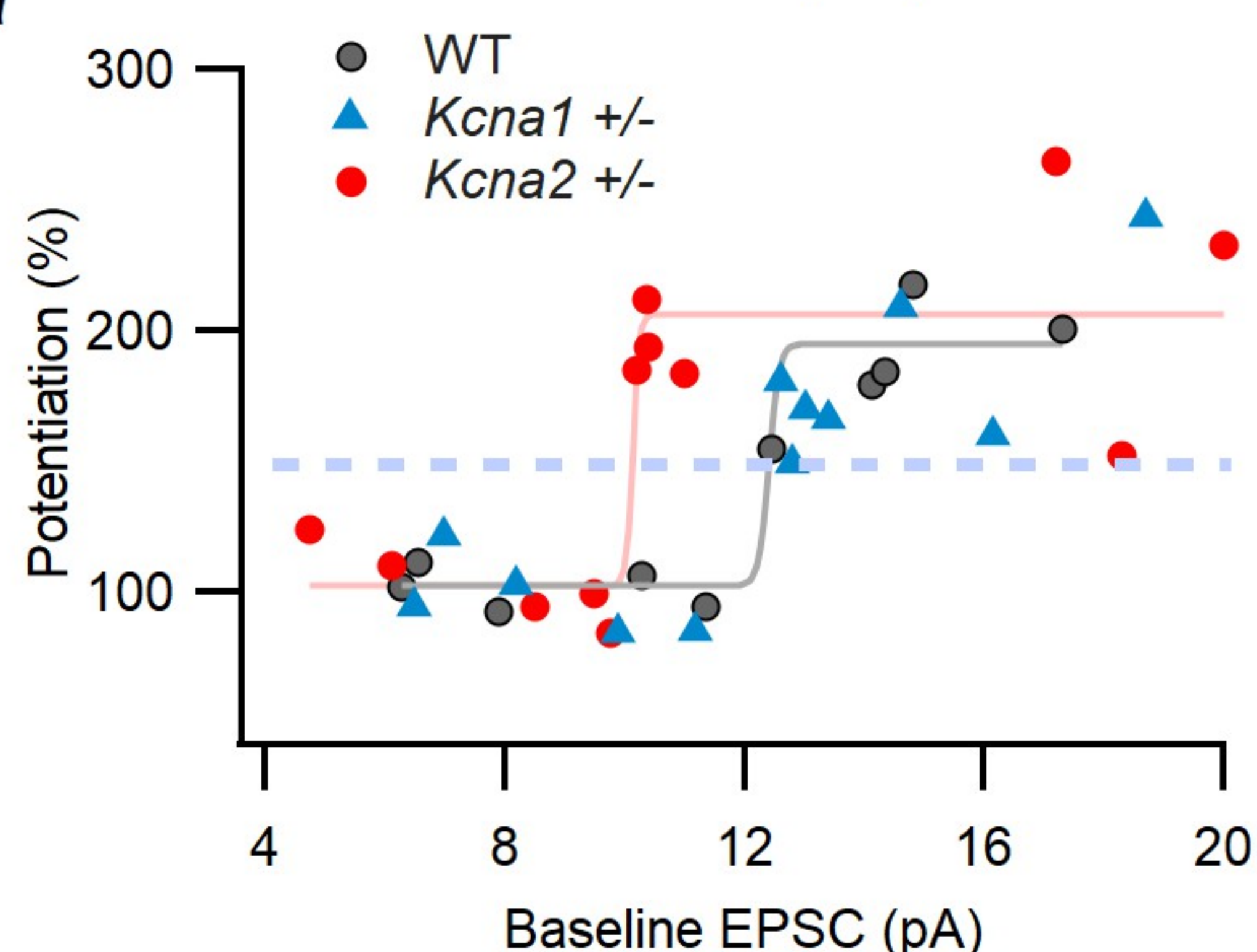
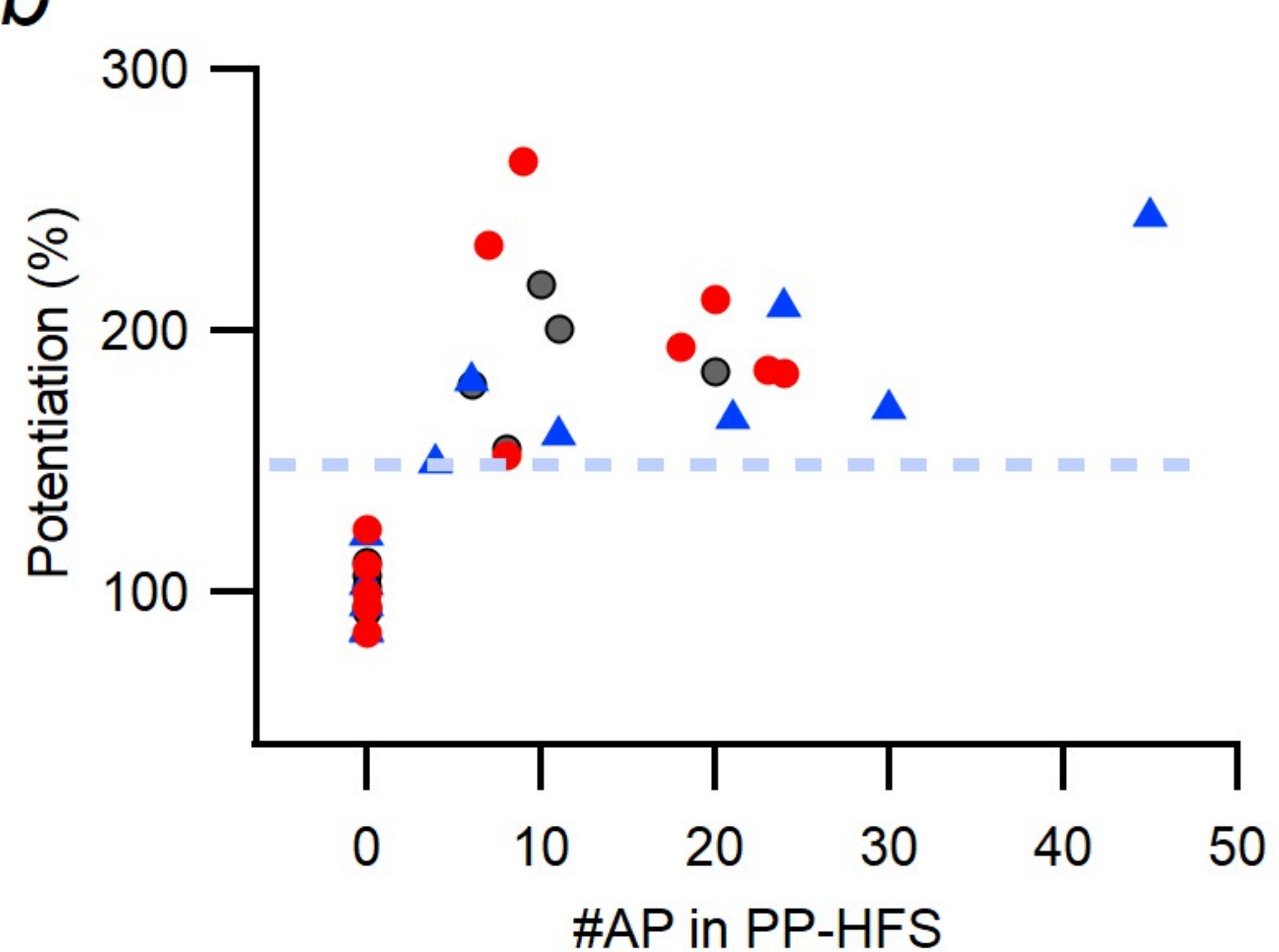
**Aa****Ab****Ac**

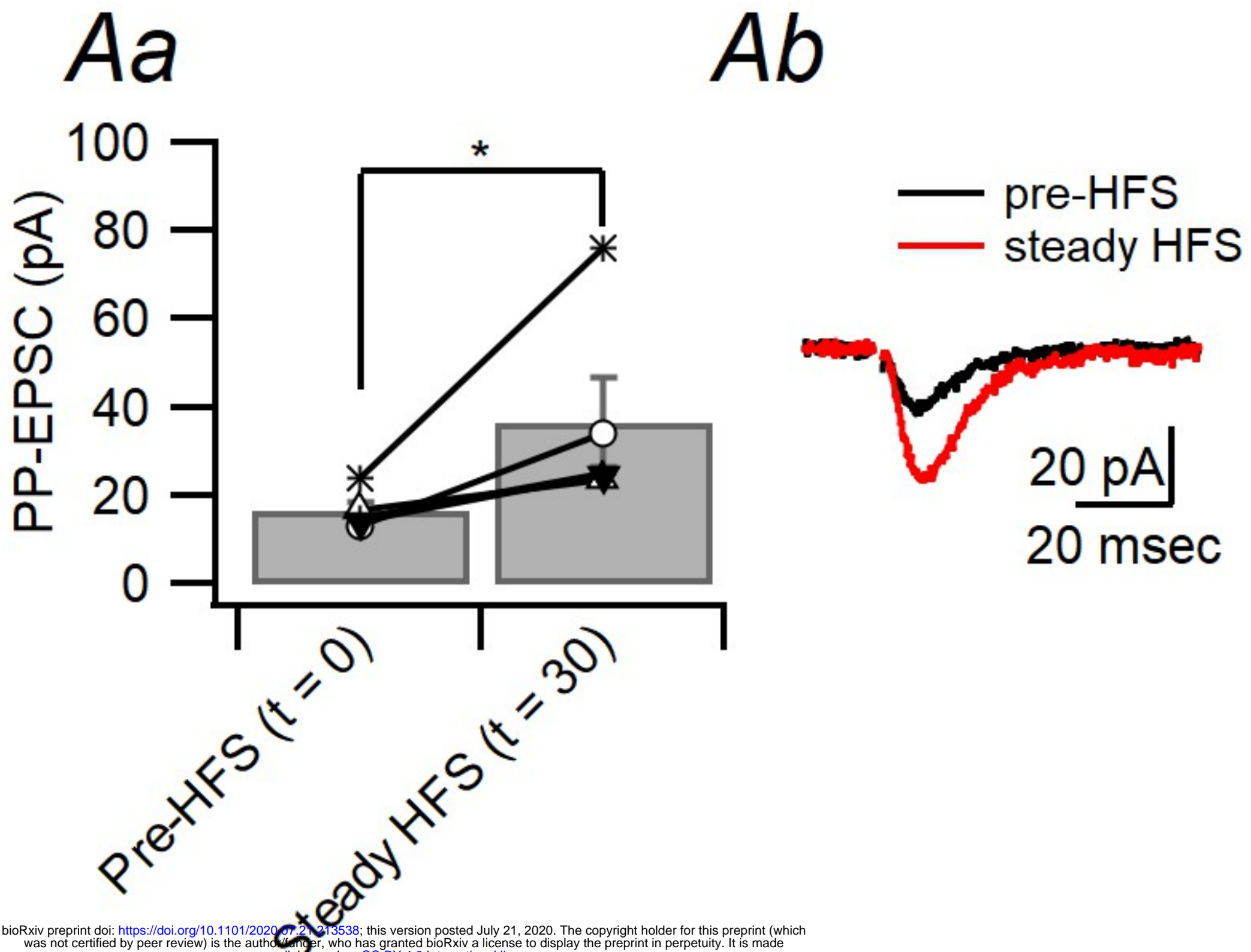
— Baseline  
—  $t = 30$  (no LTP)

1 weak HFS

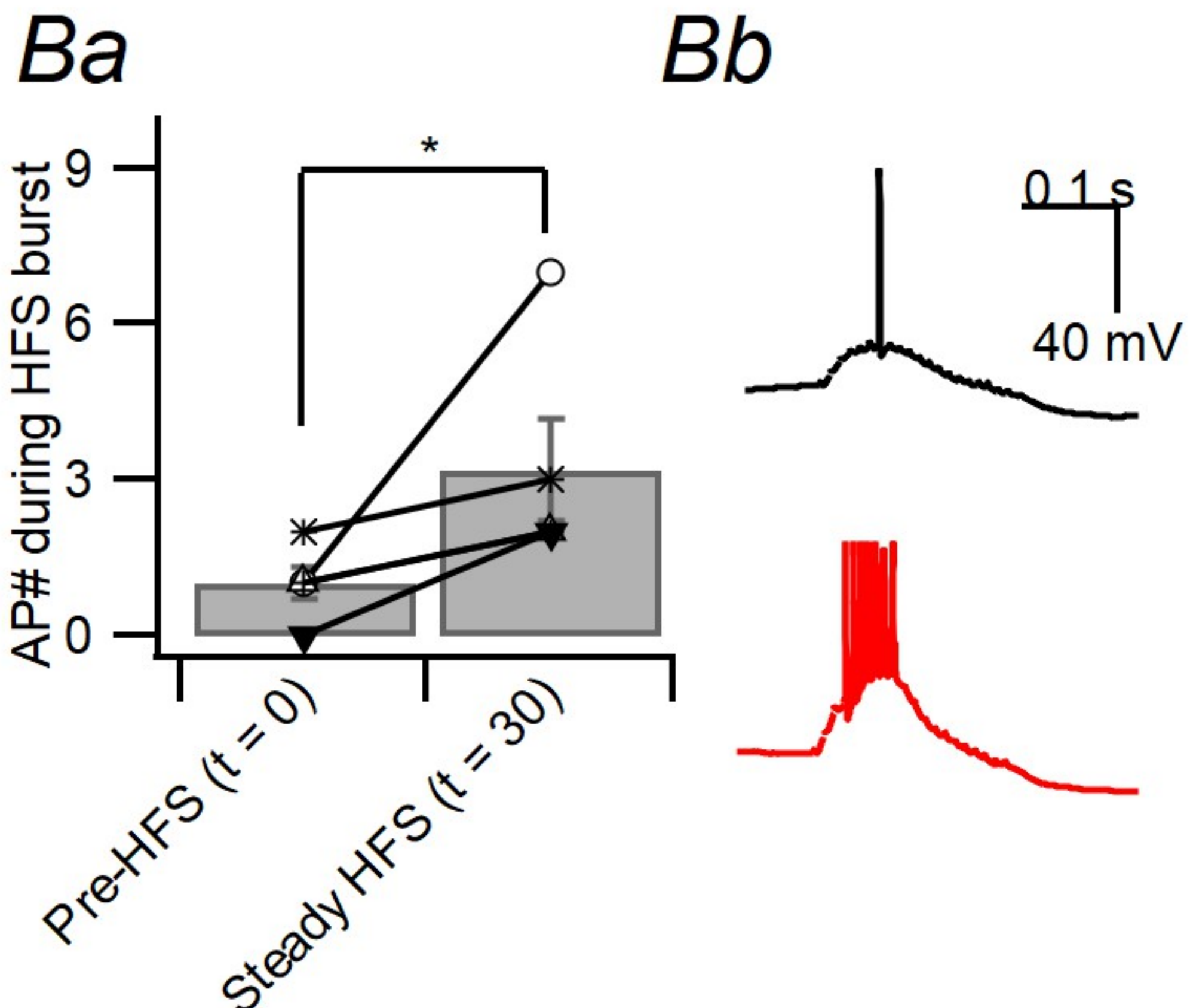
1 strong HFS

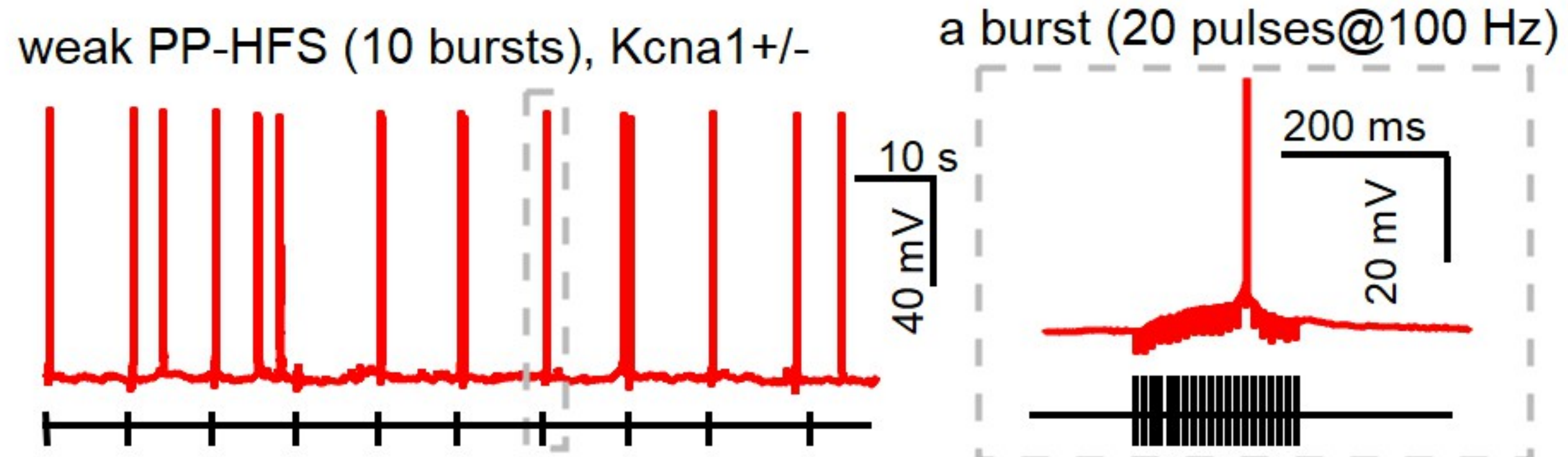
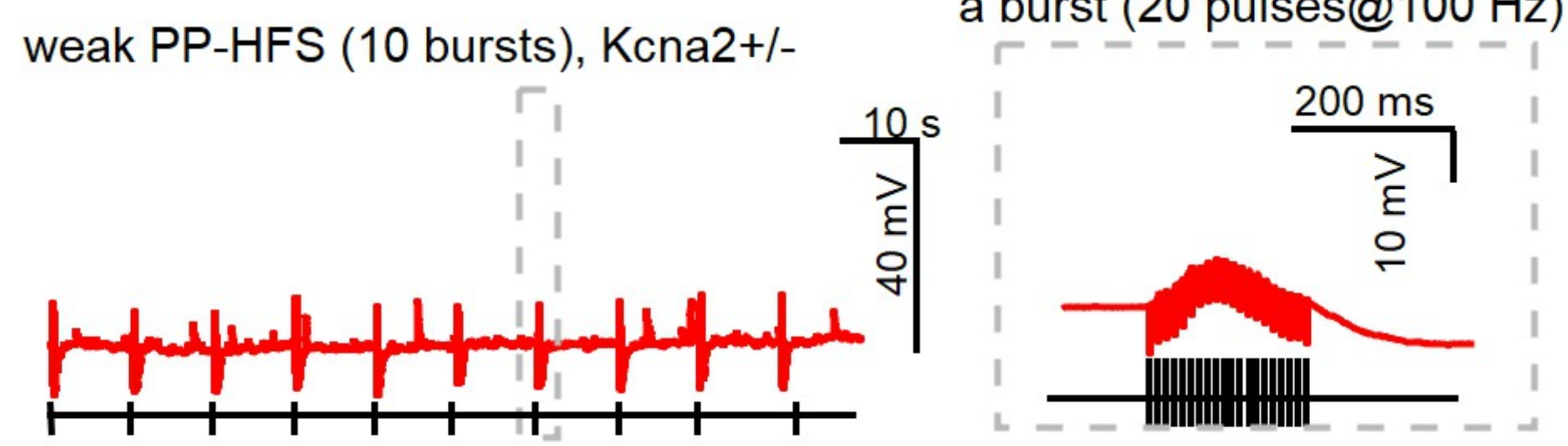
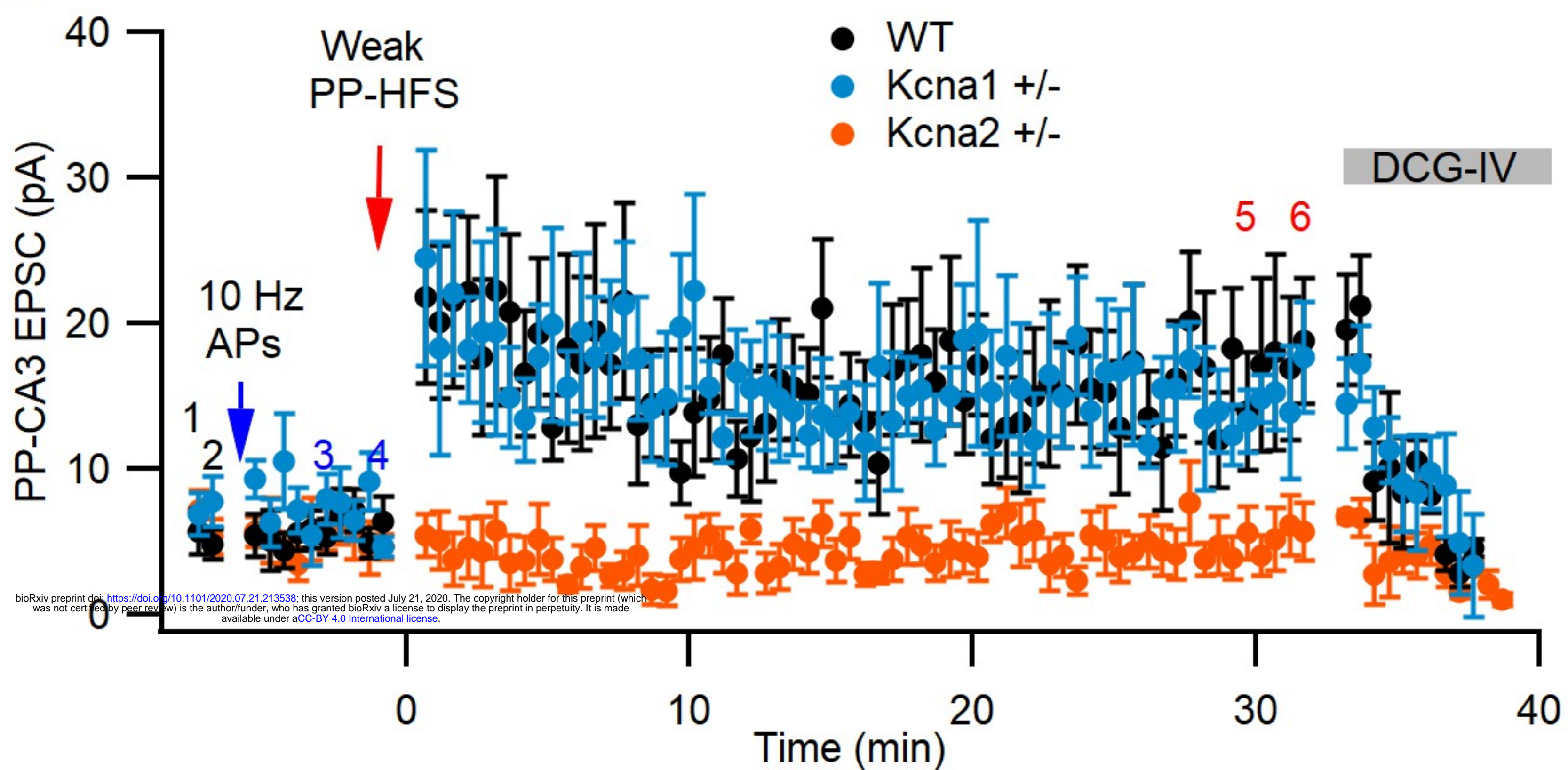
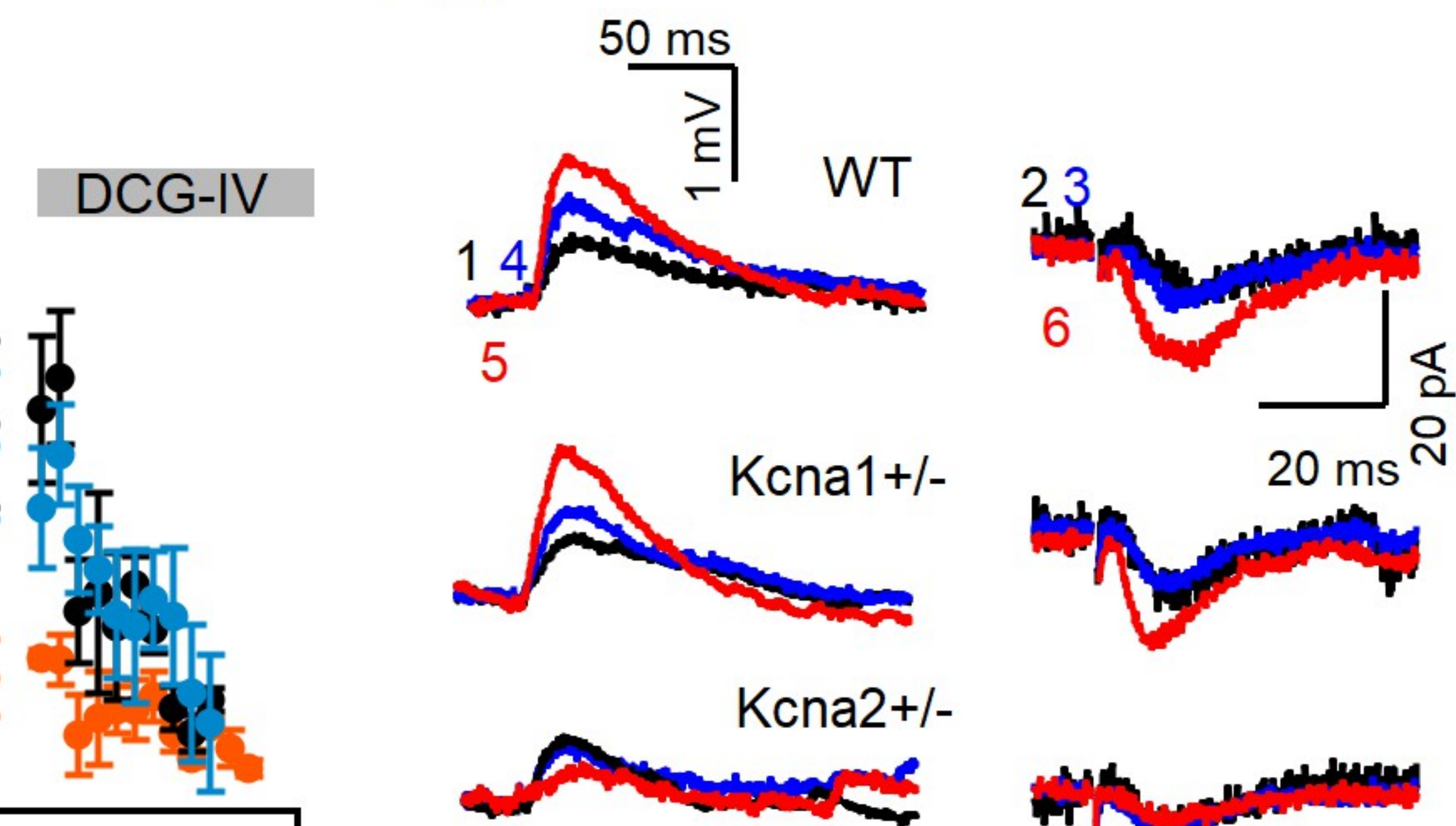
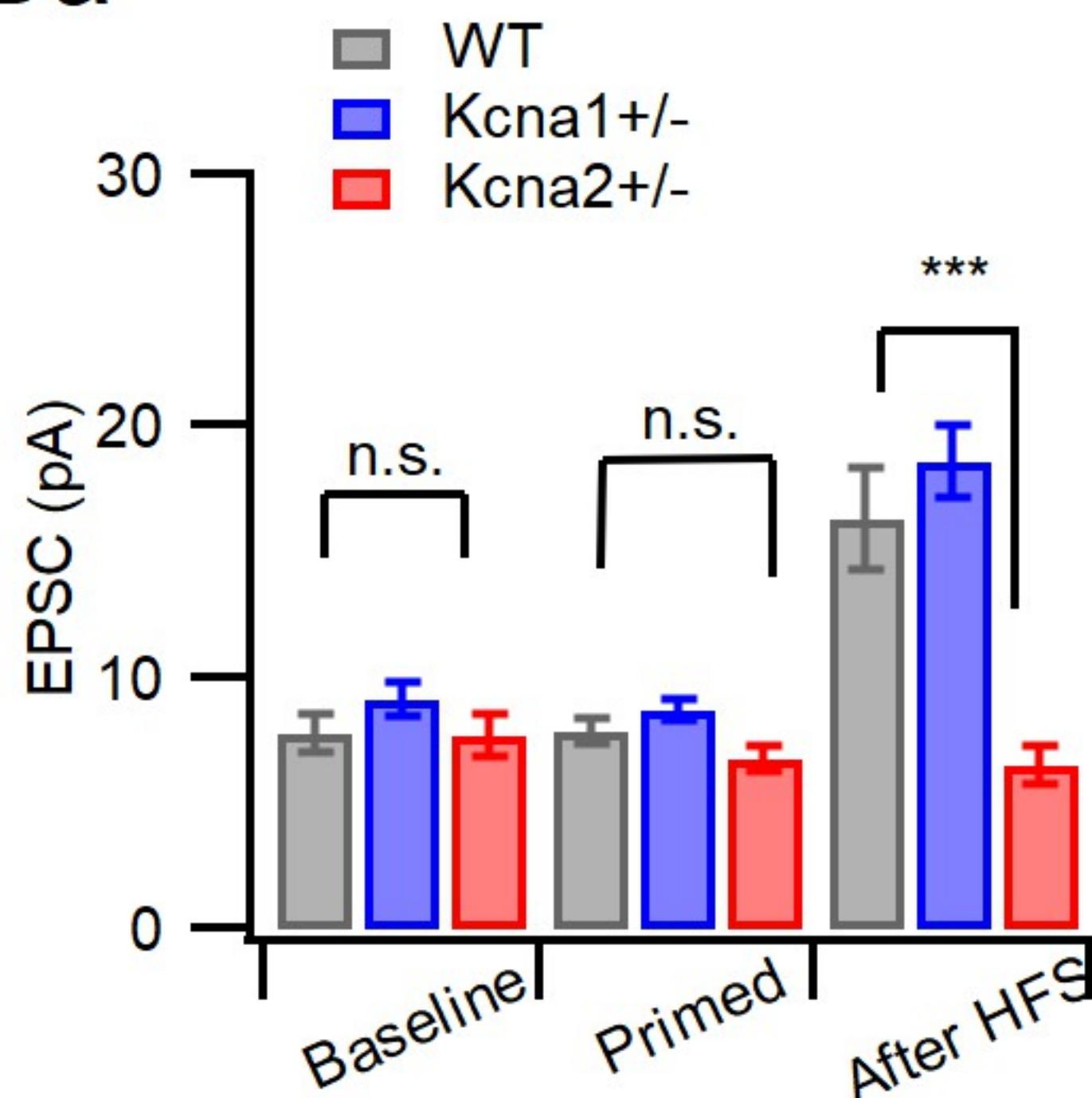
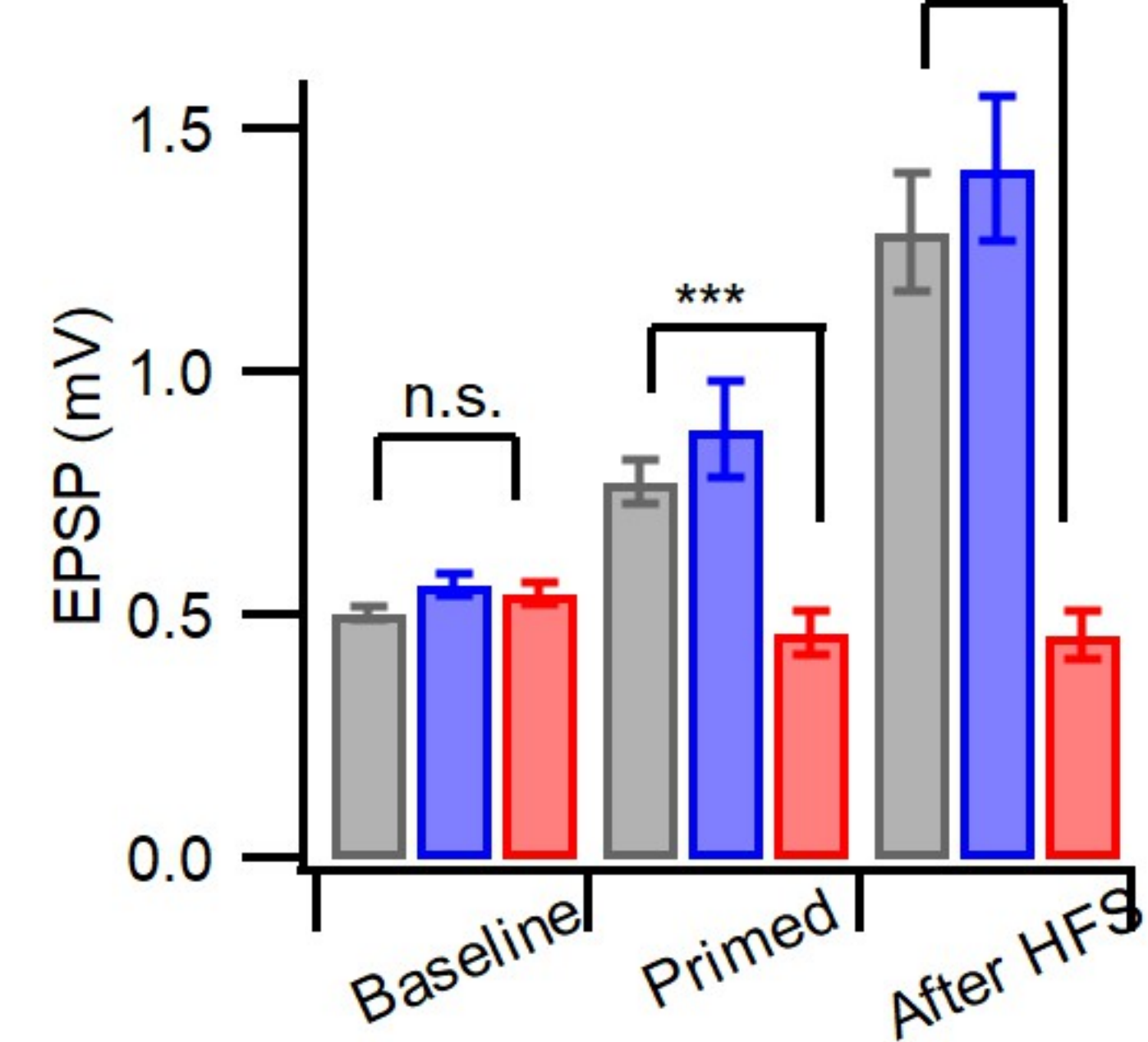
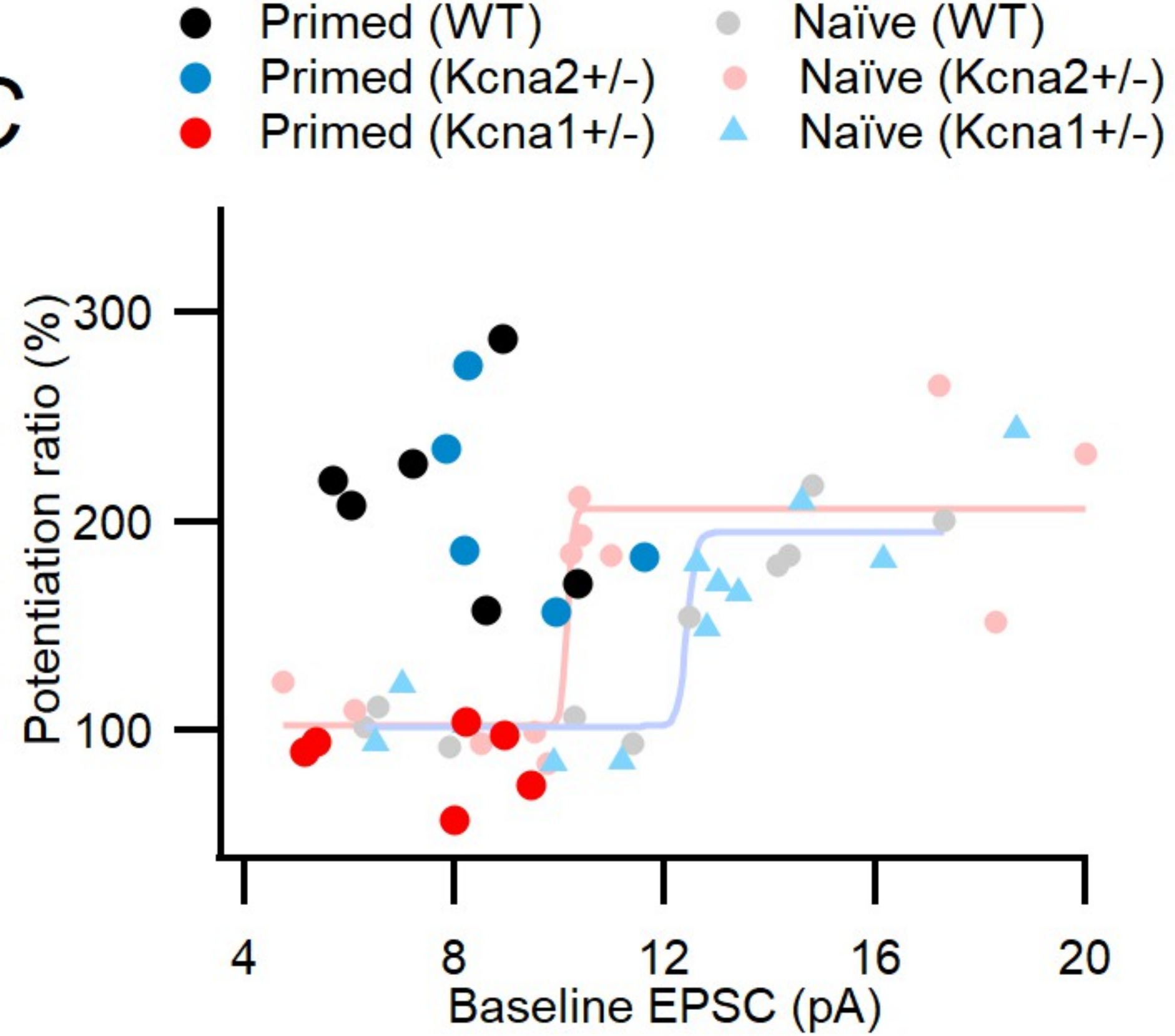
20 ms 20 pA

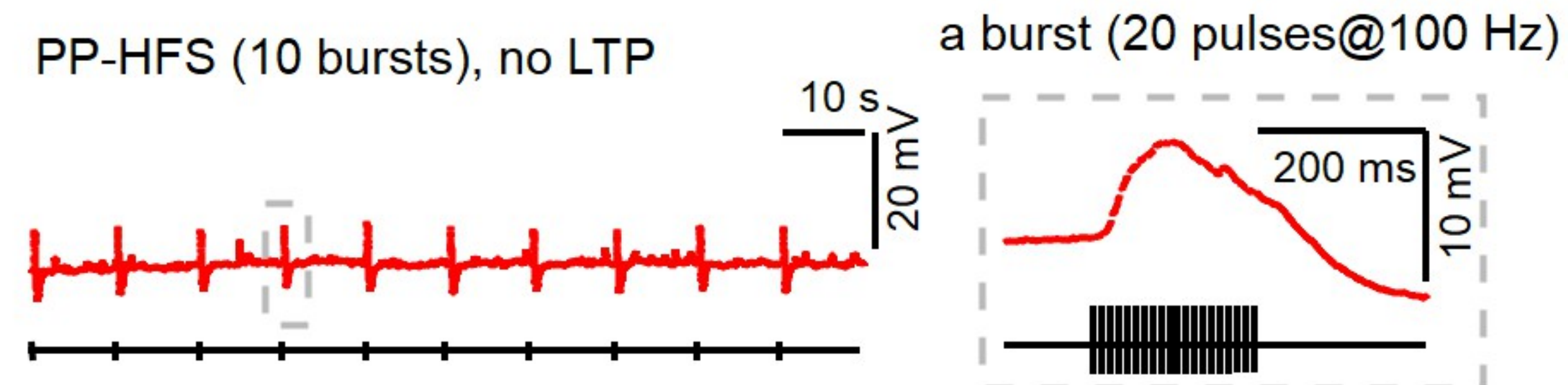
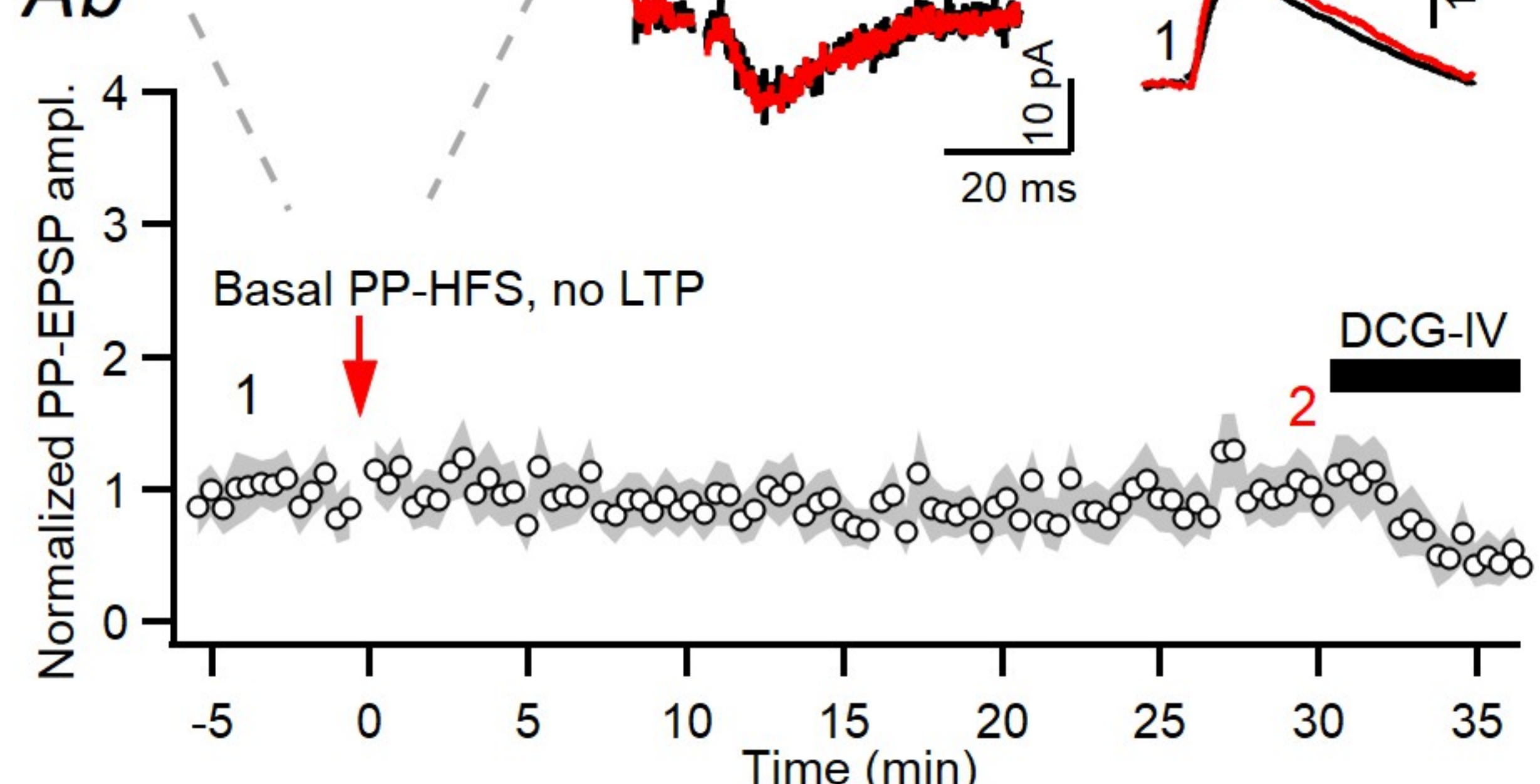
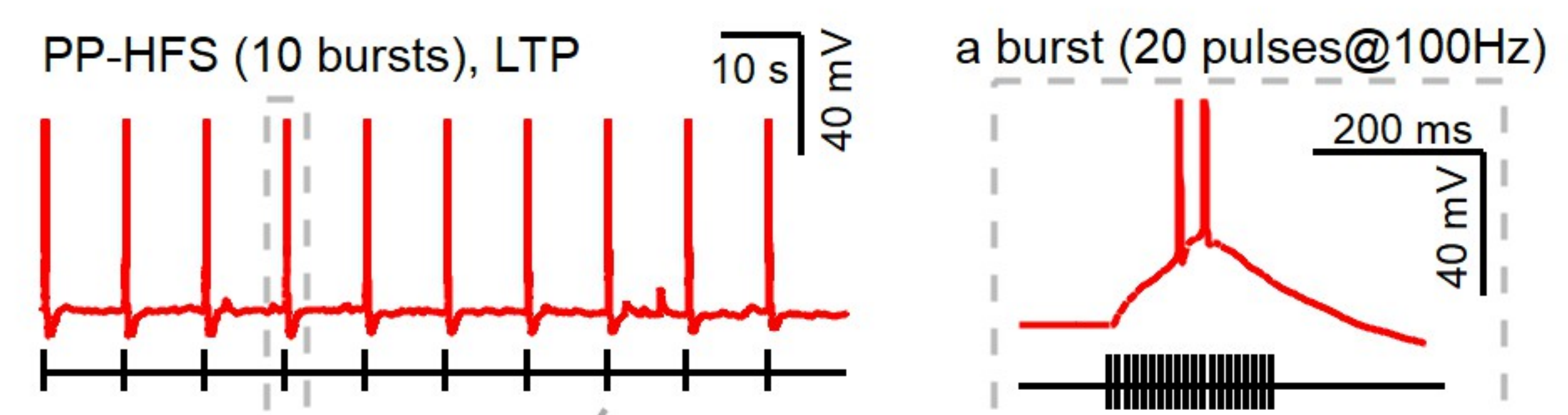
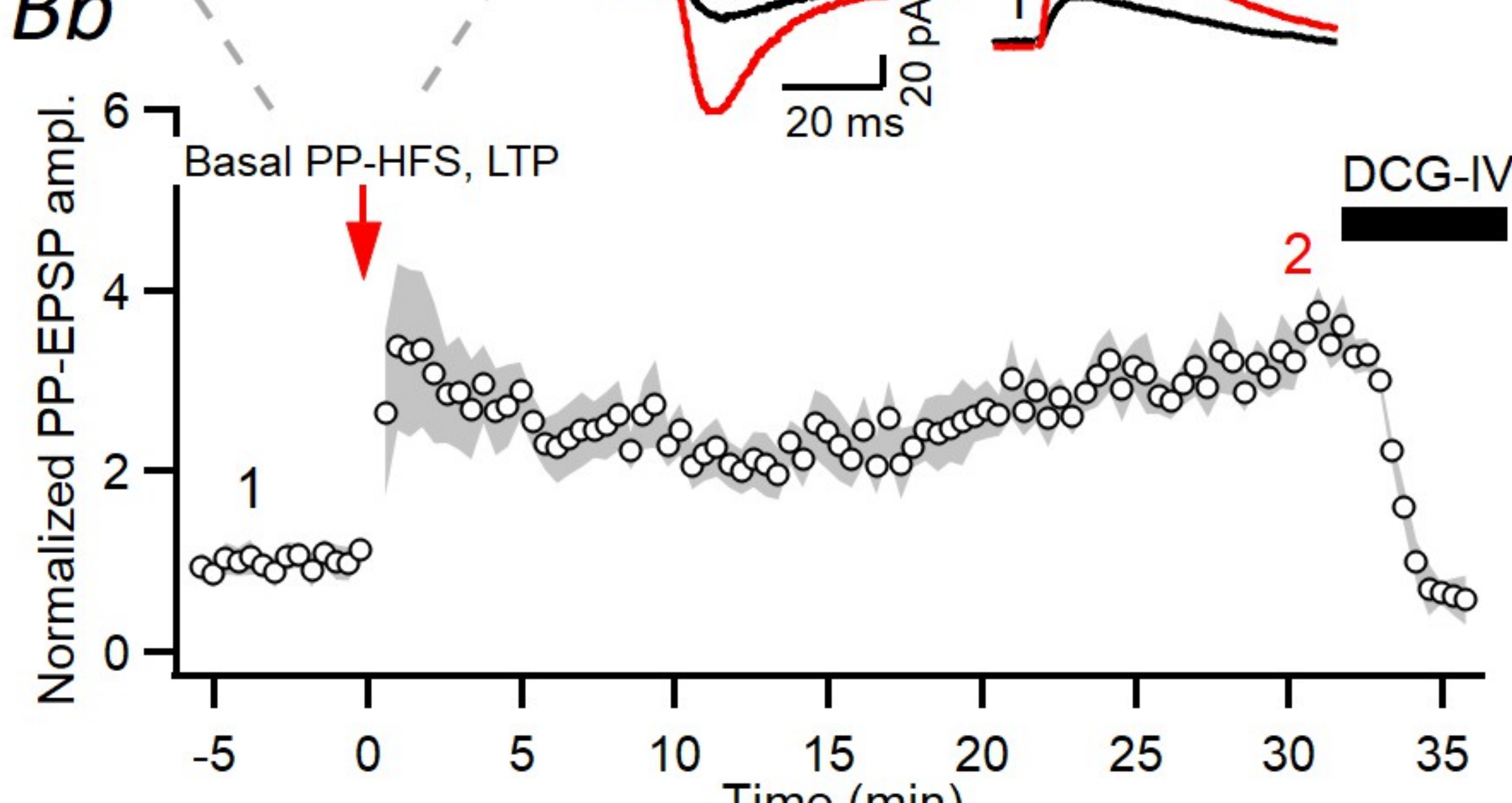
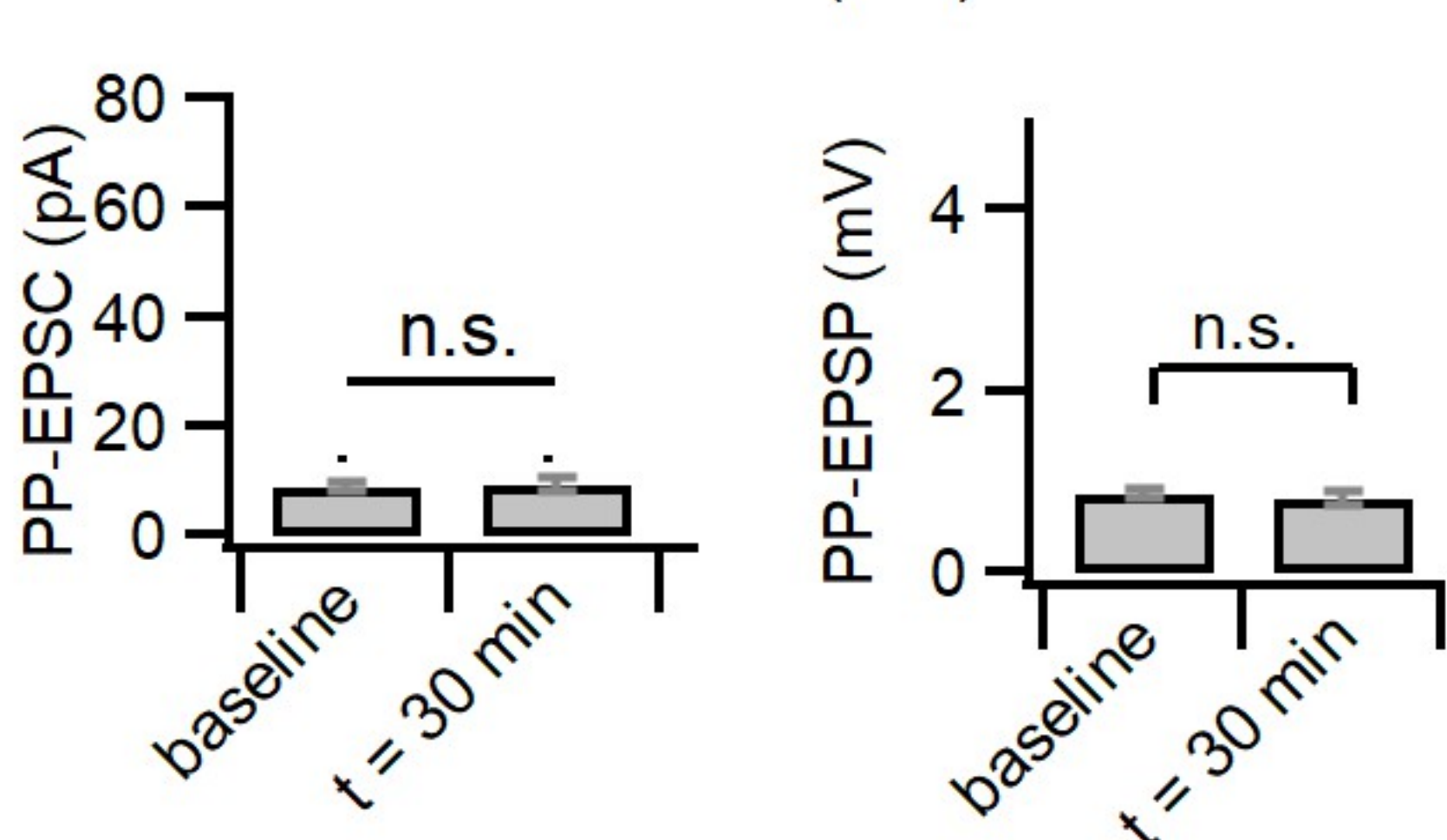
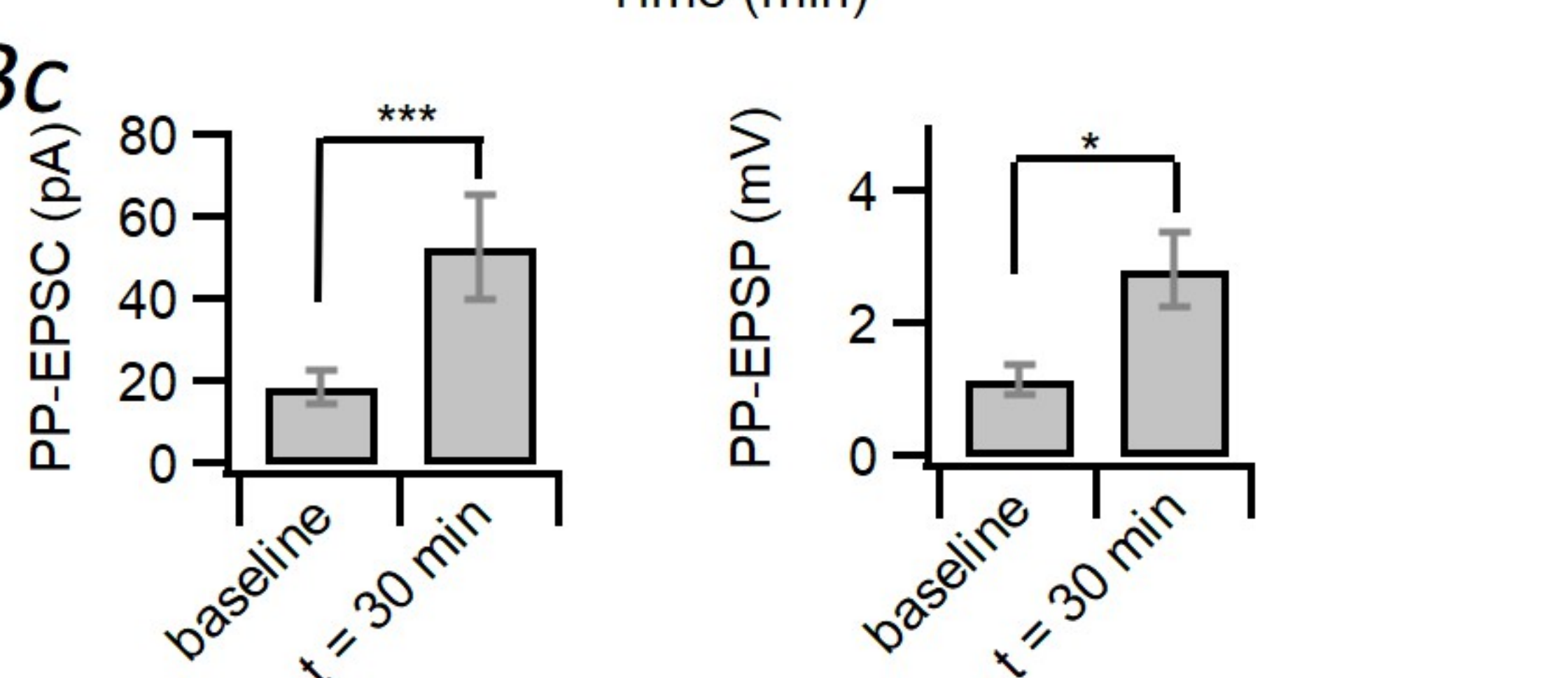
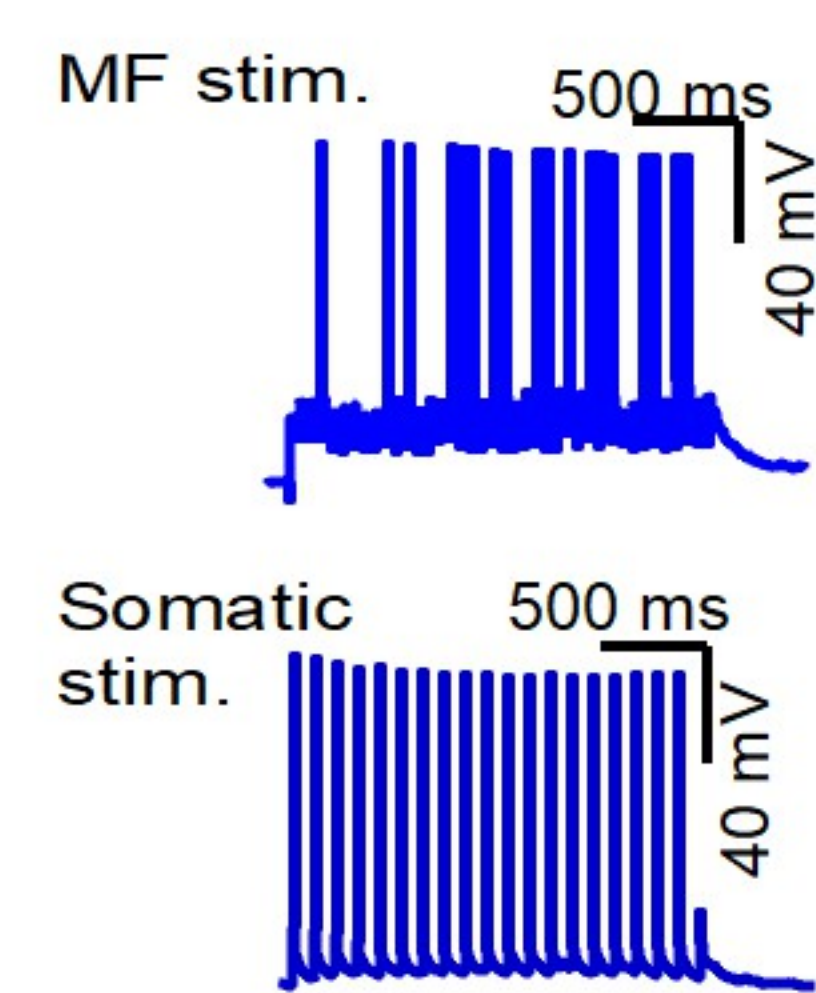
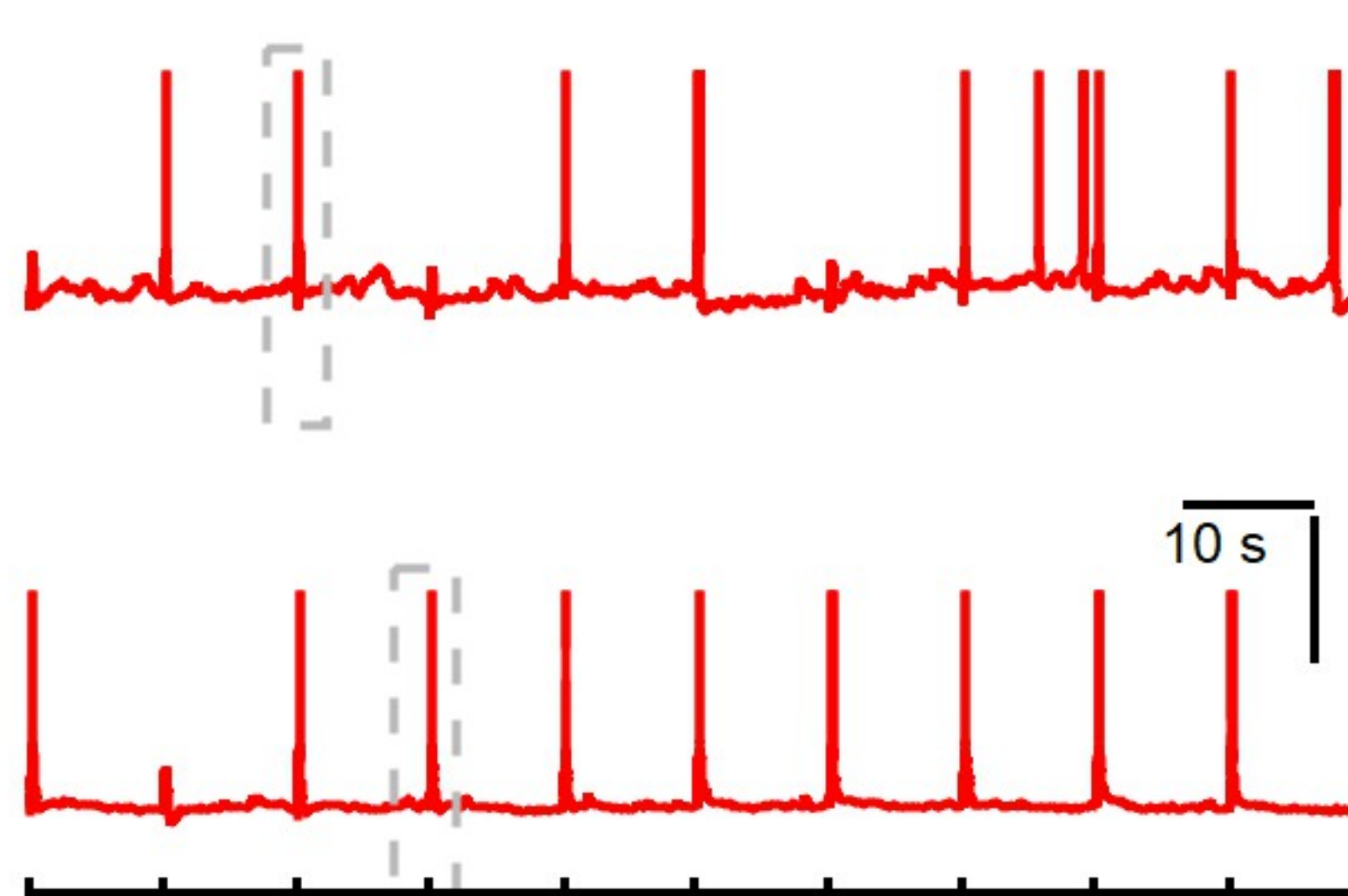
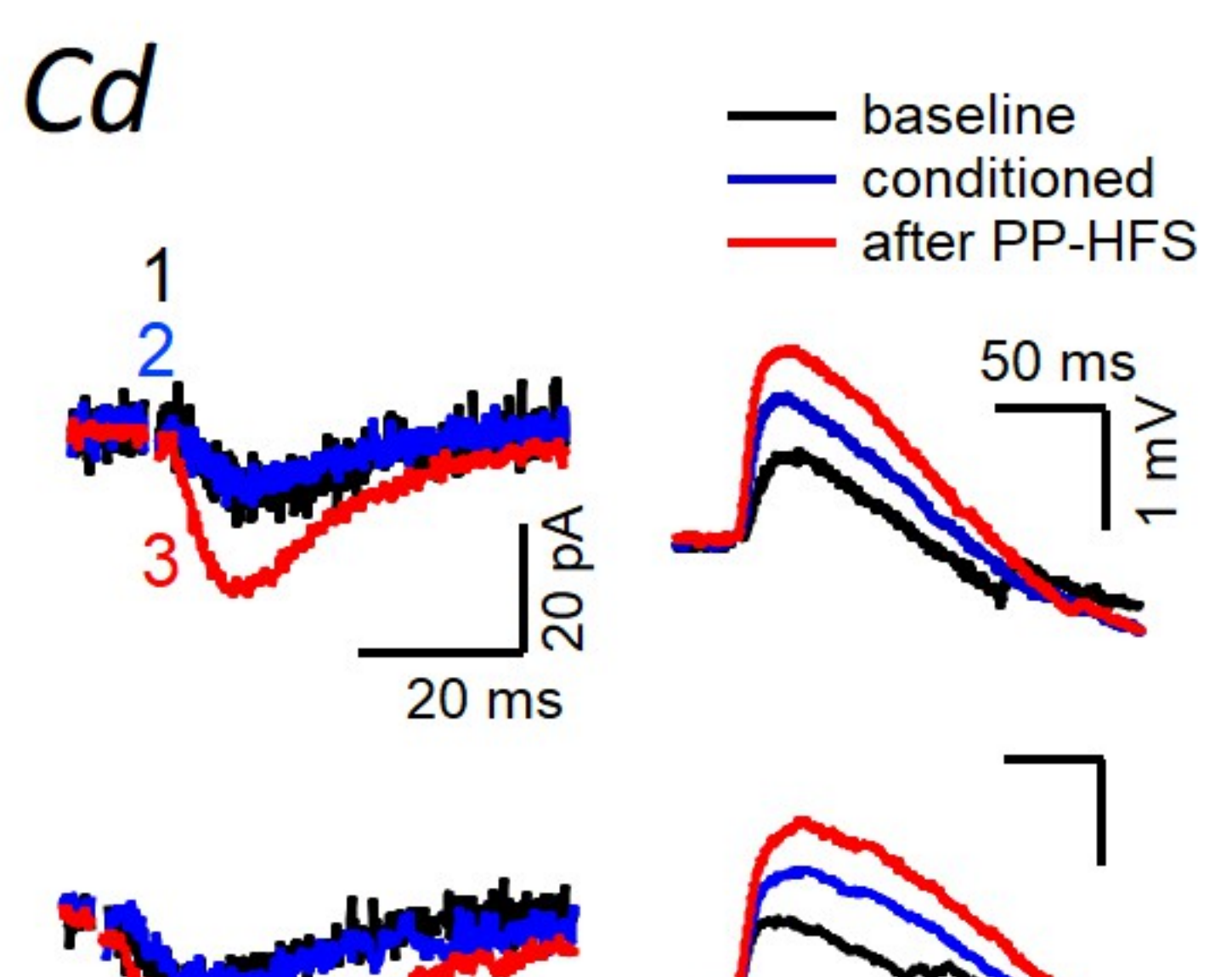
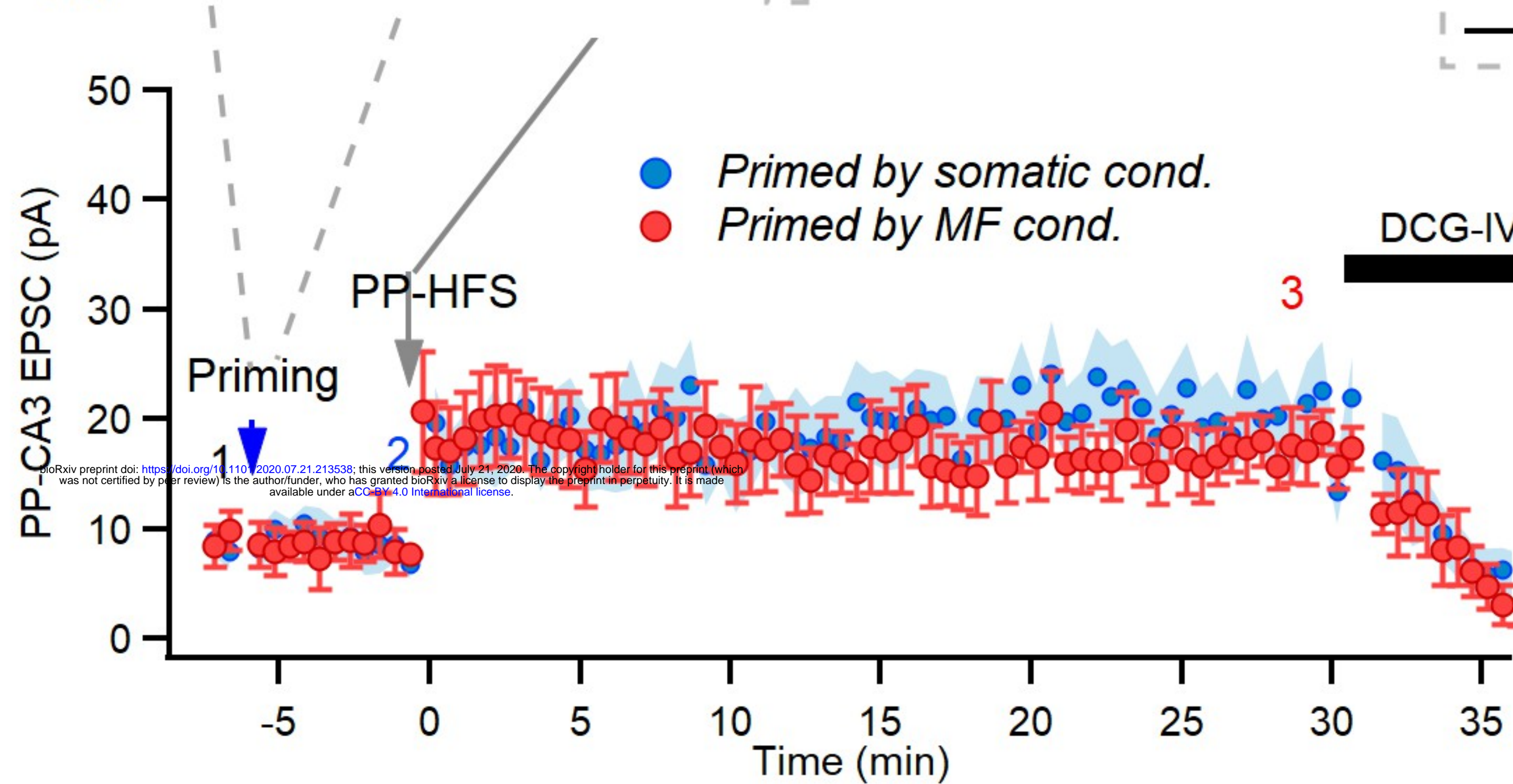
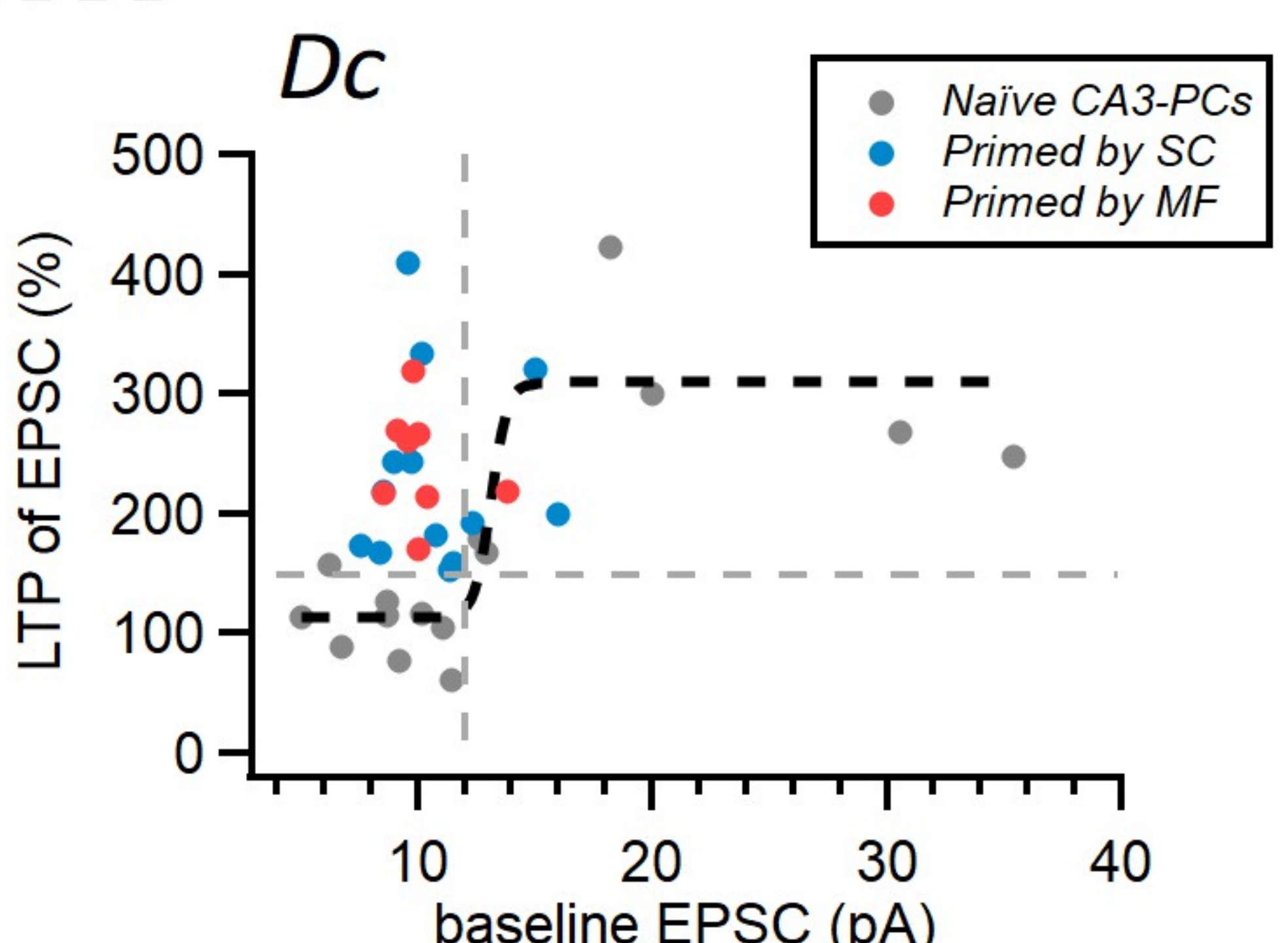
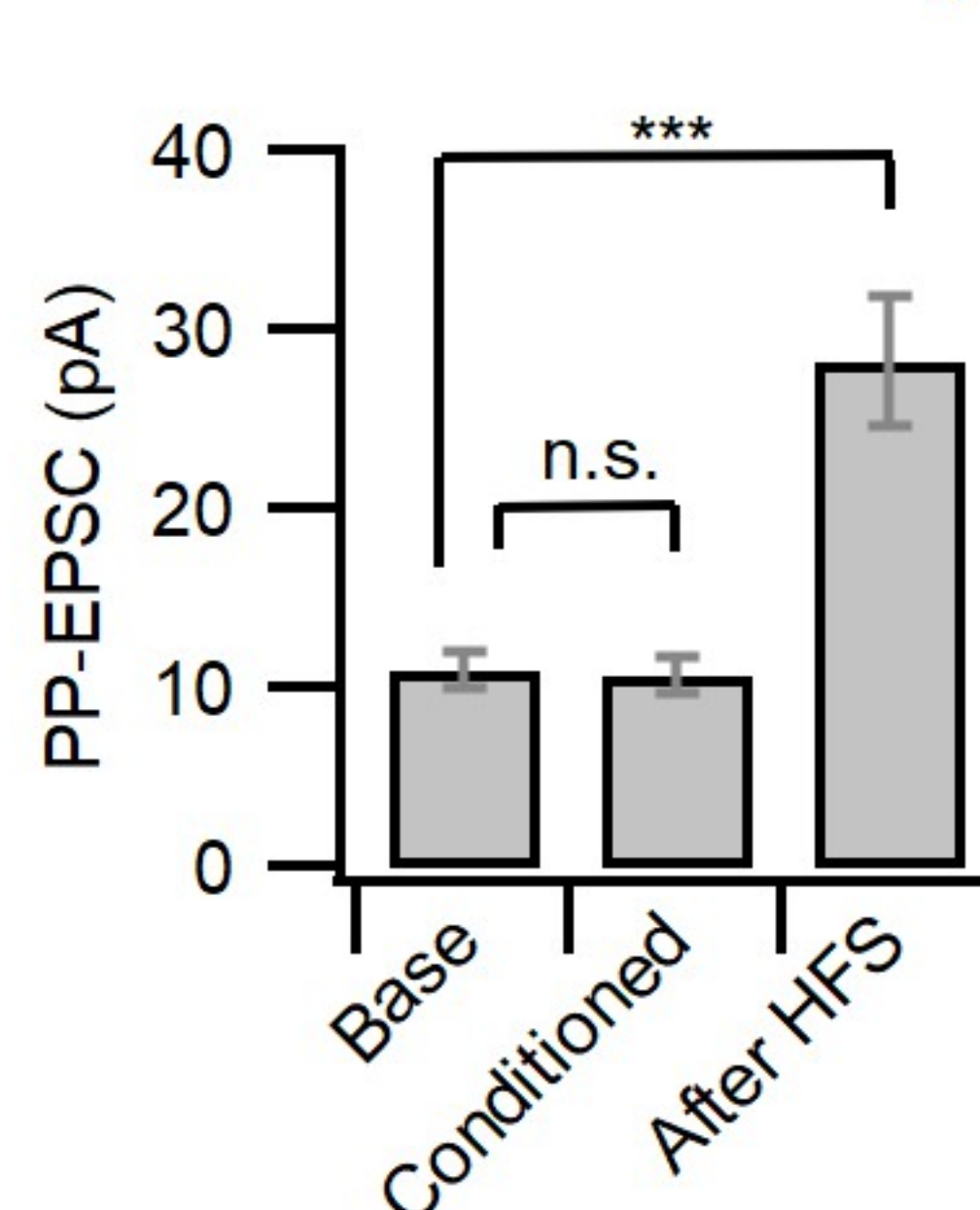
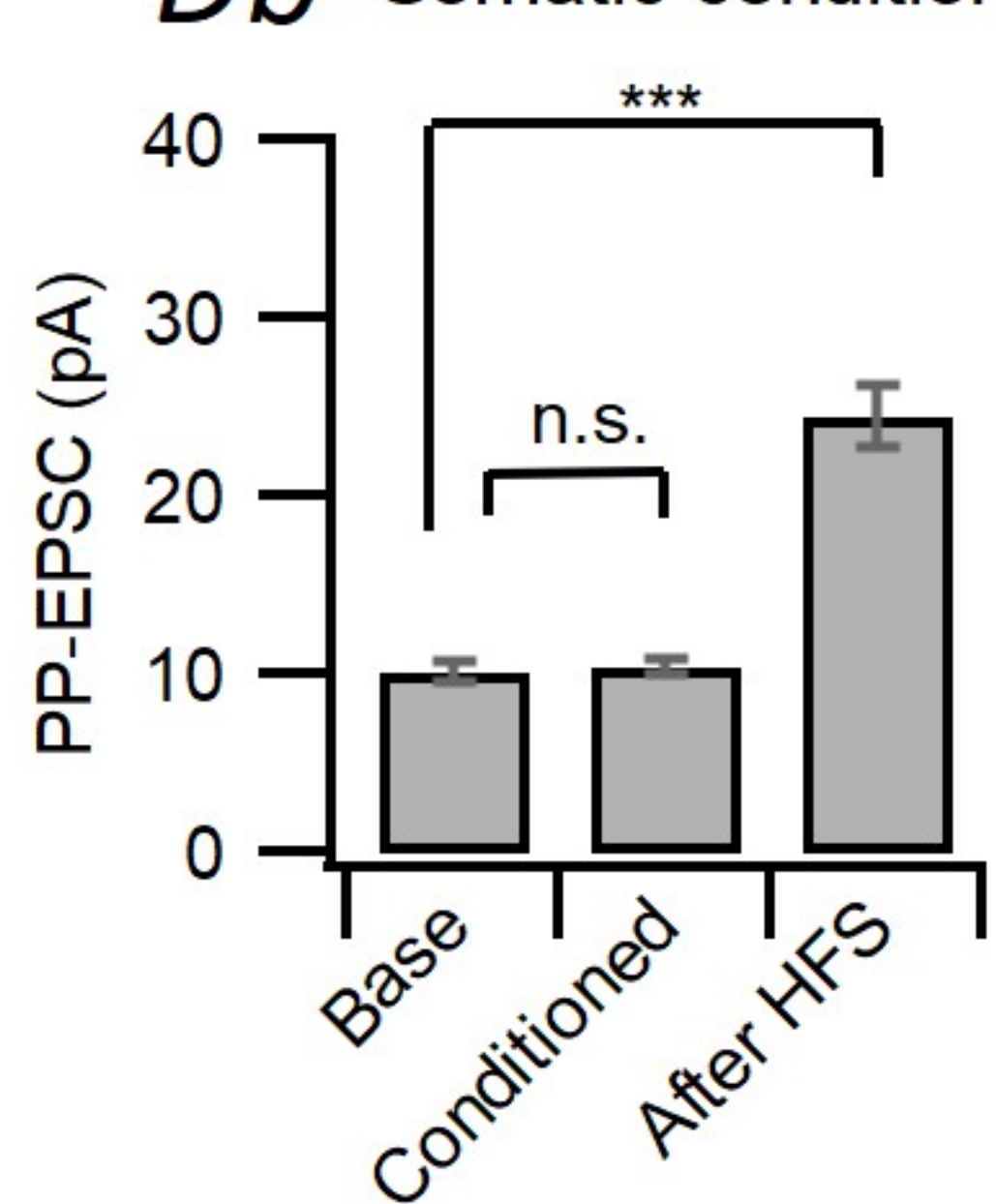
**Ad****Ba****Bb****Bc****Bd****Ca****Cb****Da****Db**

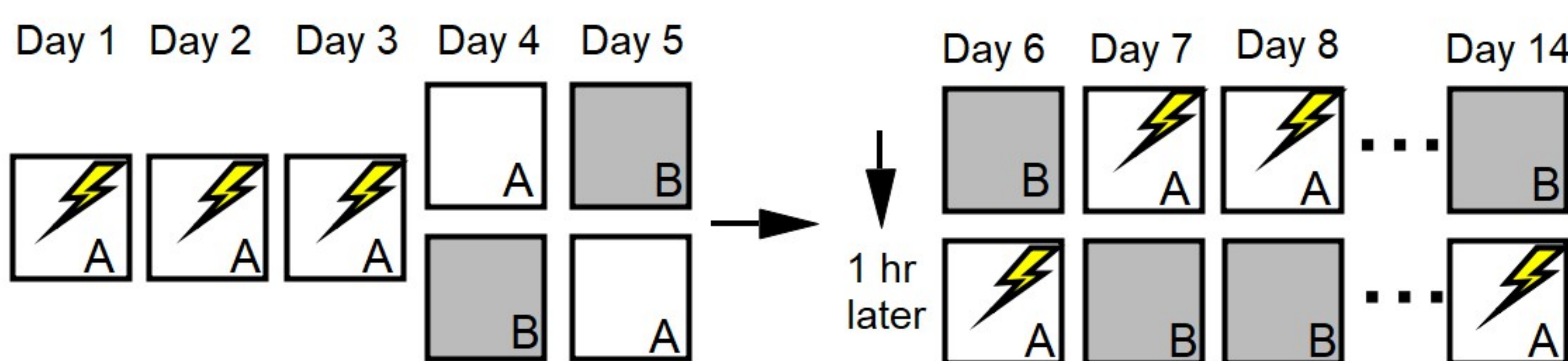
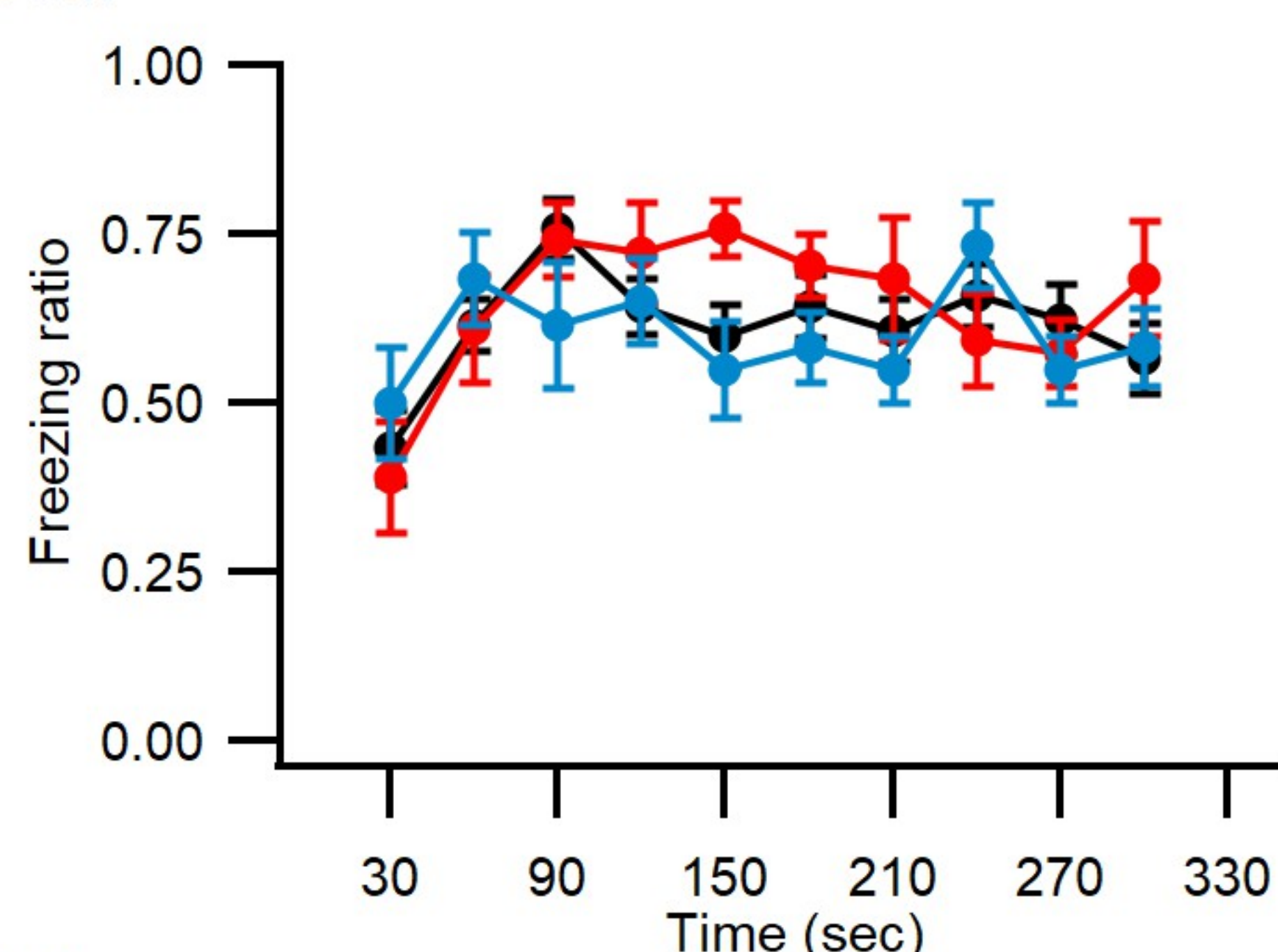
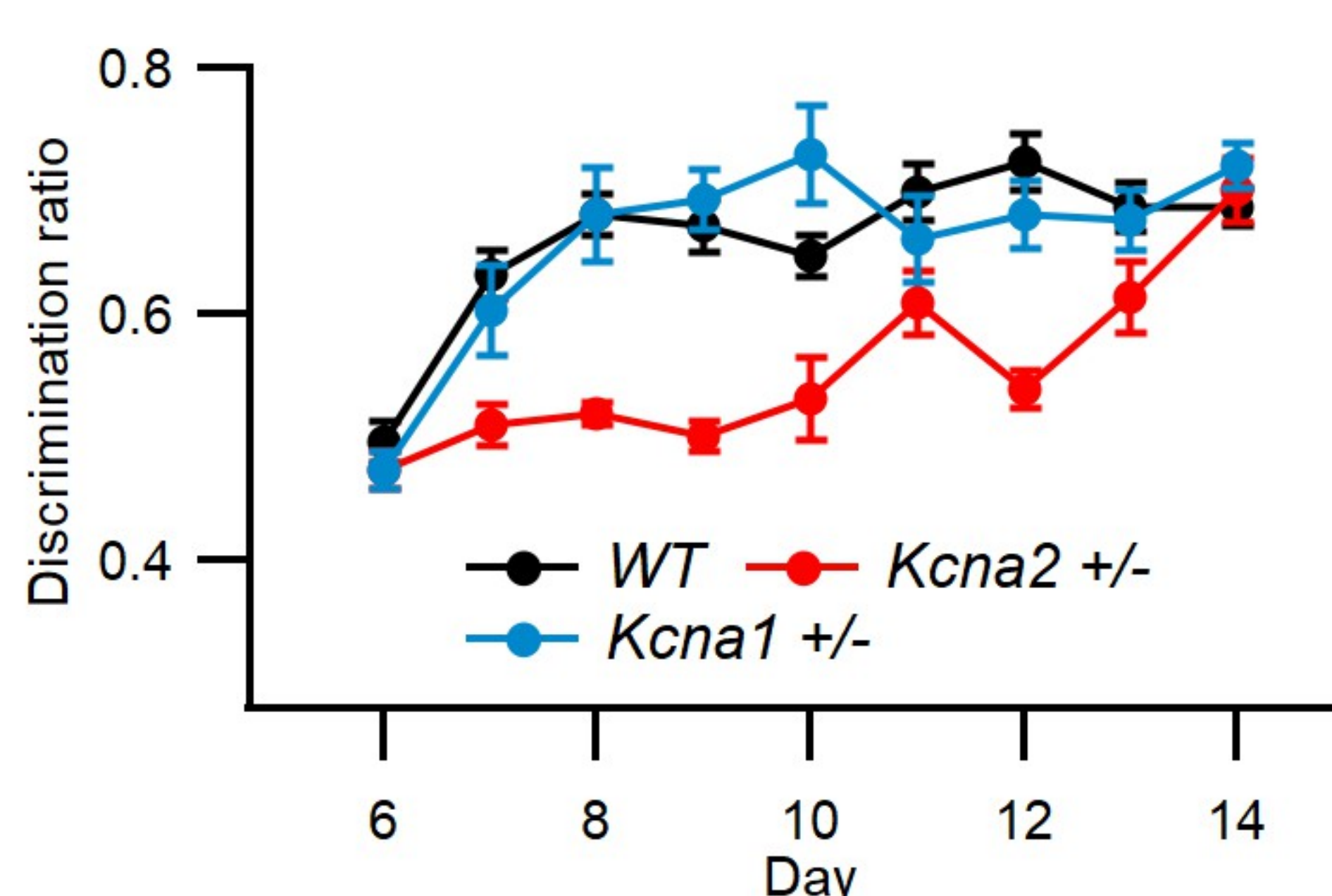
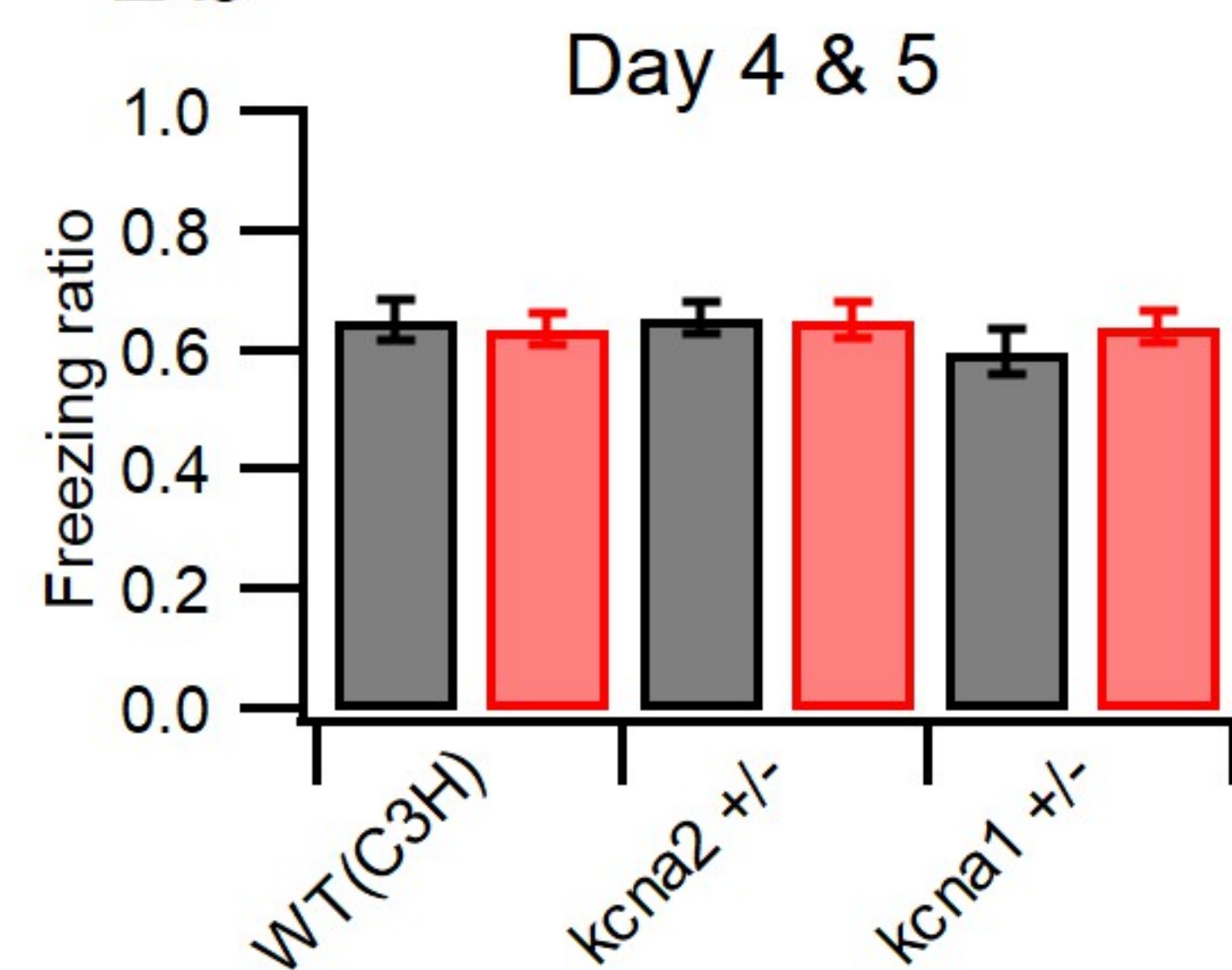
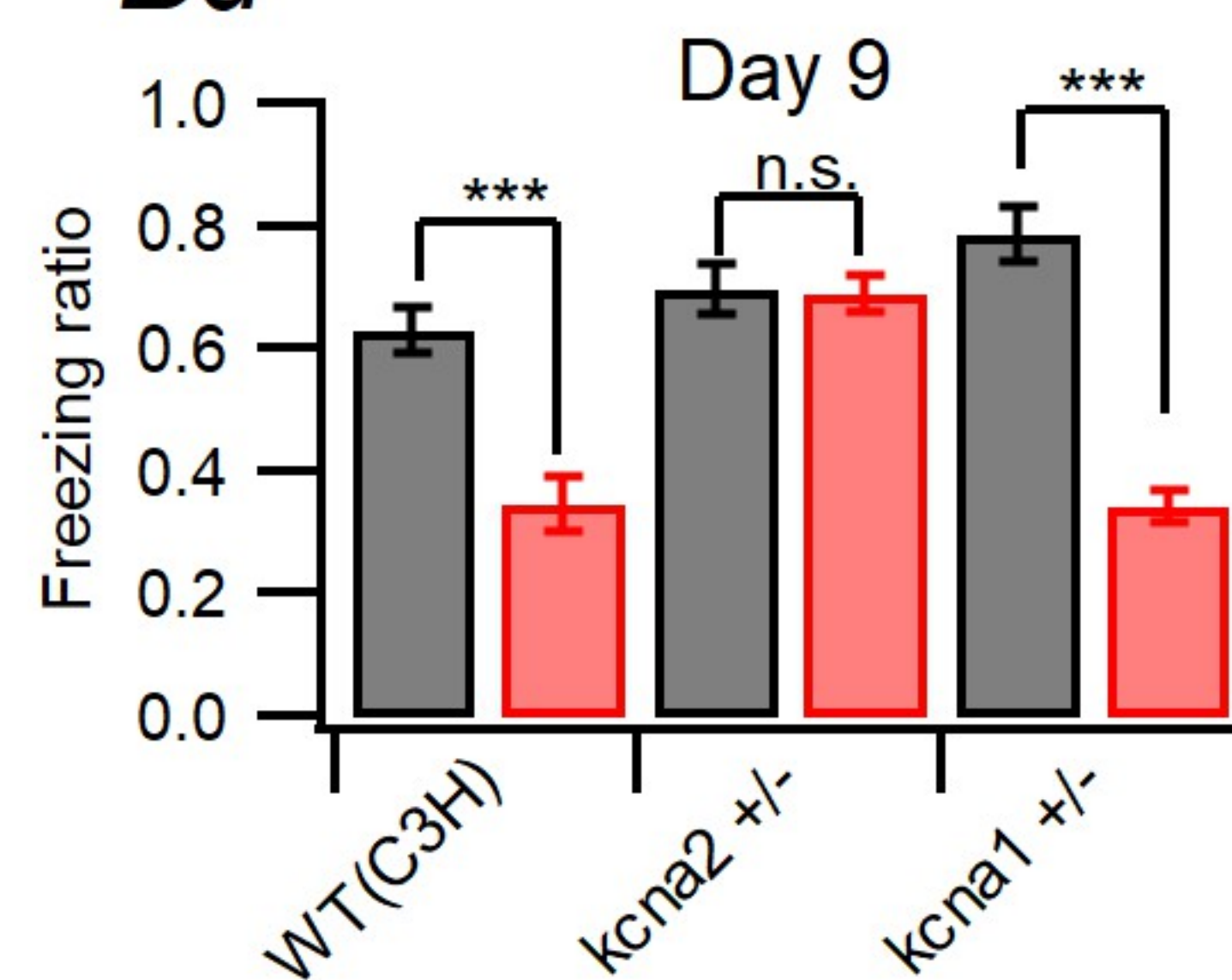
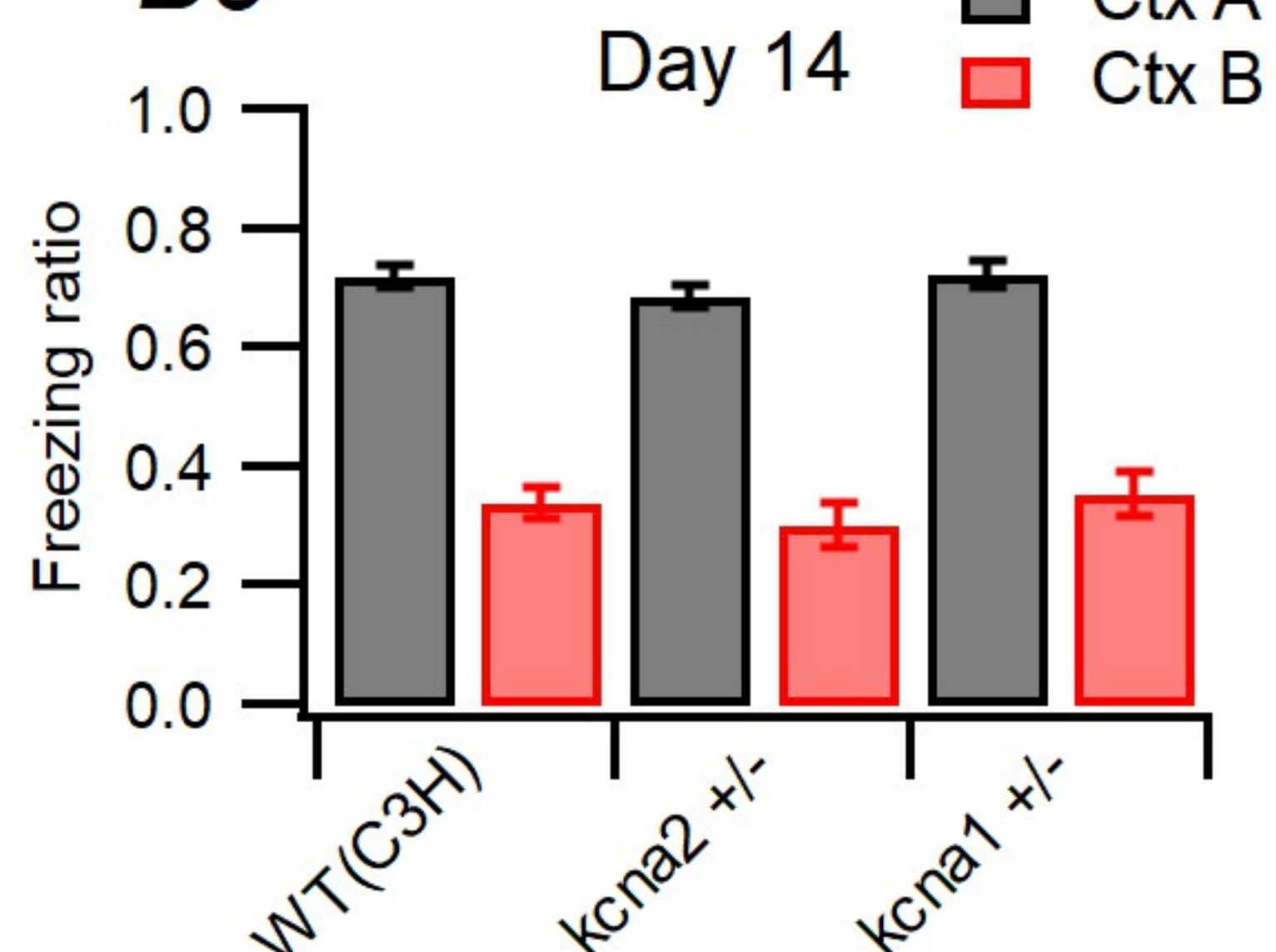
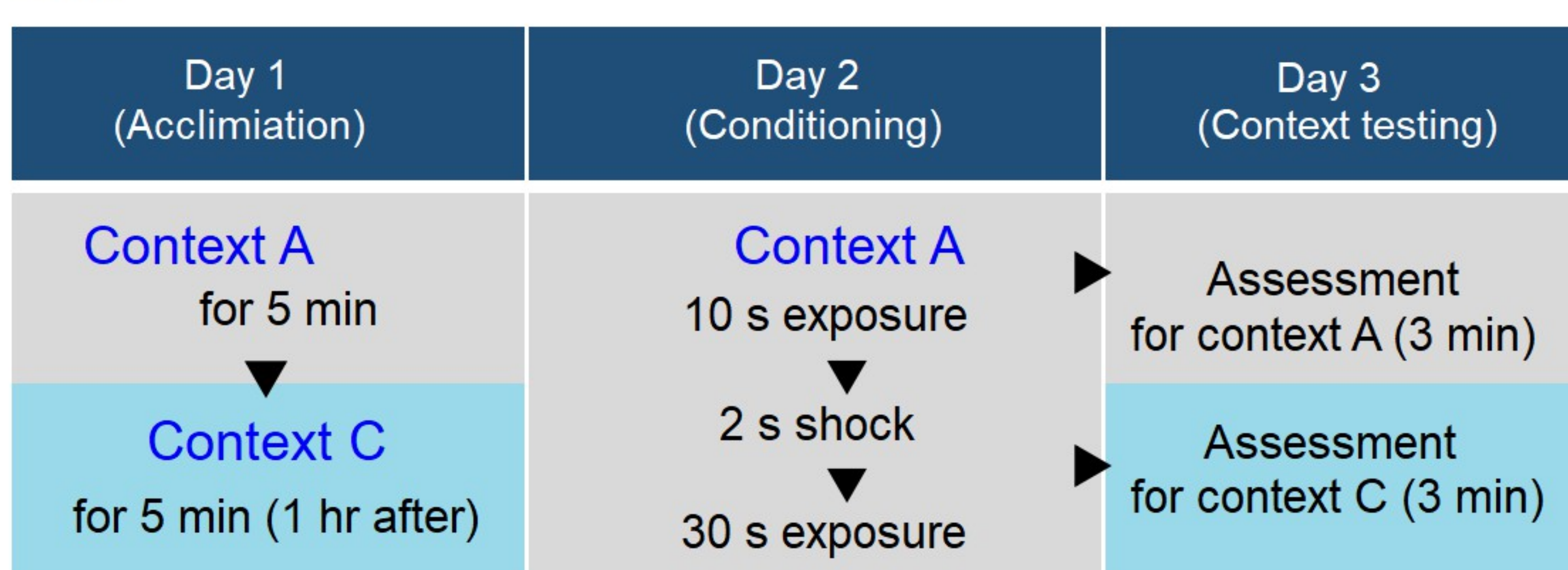
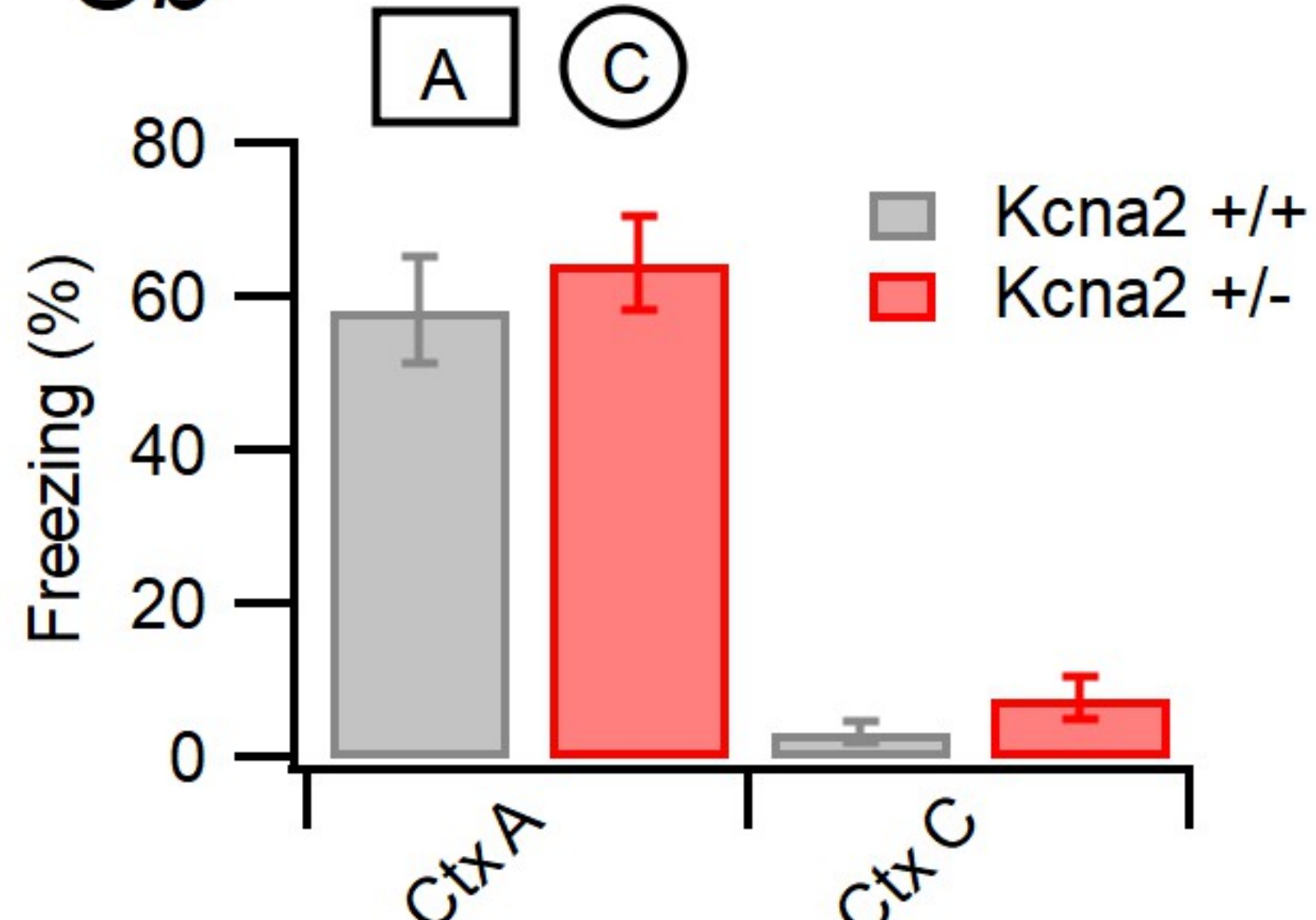
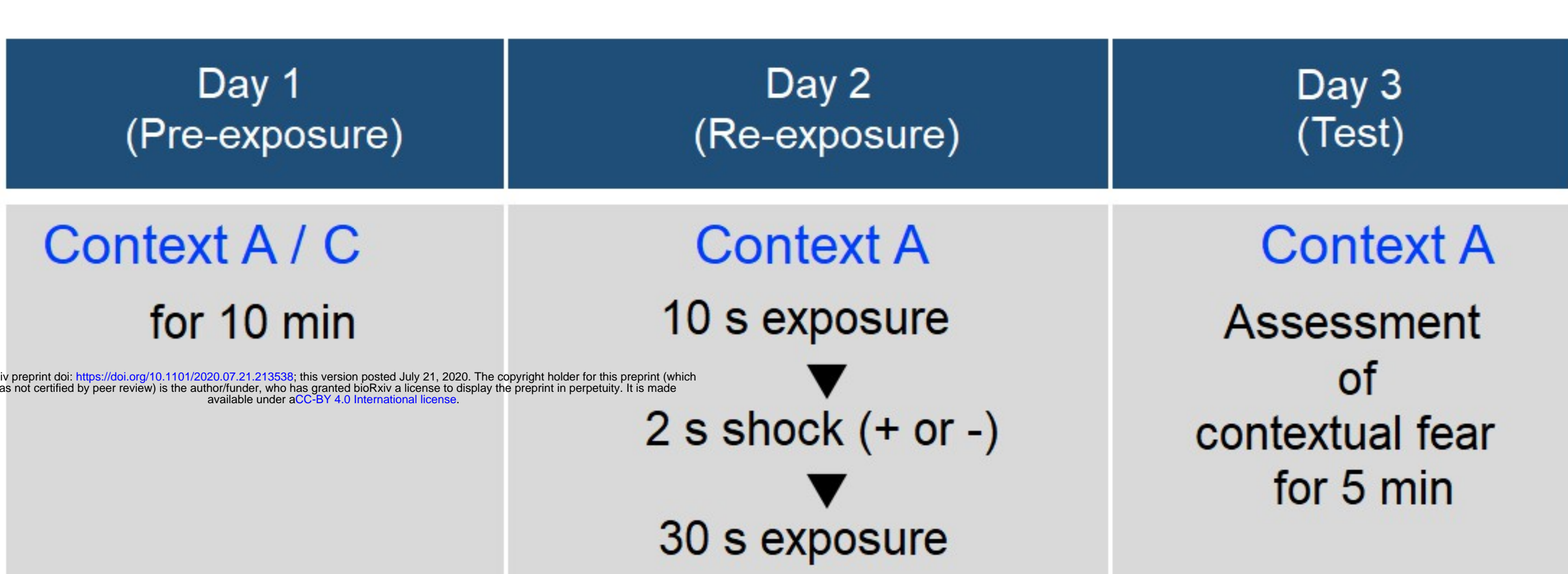
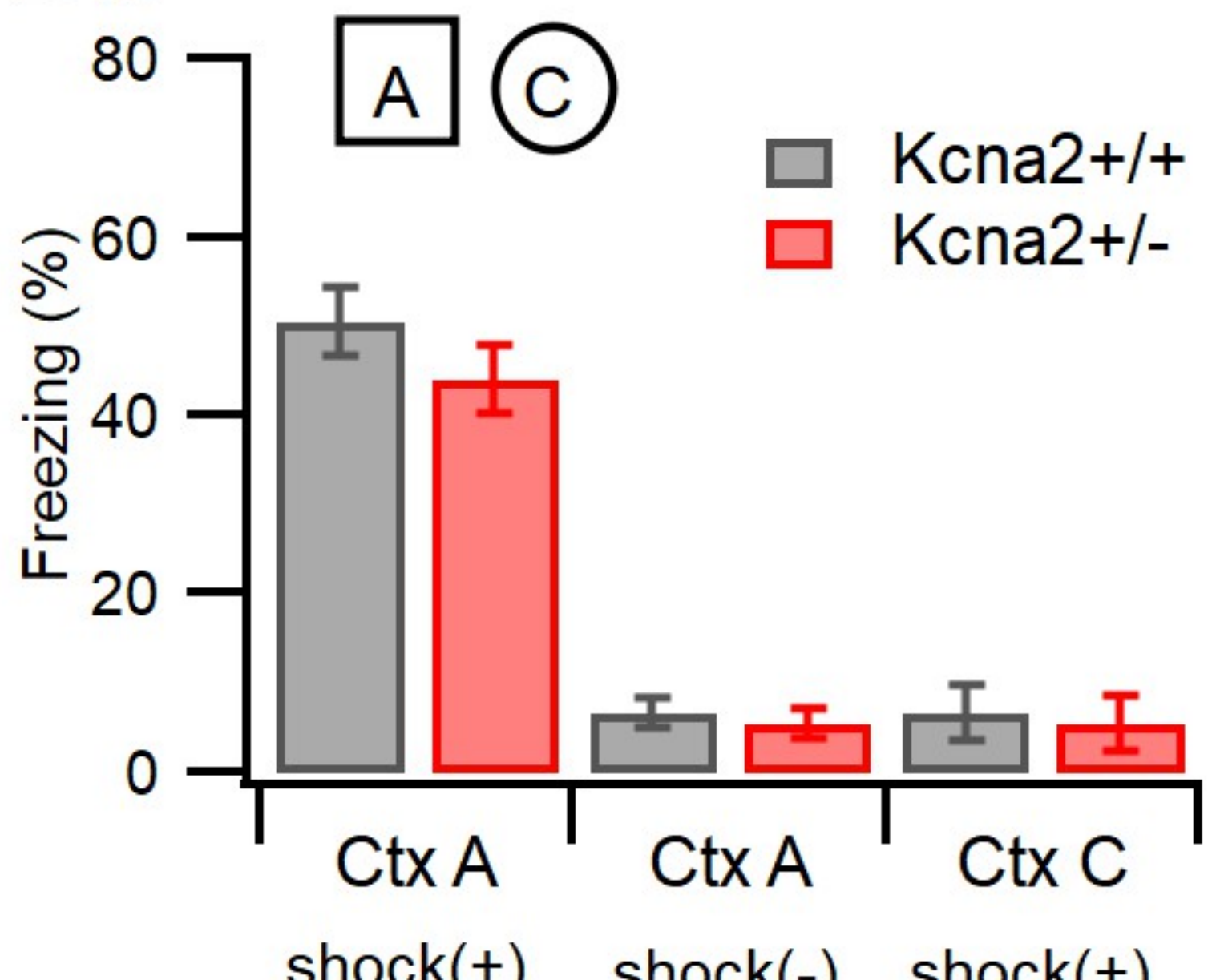
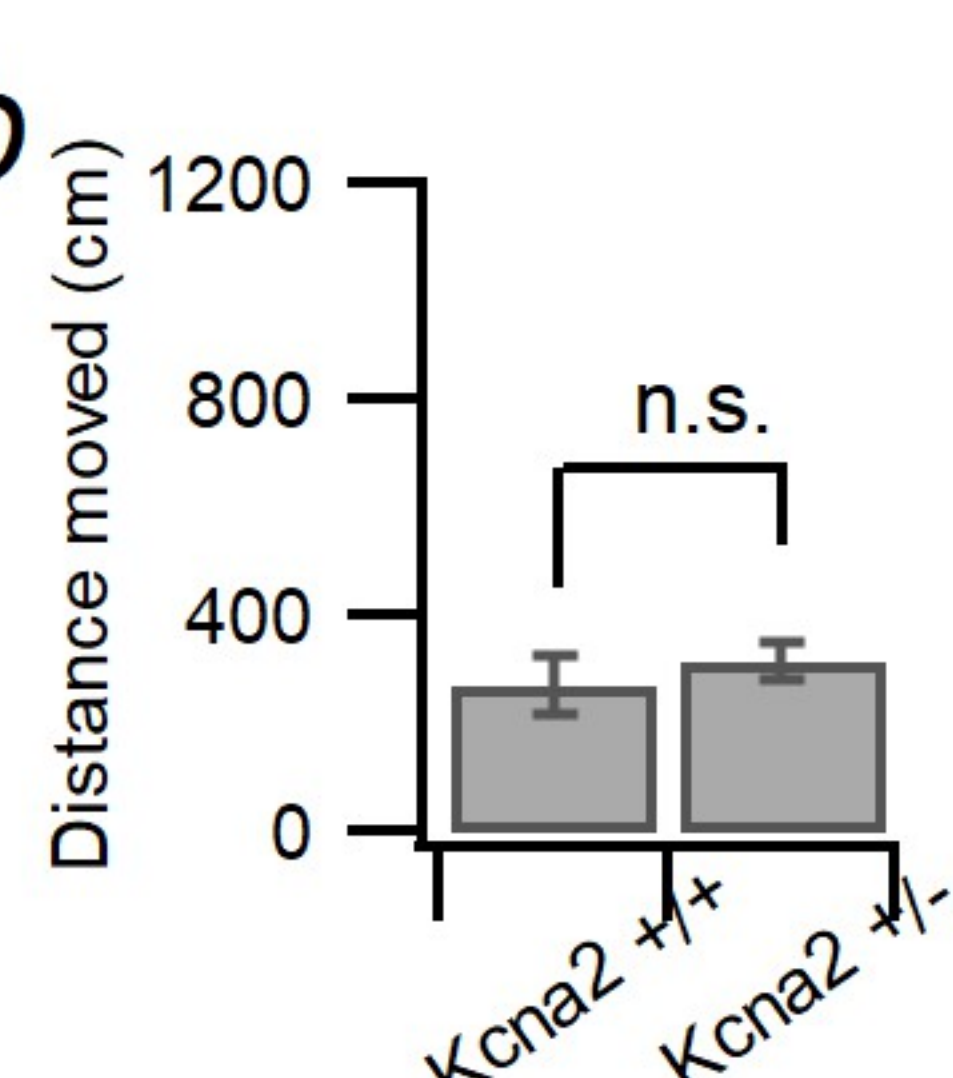
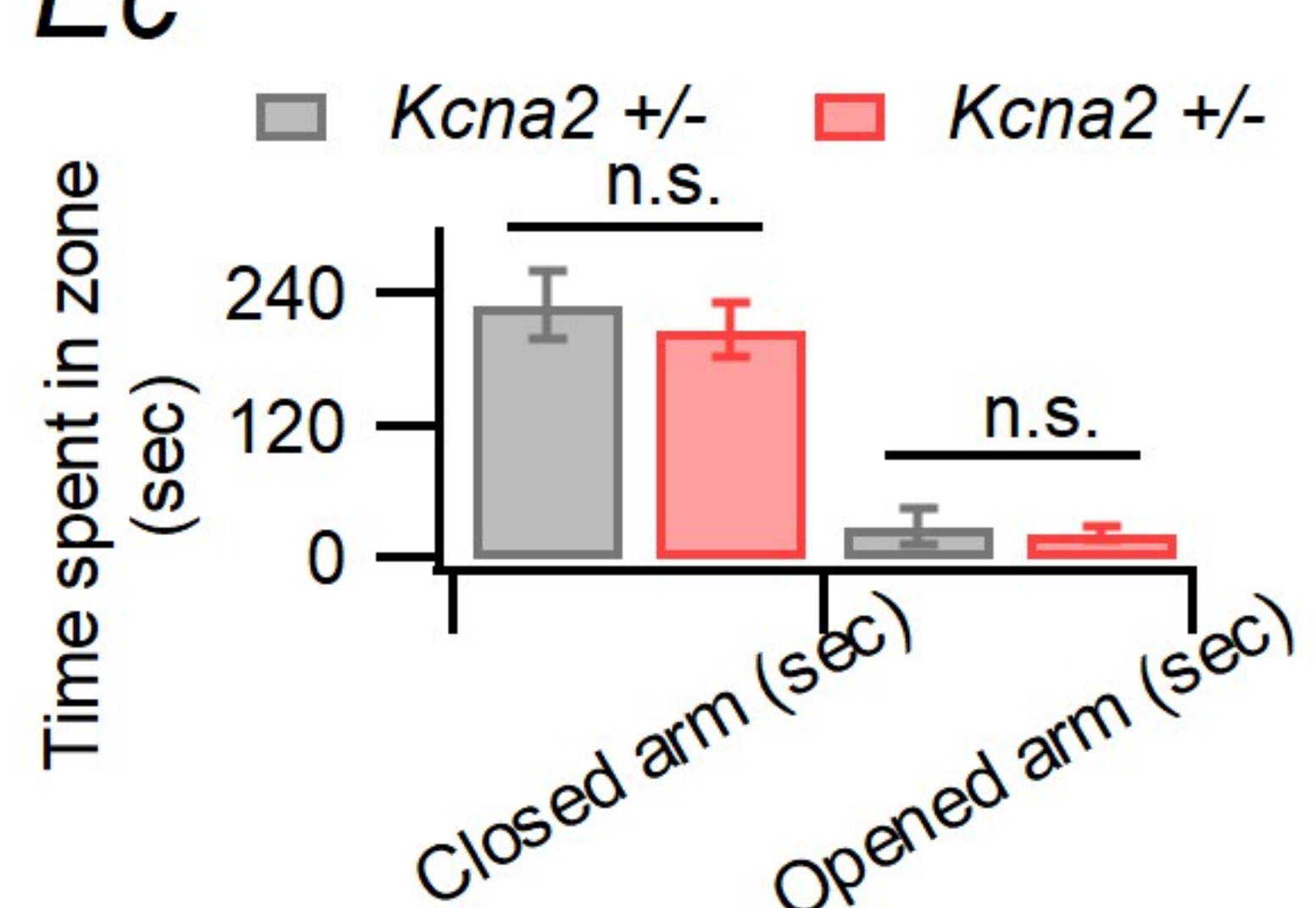


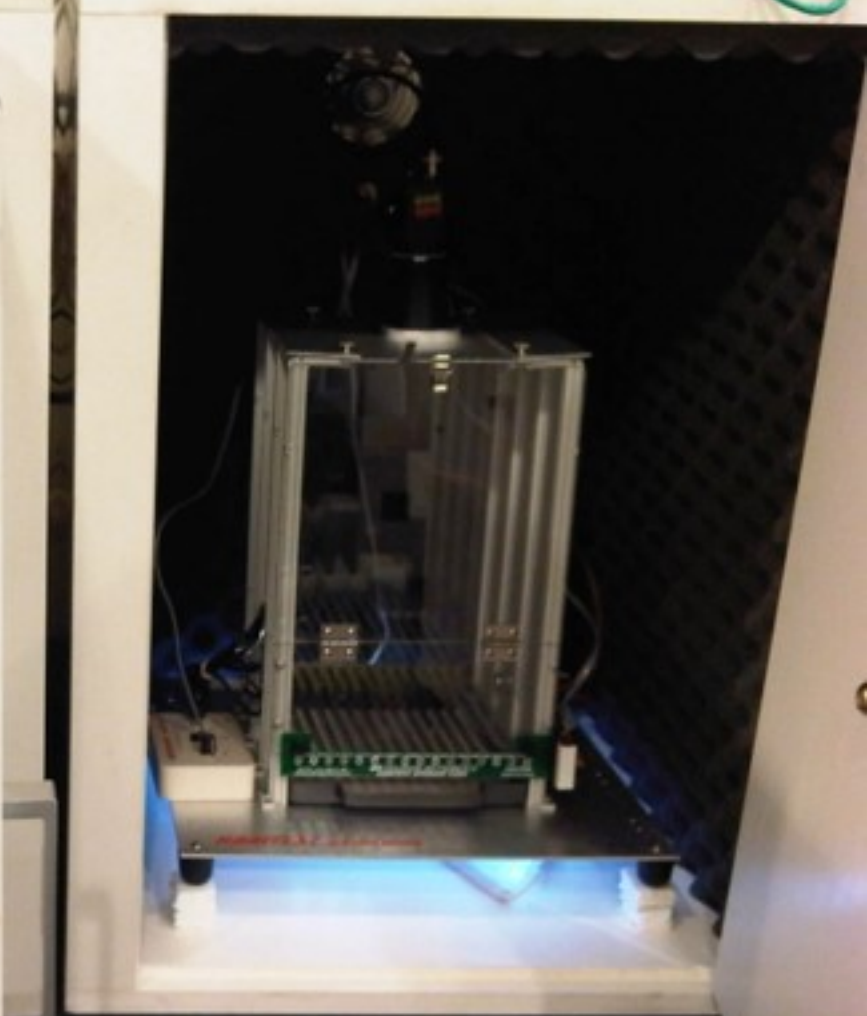
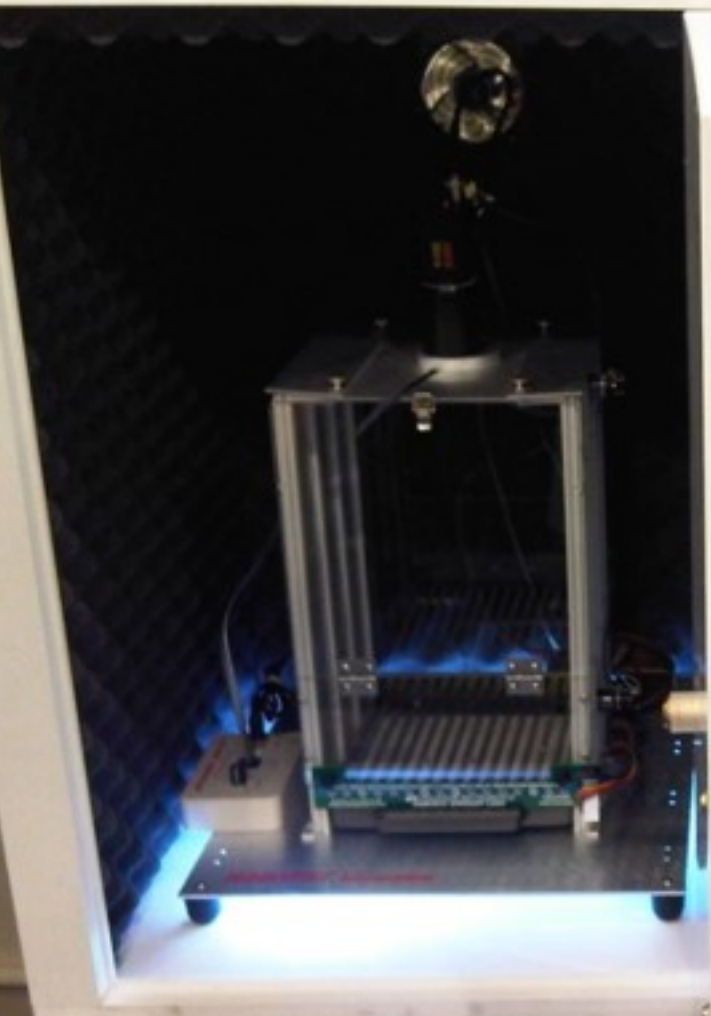
bioRxiv preprint doi: <https://doi.org/10.1101/2020.07.21.213538>; this version posted July 21, 2020. The copyright holder for this preprint (which was not certified by peer review) is the author/funder, who has granted bioRxiv a license to display the preprint in perpetuity. It is made available under aCC-BY 4.0 International license.

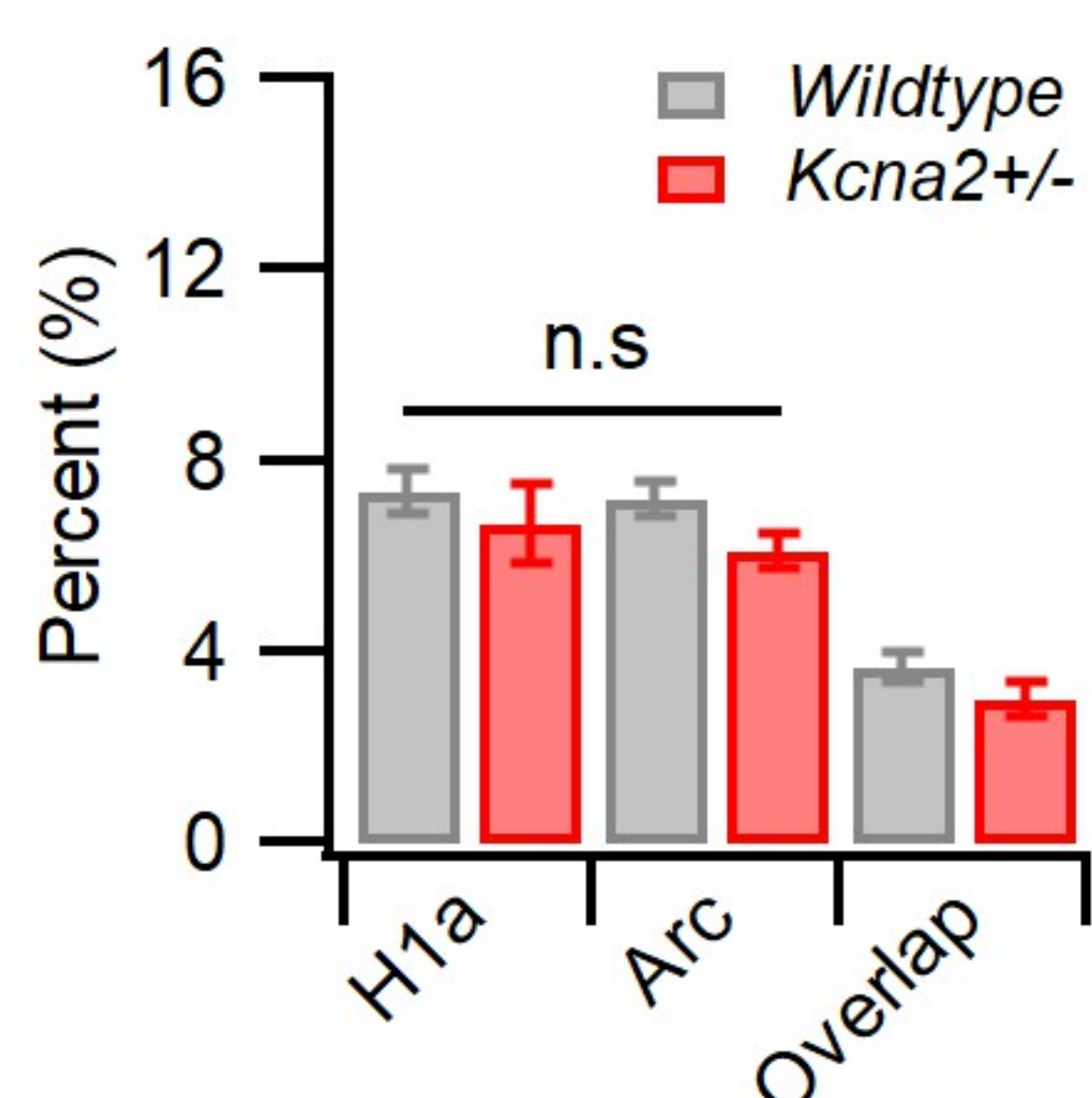
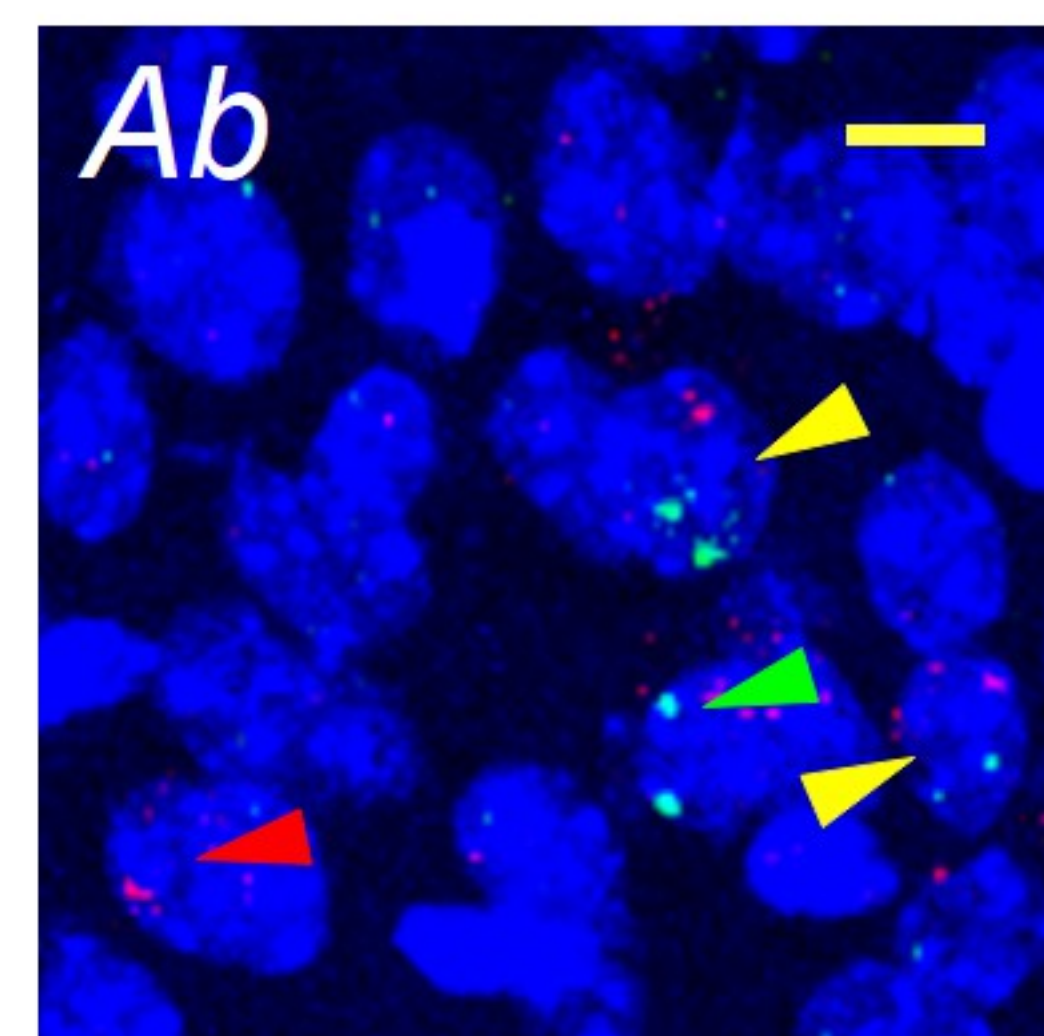
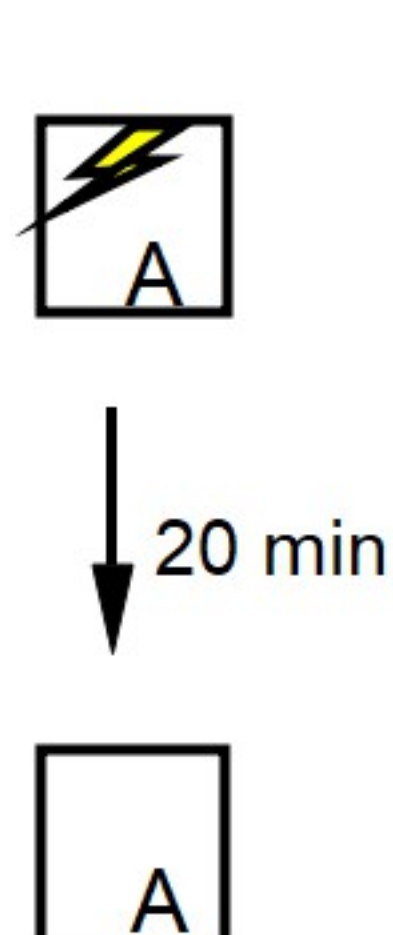
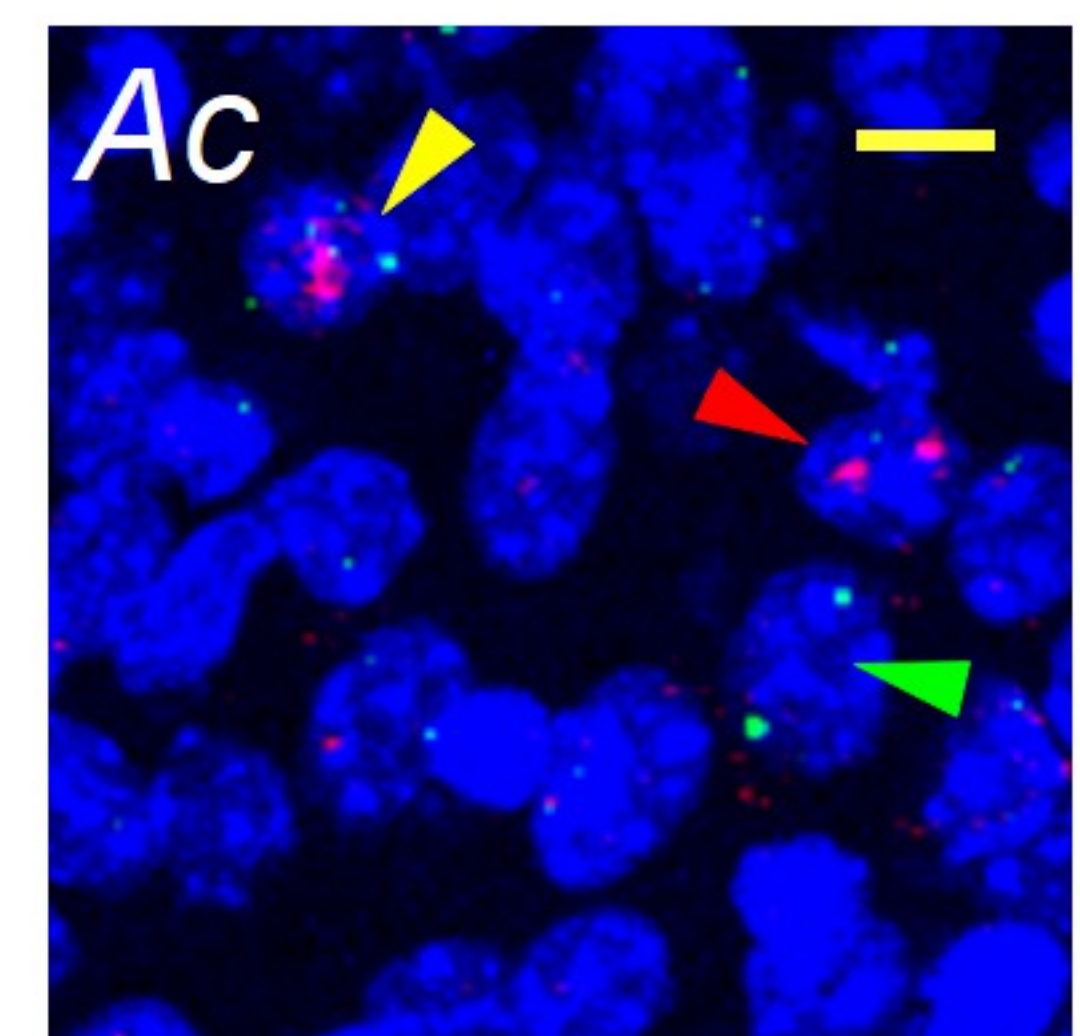
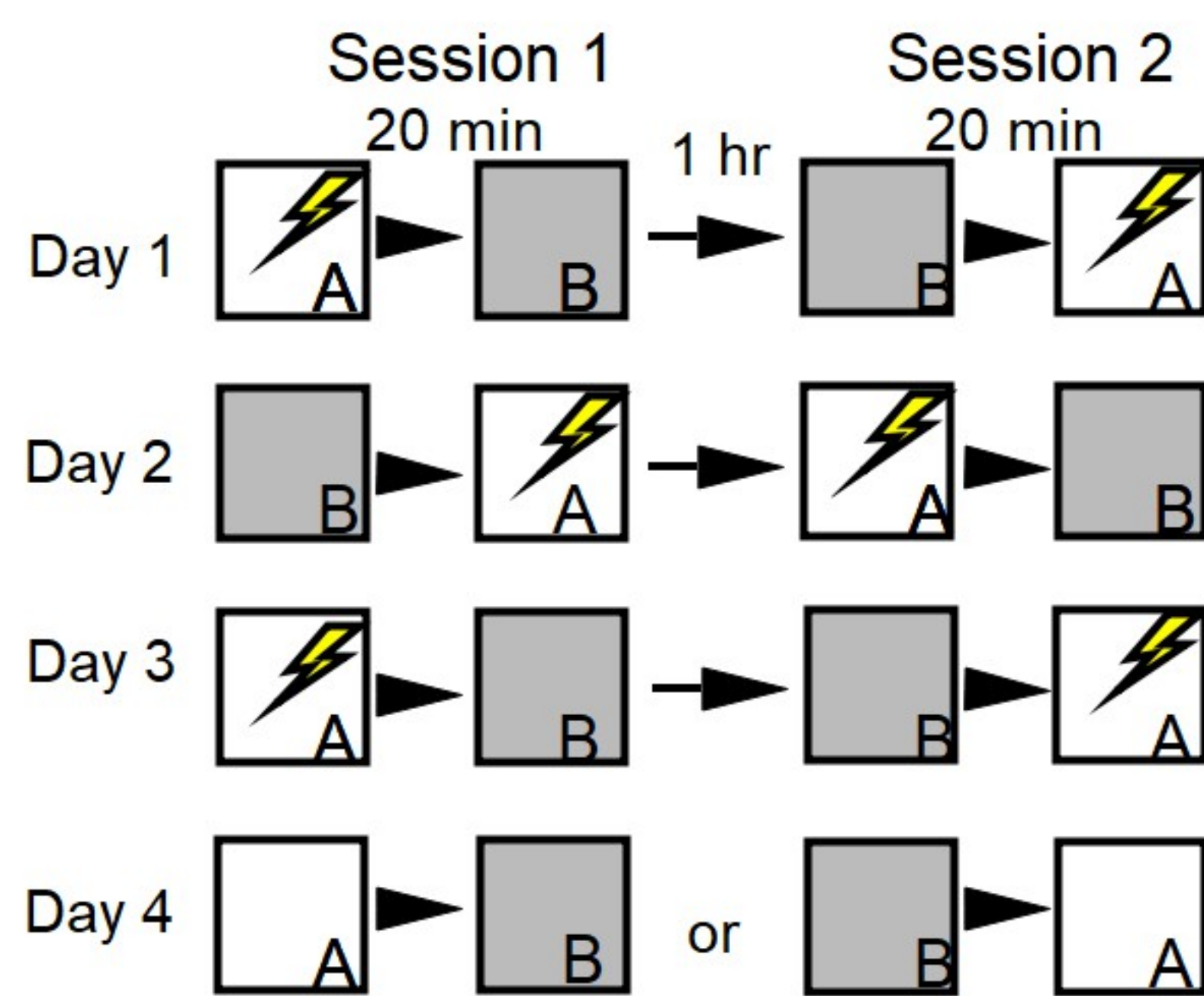
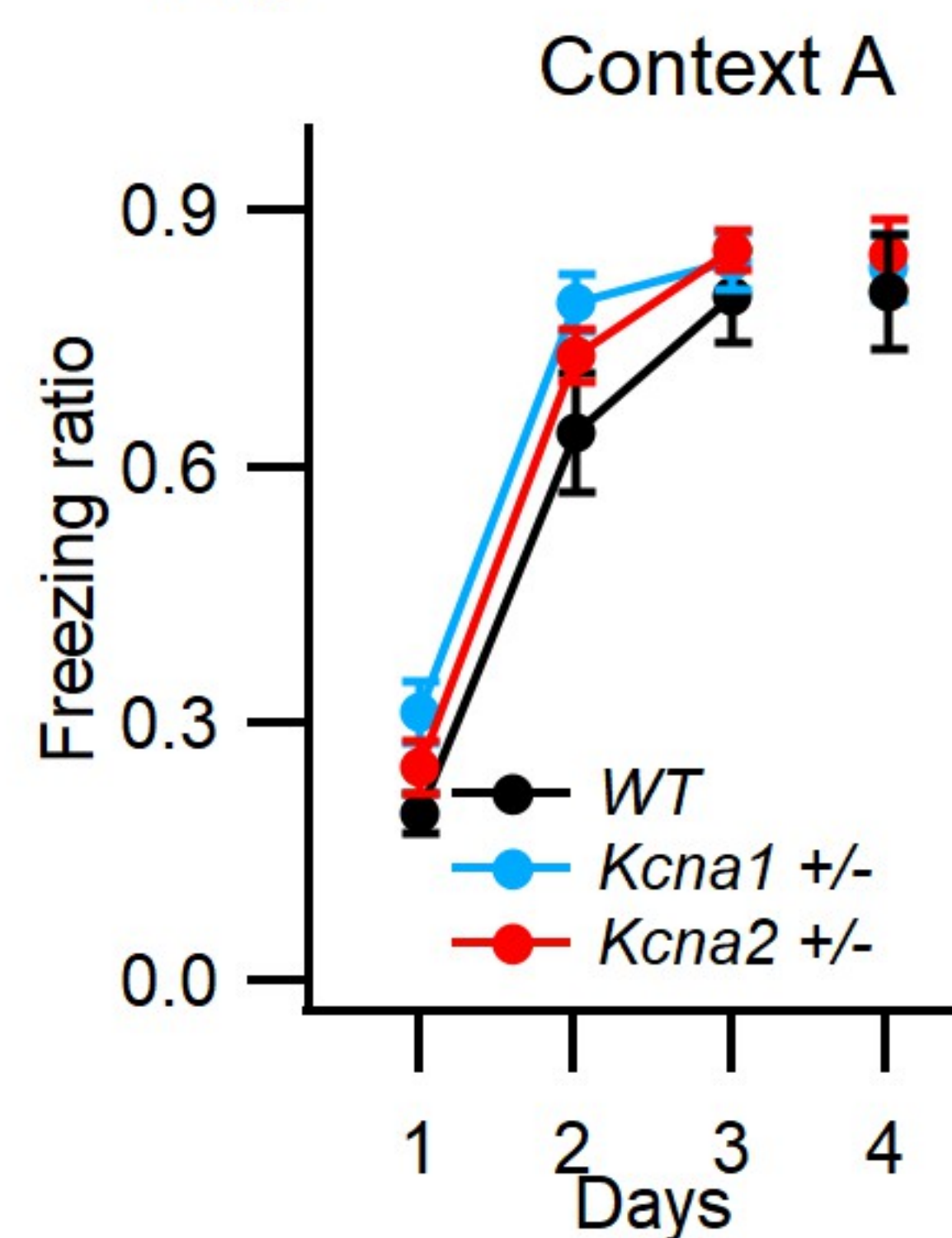
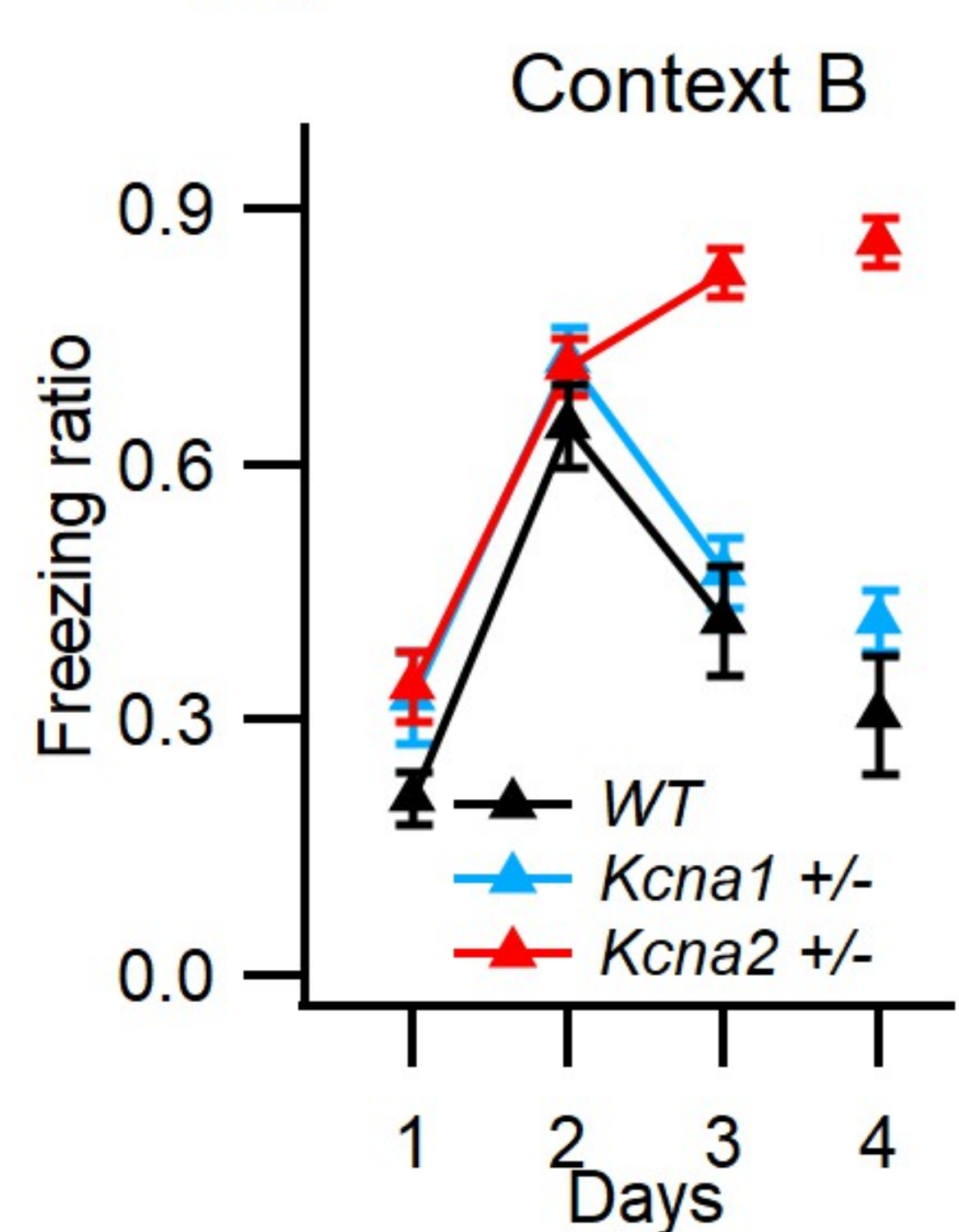
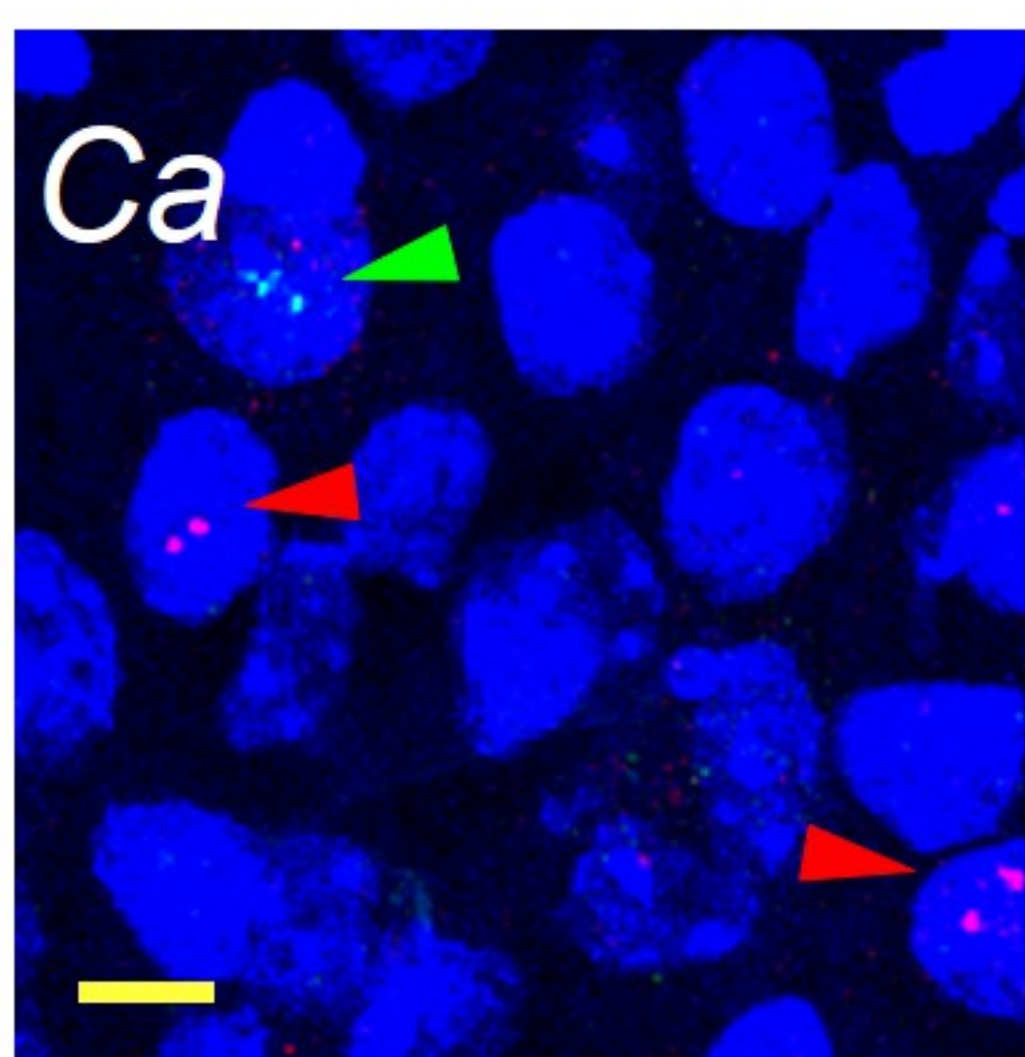
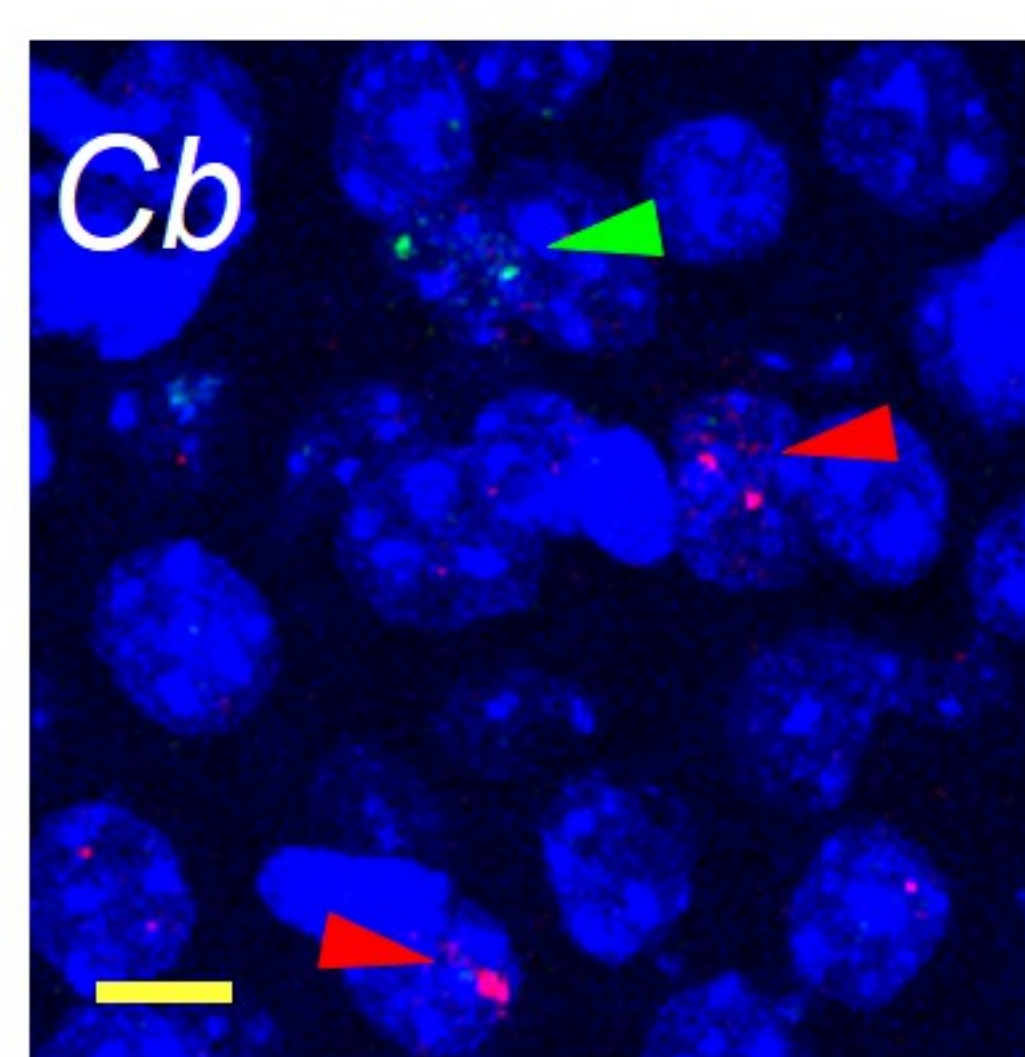
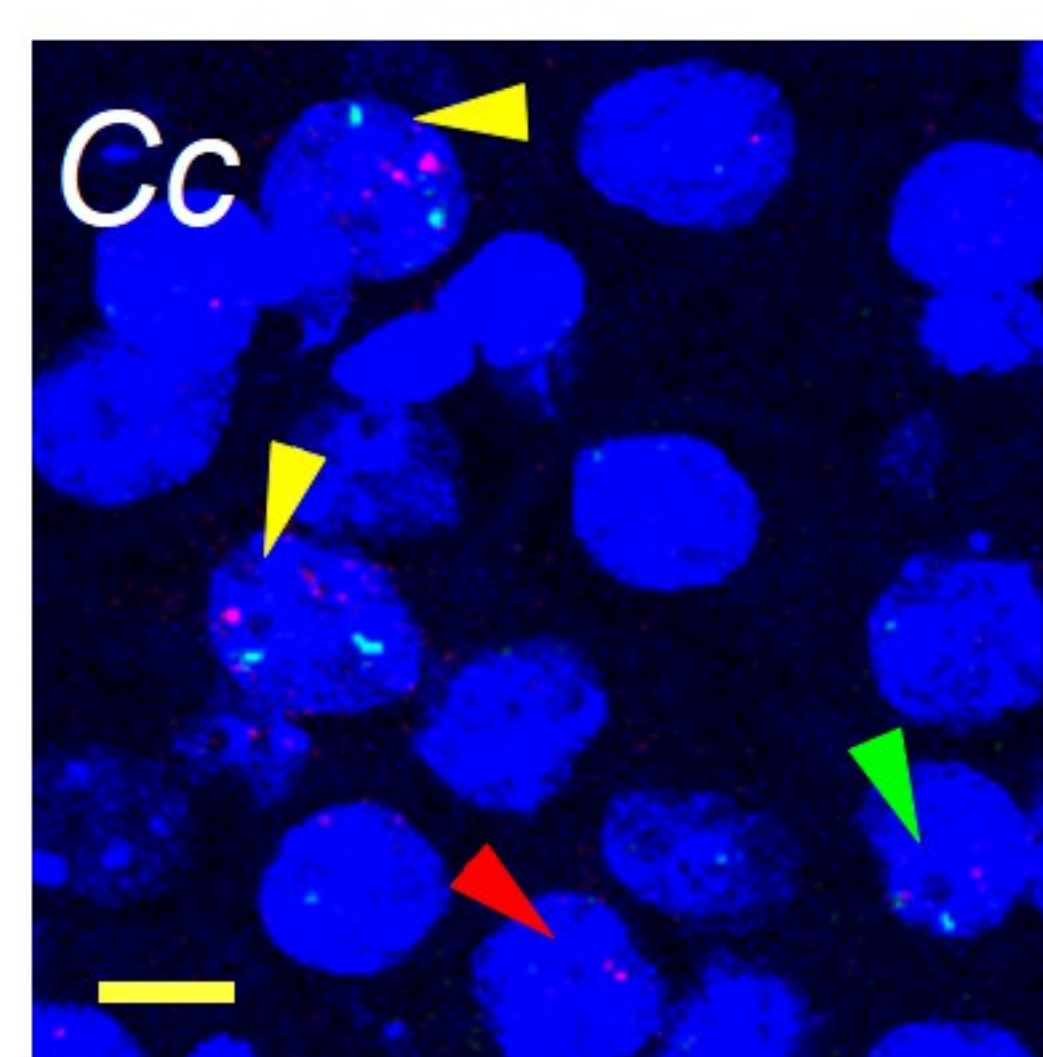
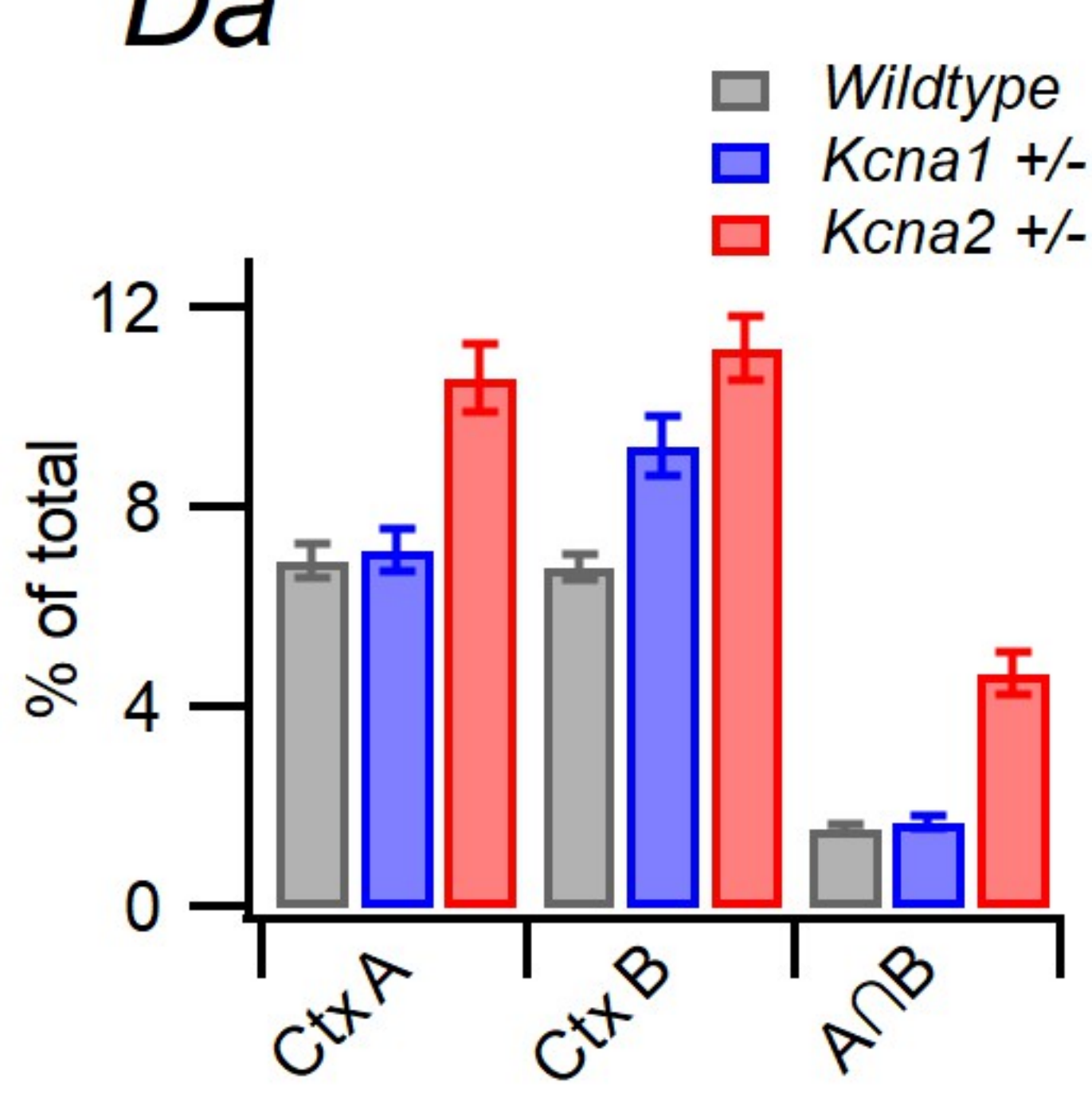
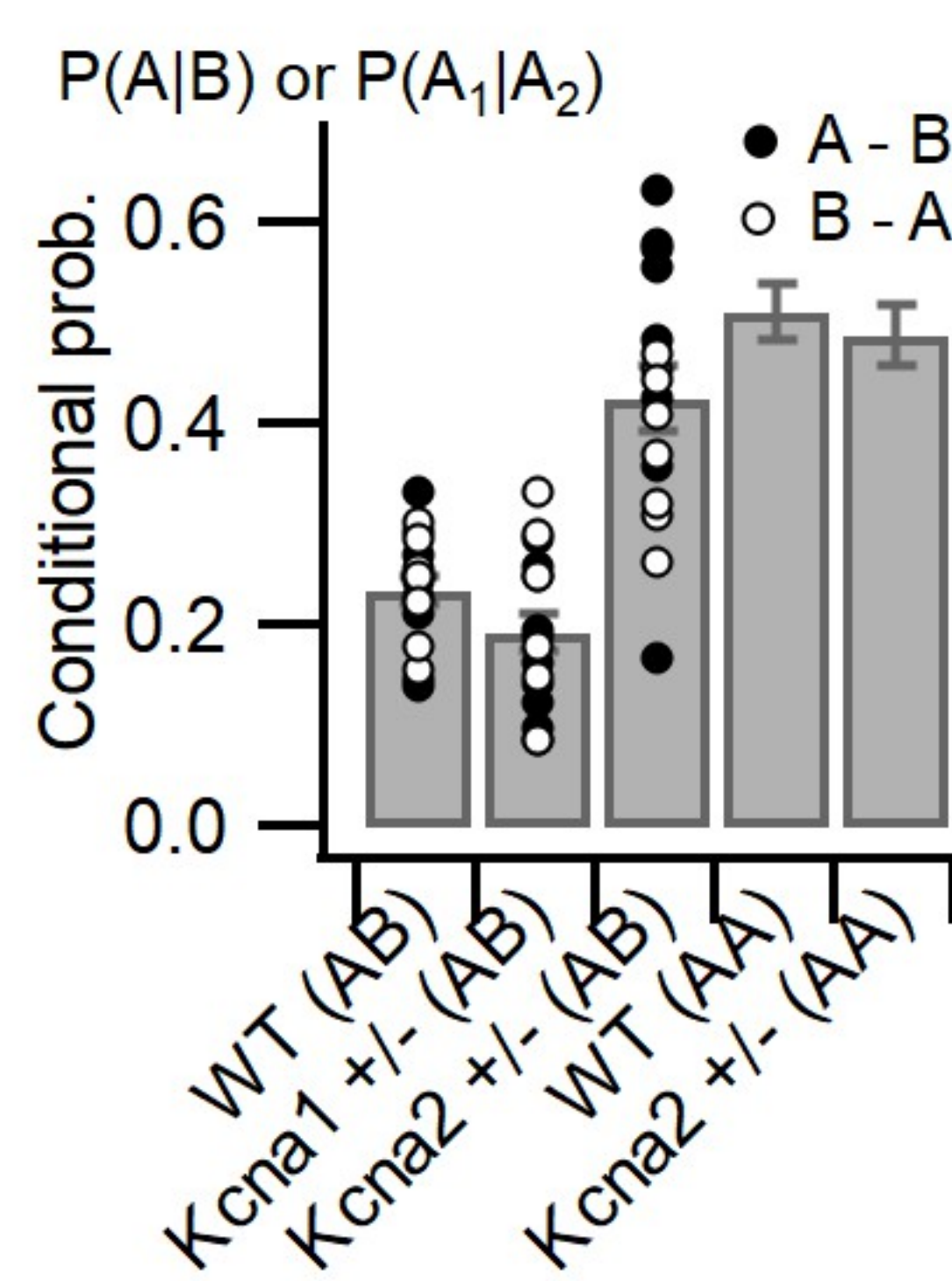


**Aa****Ab****Ac****Ad****Ba****Bb****C**

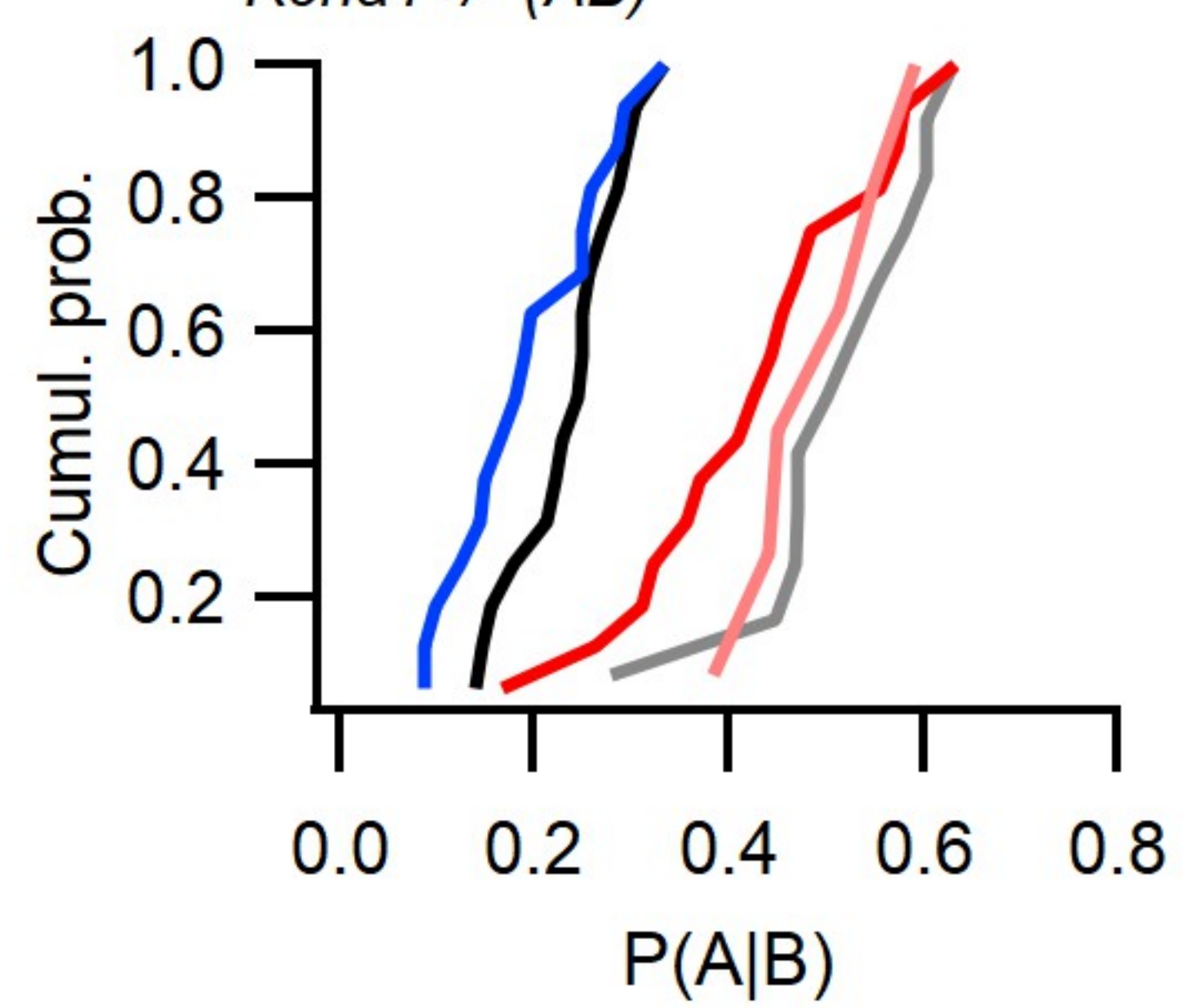
**Aa****Ab****Ba****Bb****Ac****Bc****Cb****Cc****Cd****Ca****Dc****Da****Db**

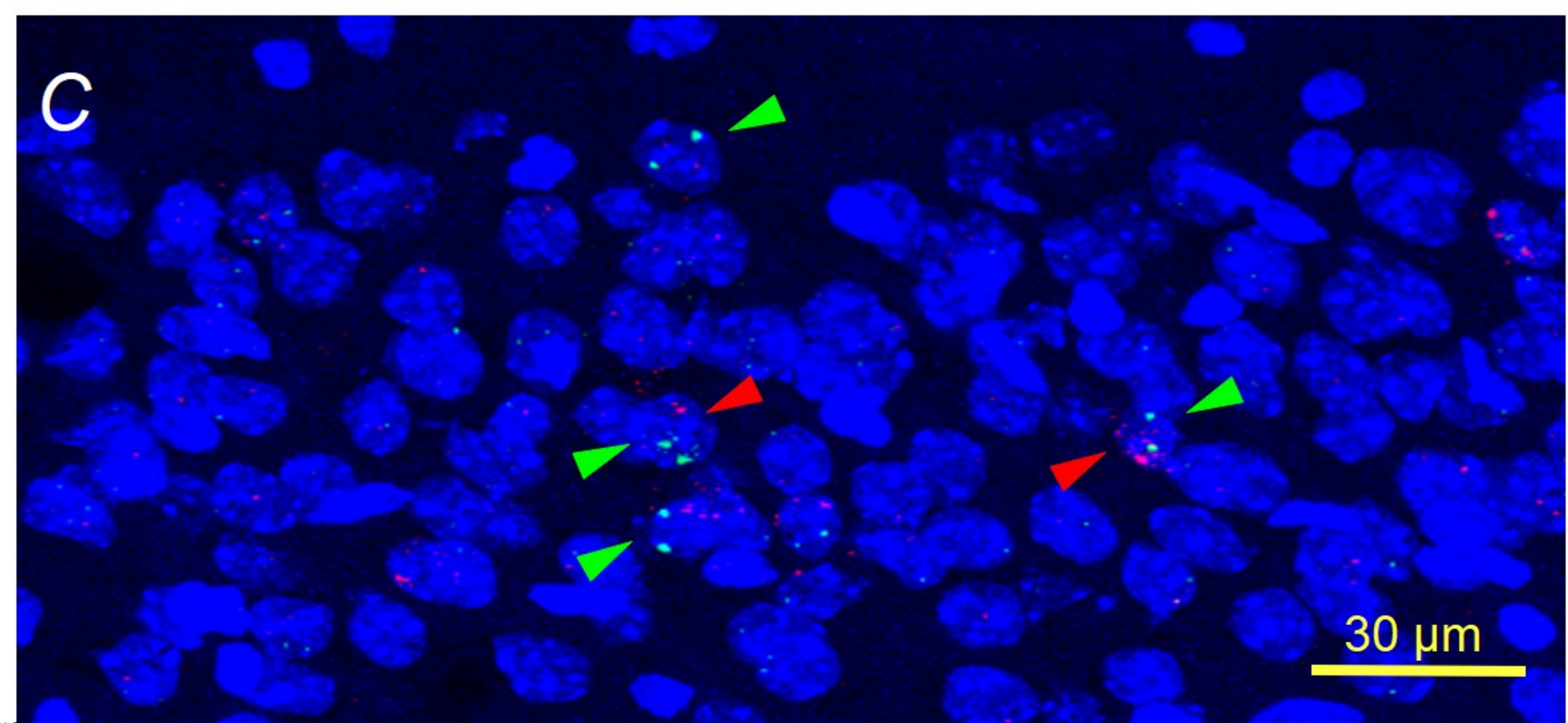
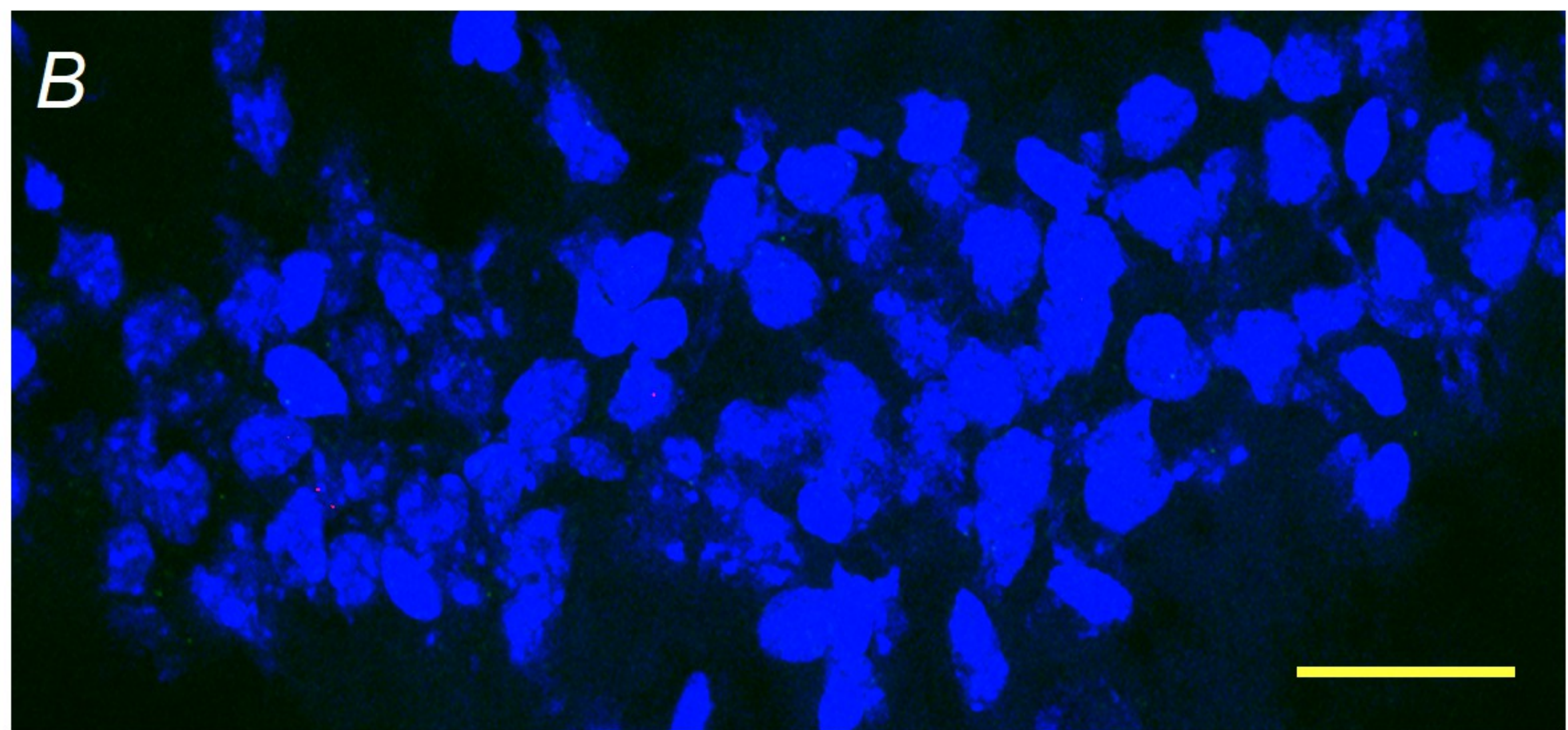
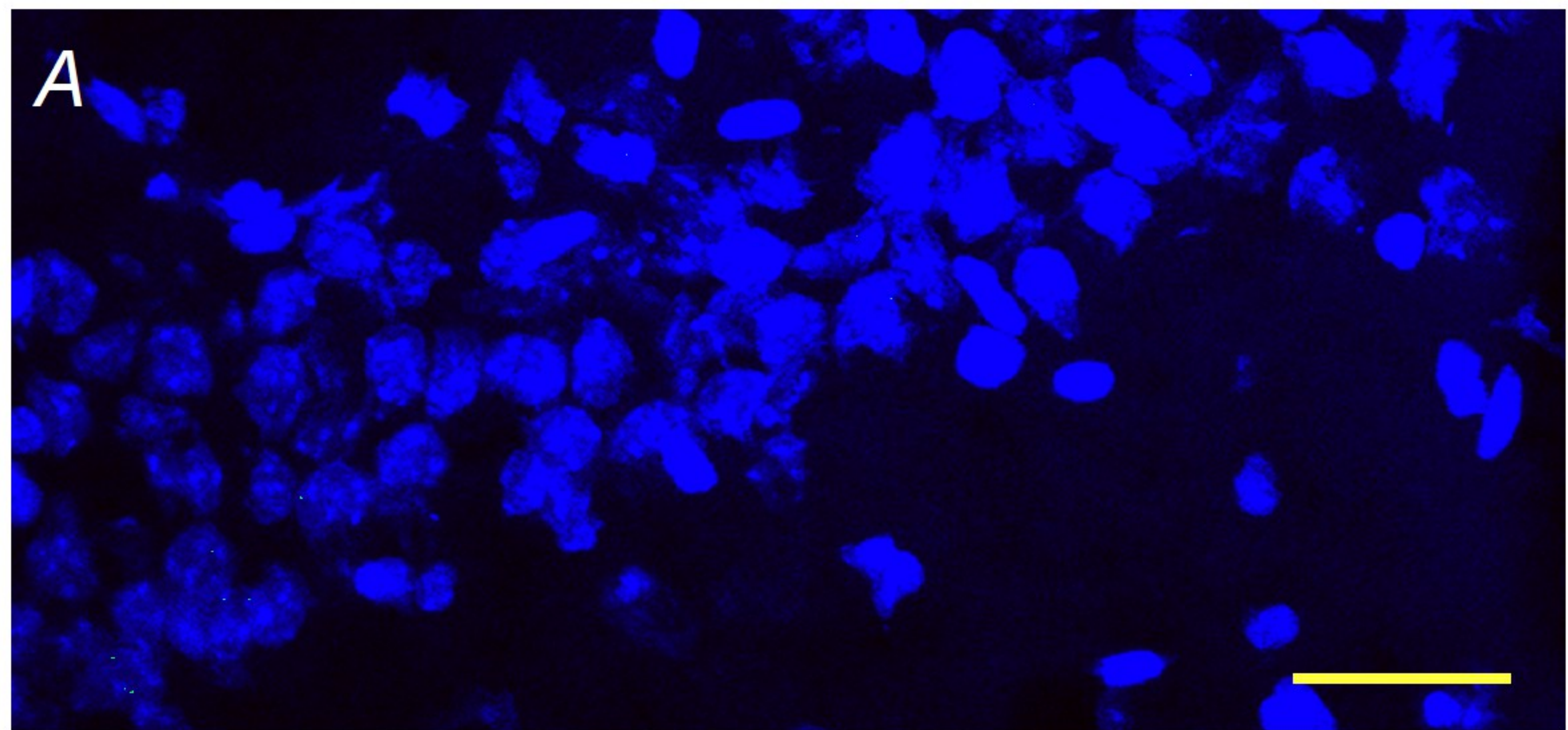
**A****Ba****Bc****Bb****Bd****Be****Ca****Cb****Da****Db****Ea****Eb****Ec**



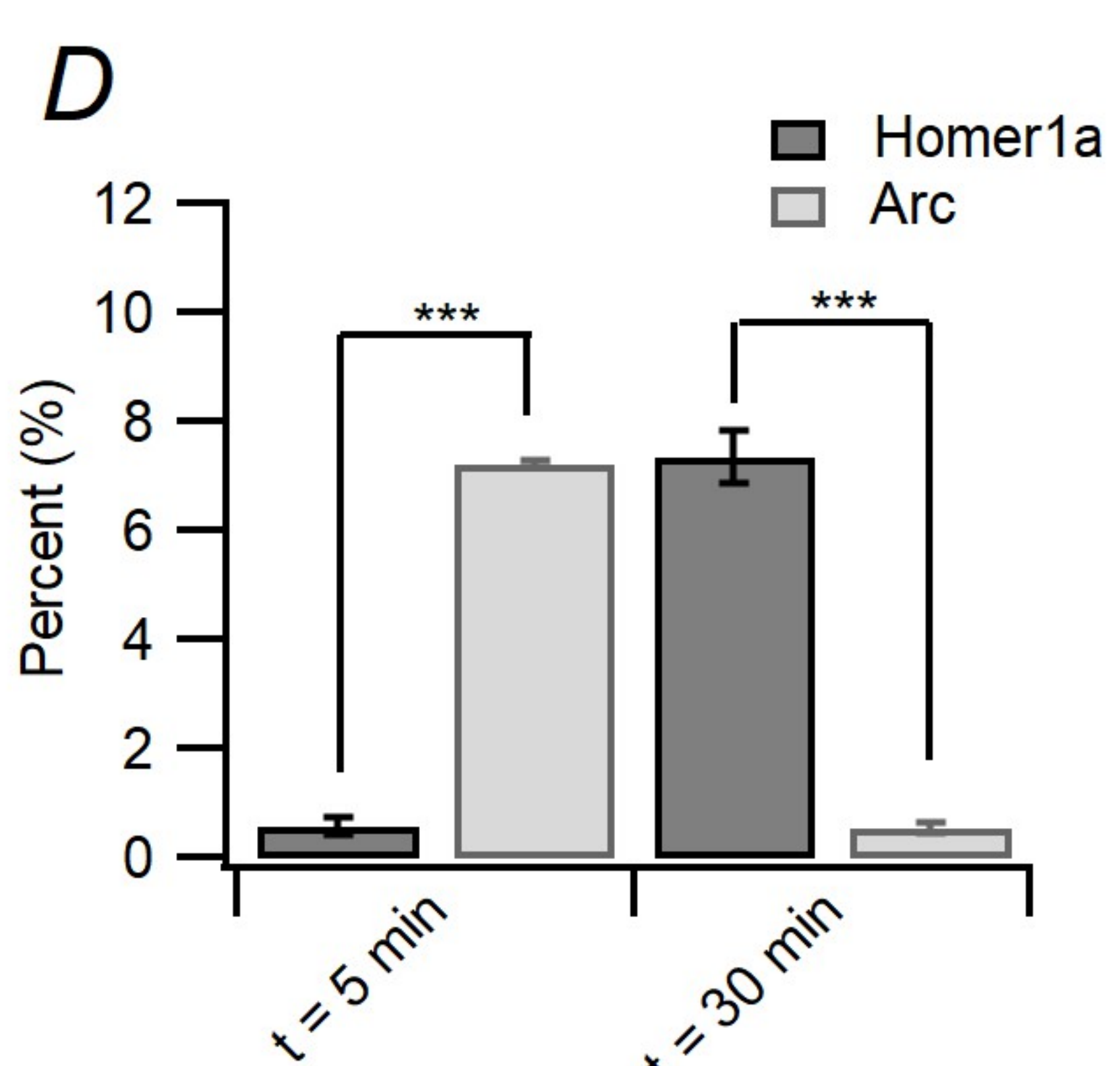
**Aa****WT (AA)****Kcna2+/- (AA)****Ba****Bb****Bc****WT****Kcna1 +/-****Kcna2 +/-****Da****Db****Dc**

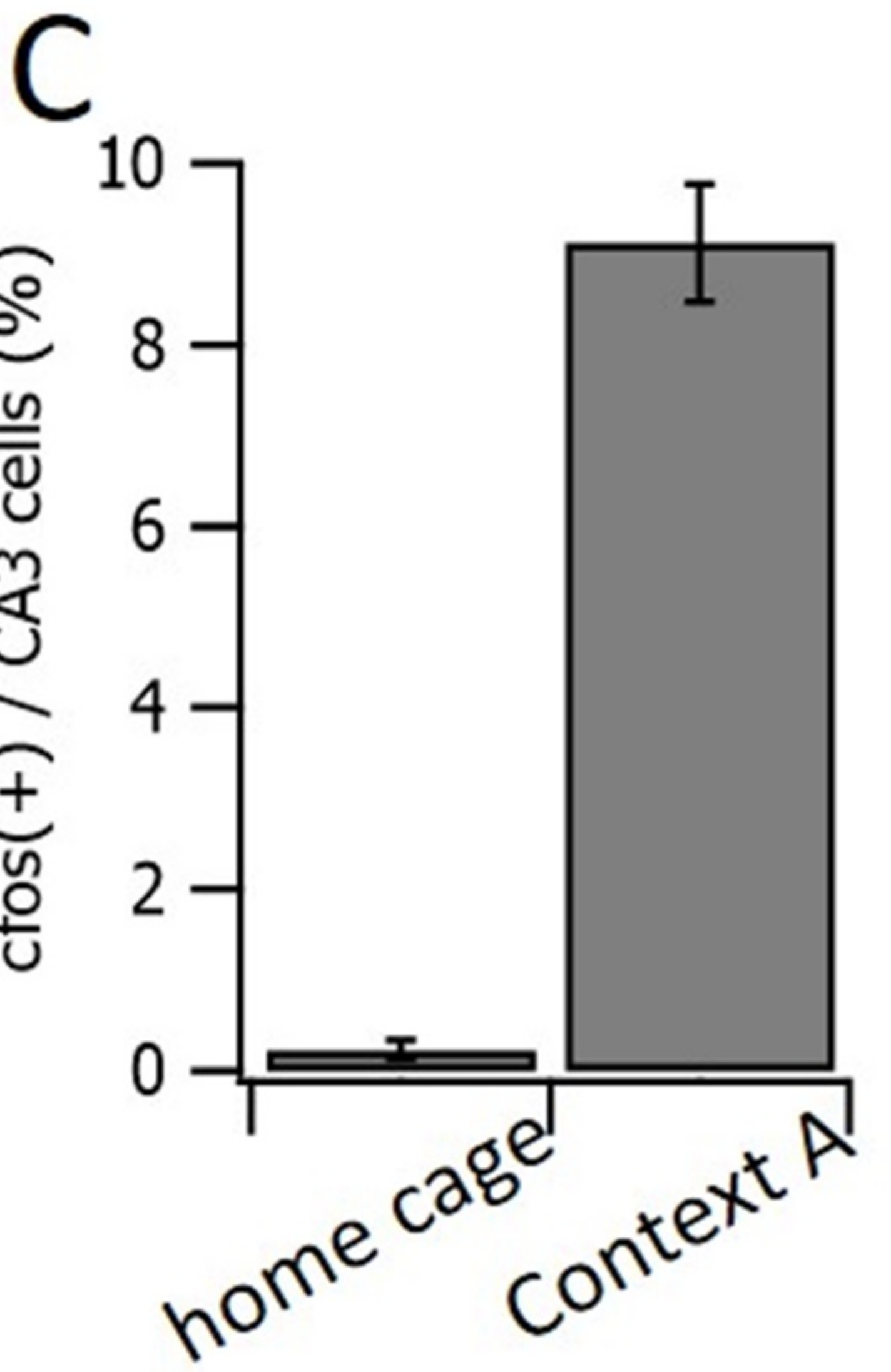
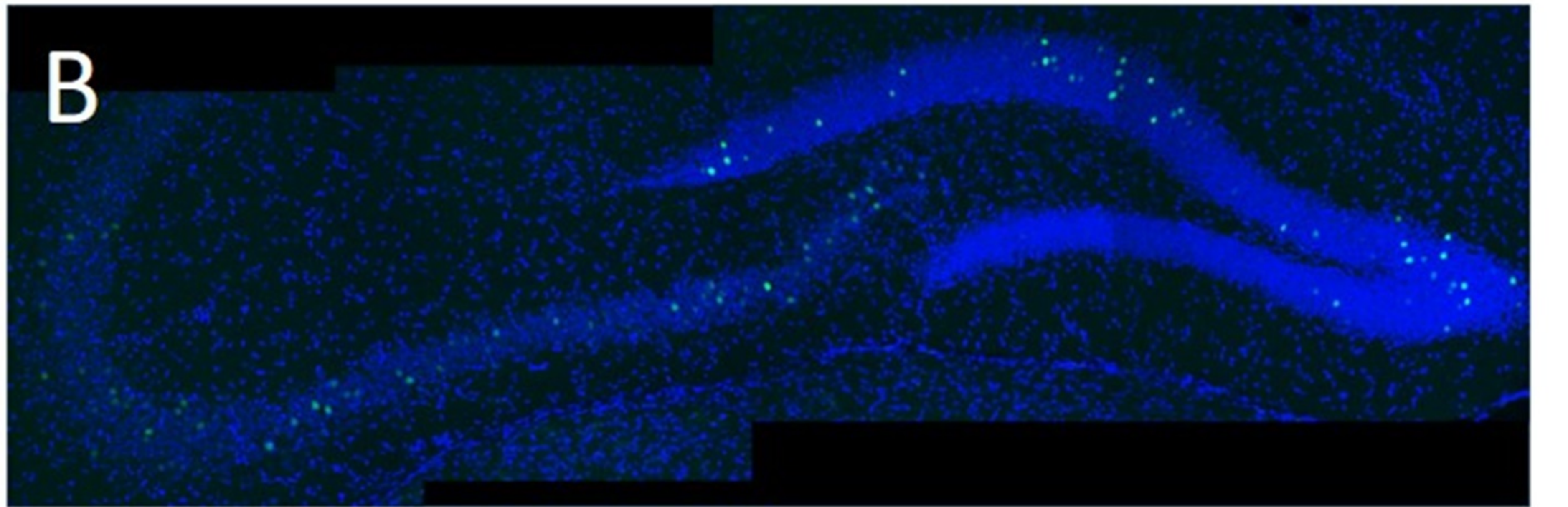
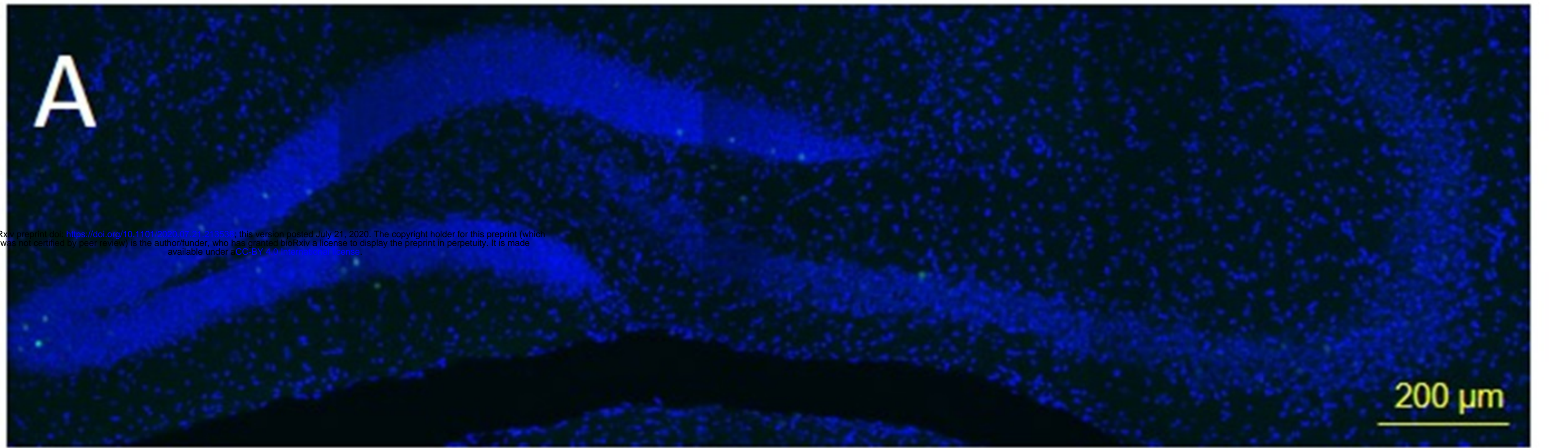
Legend:   
Wildtype (AA)   
Wildtype (AB)   
Kcna2 +/- (AA)   
Kcna2 +/- (AB)   
Kcna1 +/- (AB)

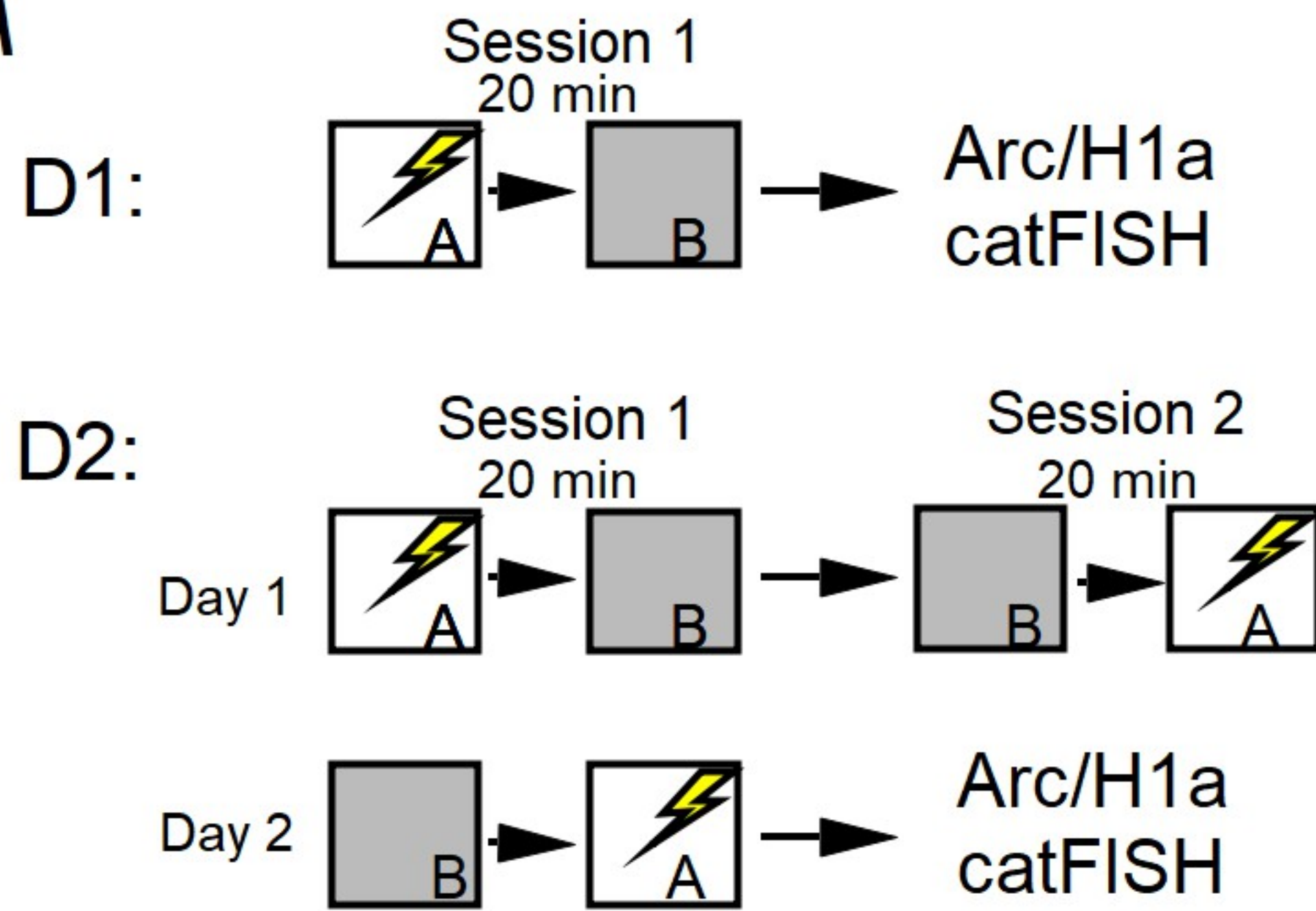
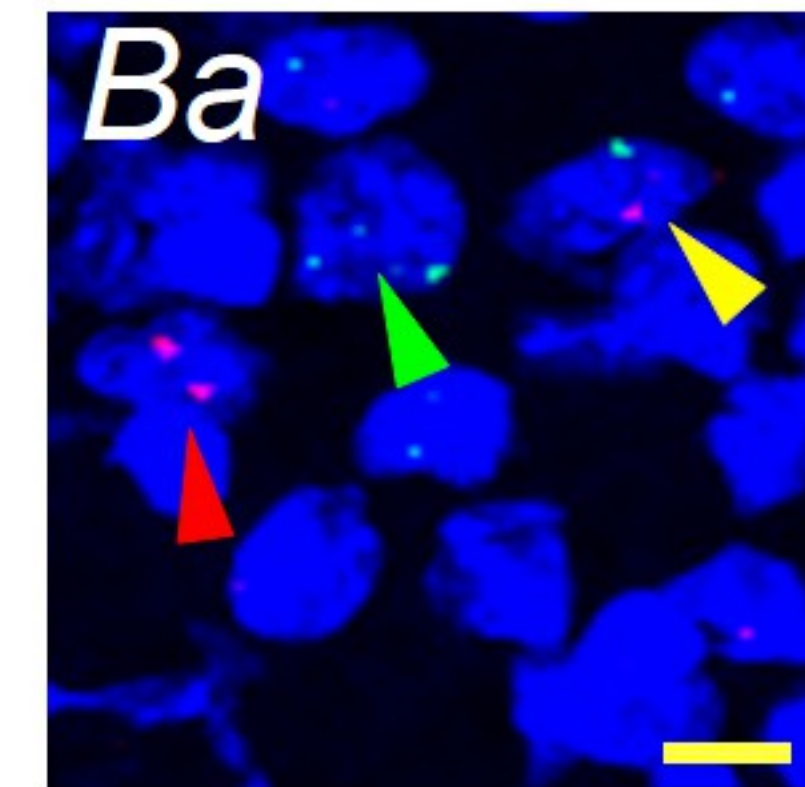
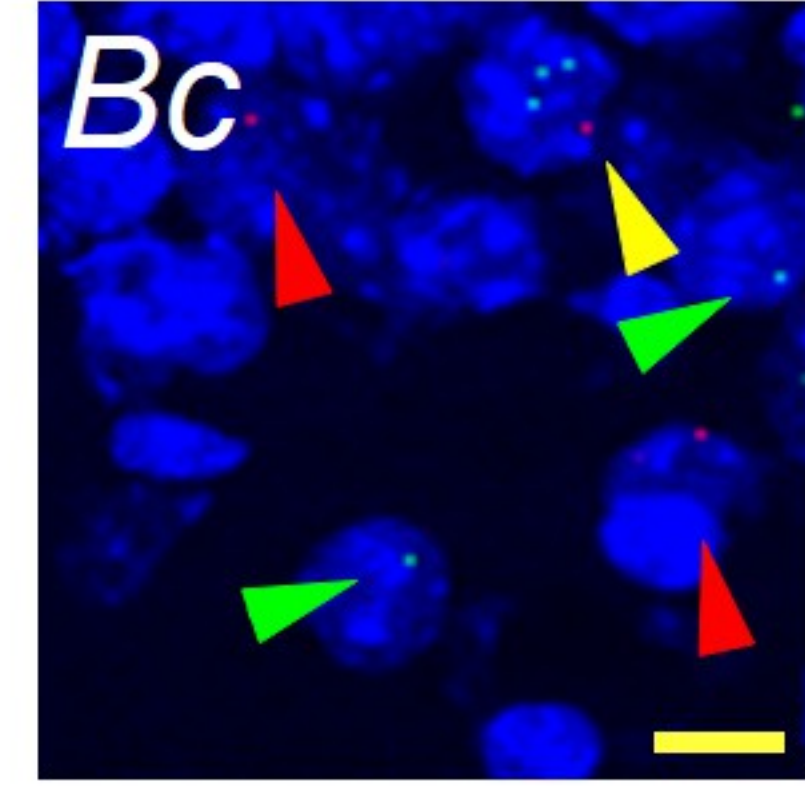
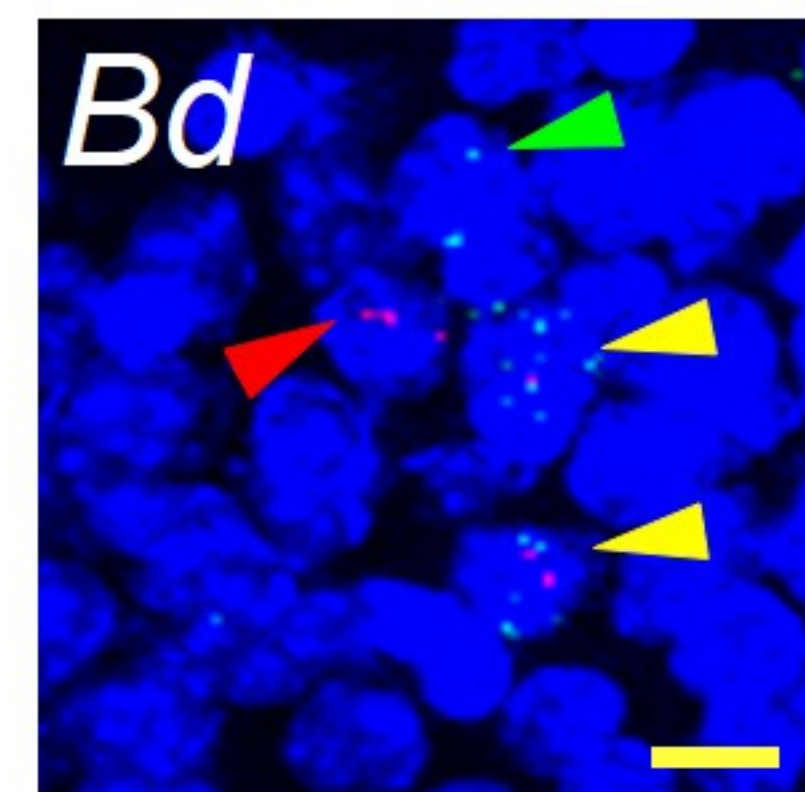
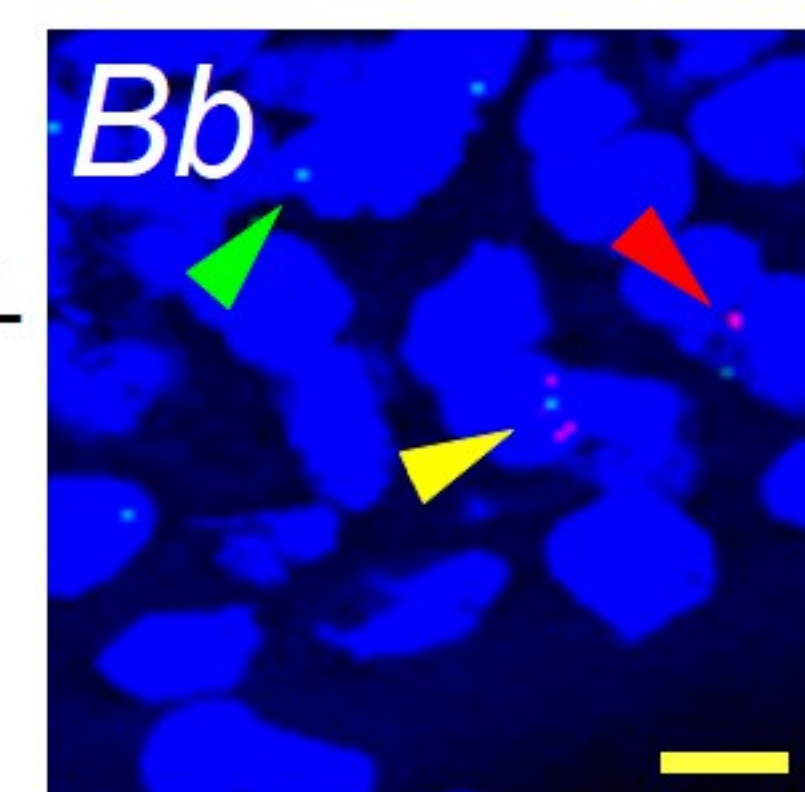
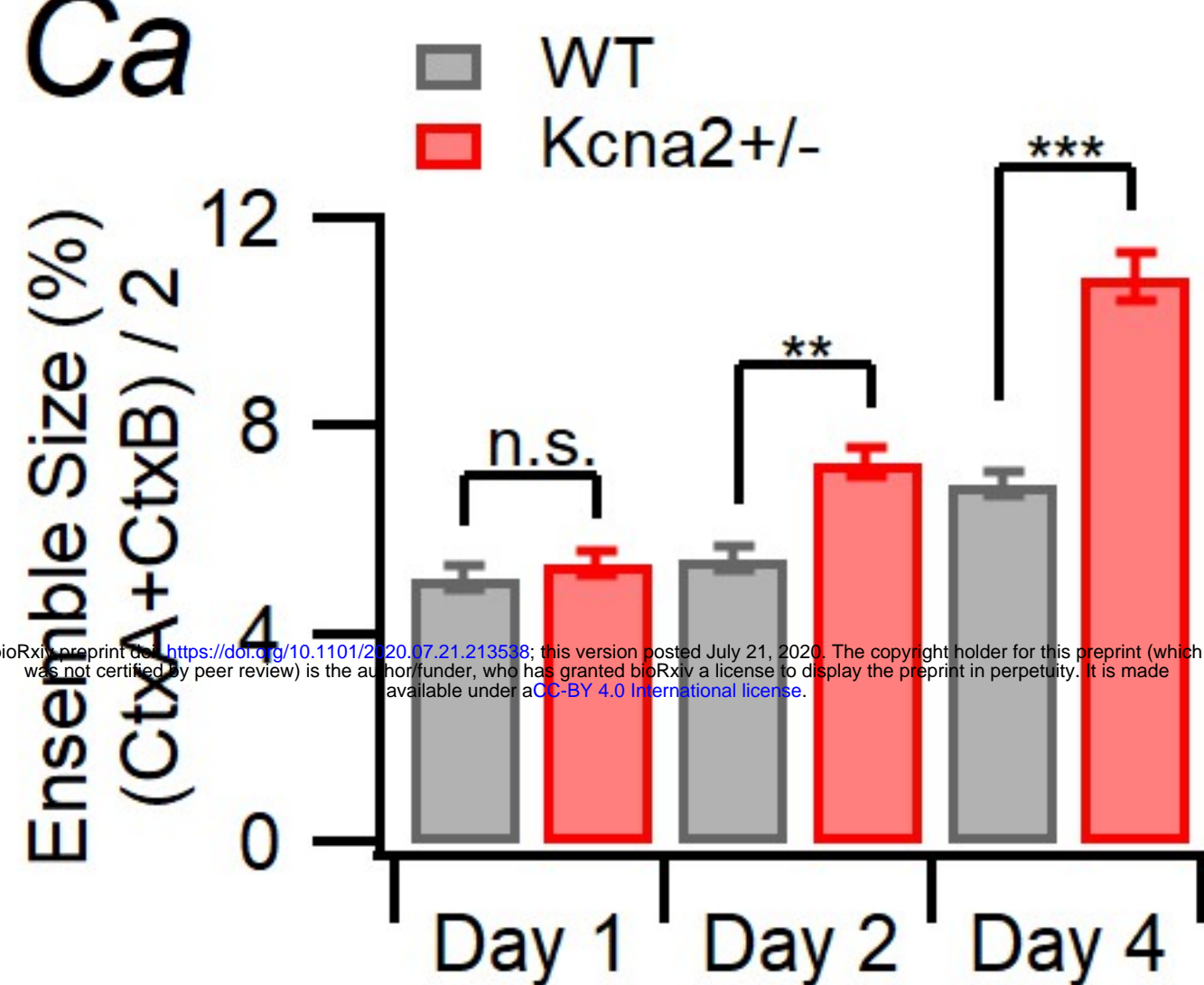
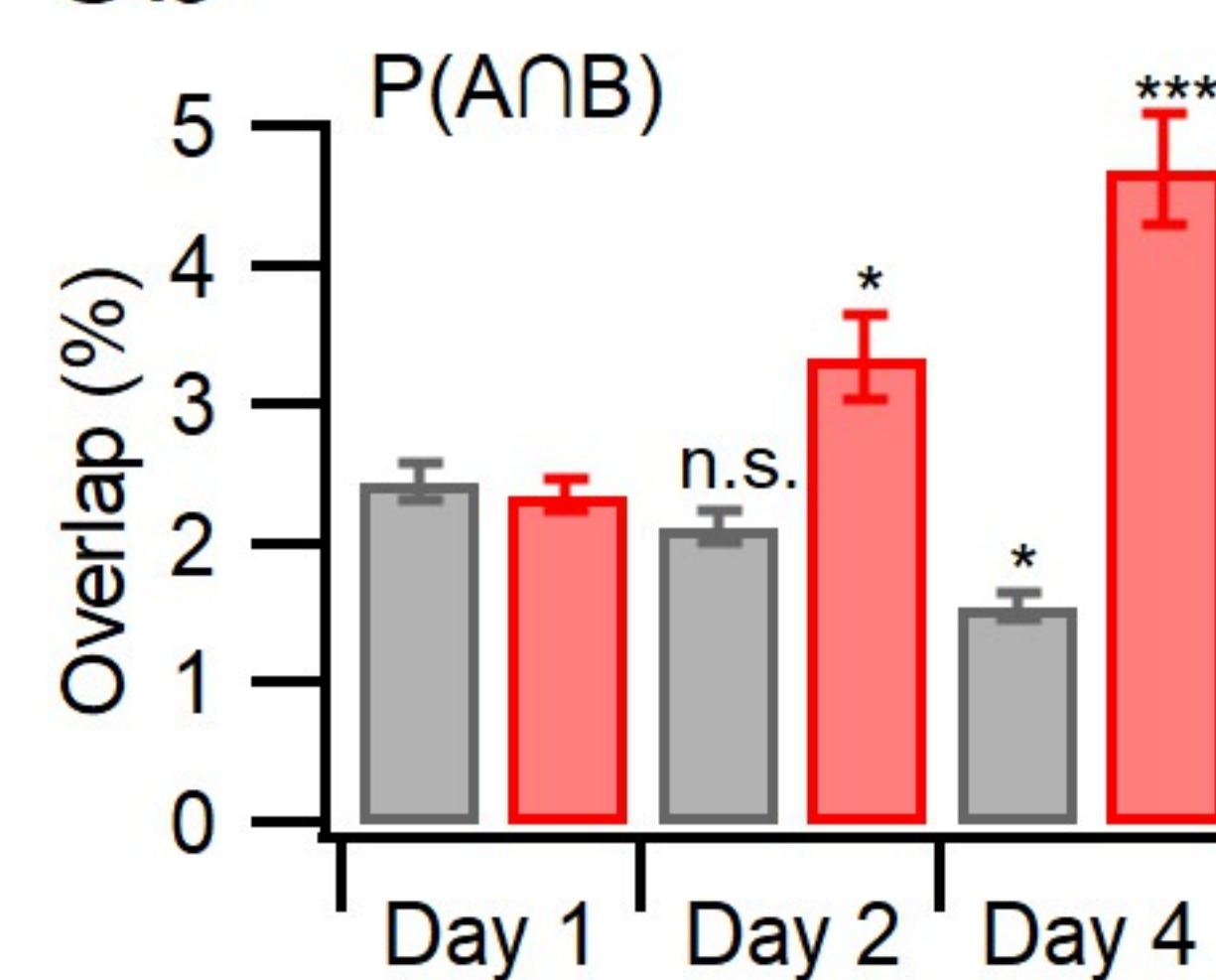
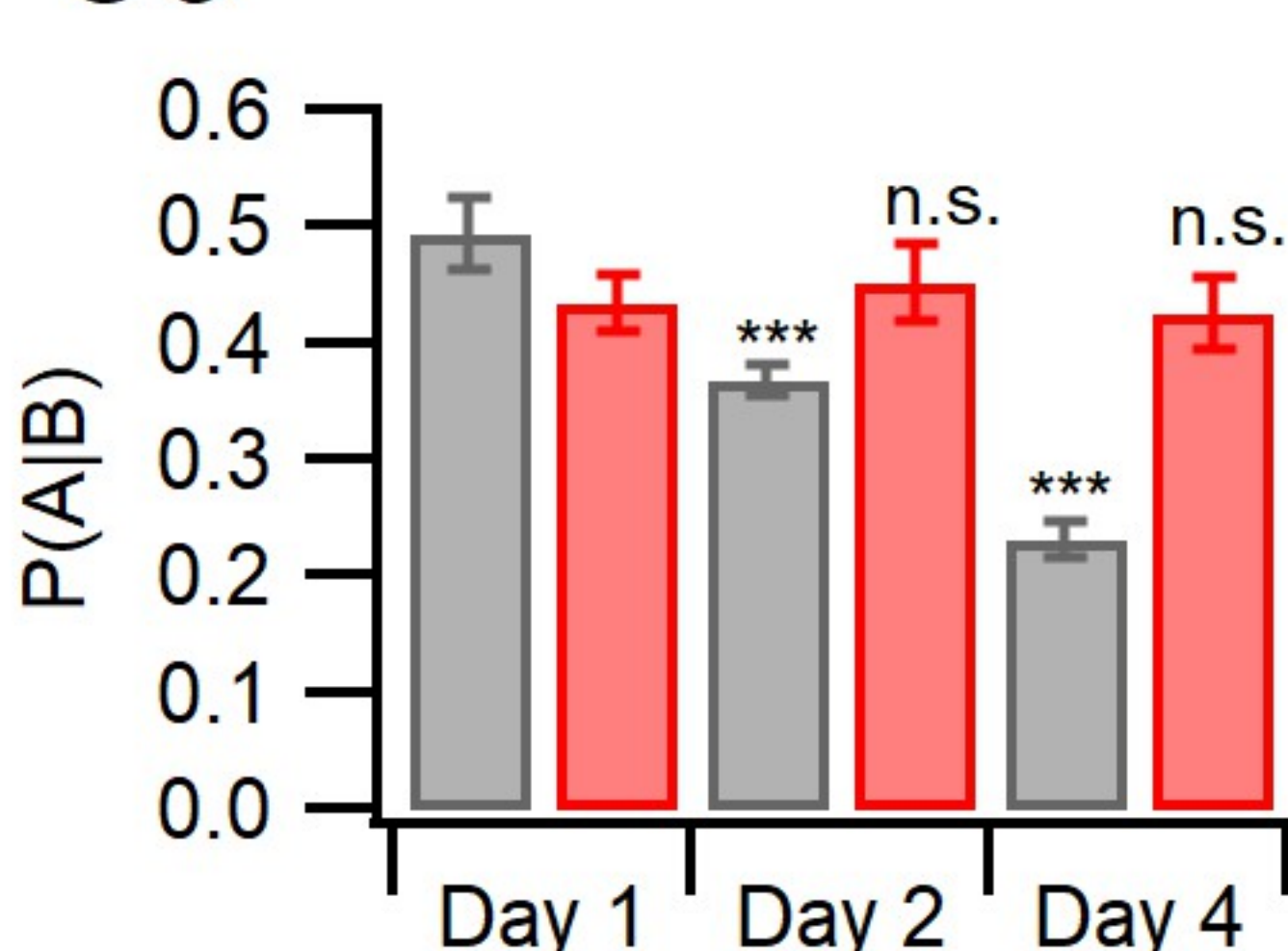
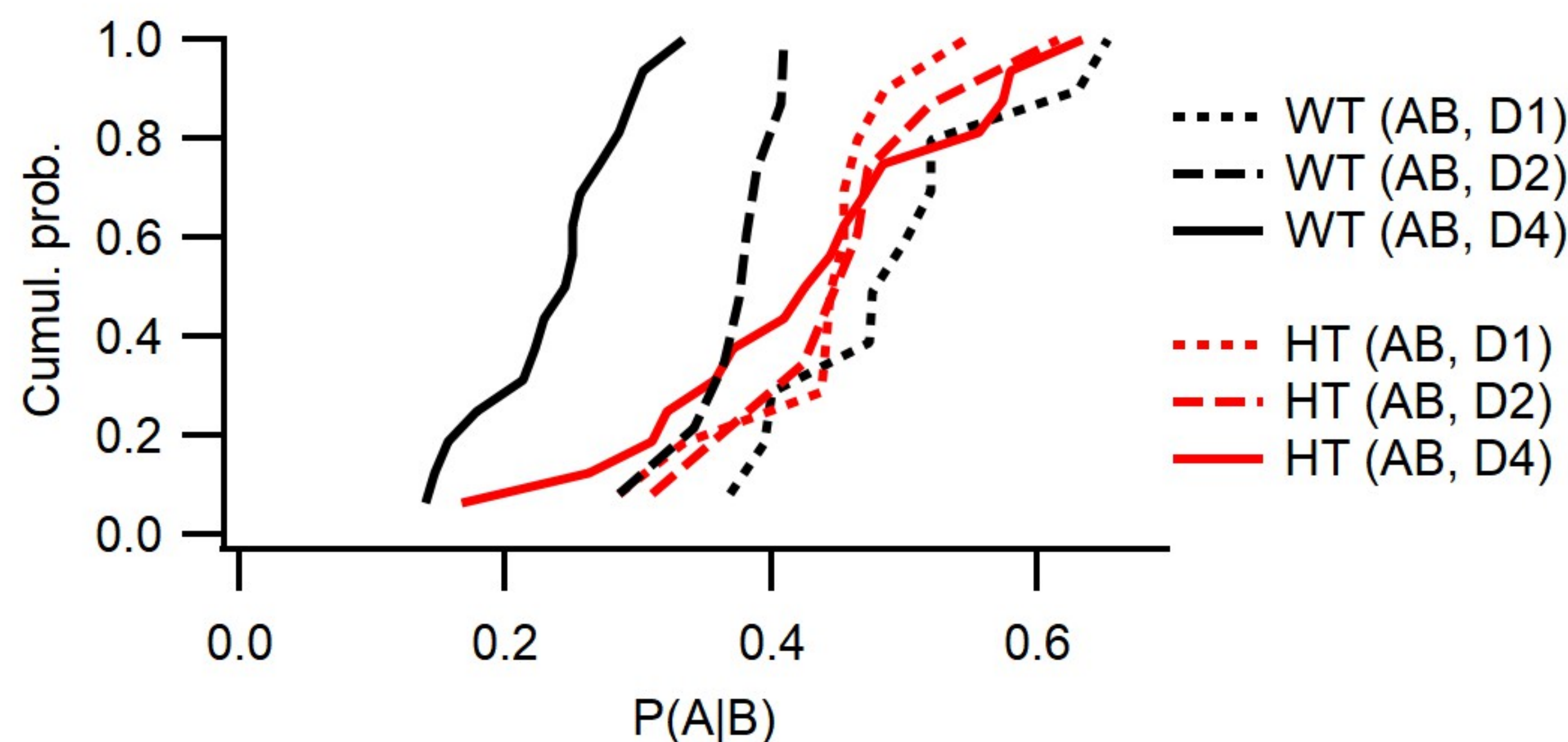


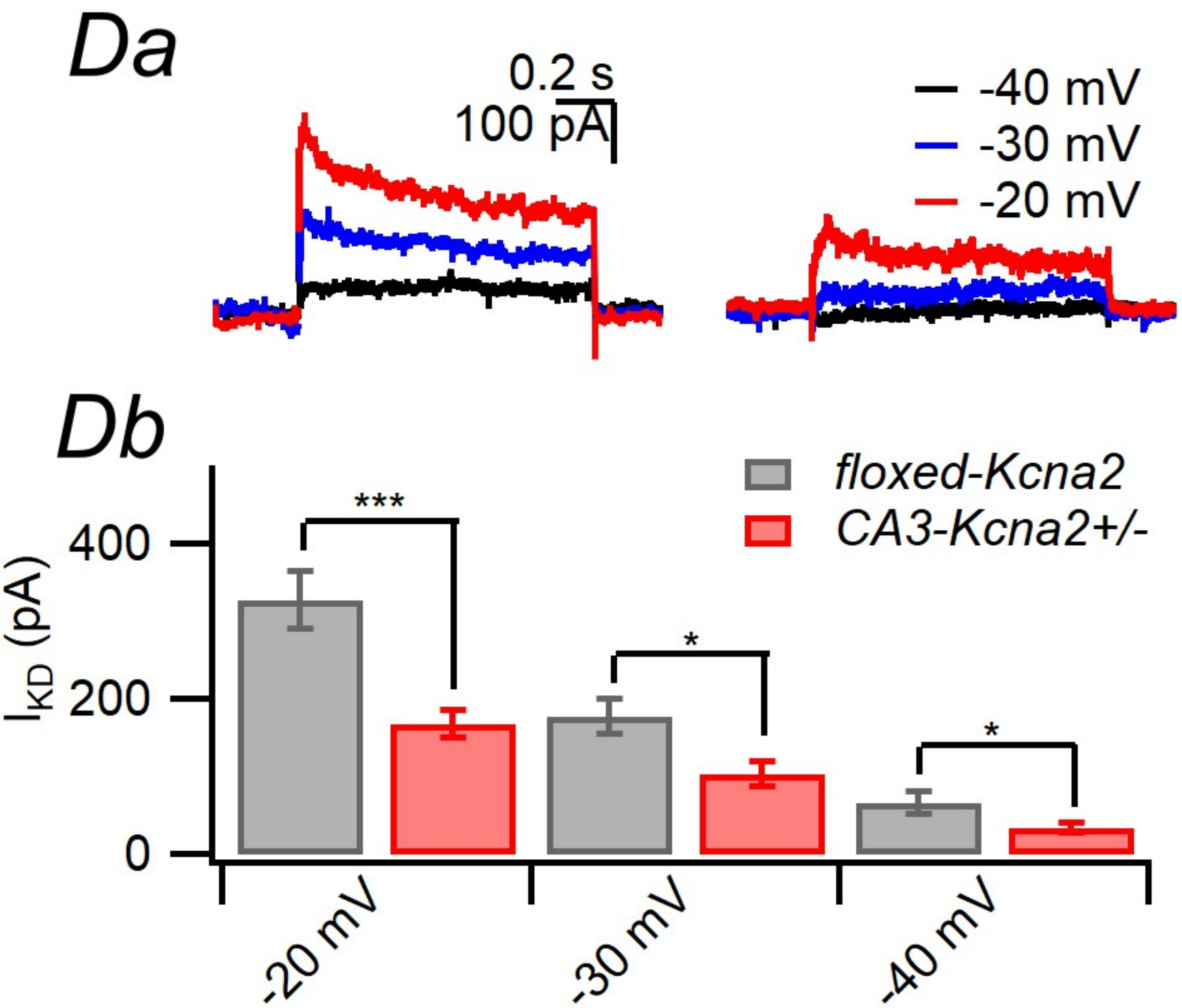
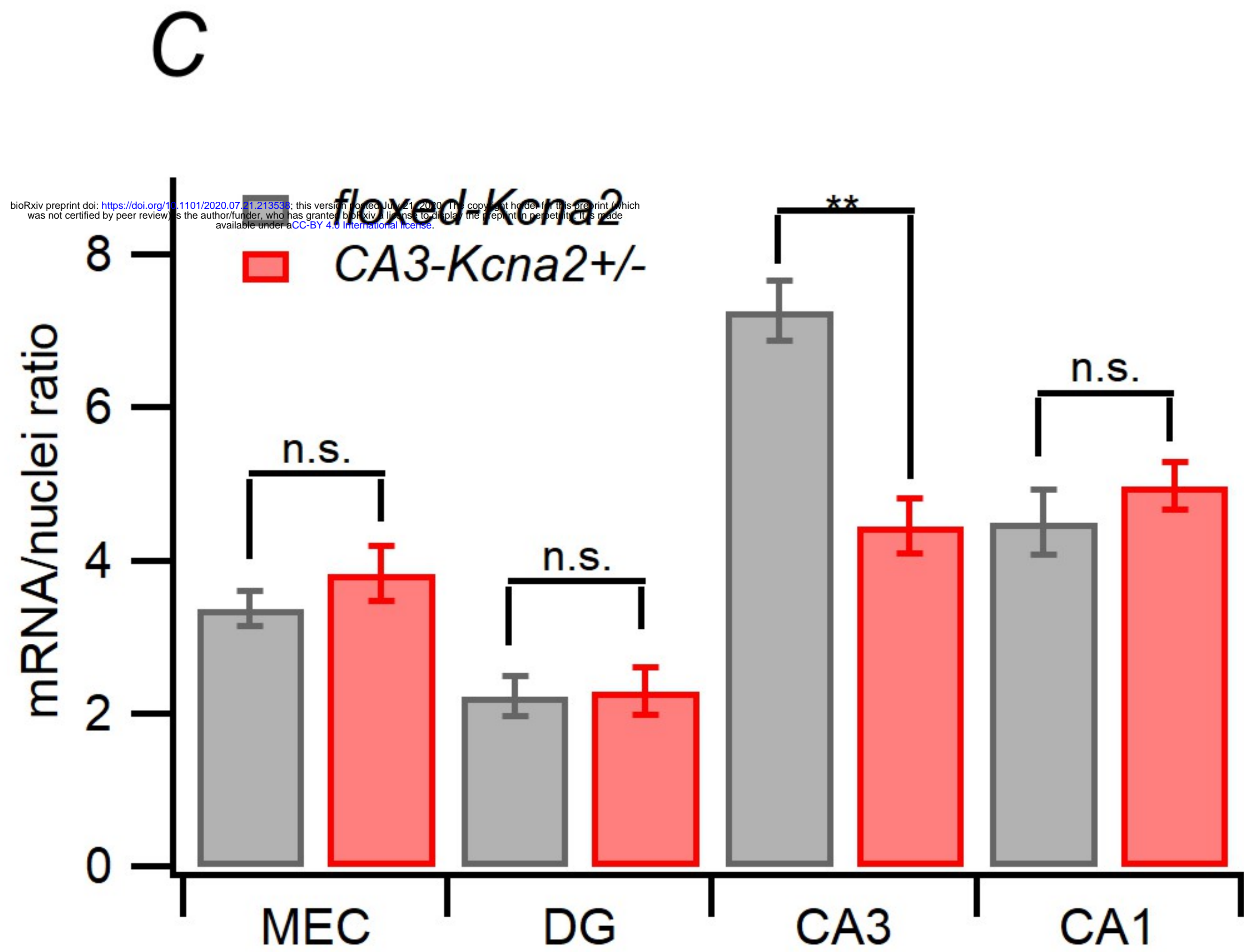
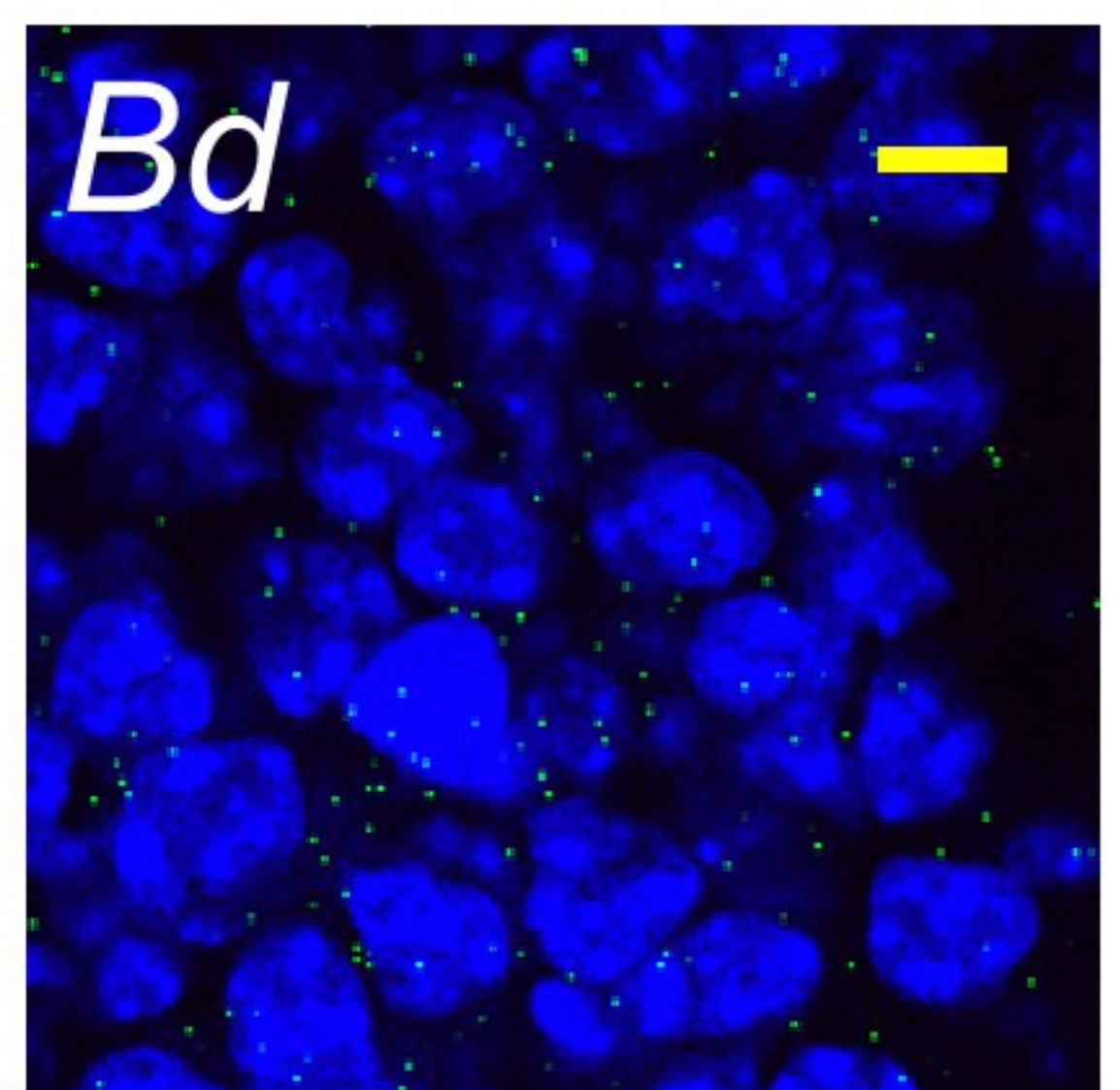
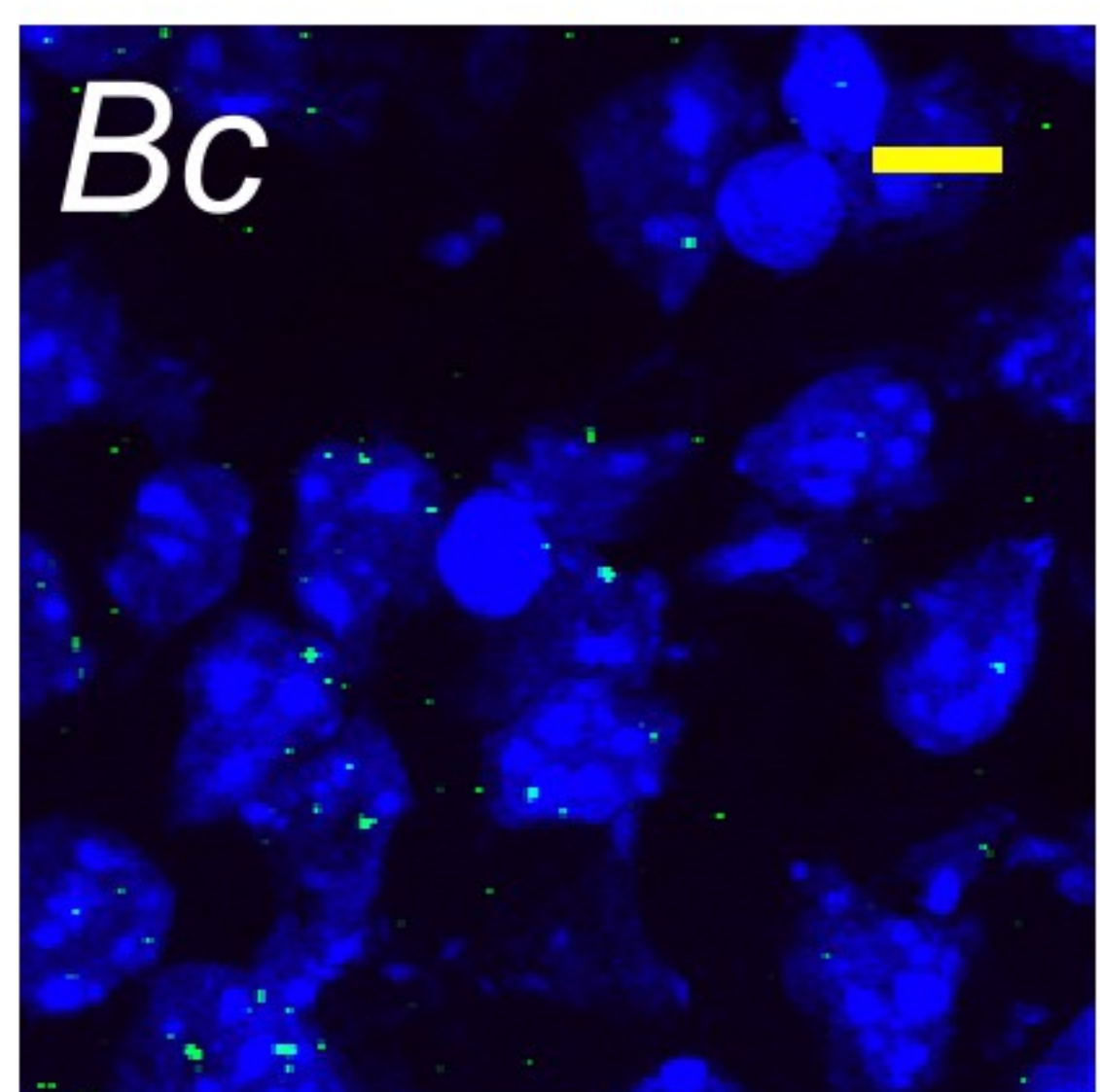
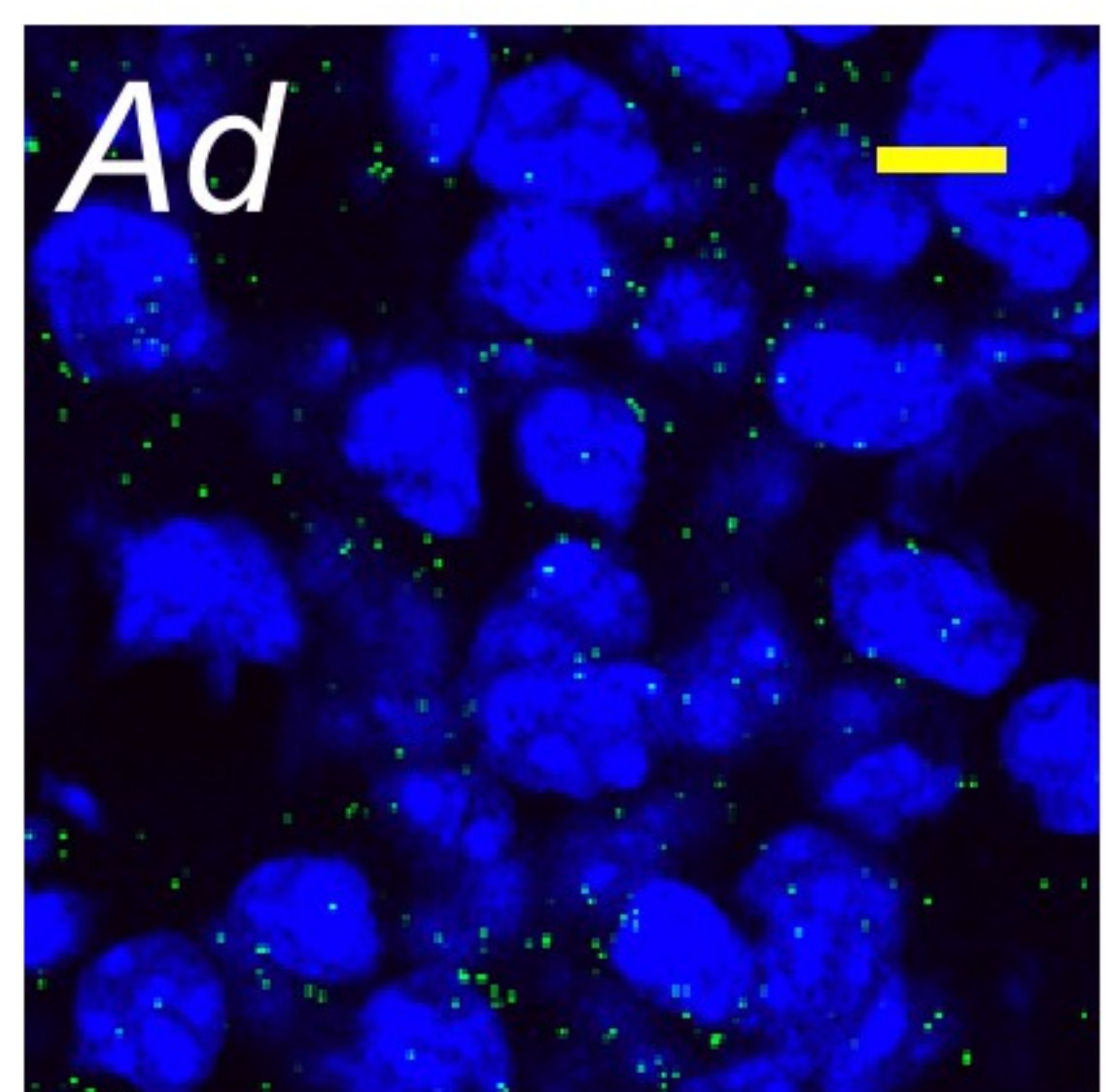
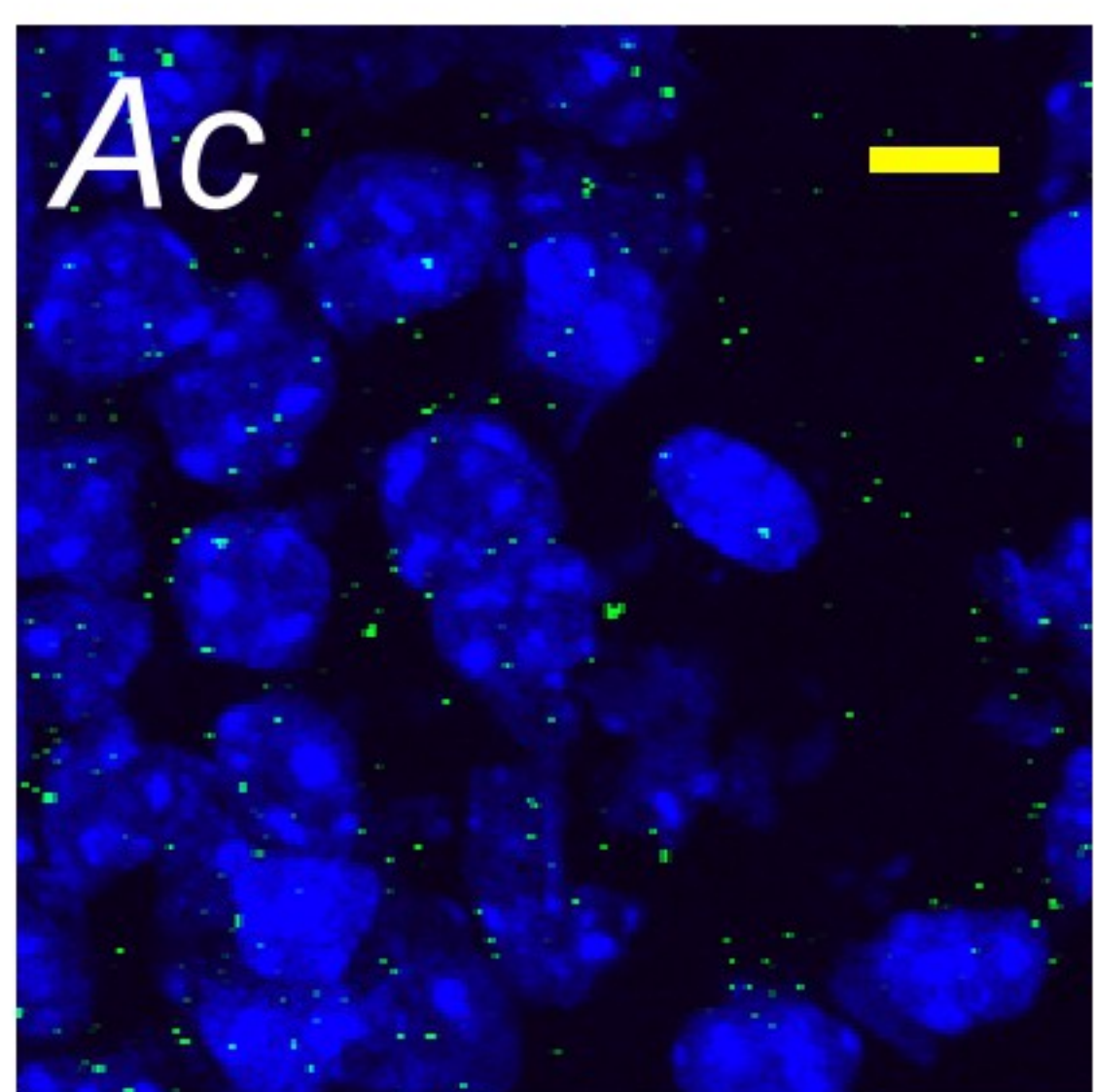
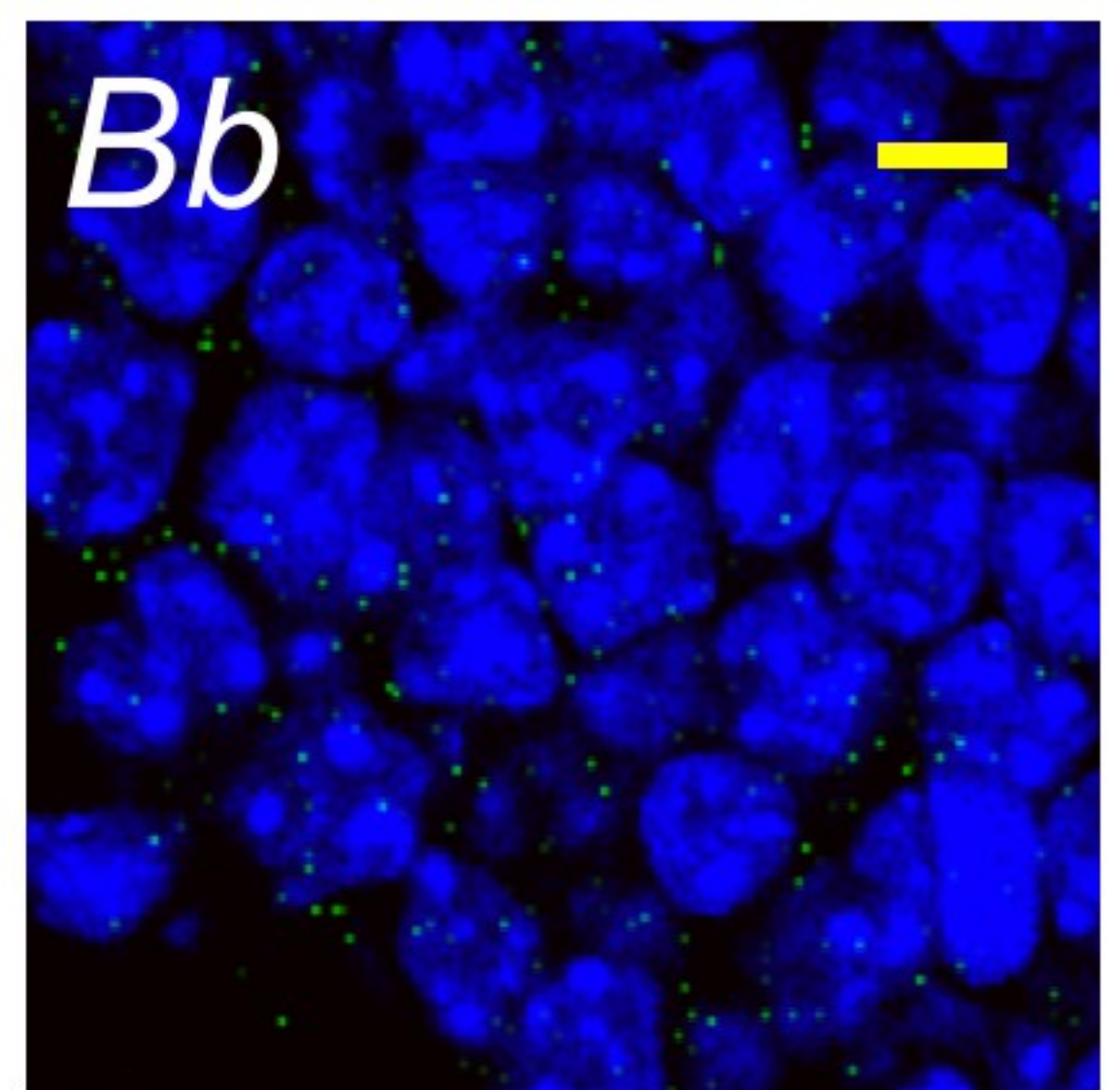
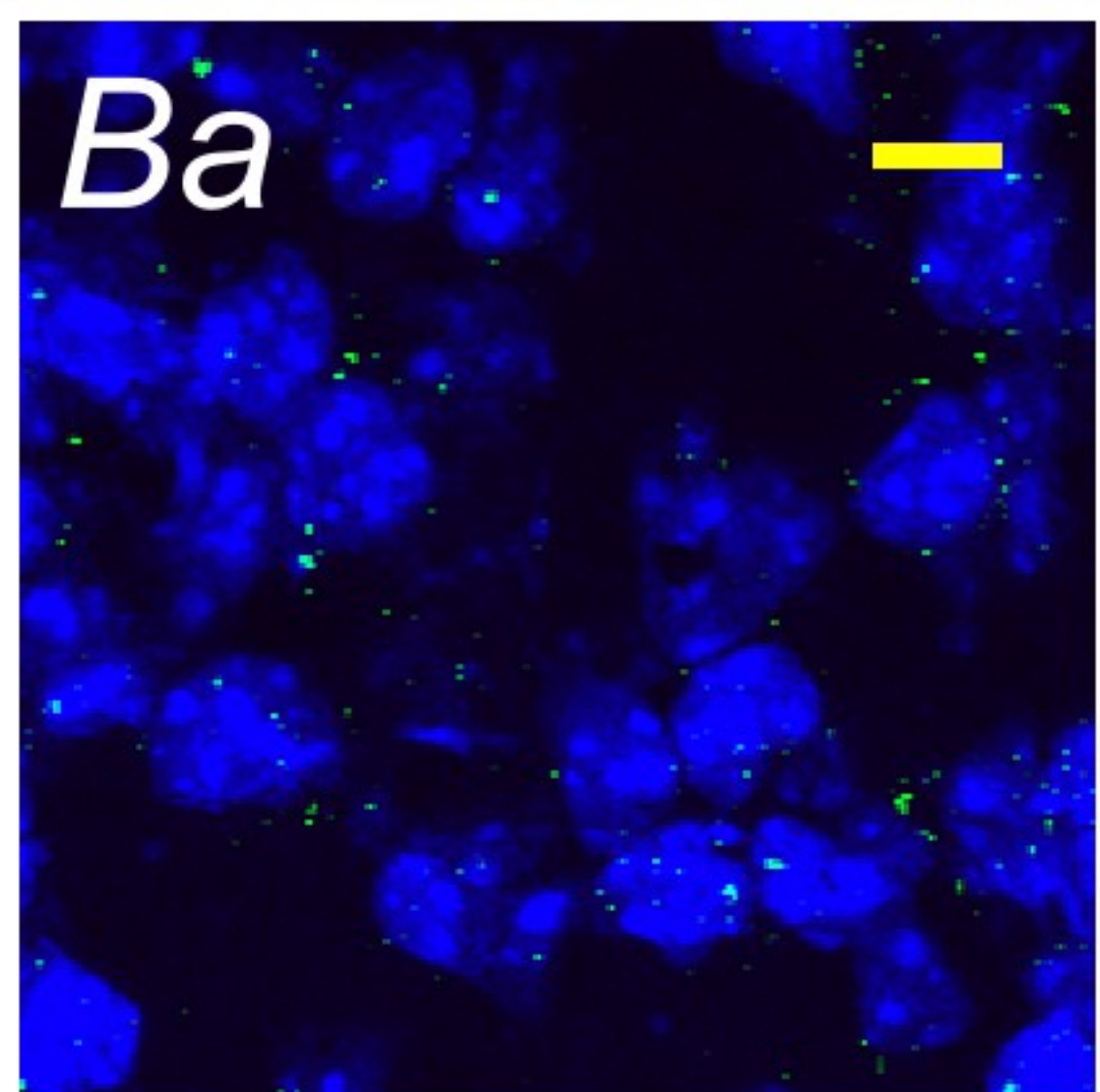
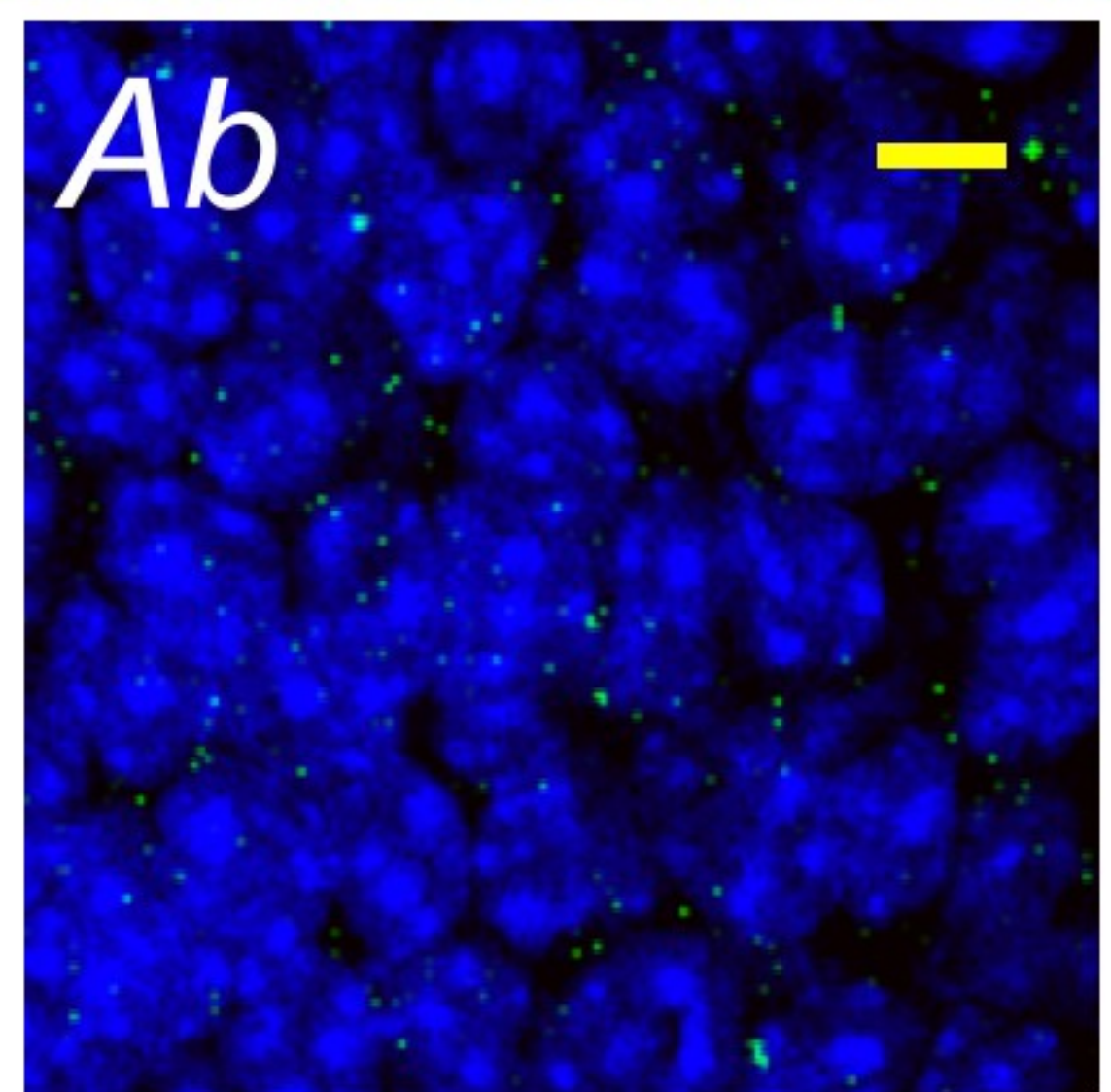
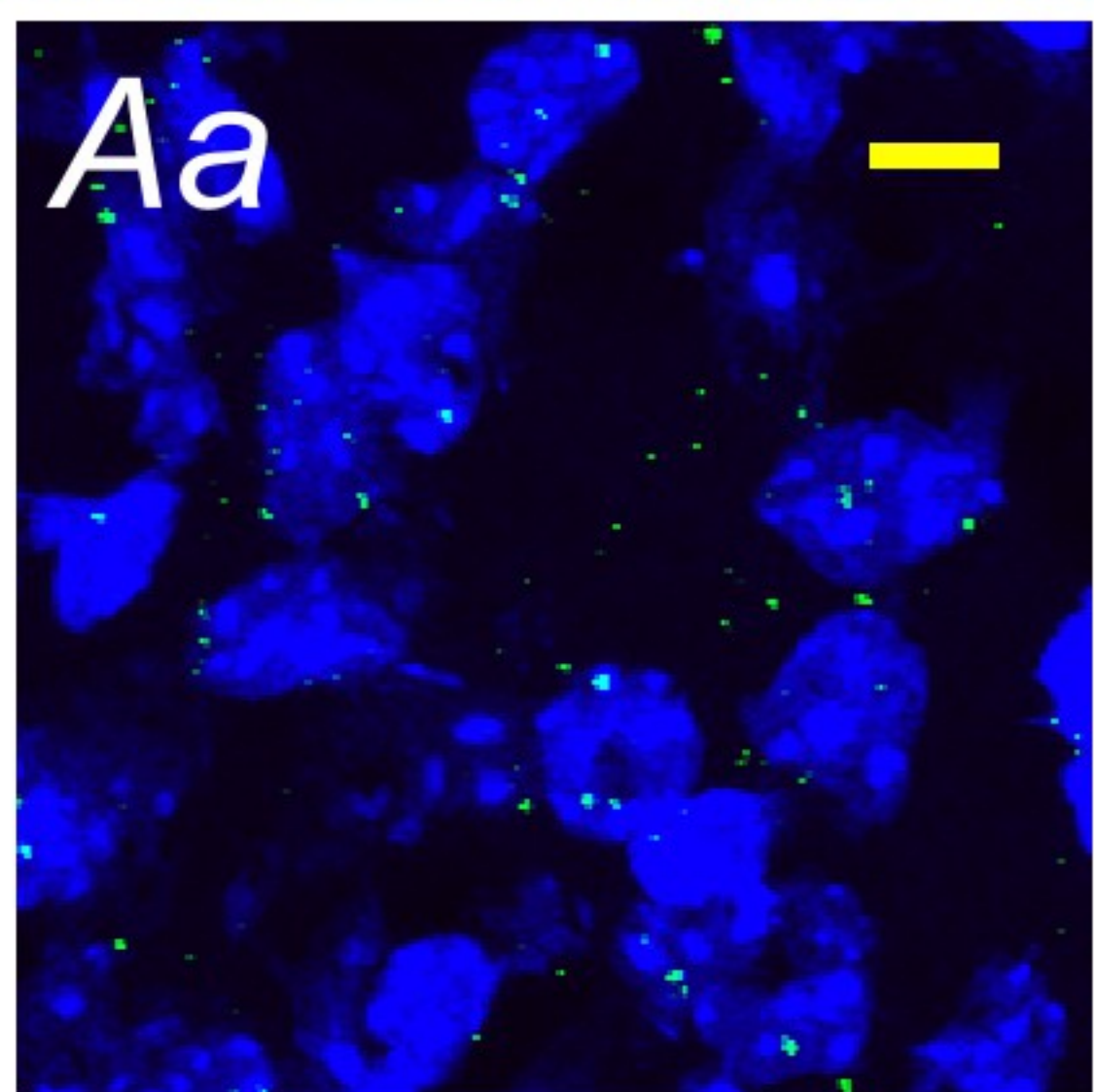
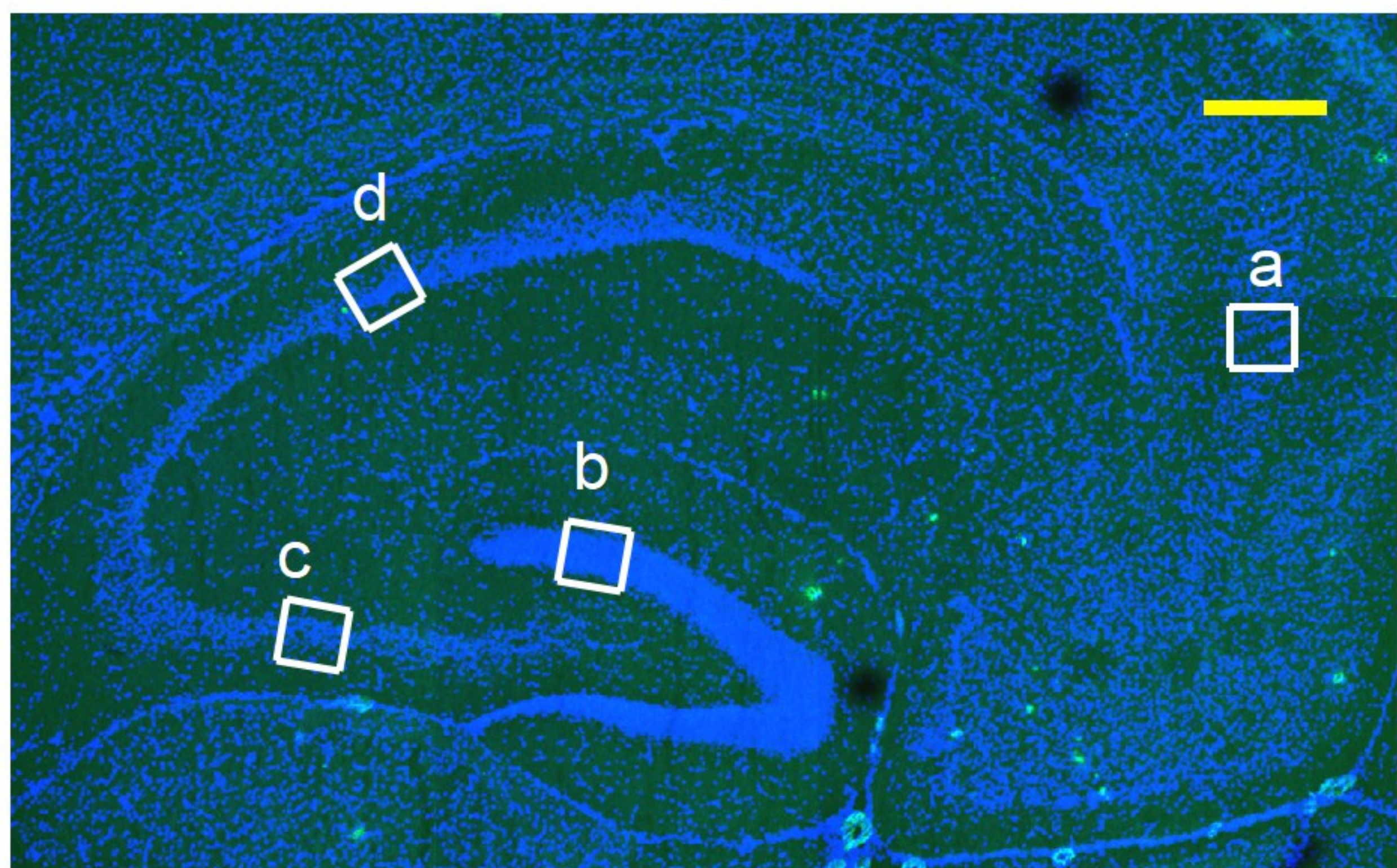
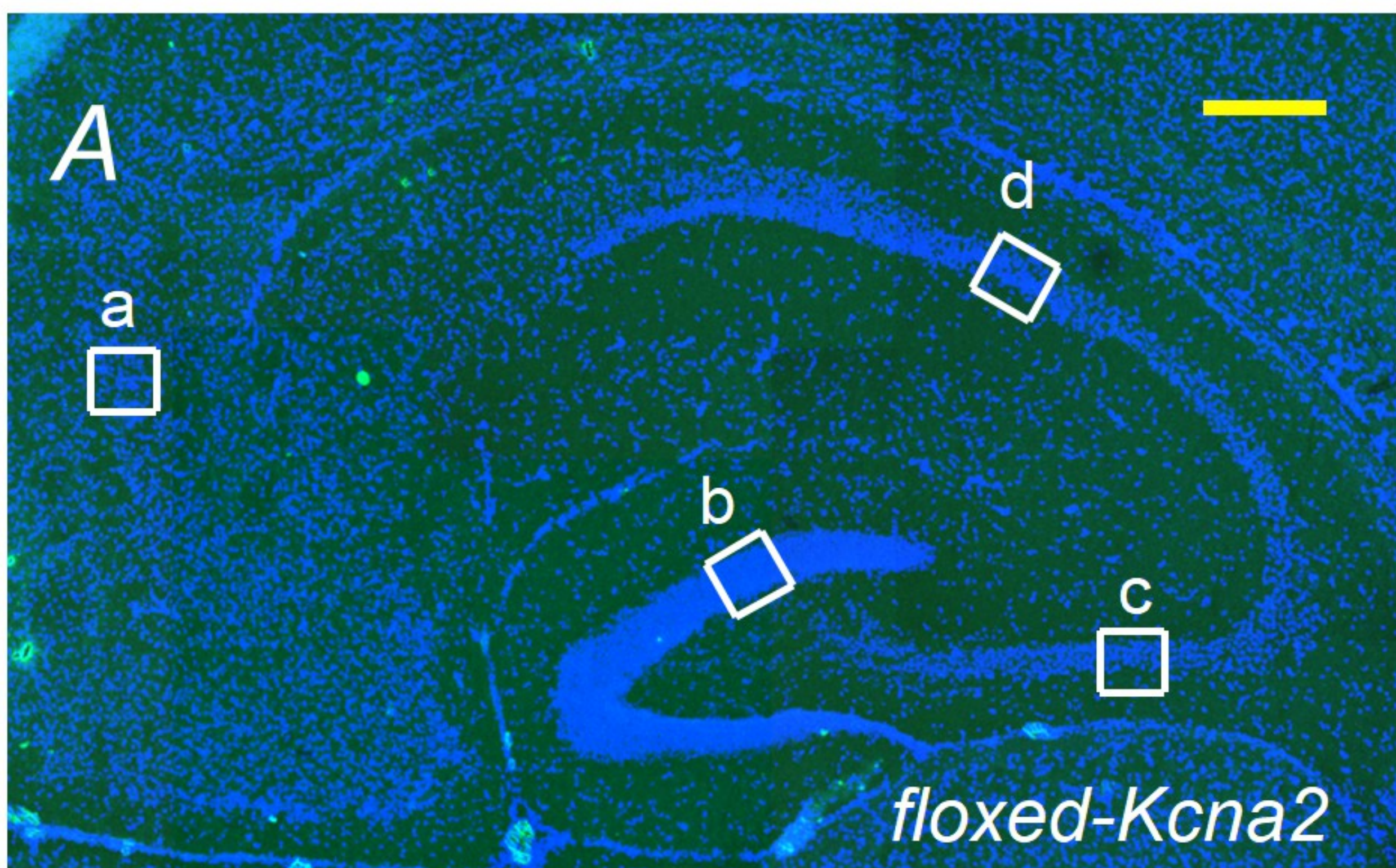


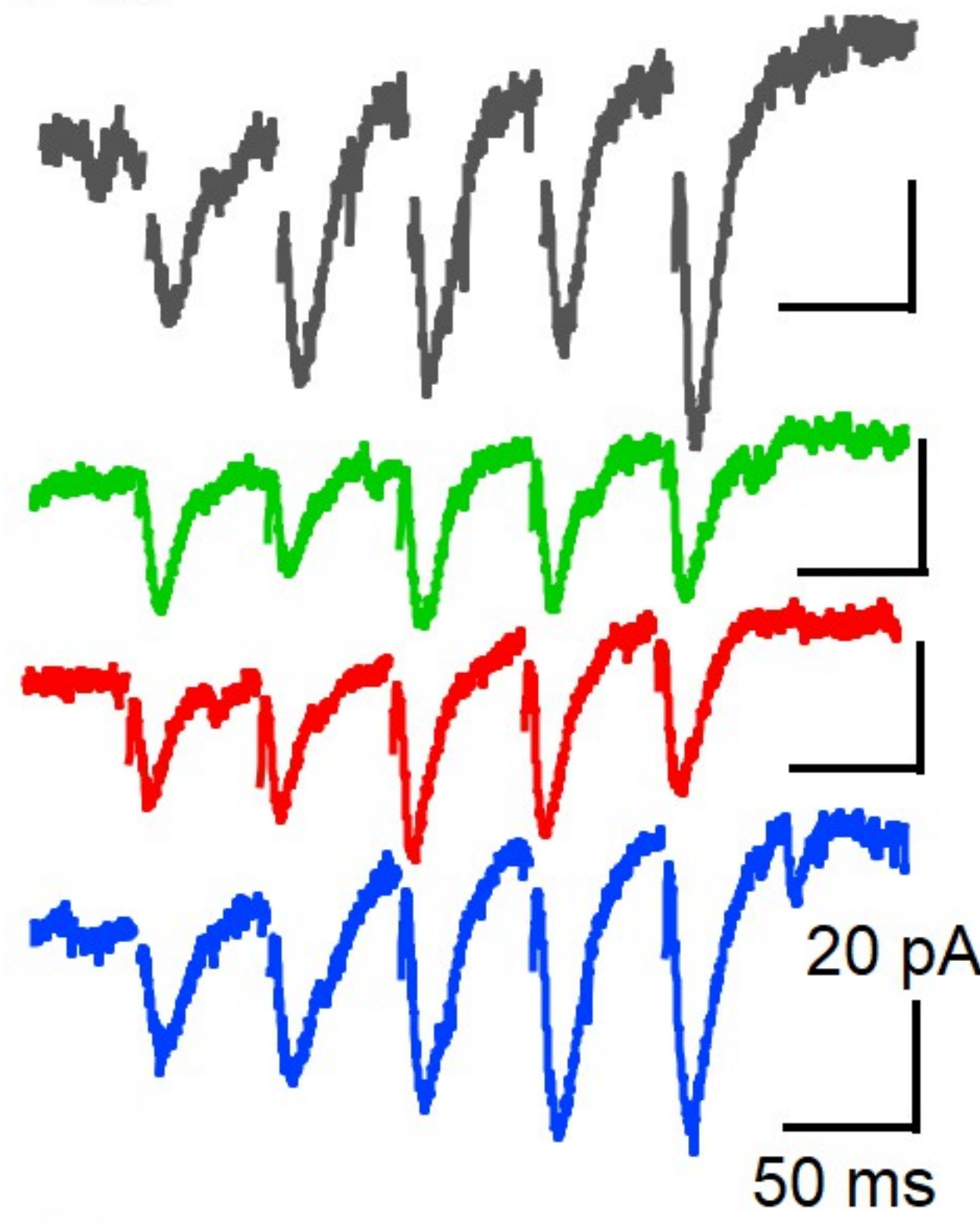
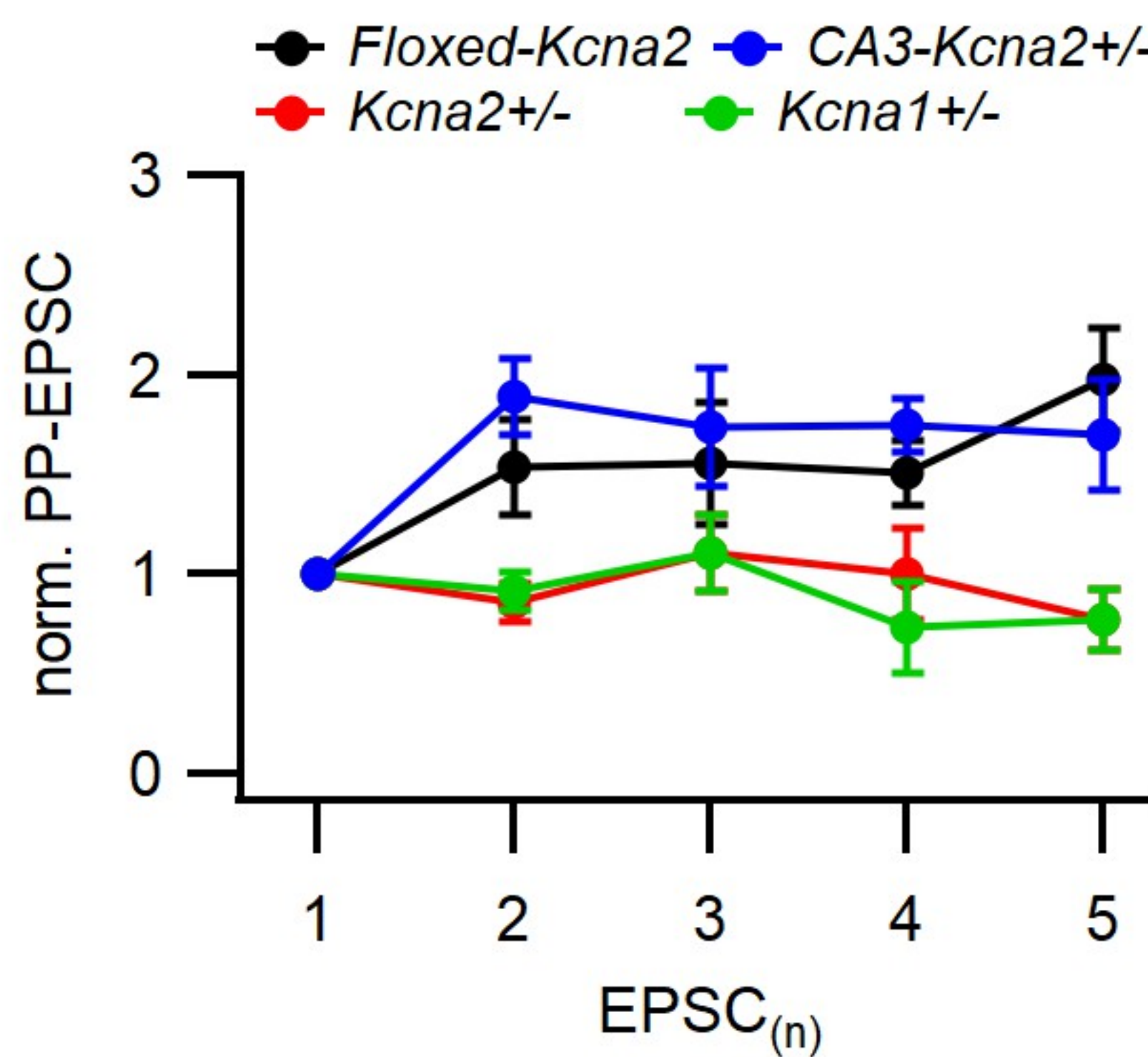
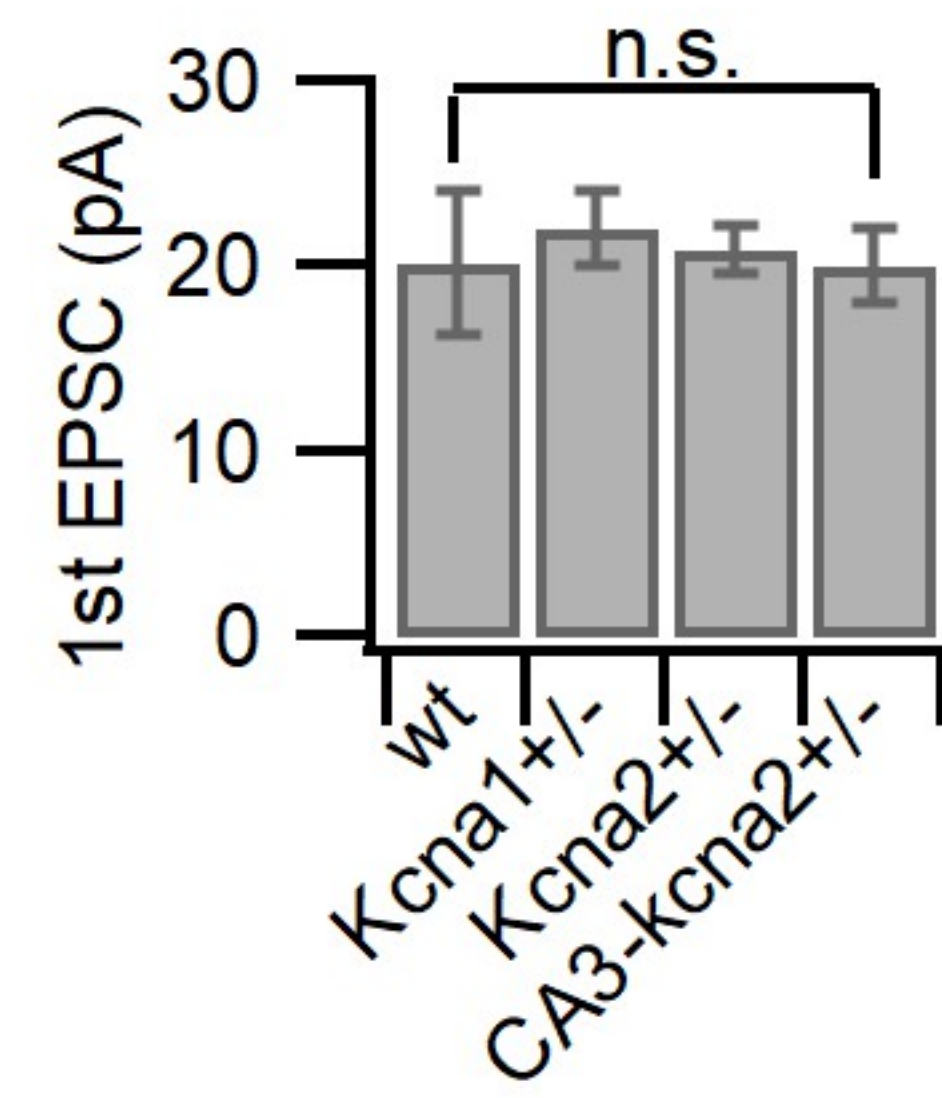
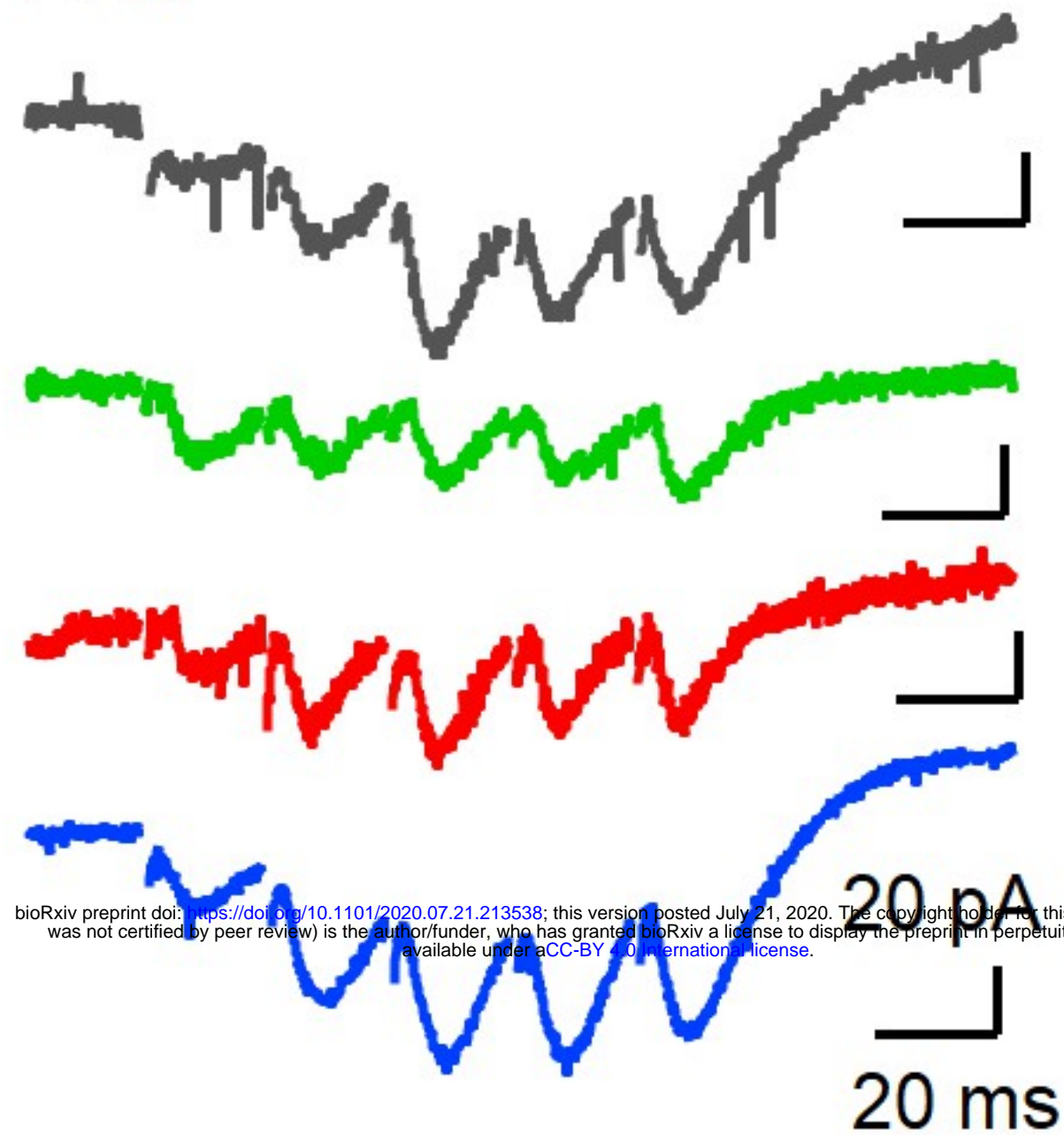
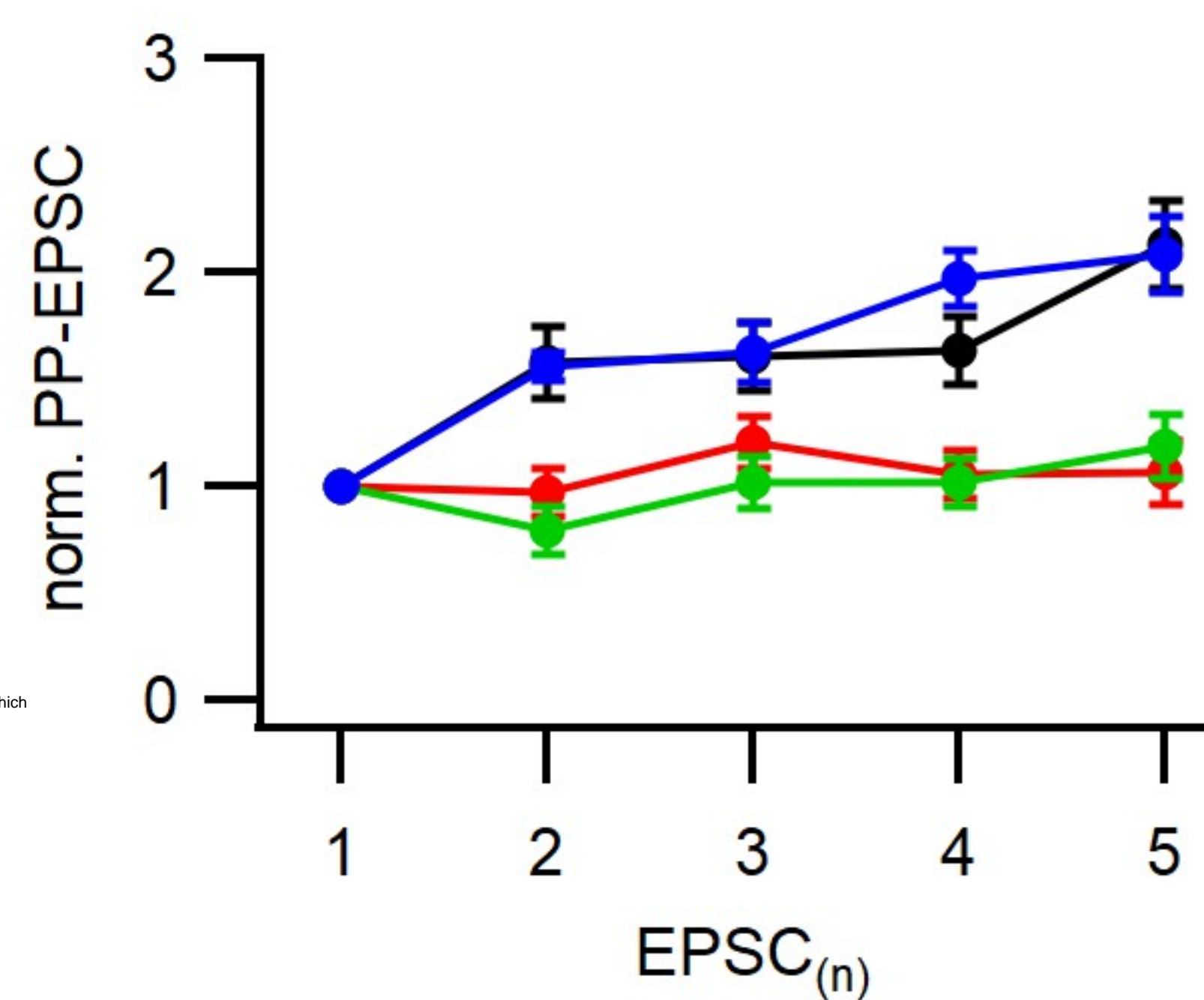
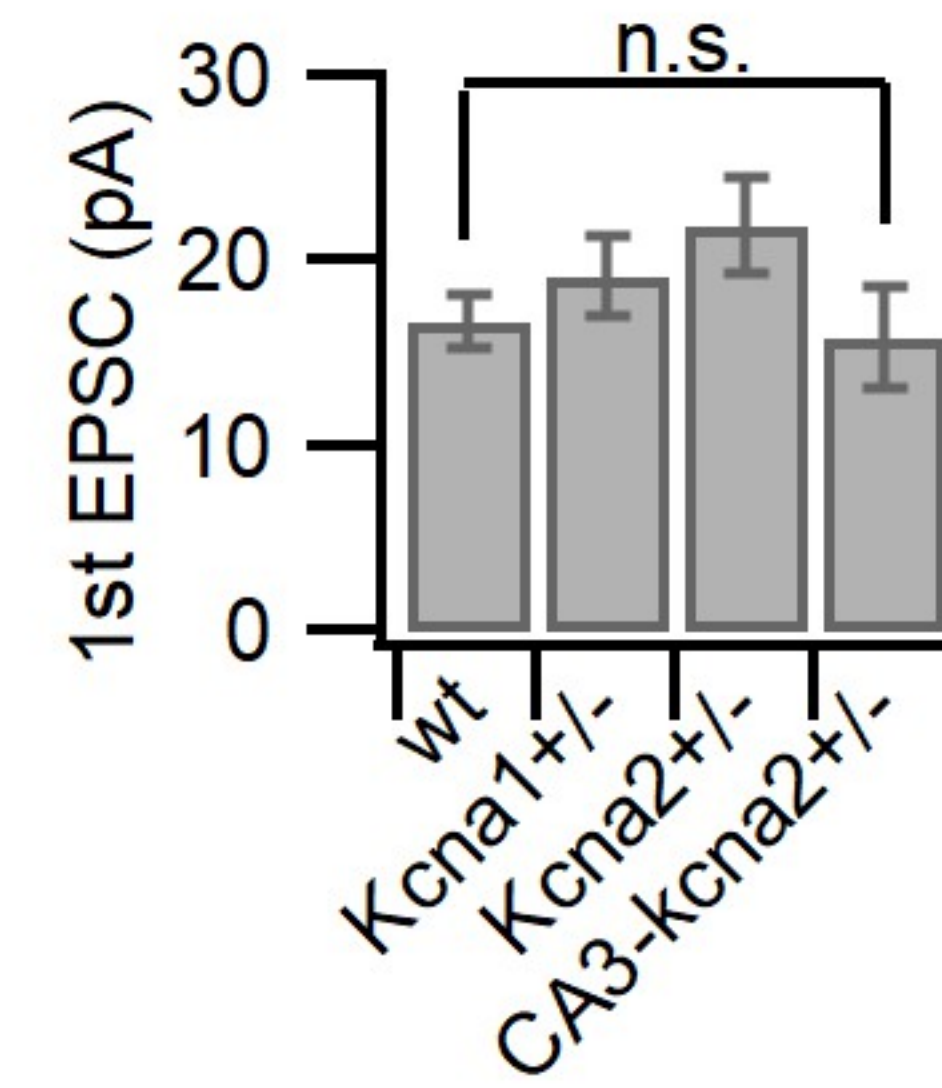
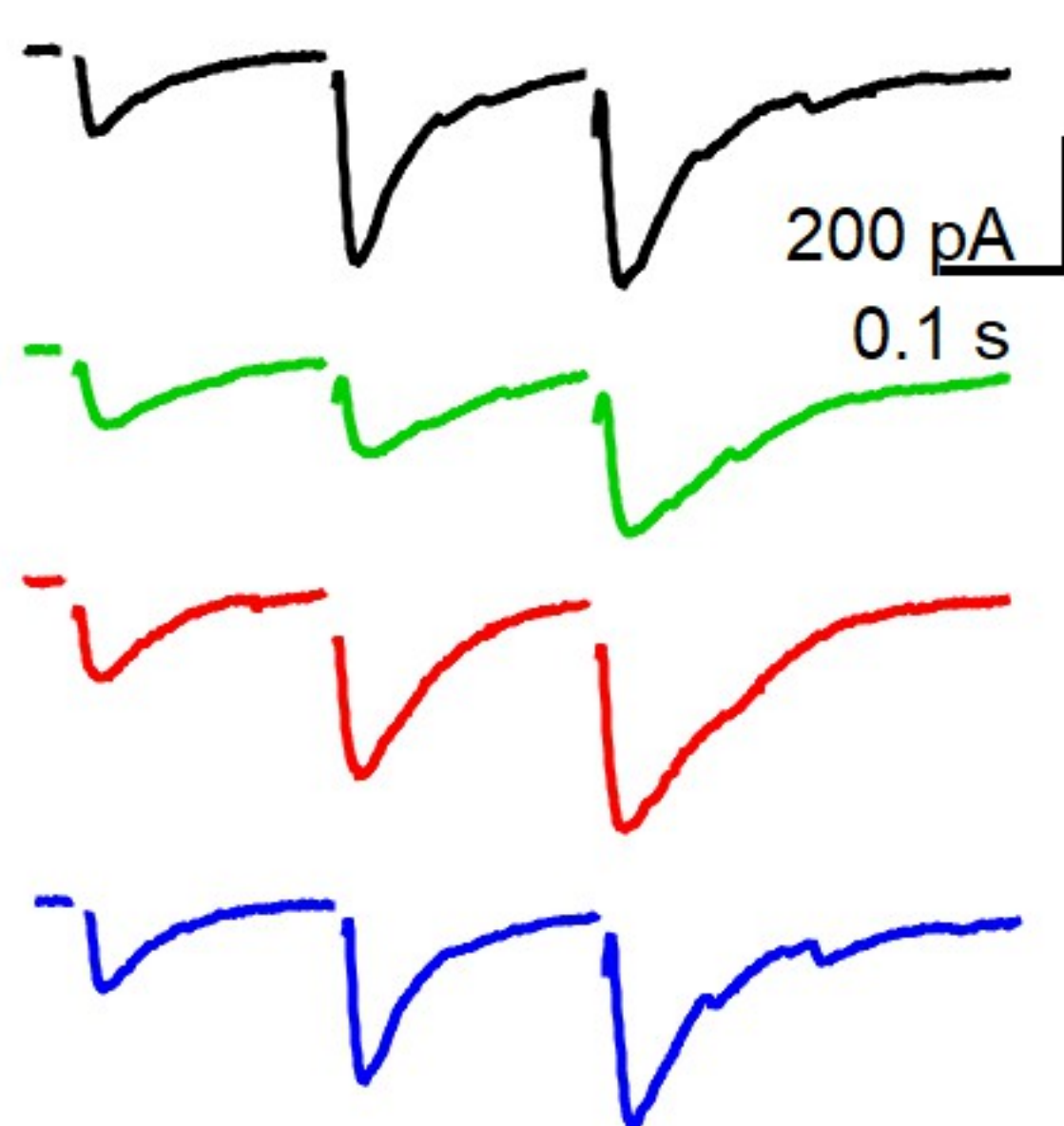
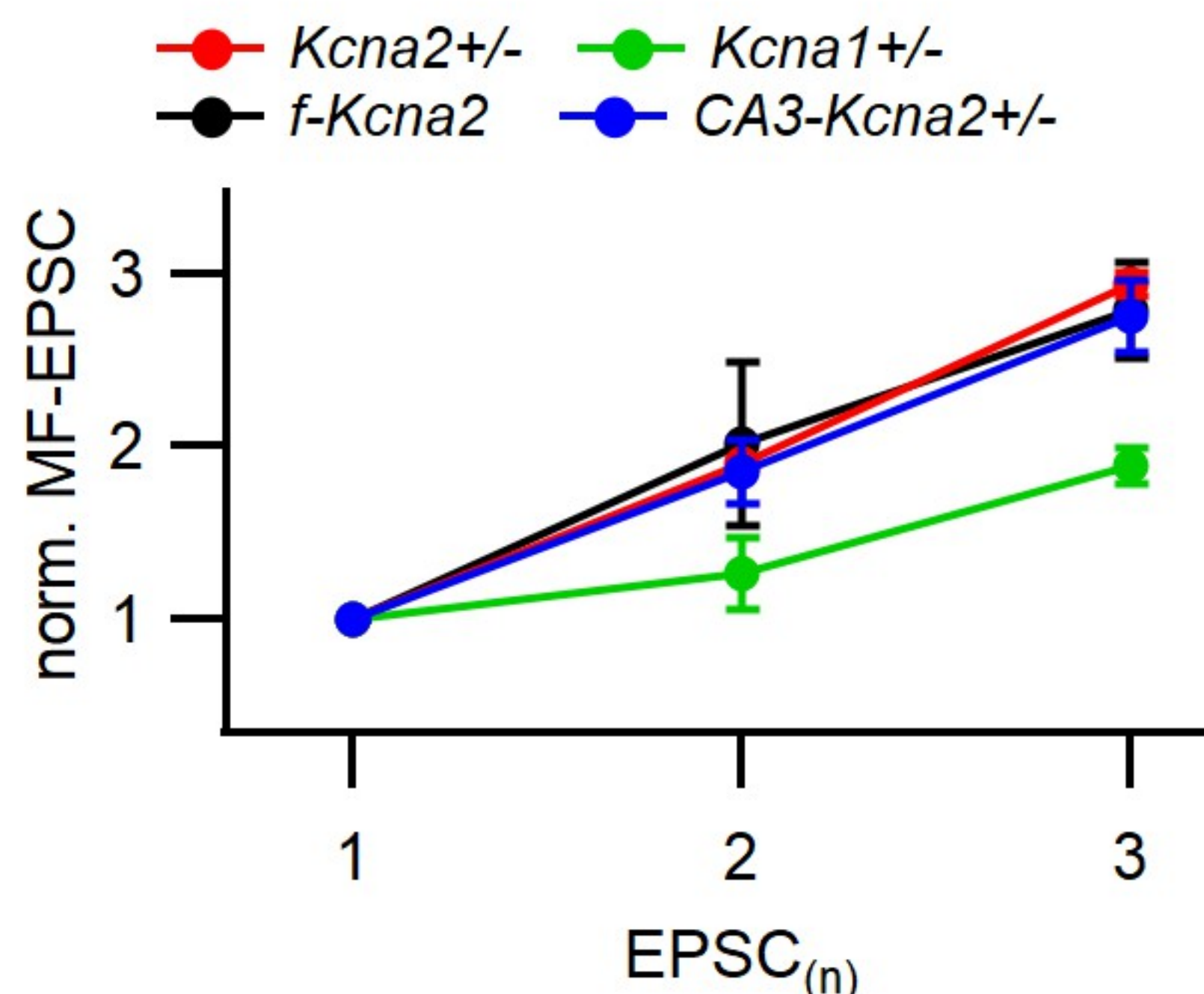
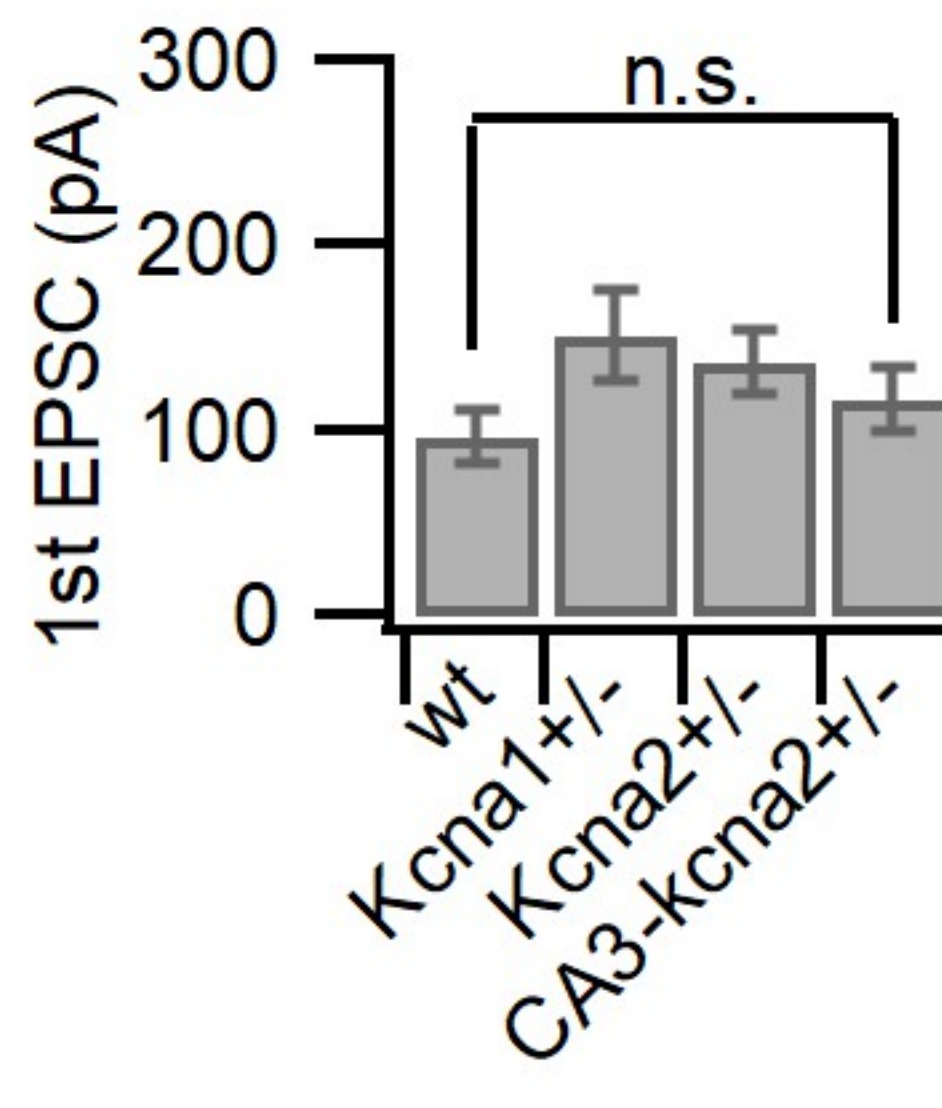
bioRxiv preprint doi: <https://doi.org/10.1101/2023.06.05.538100>; this version posted June 2023. The copyright holder for this preprint (which was not certified by peer review) is the author/funder, who has granted bioRxiv a license to display the preprint in perpetuity. It is made available under aCC-BY 4.0 International license.

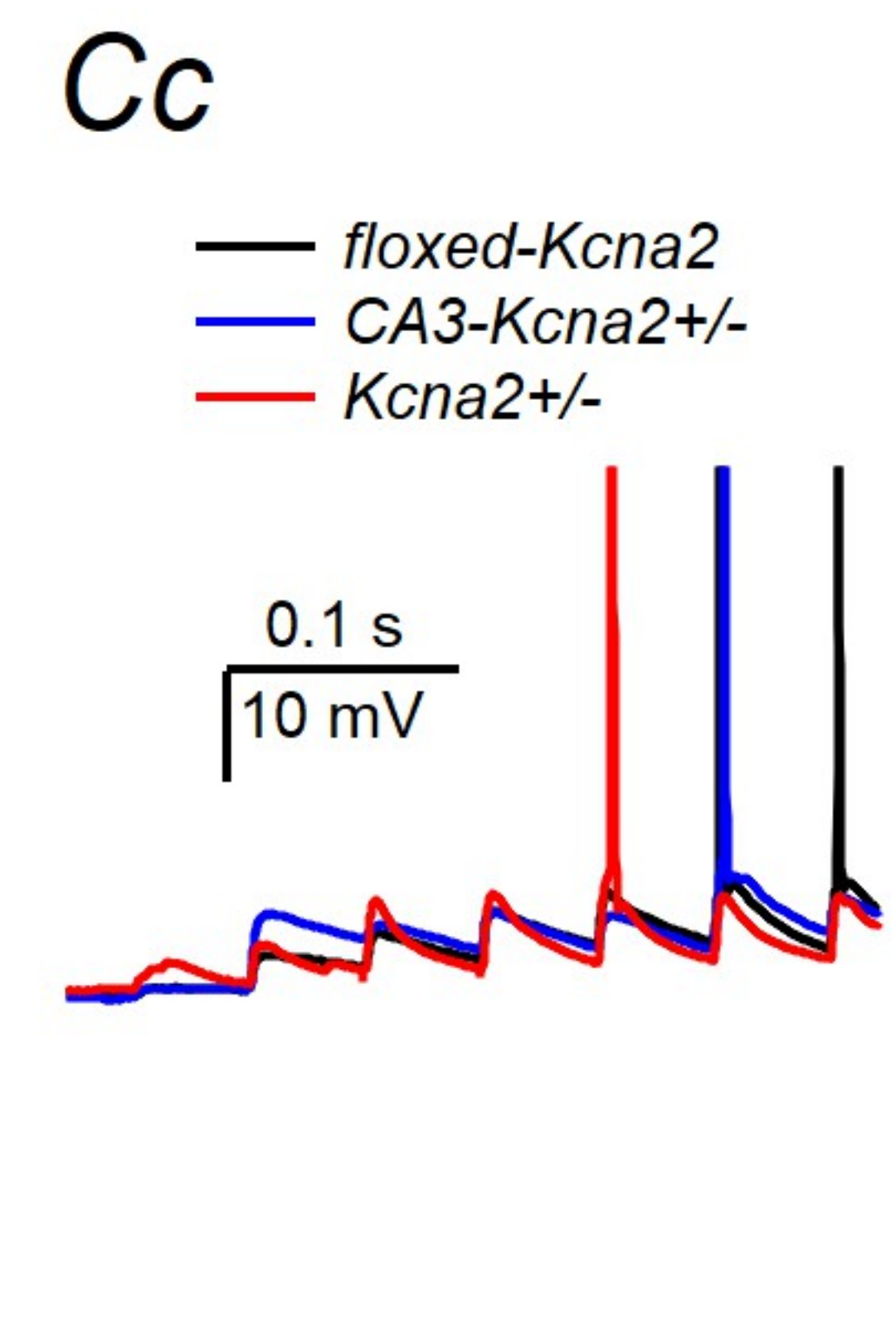
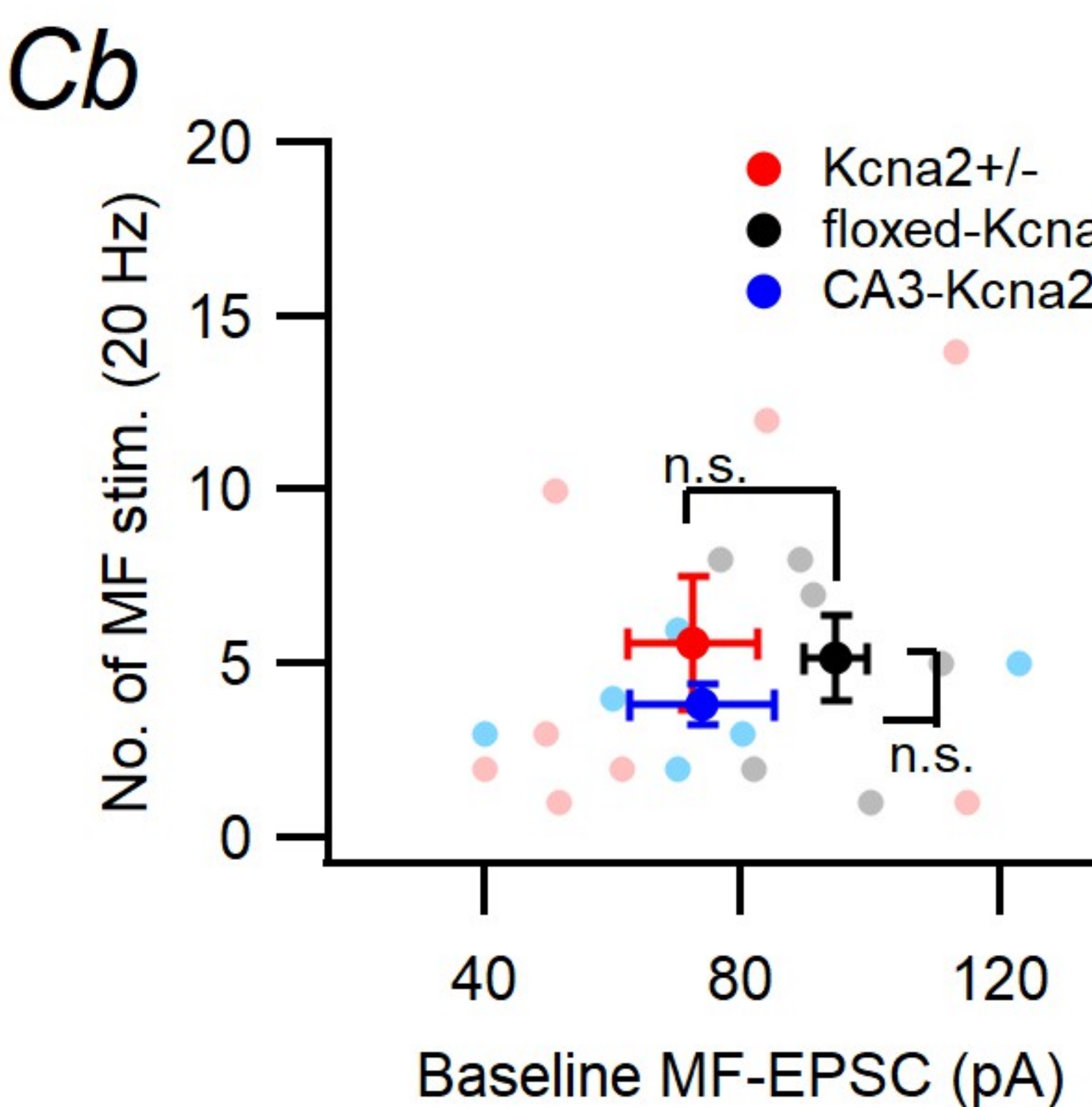
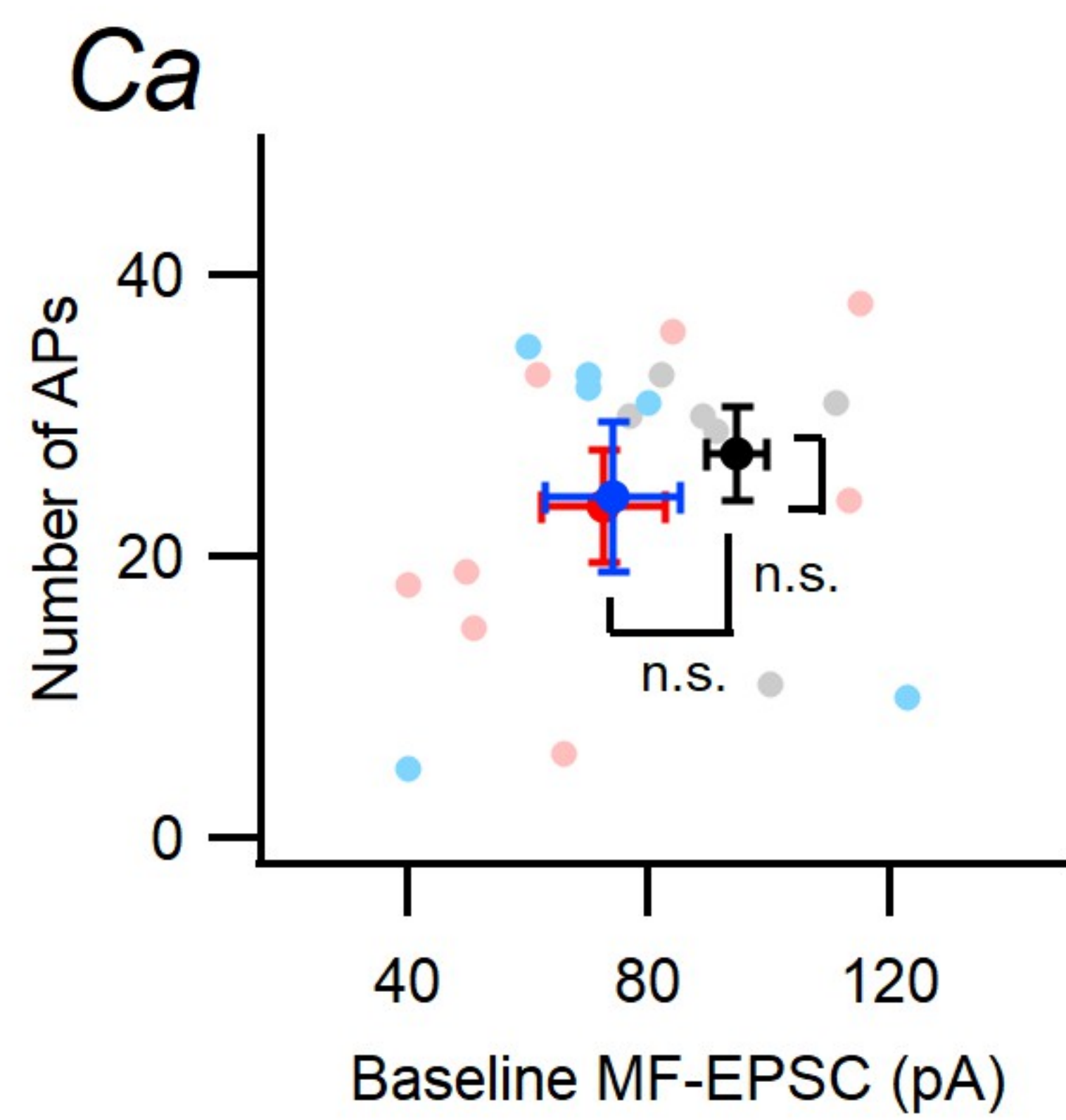
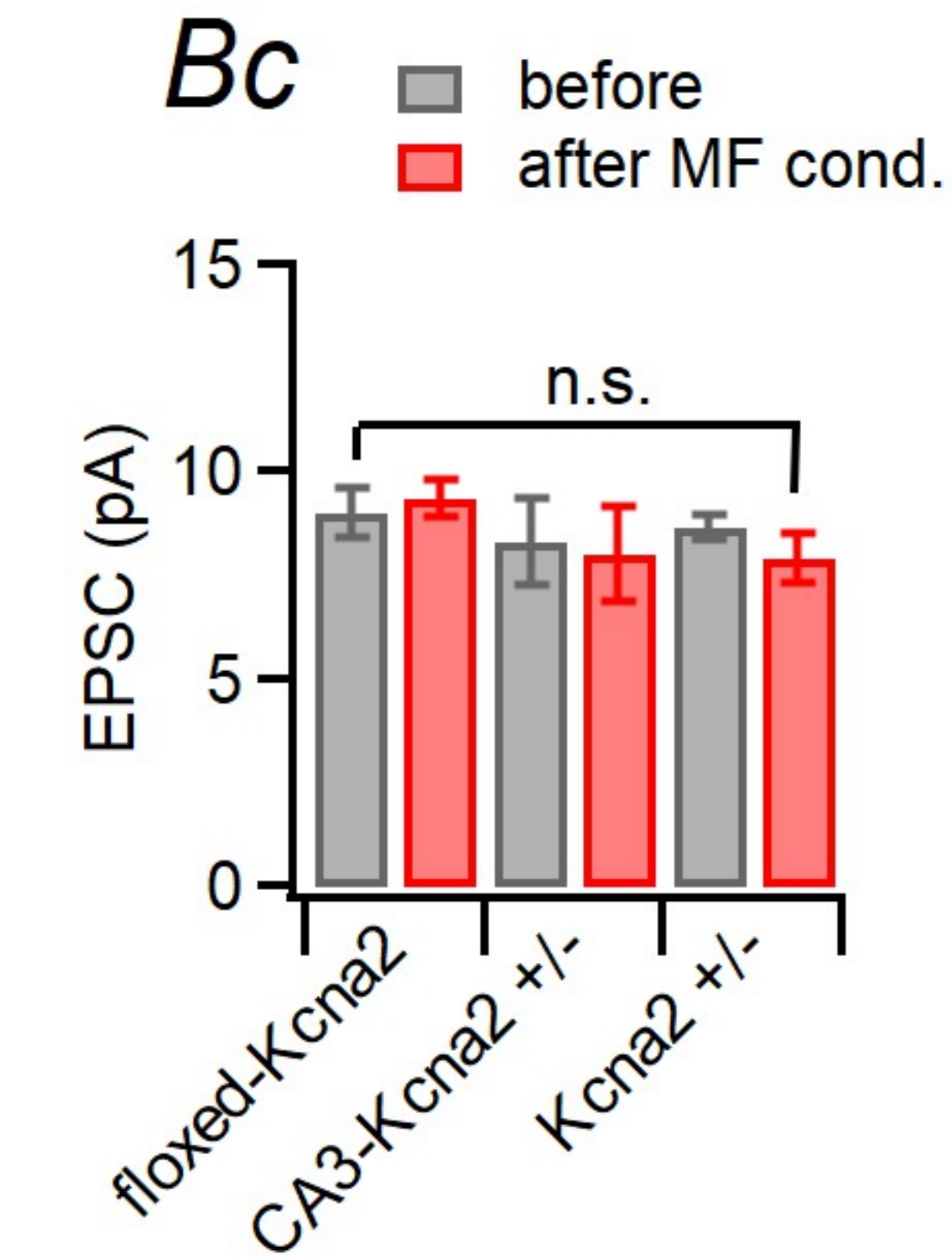
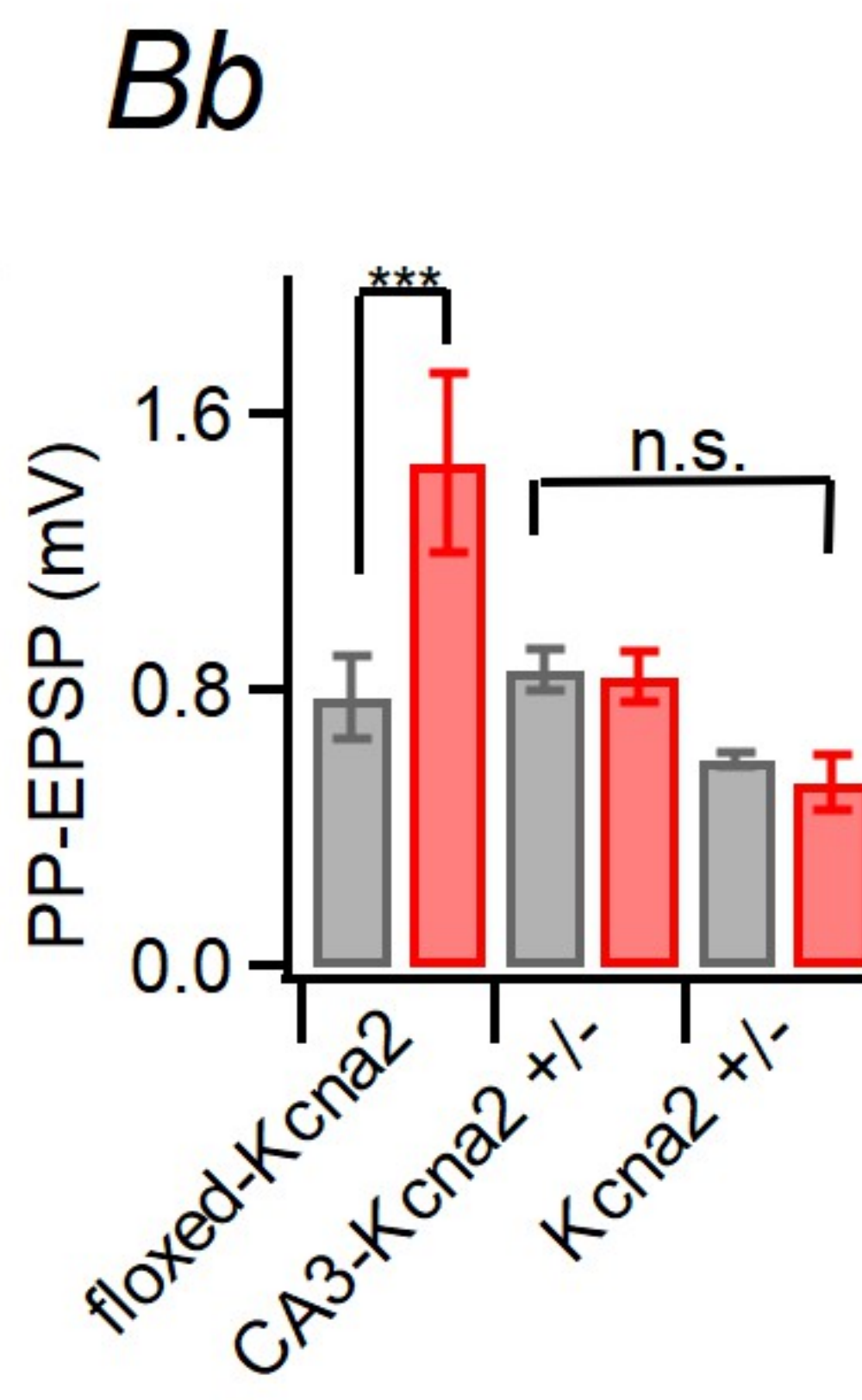
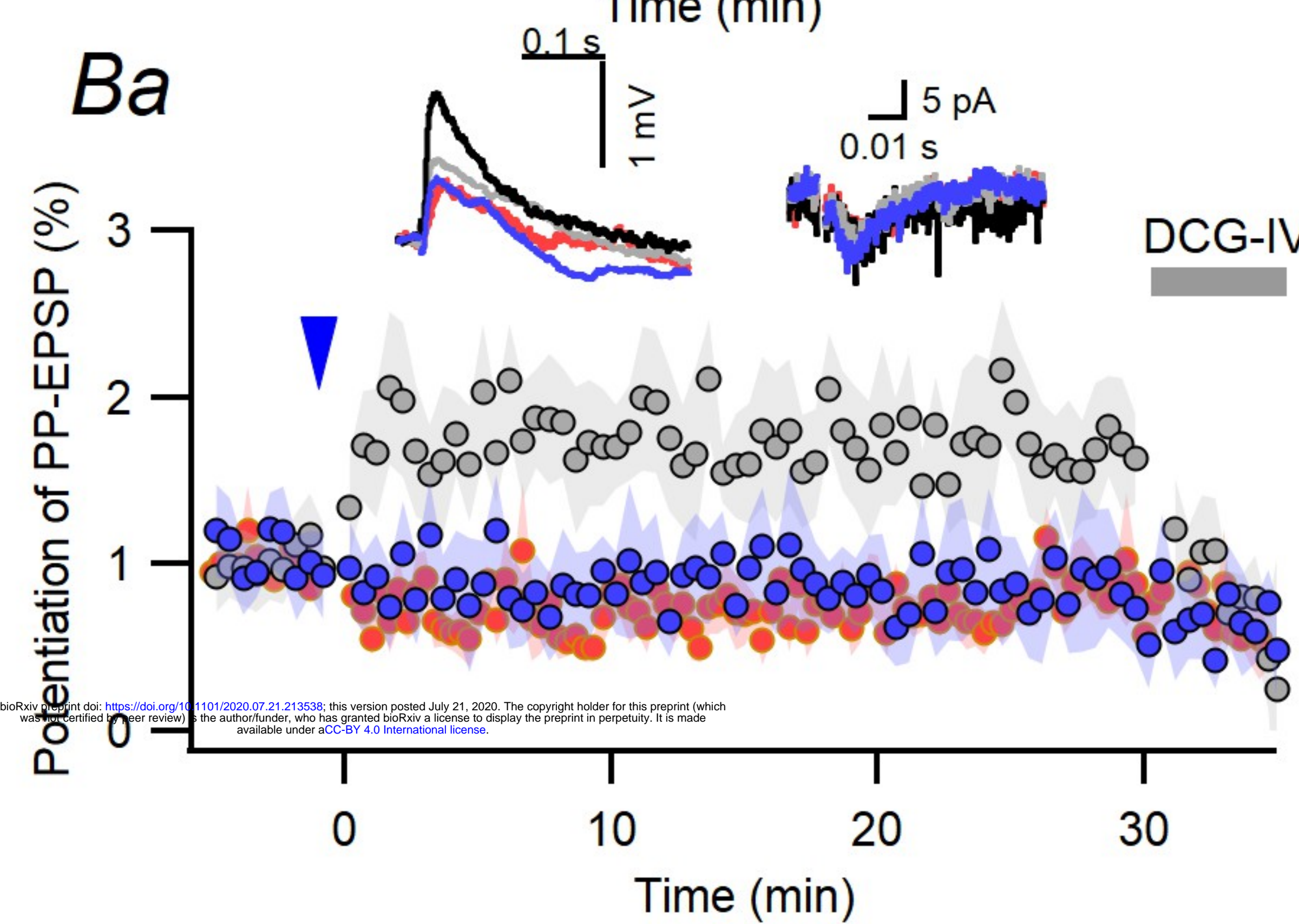
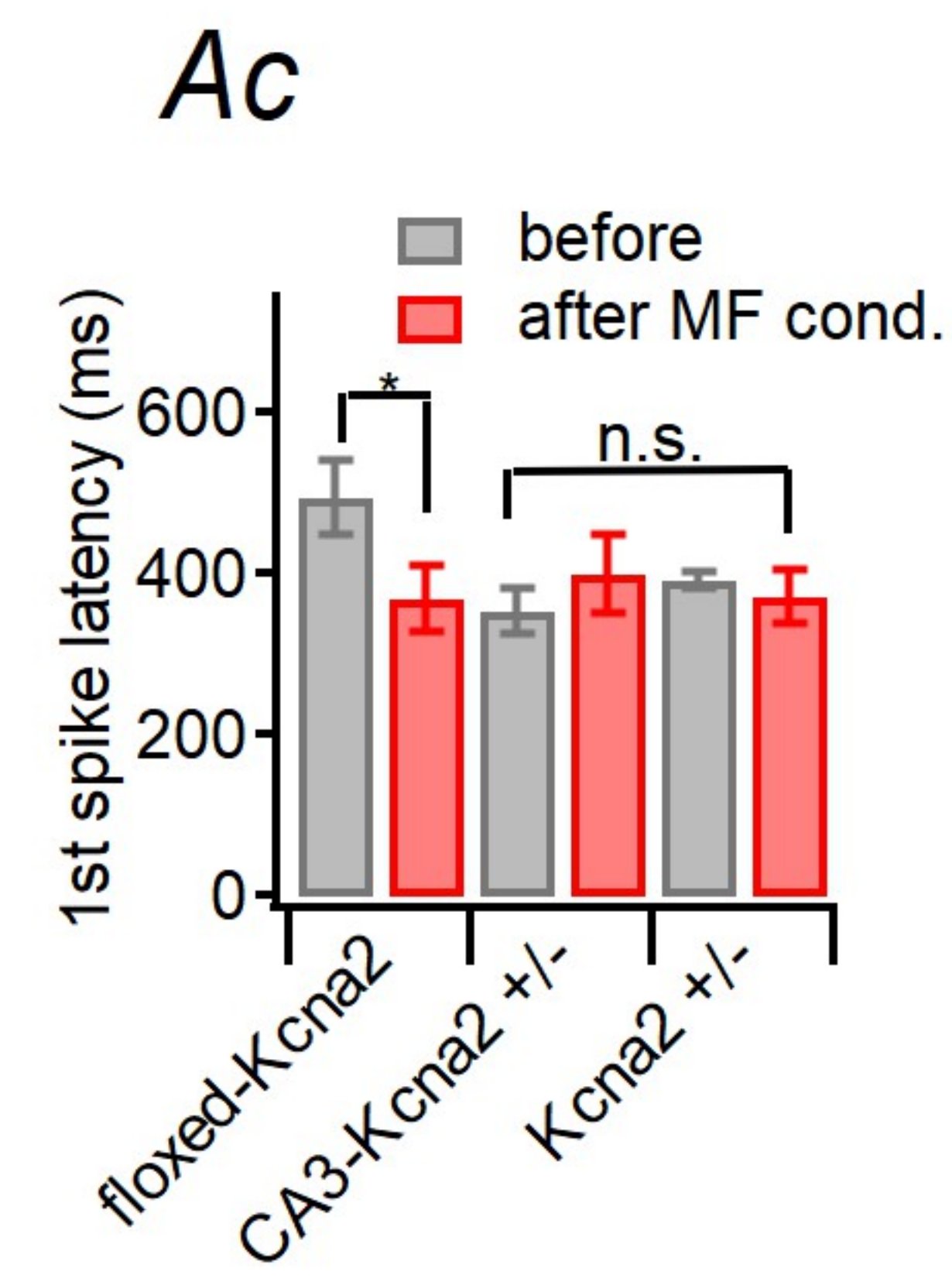
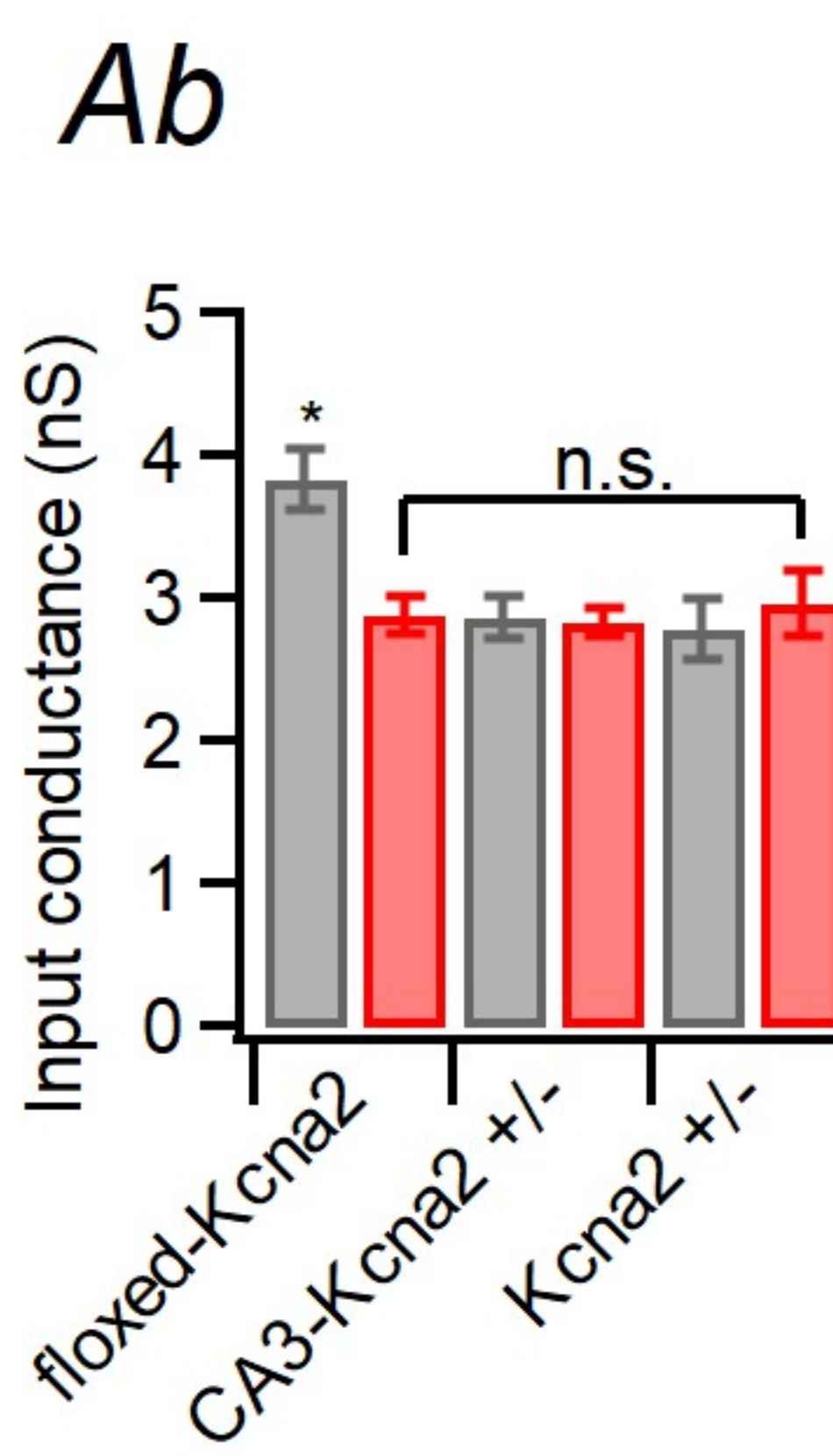
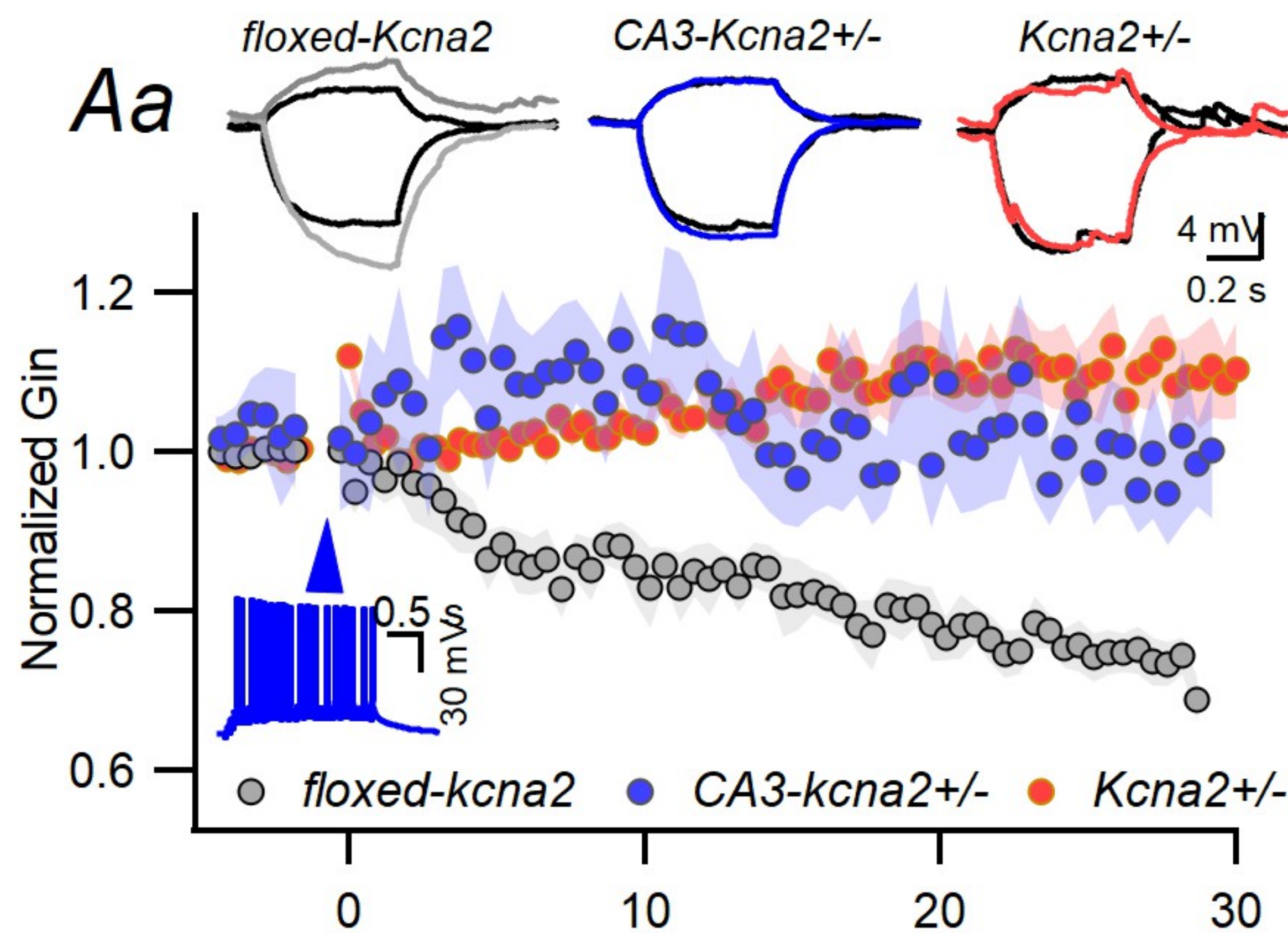


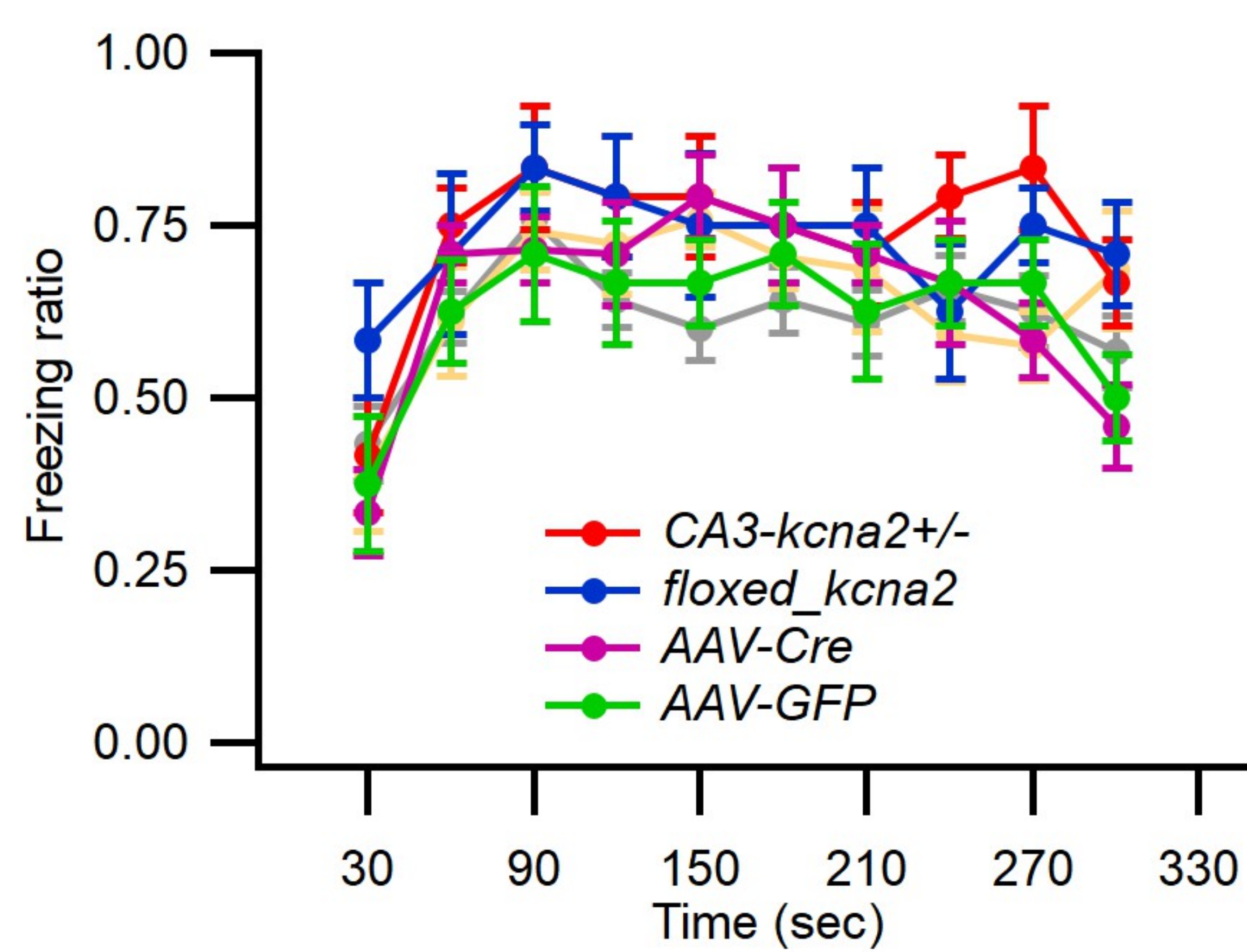
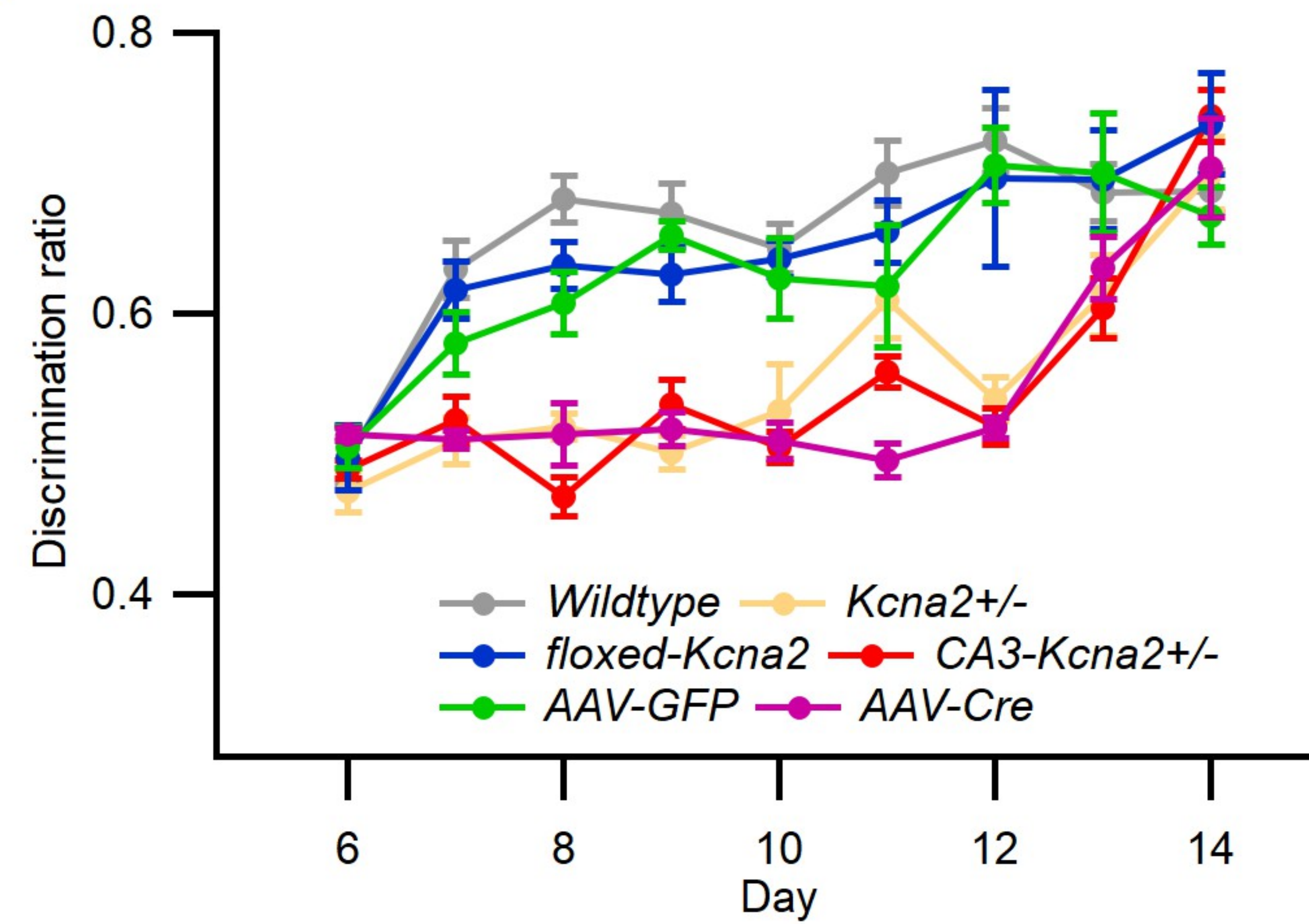
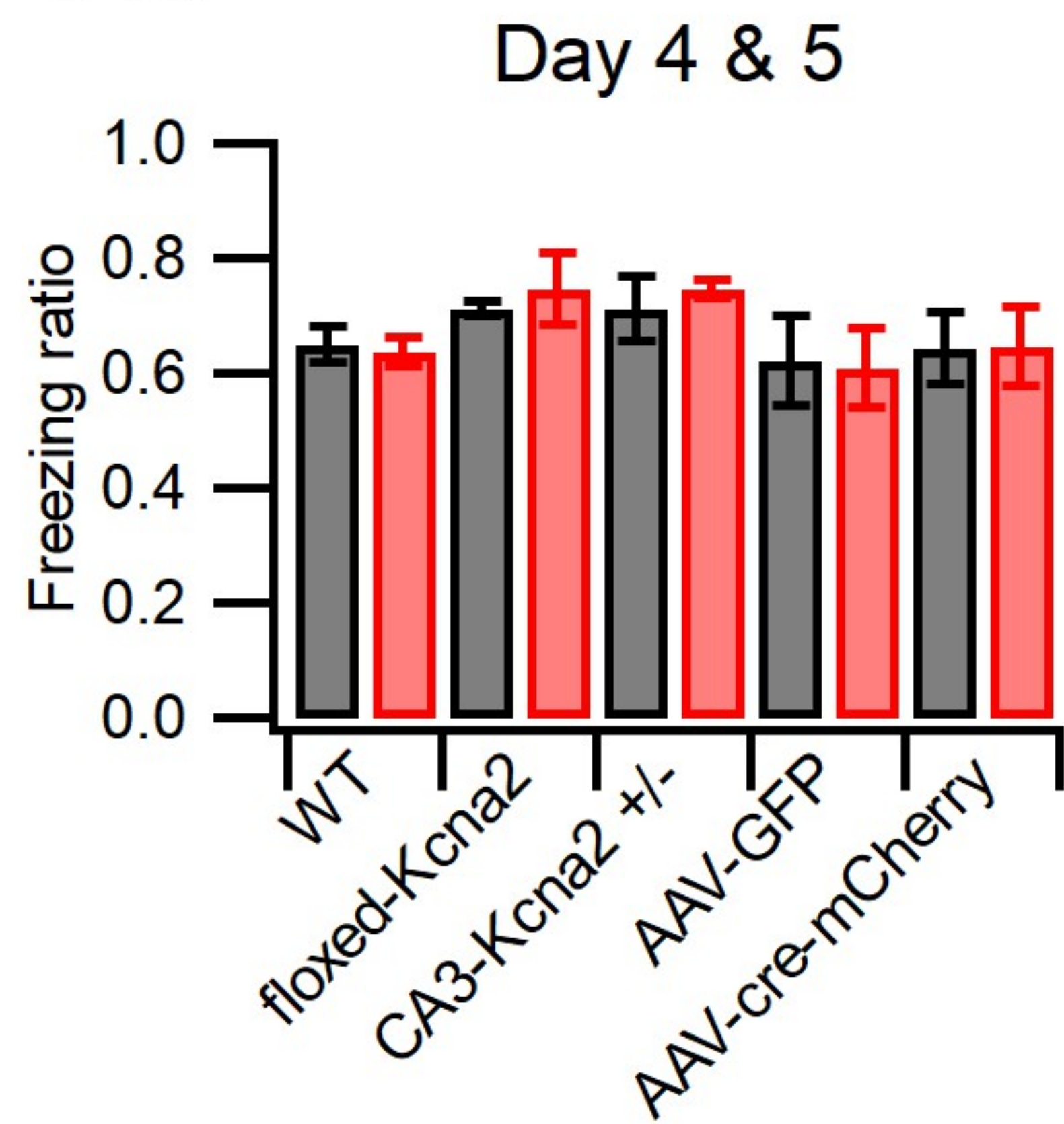
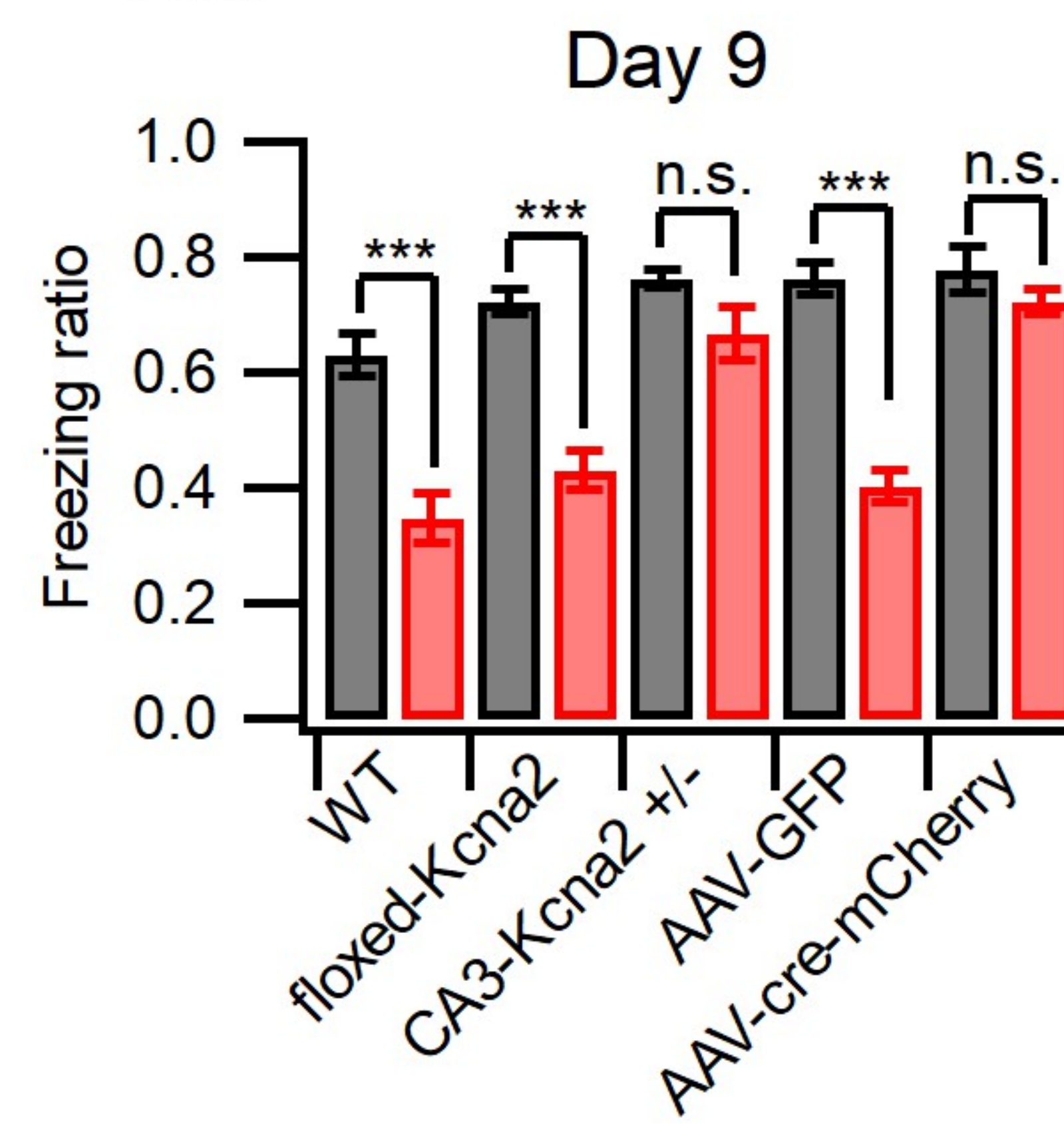
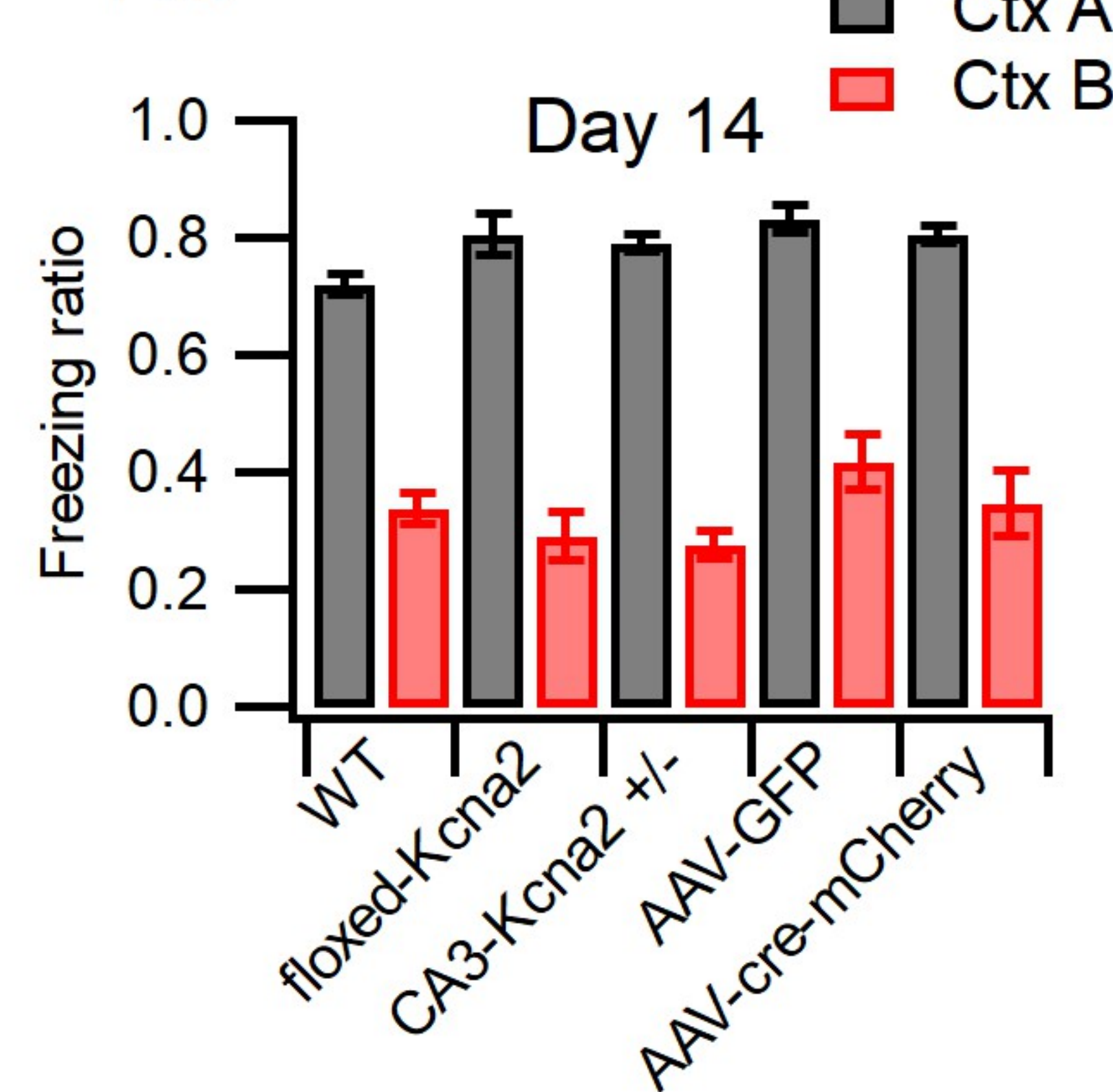


**A****Day 1****Day 2****Kcnna2<sup>+/−</sup>****Ca****Cb****Cc****Cd**

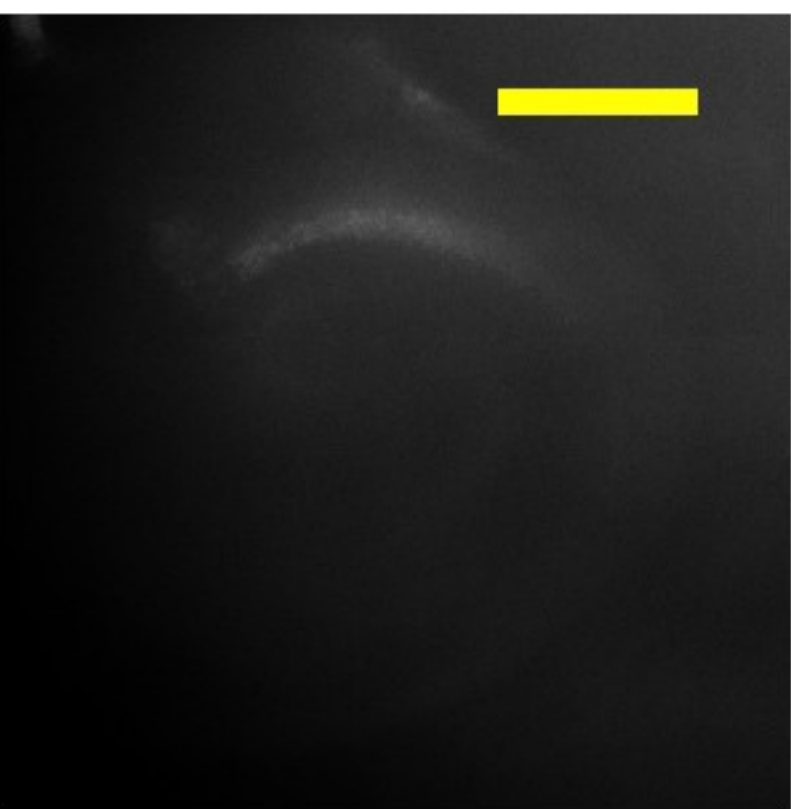
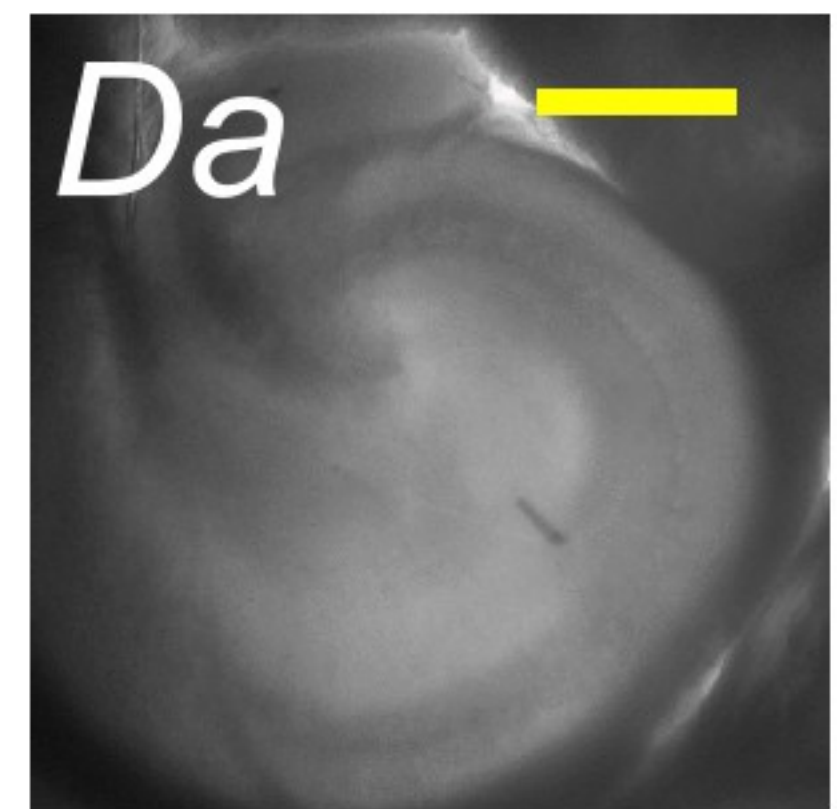
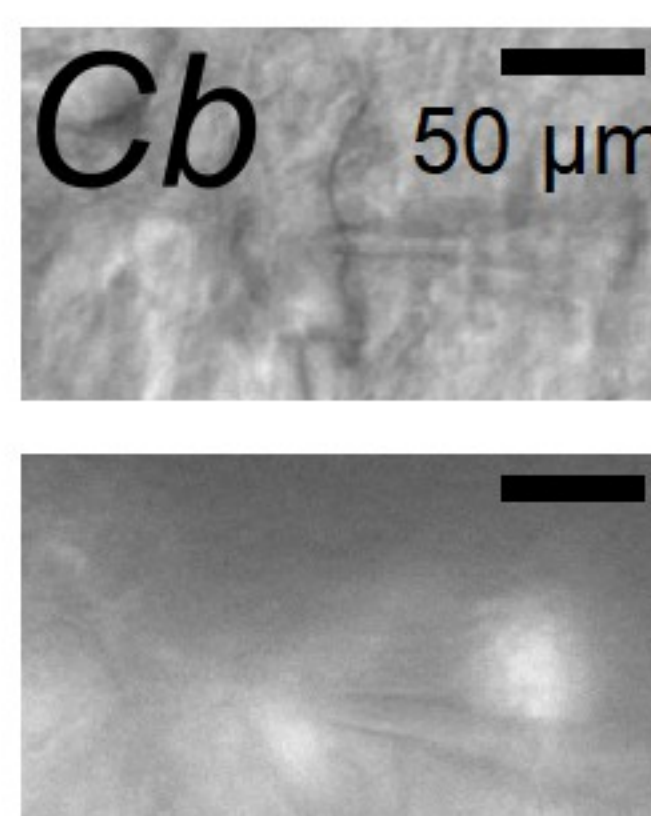
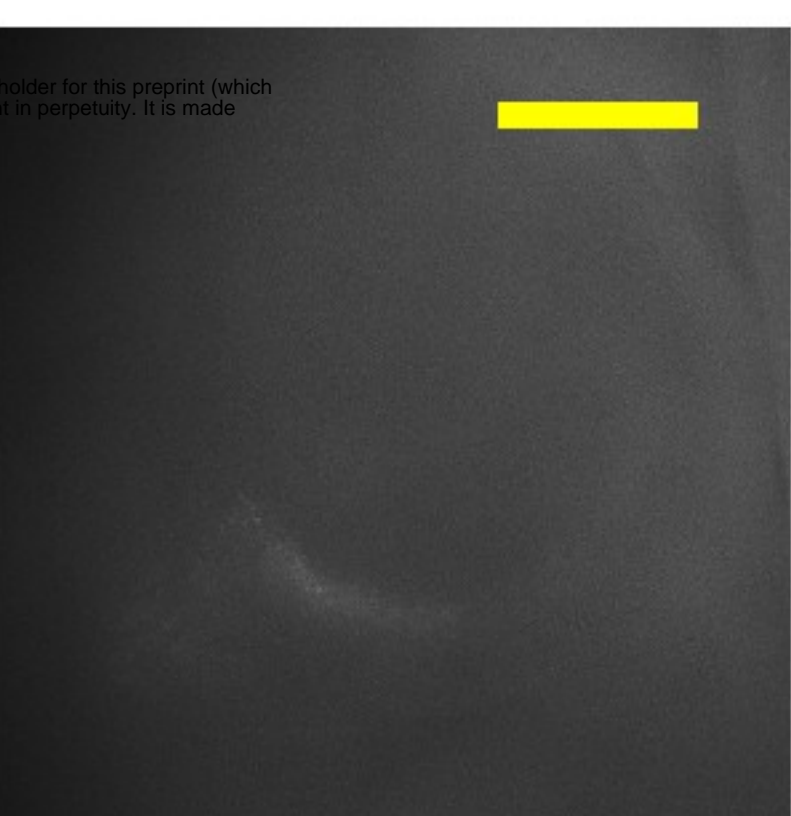
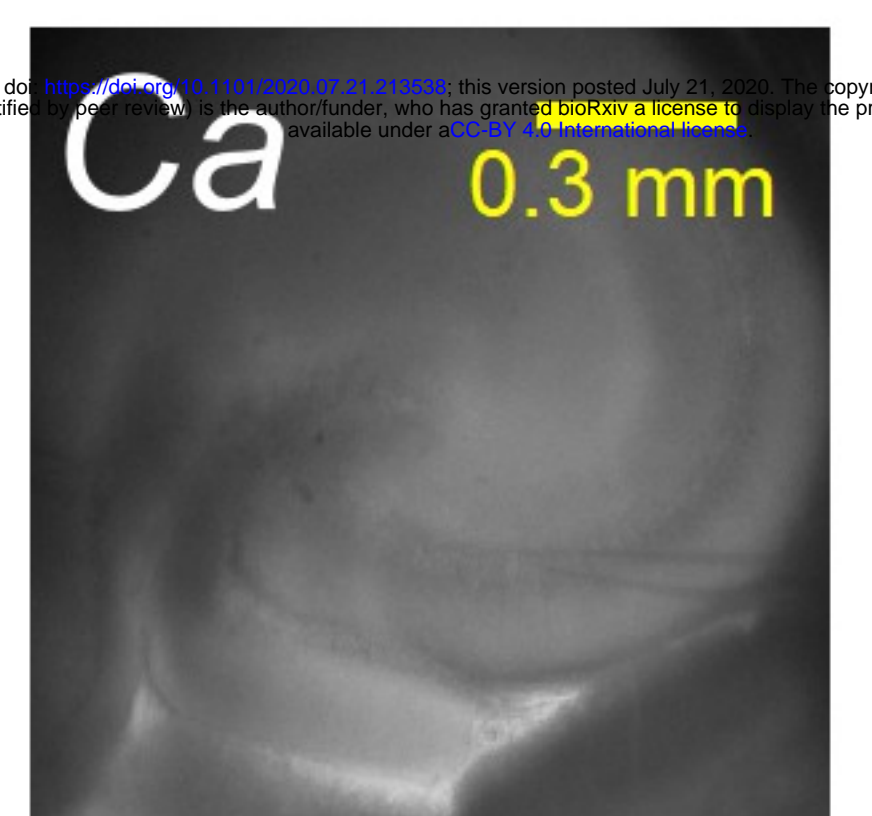
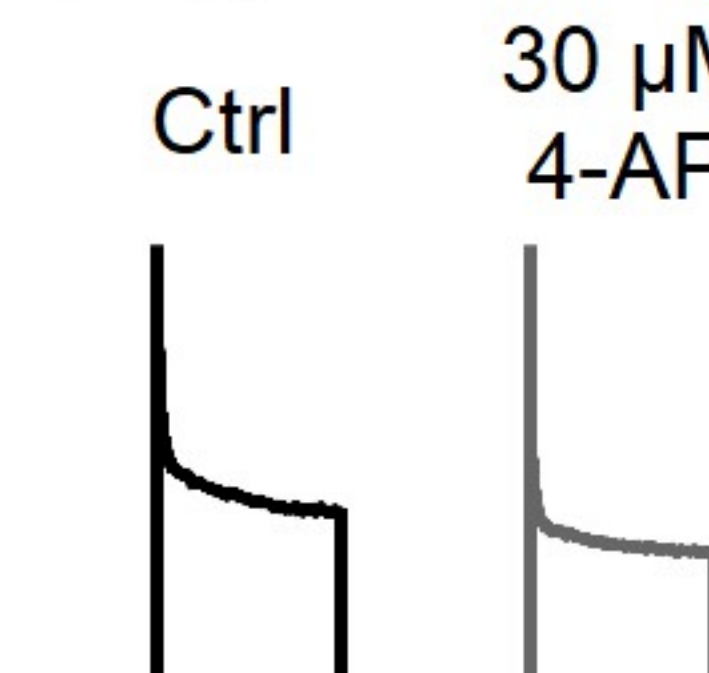
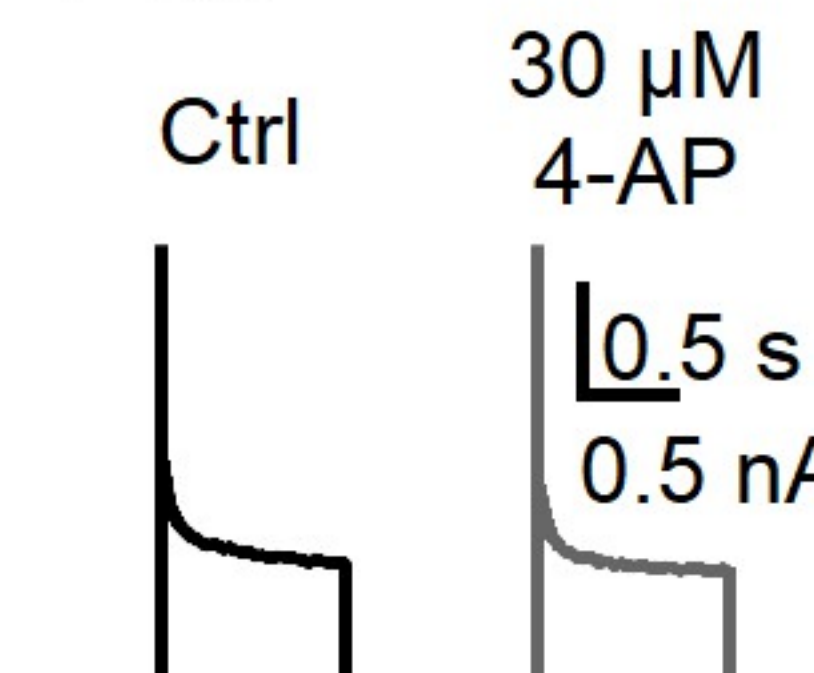


**Aa****Ab****Ac****Ba****Bb****Bc****Ca****Cb****Cc**



**Aa****Ba****Ab****Bb****Bc**

bioRxiv preprint doi: <https://doi.org/10.1101/2019.07.24.269000>; this version posted July 24, 2019. The copyright holder for this preprint (which was not certified by peer review) is the author/funder, who has granted bioRxiv a license to display the preprint in perpetuity. It is made available under a [aCC-BY-ND 4.0 International license](https://creativecommons.org/licenses/by-nd/4.0/).

**Ea****Eb****Ec**